# Skin-targeting platforms based on poly (β-amino ester)s for local immunotherapy

**Núria Puigmal Domínguez**

http://hdl.handle.net/10803/672238

UNIVERSITAT
**RAMON LLULL**

# DOCTORAL THESIS

| | |
|---|---|
| Title | Skin-targeting platforms based on poly(β-amino ester)s for local immunotherapy |
| Presented by | Núria Puigmal Domínguez |
| Centre | IQS School of Engineering |
| Department | Bioengineering |
| Directed by | Dr. Víctor Ramos Pérez |

**A la meva família**

This page left blank intentionally

"What you do makes a difference,
and you have to decide what kind of difference you want to make."
**Jane Goodall**

This page left blank intentionally

# ACKNOWLEDGEMENTS

En primer lloc, vull agrair al meu director de tesi, el Dr. Víctor Ramos, el seu suport i confiança durant la realització d'aquesta tesi. Víctor, gràcies pel teu recolzament. Des del primer moment, el teu optimisme em va inspirar a superar-me, i crec de debò que aquesta tesi transpira aquest entusiasme i passió per la ciència que m'has contagiat. T'estic molt agraïda per haver-me cuida't i guiat durant tots aquests anys a nivell professional i personal. Moltes gràcies de tot cor Víctor.

Junt amb el Dr. Ramos, m'agradaria agrair-li al Dr. Salvador Borrós l'oportunitat de realitzar aquesta tesi doctoral al seu grup. Salvador, sempre has vetllat per mi en la distància, però sé que totes les portes que se m'han obert han sigut gràcies a tu. L'equip que has format a GEMAT és especial i únic perquè és un reflex de la teva persona i dels valors de respecte, solidaritat i rigor científic que sempre ens has inculcat. Gràcies per una etapa inoblidable a IQS que m'ha fet millor científica i persona.

I am very grateful to Professor Natalie Artzi for welcoming me in her lab with open arms and make me feel at home. Thankyou Natalie for trusting in me from the very first minute and providing me with the mentoring, encouragement and resources to become the greatest scientist I could have ever dreamed of. I would also like to express my gratitude to Dr. Jamil Azzi for granting me the opportunity to collaborate with his prestigious lab. Working with you and your team has been a pleasure.

He de començar els agraïments dels GEMATOS amb en Pere, ja que has sigut el meu mentor tant a Barcelona i Boston. Tot lo professional queda relegat a un segon pla però si penso en tots els moments en que has sigut el meu pilar durant la tesi. Gràcies per ser un germà gran quan més l'he necessitat. Gràcies a la Dra. Cristina Fornaguera per ajudar-me sempre, i parar-ho tot per mi sense importar les mil tasques que tinguessis aquell dia. Juntament amb la Dra. Marta Guerra heu sigut unes grans guies per aquesta tesi. Gràcies noies! A Cris García, gracias por tu entusiasmo, siempre dispuesta a organizar y poner tu granito de arena, ¡faltan mujeres como tú! Polete, t'agraeixo que m'ajudessis amb la química orgànica, però encara més que ens preparessis els millors gintònics i tiberis, gràcies per la teva generositat i sempre estar disposat a donar-me un cop de mà. Anna Mas, gràcies per la teva amistat, pel teu sofà a Sant Antoni, per escoltar-me, ets una inspiració i tant debò sigui una científica tant valenta com tu algun dia. Robert, m'ha fet molt molt feliç treballar al teu costat. El teu humor i la teva fantàstica veu de tenor feien que venir al laboratori fos un plaer. Gràcies per ser el meu verdader senpai. Joan, qui m'ho hagués dit fa un temps però... et fas enyorar eh? Sota aquest mig somriure de "ladrón" tens amagat un gran cor i estic molt contenta d'haver format part de la família Tractivus. Alba, gracias por iluminar nuestros días. Tuvimos tanta suerte que os adoptaran en GEMAT

junto a Mire. Mire, gràcies pels moments dins GEMAT, però sobretot els de fora. Ets indispensable pel grup i el teu optimisme s'encomana. Patri, m'emporto molt bons records i riure compartits amb tu. Antonio, aunque te acogiéramos más tarde, lo compensaste con creces con tu locura y tu buen humor. Tampoc vull oblidar-me dels nois, Tito, Germancito, Mario, us desitjo lo millor en les vostres futures aventures. Finalment, a les TFMs; la Laura, l'Anna López, l'Aricookies i la Coral, moltes gràcies per aportar tant al grup.

He de fer una categoria a part per les Antonies de IQS per haver-me acompanyat des de 2015 (nenas, que ens fem velles). No sé que hagués fet sense els nostres bon moments a Barcelona, Roses, Sabadell i mil més, sou lo millor que m'emporto de IQS, de veritat. Laura ha sigut un plaer tenir-te de companya de viatge durant la tesi, gràcies per evitar que ens tornéssim boges entre tant "pamort". A la Mire, gràcies per fer-me riure sempre inclús en els dies més foscos, tens un do per treure lo millor de la gent. Cris, estic molt feliç de que ens haguem pogut retrobar a Boston, ets la millor amfitriona i amiga.

Vull tancar el capítol IQS amb els meus amics bioquímics (i companys de Torreta). Sergi, jo i tota la residència Roca et trobarem a molt a faltar. A la Laia i la Núria, per ser unes auxiliars genials i unes bones amigues/companyes de xafarderies i gràcies també al Marc i el Bernat pels bon moments.

Let's move to the Artzi team. Ana Pau, fuiste mi fuente de risas, alegría y mi primera y gran amiga de Boston, gracias por ayudar-me tanto con el proyecto y por llenar-lo todo de tu optimismo. Pinche güey, te echo de menos. Gonzalo, te incluyo dentro del Artzi Lab, pero tu apoyo ha ido mucho más allá de lo científico. Banquero, mecánico, chofer, chef, tienes muchos títulos, pero por encima de todo, está el de amigo. Grazas. Pau, va ser genial poder treballar al teu costat, arribar al lab i que et rebin amb un somriure com el teu no té preu. T'hem enyorat molt i espero que puguem tornar a coincidir i per fi poder fer tots els viatges que ens queden pendents. Cynthia, agradecerte mucho tu esfuerzo y trabajo en el laboratorio. Todos mis éxitos científicos los comparto contigo. Michelle, it meant the world having someone in the lab to talk to; for the good (and for the bad…!). But because of that, I am glad I can call you my friend. Alex, I am very grateful for your support both on the professional and on the personal level. Thanks for having the best words of wisdom and encouragement when I needed them. También quiero agradecer enormemente a Kalaumari su ayuda y tenacidad para sacar adelante nuestro proyecto. Fiona, not even the language barrier (and I mean your Irish) could stop us from having the most fun and I hope we can work together again, you are grand! Daniel, llegaste al laboratorio como un torbellino de alegría y good vibes. Siento no haber compartido más tiempo juntos, pero te deseo todo el éxito del mundo. Shiran, I really appreciate your scientific guidance and support in the lab. I really miss our moments together (specially, the laughs

during our Zumba lessons). Mica, ha sido un placer trabajar contigo. ¡Mil ganas de volver a verte! Orlando, gracias por ayudarnos tanto al team Microneedles, no lo habríamos logrado sin ti.

To the Azzi team, it was the highlight of my stay working with you. No wonder I wanted to stay with you past midnight staining Tregs (just kidding). Despite our overall sleep deprivation and stress, you always greeted me with the warmest smile, the loudest laughs and the greatest professionalism. Zhabiz, Karim, John, thanks for your support throughout these challenging times, our next frozen yogurt at the Harvard yard is on me.

A mis Brookline Babies, Mireia, Lidi, Vicky y Stella (soon-to-be roomie), qué bonito es hacer nuevas amigas verdaderas cuando menos lo esperas. Sois mis mujeres valientes, gracias por inspirarme a perseguir mis sueños. Mireia, gràcies pels mesos a la nostra mansió/paradís. Ets un bàlsam de tranquil·litat i energia positiva i m'alegro que poguéssim estar juntes quan més falta ens fèiem. Lidi, gracias por enseñarme que el cielo es el límite, por aconsejarme y por creer en mí siempre. Vicky, me acogiste en tu casa con los brazos abiertos y fuiste mi amiga y parte de mi familia cuando más lo necesitaba. Nunca lo olvidaré. Stella, ¿cómo pude tener tanta suerte de encontrarte? Your enthusiasm and passion is contagious, cannot wait for our next chapter together in Longwood Av.

També agrair-vos als Bostonianos tots els bon moments junts i que em féssiu sentir com a casa quan érem tant lluny. Ferran, Gemma, Nina, Guillem, Armand, Àlex, Hèctor, Carmen, Mireia, Anna...gràcies!

Peter, you've been my working week and my Sunday rest; my noon, my midnight, my talk, my song. Thank you.

Gràcies als biotecs pel vostre suport. Només cal que ens veiem un cop per l'any per saber que sempre sereu allà per ajudar-me. Adrià, Xec, Paula, Romà, Aina, Txell, Sònia i Robert sou genials.

Rosinques, vull agrair-vos tot el vostre suport incondicional durant tants anys. Xènia, Marta, Anna, Rosa, Raquel, Carla, gràcies per tot.

A la Martuel, només dir-te que no sé que faria sense tu. Tinc molta sort de tenir-te al meu costat. Ets la millor amiga que es pot desitjar i simplement, aquesta tesi no hagués estat possible sense tu.

Avis, Marieta, Mama, Papa, us dedico aquesta tesi. Gràcies per recolzar-me sempre i creure en mi, inclús quan ni jo ho feia. Veure que esteu tant orgullosos de mi és el que m'ha donat la força i el coratge per seguir superant-me. M'ho heu donat tot i sempre m'heu animat a que seguís els meus somnis. Per tot això, us estaré eternament agraïda. Us estimo molt.

Núria Puigmal Domínguez, 27 d'abril de 2021

This page left blank intentionally

This page left blank intentionally

# Abstract

**Skin-targeting platforms based on poly(β-amino ester)s for local immunotherapy**

The curative potential of immunotherapies to augment or suppress immune responses has shifted the paradigm for managing various diseases including cancer and autoimmune disorders, yet broad implementation has been curtailed by detrimental off-target toxicities. Given the ability of nanomaterials to direct immunomodulators to target tissues, nanomedicine-based delivery platforms formulated in carrier biomaterials could surmount the most pressing needs in the field being cell-specific targeting, local —rather than systemic— administration, and tissue accumulation to ultimately enhance the safety and potency of these therapeutic products. Using poly(β-amino ester)s (PBAEs) as foundational nanocarriers, this thesis proposes to engineer PBAE-based delivery platforms to target the immunologically rich milieu of the skin for local immunomodulation in the contexts of nucleic acid vaccination, cancer immunotherapy and adoptive T cell therapy.

First, a novel library of oligopeptide- and mannose-modified PBAEs is presented for refined targeting of dendritic cells (DCs) as primary orchestrators of antigen presentation in the skin. The synergistic potential of oligopeptide and ligand decoration to target dermal DC subsets has been demonstrated as a powerful tool to upgrade delivery vectors for gene vaccination. Nanoparticle- and solvent-free delivery of nucleic acids using PBAEs formulated as polyelectrolyte films (PEMs) has also been confirmed. PBAEs can be successfully integrated in transdermal devices such as microneedles, either as PEMs or as polyplexes, to mediate minimally-invasive gene transfer. Moving to cancer immunotherapy, a hydrogel-based MN platform is presented for delivery of an immunostimulatory drug and retrieval of interstitial skin fluid (ISF) for *in situ* immune surveillance of the response to therapy. It has been proven that PBAE-loaded MNs suppress tumor growth and modulate the immune signature of the tumor microenvironment, which appears to correlate with that from MN-sampled ISF. Finally, hydrogel MNs are proposed for restoring immune homeostasis in transplanted skin allografts. Recruitment of adoptively-transferred regulatory T cells into the allografts has been achieved by delivering chemoattractant chemokines with the MNs while also monitoring the $T_{reg}$ homing process via ISF sampling, confirming the potential of MNs as a mode of tissue surveillance.

In conclusion, this thesis demonstrates the potential of transdermal platforms derived from PBAEs for local immunomodulation. Shifting from hypodermic administration to solvent-free, local, and minimally-invasive approaches, PBAE-based systems have been engineered with microneedles for immunotherapy delivery.

This page left blank intentionally

# Resumen

**Skin-targeting platforms based on poly(β-amino ester)s for local immunotherapy**

El potencial curativo de las inmunoterapias para estimular o suprimir el sistema inmune ha revolucionado el paradigma bajo el que enfermedades como el cáncer o trastornos autoinmunes son tratados; no obstante, la implementación de dichas terapias se ha visto restringida por su toxicidad. Dada la capacidad de los nanomateriales para redirigir fármacos inmunomoduladores a tejidos dianas, las plataformas de liberación basadas en biomateriales podrían solventar las mayores necesidades del ámbito incluyendo, liberación específica a células diana, localizada —en vez de sistémica— y acumulación en tejidos diana para así aumentar su potencia y seguridad. Usando los poly(β-amino ester)s (PBAEs) como piedra angular, esta tesis propone desarrollar vectores dirigidos hacía la piel con el fin de modular el sistema inmune a nivel local en ámbitos tales como vacunación con ácidos nucleicos, inmunoterapia contra cáncer y terapia celular adoptiva.

Se ha presentado una nueva librería de PBAEs modificados con oligopéptidos y manosa que poseen especificidad celular hacia células dendríticas, las principales instigadoras en la presentación de antígenos en la piel. El efecto sinérgico entre oligopéptidos y ligando ha permitido mejorar sustancialmente estos vehículos de transporte para vacunación. Además, los PBAEs se han podido formular como vectores alternativos a las nanopartículas y que no precisan solventes, así como integrarlos en dispositivos médicos como microagujas, ya sea en forma de partículas o de films, para transferir genes de manera no invasiva. Como terapia contra el cáncer, se han diseñado microagujas de hidrogel que permiten la liberación de un fármaco inmunoestimulante además de colectar líquido intersticial para monitorear la respuesta a la terapia *in situ*. Las microagujas cargadas con PBAEs pudieron reducir el tamaño de los tumores y modular el microambiente tumoral, la composición del cual correlaciona con la del líquido intersticial colectado con dicha plataforma. Finalmente, las microagujas fueron usadas para restablecer el equilibrio inmunológico en trasplantes de piel. Las microagujas pudieron reclutar células T reguladoras hacia el trasplante mediante la liberación de citoquinas quimioatrayentes además de informar sobre su proceso de migración hacia el trasplante.

En conclusión, esta tesis demuestra el potencial de las plataformas transdérmicas basadas en PBAEs para inducir inmunomodulación local. Priorizando plataformas sin solventes, locales, y poco invasivas, se han desarrollado sistemas basados en PBAEs e integrados con microagujas para inmunoterapia.

This page left blank intentionally

# Resum

**Skin-targeting platforms based on poly(β-amino ester)s for local immunotherapy**

El potencial curatiu de les immunoteràpies per a estimular o suprimir respostes immunes ha revolucionat el paradigma sota el qual malalties como el càncer o trastorns autoimmunes son tractats; no obstant, una implementació extensa d'aquestes no ha sigut possible degut a la seva toxicitat. Donada la capacitat dels nanomaterials de reconduir fàrmacs immunomoduladors cap a teixits diana, les plataformes per alliberar fàrmacs dissenyades a partir de biomaterials podrien solucionar les necessitats més urgents d'aquest camp com l'alliberació específica a cèl·lules diana, l'alliberament local —en comptes de sistèmic— i l'acumulació a teixits diana per tal d'augmentar la seva eficàcia i seguretat. Aquesta tesi proposa l'ús de poly(β-amino ester)s (PBAEs) per al desenvolupant de vehicles d'alliberament dirigits cap a les pell amb l'objectiu de modular el sistema immune a nivell local en els àmbits de la vacunació amb àcids nucleics, la immunoteràpia contra el càncer y la teràpia adoptiva.

S'ha presentat una nova llibreria de PBAEs modificats amb oligopèptids i manosa amb especificitat cel·lular cap a les cèl·lules dendrítiques, les principals presentadores d'antigen a la pell. L'efecte sinèrgic entre els oligopèptids i el lligand ha permès millorar substancialment el rendiment d'aquests vector per a vacunació amb mRNA/DNA. Addicionalment, aquest s'han pogut formular sense necessitar de fer servir solvents ni en forma de nanopartícules, a més de poder-los integrar en dispositius mèdics com microagulles, ja sigui en forma de partícules o films, per tal de transferir gens de manera no invasiva. Com a teràpia contra el càncer, una microagulles innovadores fetes a partir d'hidrogels s'han utilitzat per a alliberar un fàrmac immunomodulador mentre recol·lectaven líquid intersticial simultàniament per tal monitoritzar l'eficiència de la teràpia. Les microagulles carregades amb PBAEs foren capaces de reduir la mida de tumors y modular el microambient tumoral, la composició immunològica del qual correlaciona amb la del líquid intersticial mostrejat. Finalment, les microagulles s'han reciclat com a plataforma per a restablir l'equilibri immunològic en transplantaments de pell. Les microagulles reclutaren cèl·lules T reguladores cap als transplantaments gràcies a l'alliberació de citocines mentre vigilaven *in situ* la migració d'aquestes.

En conclusió, aquesta tesi demostra el potencial de les plataformes transdèrmiques derivades de PBAEs per a induir immunomodulació a nivell local. Prioritzant plataformes sense solvents, locals i no-invasives, en aquesta tesi s'han optimitzat nous sistemes basats en PBAEs i integrats en dispositius mèdics com microagulles per a immunoteràpia.

This page left blank intentionally

# Table of Contents

# Index of Figures

# Index of Tables

# List of Abbreviations

| | |
|---|---|
| $^1$**H-NMR** | Nuclear magnetic resonance |
| **ACK** | Ammonium-Clhoride-Potassium |
| **AcONa** | Sodium acetate |
| **ADM** | allyl-α-D-Mannopyranoside |
| **APC** | Antigen Presenting cells |
| **CCL22** | C-C motif Chemokine Ligand 22 |
| **CDNs** | Cyclic dinucleotides |
| **$CO_2$** | Carbon dioxide |
| **COS-7** | African green monkey kidney fibroblast-like cell line |
| **CpG** | Cytosine-phosphate diester-guanine- rich oligonucleotides |
| **CTLA-4** | Cytotoxic T-lymphocyte-associated protein 4 |
| **$D_2O$** | Deuterium oxide |
| **DAB** | 3,3'Diaminobenzidine |
| **DCs** | Dendritic cells |
| **dDCs** | Dermal dendritic cells |
| **DEPC** | Diethyl pyrocarbonate |
| **DLS** | Dynamic Light Scattering |
| **DMEM** | Dulbecco's Modified Eagle Medium |
| **DMSO** | Dimethyl Sulfoxide |
| **DNA** | Deoxyribonucleic Acid |
| **dsDNA** | Double-stranded Deoxyribonucleic Acid |
| **EDC** | N-(3-(dimethylamino)propyl)carbodiimide |
| **FDA** | Food and Drug Administration |
| **FoxP3** | Forkhead box P3 |
| **GAPDH** | Glyceraldehide-3-Phosphate Dehydrogenase |
| **GFP** | Green Fluorescent Protein |
| **GM-CSF** | granulocyte-macrophage colony-stimulating factor |
| **GPa** | Gigapascal |
| **HA** | Hyaluronic acid |
| **HaCaT** | Human epidermal keratinocyte line |
| **HADA** | Dopaminated hyaluronic acid |
| **HBSS** | Hanks' Balanced Salt solution |
| **HEPPES** | 4-(2-hydroxyethyl)-1-piperazineethanesulfonic acid |
| **HNDF** | Human normal dermal fibroblast |
| **HRP** | Horseradish Peroxidase |
| **IHC** | Immunohistochemistry |
| **IHF** | Immunohistofluorescence |

| | |
|---|---|
| **IL-2** | Interleukin-2 |
| **IL-6** | Interleukin-6 |
| **ISF** | Interstitial skin fluid |
| **kDa** | kilodalton |
| **kPa** | kilopascal |
| **LbL** | Layer-by-Layer |
| **LCs** | Langerhans Cells |
| **LN** | Lymph node |
| **M** | Molar |
| **MC38** | Murine Colon Adenocarcinoma 38 cells |
| **MDDCs** | Monocyte-derived Dendritic Cells |
| **MDSCs** | Myeloid-derived suppressor cells |
| **MEM-α** | Minimal essential medium alpha |
| **MHC** | major histocompatibility complex |
| **mM** | Millimolar |
| **MM-** | Mannose-modified |
| **MNs** | Microneedles |
| **MoLCs** | Monocyte-derived Langerhans Cells |
| **MR** | Mannose receptor |
| **mRNA** | Messenger Ribonucleic acid |
| **MTT** | 3-(4,5-dimethylthiazol-2-yl)-2,5-diphenyltetrazolium |
| **MTS** | 3-(4,5-dimethylthiazol-2-yl)-5-(3-carboxymethoxyphenyl)-2-(4-sulfophenyl)-2H-tetrazolium |
| **MUTZ-3** | Human monocytic cell line |
| **NHS** | N-hydroxysuccinimide |
| **NK** | Natural Killer |
| **OCT** | Optimal cutting temperature compound |
| **ODN** | oligodeoxynucleotides |
| **OM-** | Oligopeptide modified- |
| **PB** | Phosphate buffer |
| **PBAE** | Poly (β-amino ester) |
| **PBS** | Phosphate-Buffered Saline |
| **PCL** | Polycaprolactone |
| **PD-1** | Programmed cell death protein 1 |
| **PDA** | Polydopamine |
| **PDI** | Polydispersivity Index |
| **PD-L1** | Programmed death-ligand 1 |
| **PDMS** | Poly(dimethylsiloxane) |
| **pDNA** | Plasmid Deoxyribonucleic Acid |
| **PECVD** | plasma enhanced chemical vapor deposition |
| **PEG** | Polyethylene glycol |
| **PEMs** | Polyeletrolyte multilayers |

| | |
|---|---|
| **PFM** | Pentafluorophenyl Methacrylate |
| **PLGA** | Poly(lactic-co-glycolic acid) |
| **pp** | plasma-polymerized |
| **PRR** | Pattern recognition receptor |
| **PVA** | Poly(vinyl alcohol) |
| **qPCR** | quantitative real-time PCR |
| **RF** | Radio frequency |
| **RhoB** | Rhodamine B |
| **SC** | Stratum corneum |
| **SD** | Standard deviation |
| **TA** | Tumor Antigen |
| **TCEP** | Tris (2-carboxyethil) phosphine |
| **tdLN** | Tumor-draining lymph nodes |
| **TGF-β1** | Transforming growth factor β1 |
| **THP-1** | Human monocytic cell line |
| **TLR9** | Toll-like receptor 9 |
| **TNF-α** | Tumor necrosis factor α |
| **T$_{reg}$** | Regulatory T cell |
| **v/v** | Volume/volume fraction |
| **w/v** | Weight/volume fraction |
| **µl** | Microlitre |
| **µm** | Micrometre |

This page left blank intentionally

**Chapter I:    Motivation and objectives**

This page left blank intentionally

## 1.1 Introduction

The cellular mechanisms driving immune regulation can be a tug of war; effector cells play against the regulatory compartment of the immune system and this game results in the maintenance of immune homeostasis in healthy patients. In the advent of disease, modulating the immune system via immunotherapies can restore that balance, yet it is also a double-edged sword since activation of the immune sentinels cascades non-specific systemic inflammation and autoimmune side effects. For this reason, drug delivery technologies are important, if not central, to fully exploit the potential of immune therapeutics while avoiding detrimental off-target effects. This doctoral thesis proposes the use of PBAEs-derived systems for both targeted and local delivery of immunomodulators to the skin. Leveraging their versatility and chemical flexibility, platforms based on PBAEs and integrated with interventional medical devices such as microneedles are here projected for translation into three cardinal applications of the immunotherapy field: nucleic acid vaccination, checkpoint blockade for cancer treatment and adoptive T cell therapy in the context of transplantation.

Immunotherapies, treatments that educate the patient's own immune system to activate or suppress natural immune mechanisms, have shifted the paradigm for the management of multiple conditions including infectious diseases, autoimmunity, allergies, transplant rejection, graft versus host disease, and cancer.[1] Among these therapeutic areas, cancer immunotherapy has experienced tremendous progress,[2,3] energizing the scientific community to further explore alternative treatments that equip the immune system against other disorders. Some of the most thoroughly investigated approaches include nucleic acid vaccines, checkpoint inhibitors and adoptive cellular therapies that will be next discussed, yet the field is constantly being fed with new emerging strategies.[4]

Nucleic acid therapeutics, including DNA-based and mRNA-based vaccines, represent a promising alternative to conventional vaccines due to their increased potency, scalable manufacturing and outstanding safe profile.[5,6] Their course of action relies on the intracellular internalization of exogeneous nucleic acids by target cells where the nucleic acids will be translated to induce antigen expression and trigger both humoral and cell-mediates responses.[7,8] The main difference between DNA and mRNA vaccines is the target location for the delivery of the oligonucleotides, set in the nucleus for DNA therapeutics and in the cytosol for mRNA vaccines,[9] which prevents potential genomic integration in the lastest.[10] Due to the multiple biological barriers,[11] nucleic acid vaccines have greatly benefited from delivery technologies based on biomaterials to succeed in their

translation to the clinic,[12] specially for infectious diseases[13] and cancer vaccines,[14] both in prophylactic and therapeutic settings.

The real breakthrough in cancer immunotherapy occurred a decade ago following the approval of checkpoint inhibitors by the FDA.[15] Immune checkpoints are inhibitory pathways hardwired into the immune system that are crucial for maintaining self-tolerance and modulating physiological immune responses.[16] Tumoral cells disarm immune checkpoint pathways as a major mechanism of immune resistance to evade recognition and restrain host T-cell response against tumors.[17] Since immune checkpoints are activated upon ligand-receptor interactions, blockade by recombinant antibodies or ligands can restore T-cell mediated tumor cell death (PD-1/PD-L1 blockade) or maintain T-cell activation (CTLA4 blockade).[17] Nevertheless, severe toxicity and patient unresponsiveness has limited their widespread implementation, which could be addressed if using advanced delivery technologies.

Steady advances in the field of adoptive T cell therapy for cancer treatment heralded a new era of promise for managing other diseases such as solid organ rejection.[18] In recent years, a growing number of clinical trials have explored the use of T cell subsets other than effector T cells such as regulatory T cells ($T_{regs}$) as an alternative to systemic immunosuppressants.[19,20] A major limitation of adoptive T cell therapies is that the viability and function of the transplanted cells rapidly declines after administration,[4] highlighting the need for nanomedicine-based approaches capable of enhancing longevity, phenotype and function of cell therapy products.

As evidenced here, broader success with immunotherapy treatments has not been limited by a lack of reasonable therapeutic targets but rather how the timing and location of immunomodulation was controlled.[21] It appears that the drug delivery paradigm prioritizing systemic administration should be obviated and efforts focused in targeting cells and tissues instead. As our major barrier to the outside world, the skin harbors a unique and complex immune cell reservoir that finely coordinates immune homeostasis.[22–24] Therefore, the skin offers direct and easy access to an intricate network of immune cells that could be leveraged for targeted, transcutaneous delivery of immunotherapies.

Therapeutics formulated in carrier biomaterials could easily surmount some of the most pressing needs of the field being cell-specific targeting, local —rather than systemic— immunomodulation, and tissue accumulation. As of today, a myriad of synthetic biomaterials have been developed for drug delivery purposes,[25] and where a particular candidate, the PBAE family, could effectively harness immunotherapies and improve their potency while reducing off-target effects.

PBAEs were first developed by David Lynn and co-workers in 2000 as a new class of cationic polymers,[26] rising in two decades as an unmatched vehicle for therapy delivery and being considered the most potent alternative to viral vectors.[27,28] Such regard derives from their inherent biocompatibility, biodegradability and ease of synthesis without solvents, catalysts, or by-products.[29] Cationic PBAEs can condense commonly used immunomodulators such as nucleic acids and assemble them into nanoscopic scale polyplexes via electrostatic interactions with the negatively charged phosphate groups present in their backbone. These stable nanoparticles can next penetrate the intracellular space, scape the endosomal compartment and degrade via hydrolytic cleavage of ester groups to release their therapeutic cargo.[30]

Synthesis of PBAEs is readily accomplished via Michael addition of primary amines or bis(secondary amines) and a diacrylate following a one-step growth mechanism (**Figure I-1**).[31] Through this facile synthetic strategy, extensive libraries of PBAE candidates can be generated for successive exploration of their physicochemical properties and delivery efficacy. Screening of the polymer libraries following combinatorial modification has corroborated the close relationship existing between end-modification and transfection efficiency,[32–34] and which can be exploited to rationally design PBAEs targeting specific cellular subsets. In the context of transdermal immunotherapy, where cellular targets such as Langerhans Cells (LCs) and macrophages are both scattered and scarce, an unfortunate choice of a vector could doom the chances of success. Therefore, the chemical flexibility of PBAEs offers an unparalleled opportunity for extensive screening of numerous candidates to isolate the very few formulations that could attain a therapeutic effect.
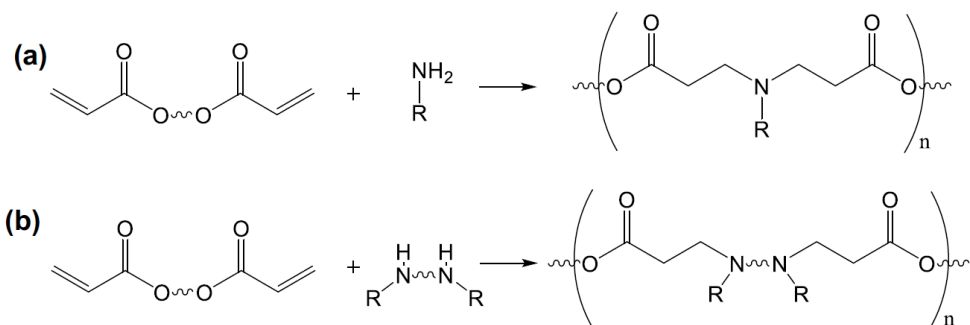


**Figure I-1. Synthetic strategy for PBAEs.**[31] Synthesis of linear PBAEs is achieved by conjugate addition of primary (a) or bis(secondary amines) (b) to diacrylates. Synthesis can be conducted either as a solvent free reaction or in anhydrous organic solvents such as DMSO, chloroform and dichloromethane to avoid hydrolytic degradation.

Our group has long reported end-capping of PBAEs with oligopeptide chains as a powerful tool for enhanced stability, biocompatibility and transfection in a cell-type dependent manner.[35–38] Specifically, surface charge tunability following decoration with oligopeptides allows a strong control over the nanoparticle composition and features such as size and zeta potential which later translates into cell-specific targeting.[39] However, restricting PBAE decoration to the inclusion of cationic and anionic moieties might not suffice to target the reservoir of immune cells present in the skin given their elusive nature. In an effort to achieve cell- and tissue-specific targeting, PBAEs can be engineered by tuning their physical characteristics as described by us and others,[40] —and generally referred as passive targeting—but also via the inclusion of stimulus-driven release motives or cell-homing ligands,[41] —known as active targeting mechanisms.

Numerous biological ligands have been proposed to facilitate active targeting of delivery vehicles including nanoparticles. These ligands bind to cell-specific endocytic receptors expressed on the surface of target cells such as antigen presenting cells (APCs), increasing cellular uptake of the drug-loaded vectors and in turn, their therapeutic efficacy.[42] Analogously, specific targeting of immune-effector cells reduces anergy-related responses associated with systemic delivery.[43] Incorporation of targeting ligands into nanoparticles can be achieved via two synthetic strategies.[27] Briefly, ligands can be covalently attached during polymer synthesis as a side-chain or as an end-cap moiety prior to nanoparticles formation. Alternatively, they can also be added after nanoparticle formulation via chemical conjugation or physical adsorption. Either way, various ligands can be integrated such as proteins, nucleic acids, peptides, small molecules and polysaccharides,[42] being the latest of special relevance in the immunotherapy field.

Targeting cell surface receptors from APCs has been long explored for vaccination and anti-cancer immunotherapy, with efforts being put into the calcium-dependent (C-type) lectin family due to their high specificity and binding-affinity to polysaccharides.[44] These receptors are ubiquitously expressed by professional APCs and can efficiently transfer antigens into endocytic compartments for loading onto MHC molecules and stimulation of T-cell responses,[45] bringing together both adaptive and innate immunity.[7] Mannose-decorated drug delivery systems have shown great effectiveness given their affinity with the most important receptors involved in antigen endocytosis such as the mannose-receptor (MR) or the Langerin receptor (CD207) predominantly expressed in macrophages and LCs, respectively.[46] In the past, Jones and colleagues showed that decoration of PBAE nanoparticles with mannose moieties rendered potent polyplexes that preferentially targeted dermal APCs both *in vitro* and *in vivo*,[41,47] supporting mannosylated PBAEs as superior delivery agents.

As previously stated, combinatorial screening of PBAE-derived polyplexes remains extremely useful to evaluate transfection efficacy, as large numbers of formulations can be studied in parallel due to their easy fabrication. However, using alternative PBAE-derived systems such as polyelectrolyte films, gels, or fibers is sometimes preferred, especially when aiming to integrate them with medical devices (**Figure I-2**).
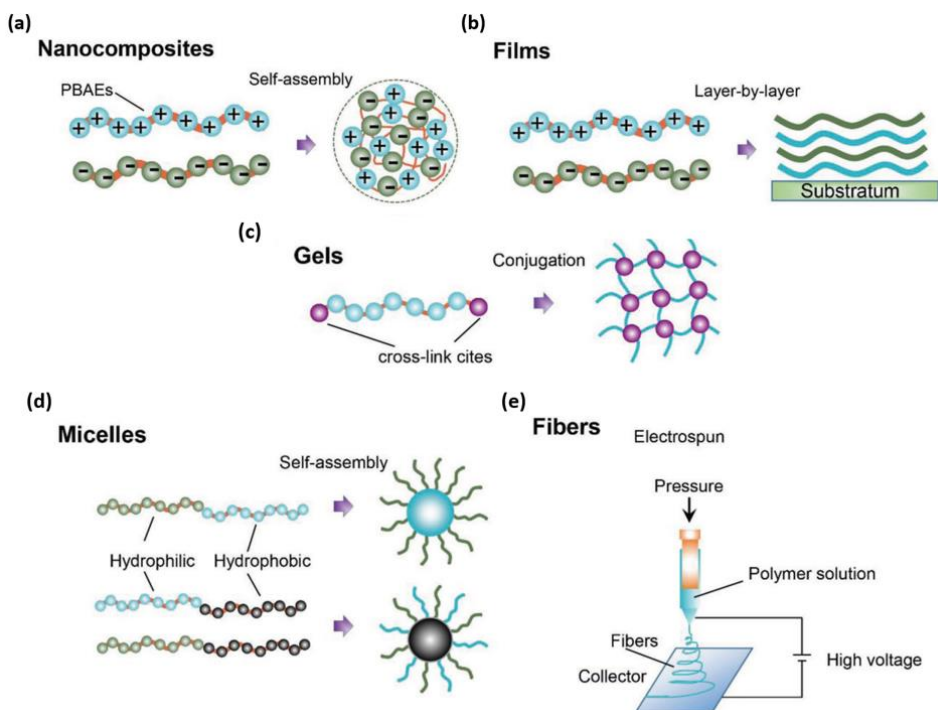


**Figure I-2. Schematic representation of PBAE-derived systems.**[48] Thanks to their chemical flexibility, PBAEs can be formulated using different approaches in accordance with their final application. Nanocomposites (polyplexes), films and micelles have been extensively described for drug delivery, yet others such as gels or fibers are of particular interest for tissue engineering.

Polyelectrolyte-based films, often referred as polyelectrolyte multilayers or PEMs, have drawn the most attention (just after polyplexes) due to their ease of production and ability to virtually coat any substrate.[49] Polyelectrolyte films are assembled using a "layer-by-layer" method via alternate deposition of nucleic acids and cationic polymers that interact electrostatically, rendering nanostructured films with bioactive cargos embedded in a dried state.[50,51] The therapeutic cargo can then be released by passive diffusion or following disassembling of the films, allowing the internalization of the nucleic acids into the cells via surface-mediated transfection mechanisms. The

solvent-free nature of the films could offer a convenient opportunity for extended storage, reduced costs and widespread distribution to developing countries as refrigeration can generally be avoided.[52]

As we move from optimization of PBAEs as therapeutic vectors to their translation into a platform for transcutaneous immunization, it becomes evident that not only a rational polymer design, but a powerful administration device is needed to succeed. As previously discussed, the skin —being an immune sentry-rich tissue— could be an exceptional route of administration for immunotherapies, but only if immunomodulators are successfully transported across the stratum corneum (SC). To facilitate their transport, PBAEs can be integrated with interventional medical devices such as microneedles (MNs) as therapeutic tandems, which have shown great promise in the vaccination field.[53–57]

MNs are transdermal devices consisting in micrometric needle-like projections capable of disrupting the epidermis for drug delivery in a minimally-invasive manner.[58] MN-based systems enhance the delivery of bioactive molecules, possess higher stability and immunogenicity than conventional intramuscular routes, and present dose-sparing advantages.[59] Besides, needle-free delivery prevents the hazard of needle-borne diseases associated with the re-use and inappropriate disposal of needles. Other significant advantages are their ease of administration by minimally trained personnel and independence from refrigerated transport and storage.[60] Finally, MNs can be administered in a painless manner since receptors that populate the underlaying dermis are not stimulated.[61] This feature increases patient compliance and eliminates the anxiety and injuries caused by hypodermic needles. In order to accommodate the requirements of the medical industry, an eclectic variety of MNs has been designed, which are generally divided into five categories (solid, coated, dissolving, hollow and hydrogel-forming) depending on their features (**Figure I-3**).[62]

Among these, hydrogel-forming MNs should be highlighted. First described by Donnelly and colleagues,[63] hydrogel-based MNs are prepared from crosslinked polymers in a wide range of geometries that can effectively penetrate the stratum corneum barrier in their dry state. Upon insertion, MNs rapidly swell skin interstitial fluid (ISF) and hydrate, forming hydrogel conduits with the dermal microcirculation that cannot be blocked and which ensure a continuous release of the therapeutic cargo at a rate dictated by the crosslinker.[63,64] Translation of MNs into marketable products had been hampered in the past due to their limited loading capacity, which prevented them from delivering the high doses needed to achieve therapeutic plasma concentrations. However, hydrogel-based MNs do not have drug loading limitations as they can be coupled to lyophilized drug reservoirs,[64] making them top contenders in the race for clinical applicability.
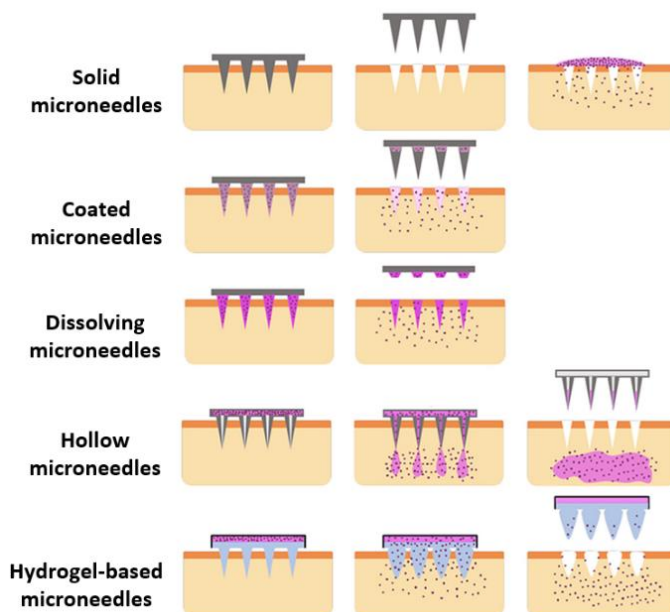
**Figure I-3.Schematic representation of the different types of microneedles.** [65] Microneedles can be classified as follows depending on their properties. Selection of  the fittest MN for drug delivery is generally dictated by the type of drug aiming to be delivered.

Complimenting their therapeutic arm, hydrogel-based MNs can also provide means for extraction of ISF, an emerging source of biomarkers for disease diagnosis and prognosis.[66,67] With recent clinical trials supporting the narrow correlation between ISF biomarkers and those present in plasma — specially the soluble fraction—,[68] widespread use of ISF for diagnosis purposes could soon become the rule rather than the exception as minimally-invasive MN platforms become more accessible.

For all the above, hydrogel-based MNs have rapidly become a favorite among the scientific community as they offer means for both therapy and diagnosis, —a distinctive feature that none of the rest allows for. Nevertheless, hydrogel MNs encompassing both abilities within the same device have rarely been explored as synchronizing both arms has proven challenging. If successfully designed, MN platforms with an almost-theranostic character could become one of the most sough-after technologies due to the numerous diseases still necessitating integral management, both therapy- and diagnosis-wise.

Most efforts in the immunotherapy field had been traditionally aimed at inducing inflammatory or immunostimulatory signaling. However, the therapeutic potential of adoptive T cell therapy for cancer treatment has energized the interest for alternative cell-based therapies that aimed at

immunosuppression instead, paving the way for $T_{reg}$ cell-based therapies to become a commonplace. Advances in $T_{reg}$ expansion protocols along with the excellent safety profiles now foresee an imminent translation into the clinic, with more than 50 clinical trials currently exploring the efficacy of adoptive $T_{reg}$ transfer for indications such as organ transplantation or autoimmune diseases.[18] $T_{regs}$ account for one of the largest subsets of immune cells in the skin, promoting local immune homeostasis and restoring normal function after a threat.[24,69–71] Hence, pharmacologic $T_{reg}$ augmentation and adoptive $T_{reg}$ transfer have gained increasing attention among the community,[72–74] with reports showing their potential to tilt the immunological balance towards an immunological homeostasis and prolong graft survival.[75–77] Since $T_{regs}$ mediate specific functions depending entirely upon their residing tissues,[22] tissue-specific therapeutic approaches should be favored to maximize their efficacy. Hence, skin allografts provide a unique opportunity for facile access to the tissue and that can be leveraged for transcutaneous delivery of an immunotherapy using MNs.

Immunotherapies are now a clinical reality spanning the treatment of multiple conditions such as infectious diseases, autoimmunity, allergies, transplant rejection, graft versus host disease, and cancer. Despite the steady advances, there is still an unmet need for enhanced drug delivery technologies capable of localizing the therapy for immune stimulation or suppression while avoiding side effects. Thus, the main aim of this dissertation is **the development of new platforms for local transdermal immunomodulation, using PBAEs as our cornerstone**. Thanks to their versatility, different formulations derived from PBAEs including polyplexes and polyelectrolyte films have been developed and combined with transdermal devices such as MNs for prospective clinical translation into three major applications: gene vaccination, cancer immunotherapy and adoptive $T_{reg}$ transfer.

In order to achieve the main objective, the following goals were proposed:

- To formulate and characterize a novel library of PBAEs by including oligopeptides and a mannose ligand for specific targeting of LCs and APCs governing antigen presentation in the skin (*Chapter II*).

- To develop PBAE-derived systems based on polyplexes or polyelectrolyte films and determine their transfection capacity when integrated with transdermal devices such as microneedles (*Chapter III*).

- To design a hydrogel-based MN platform for simultaneous delivery of PBAE-complexed immunostimulatory drugs (CpG oligodinucleotides) and retrieval of ISF in cancer settings (*Chapter IV*).

- To optimize the hydrogel-based MNs for delivery of chemoattractant chemokines and extraction of ISF to monitor the $T_{reg}$ homing process as a response to the immunotherapy (*Chapter V*).

## 1.2  Content of this dissertation

The main goal of this thesis is the development of new means for transdermal immunotherapy. To do so, novel PBAE-based systems are presented in this work that allow the delivery of various nucleic acids when administrated (1) on their own as polyplexes and polyelectrolyte films or (2) when integrated with transcutaneous devices such as microneedles.

First, the design of a new library of PBAEs for targeted nucleic acid vaccination is proposed (*Chapter II*). Using oligopeptide-modified PBAEs as our starting point, highly efficient polyplexes have been synthesized via inclusion of a mannose ligand for targeted DCs transfection. Gene transference has been examined *in vitro* in all the cell phenotypes supporting antigen presentation in the skin and *in vivo* to elucidate the impact of PBAE decoration on transfection efficiency.

In *Chapter III*, the ability of the newly synthesized PBAEs to deliver genes is further explored when deposited as polyelectrolyte films —a solvent-free, and nanoparticle-free strategy. Film deposition methods have been proposed on various substrates in combination with surface engineering methods for prospective non-invasive therapy administration.

In collaboration with the Artzi Lab (Harvard Medical School) *Chapter IV* goes a step further, with PBAEs being combined with a transdermal device, a hydrogel-based MN patch, for anti-cancer immunotherapy. The MN platform has been designed to allow for simultaneous therapy delivery and ISF extraction to surveil the immune status *in situ*. Immunostimulatory oligonucleotides have been released via PBAE-loaded MNs to activate inflammatory signaling paths and suppress tumor growth while retrieving ISF to analyze cellular biomarkers and inform on the immune state of the tissue following treatment.

Finally, MNs are proposed in the context of transplantation for the management of skin transplant rejection (*Chapter V*). Owing to their potential to deliver immunomodulators, the previously developed MN patch has been leveraged to release chemoattractant chemokines that promote $T_{reg}$ migration at the site of alloimmunity and monitor the $T_{reg}$ homing process to inquire on the immunotherapy's efficiency *in situ*.

## 1.3　References

1.　Zheng, Y., Tang, L., Mabardi, L., Kumari, S. & Irvine, D. J. Enhancing Adoptive Cell Therapy of Cancer through Targeted Delivery of Small-Molecule Immunomodulators to Internalizing or Noninternalizing Receptors. *ACS Nano.* 11, 3089–3100 (2017).

2.　Waldman, A. D., Fritz, J. M. & Lenardo, M. J. A guide to cancer immunotherapy: from T cell basic science to clinical practice. *Nat. Rev. Immunol.* 20, 651–668 (2020).

3.　Chen, Q., Chen, M., Liu, Z. & Chen, Q. Local biomaterials-assisted cancer immunotherapy to trigger systemic antitumor responses. *Chem. Soc. Rev.* 48, 5506–5526 (2019).

4.　Riley, R. S., June, C. H., Langer, R. & Mitchell, M. J. Delivery technologies for cancer immunotherapy. *Nat Rev Drug Discov* 18, 175–196 (2019).

5.　Pardi, N., Hogan, M. J., Porter, F. W. & Weissman, D. mRNA vaccines — a new era in vaccinology. *Nature* 17, 261–279 (2018).

6.　Hobernik, D. & Bros, M. DNA Vaccines — How Far From Clinical Use? *Int. J. Mol. Sci.* 19, 3605 (2018).

7.　Apostolopoulos, V., Thalhammer, T., Tzakos, A. G. & Stojanovska, L. Targeting Antigens to Dendritic Cell Receptors for Vaccine Development. *J. Drug Deliv.* 2013, 869718 (2013).

8.　Metcalfe, S. M. & Fahmy, T. M. Targeted nanotherapy for induction of therapeutic immune responses. *Trends Mol. Med.* 18, 72–80 (2012).

9.　Reichmuth, A. M., Oberli, M. A., Jaklenec, A., Langer, R. & Blankschtein, D. mRNA vaccine delivery using lipid nanoparticles. *Ther. Deliv.* 7, 319–334 (2016).

10.　Schlake, T., Thess, A., Fotin-mleczek, M. & Kallen, K. Developing mRNA-vaccine technologies. *RNA Biol.* 11, 1319–1330 (2012).

11.　Yin, H. *et al.* Non-viral vectors for gene-based therapy. *Nat. Rev. Genet.* 15, 541–555 (2014).

12.　Guan, S. & Rosenecker, J. Nanotechnologies in delivery of mRNA therapeutics using nonviral vector-based delivery systems. *Gene Ther.* 24, 133–143 (2017).

13.　Zhang, C., Maruggi, G., Shan, H. & Li, J. Advances in mRNA Vaccines for Infectious Diseases. *Front. Immunol.* 10, 594 (2019).

14.　Lopes, A., Vandermeulen, G. & Préat, V. Cancer DNA vaccines: current preclinical and clinical

developments and future perspectives. *J. Exp. Clin. Cancer Res.* 1, 146 (2019).

15.    Sahasranaman, S. Immune Checkpoint Inhibitors : An Introduction to the Next-Generation Cancer Immunotherapy. *J. Clin. Pharmacol.* 56, 157–169 (2016).

16.    Pardoll, D. M. The blockade of immune checkpoints in cancer immunotherapy. *Nat Rev Cancer* 12, 252–264 (2016).

17.    Darvin, P., Toor, S. M., Nair, V. S. & Elkord, E. Immune checkpoint inhibitors: recent progress and potential biomarkers. *Exp. Mol. Med.* 12, 1–11 (2018).

18.    Raffin, Caroline, Vo, Linda T. Bluestone, J. A. Treg cell-based therapies: challenges and perspectives. *Nat. Rev. Immunol.* 20, 158–172 (2020).

19.    Tang, Q. & Bluestone, J. A. Regulatory T-cell therapy in transplantation: Moving to the clinic. *Cold Spring Harb. Perspect. Med.* 11, a015552 (2013).

20.    Tang, Q. & Lee, K. Regulatory T-cell therapy for transplantation: How many cells do we need? *Curr. Opin. Organ Transplant.* 17, 349–354 (2012).

21.    Irvine, D. J. & Dane, E. L. Enhancing cancer immunotherapy with nanomedicine. *Nat Rev Immunol* 20, 321–334 (2020).

22.    Ali, N. & Rosenblum, M. D. Regulatory T cells in skin. *Immunology* 152, 372–381 (2017).

23.    Ho, A. W. & Kupper, T. S. T cells and the skin: from protective immunity to inflammatory skin disorders. *Nat. Rev. Immunol.* 8, 490–502 (2019).

24.    Nguyen, A. V. & Soulika, A. M. The dynamics of the skin's immune system. *Int. J. Mol. Sci.* 20, 1811 (2019).

25.    Midoux, P., Pichon, C., Yaouanc, J. J. & Jaffres, P. A. Chemical vectors for gene delivery: A current review on polymers, peptides and lipids containing histidine or imidazole as nucleic acids carriers. *Br. J. Pharmacol.* 157, 166–178 (2009).

26.    Lynn, D. M. & Langer, R. Degradable Poly (Beta-amino esters ): Synthesis, Characterization, and Self-Assembly with Plasmid DNA. *J Am Chem Soc* 122, 10761–10768 (2000).

27.    Karlsson, J., Rhodes, K. R., Green, J. J. & Tzeng, S. Y. Poly(beta-amino ester)s as gene delivery vehicles: challenges and opportunities. *Expert Opin. Drug Deliv.* 17, 1395–1410 (2020).

28.    Iqbal, S. *et al.* Poly (β-Amino Esters) based Potential Drug Delivery and Targeting Polymer; An Overview and Perspectives. *Eur. Polym. J.* 141, 110097 (2020).

29.   Green, J. J., Langer, R. & Anderson, D. G. A Combinatorial Polymer Library Approach Yields Insight into Nonviral Gene Delivery. *Acc. Chem. Res.* 41, 749–759 (2008).

30.   Akinc, A., Anderson, D. G., Lynn, D. M. & Langer, R. Synthesis of Poly (Beta-amino ester ) s Optimized for Highly Effective Gene Delivery. *Bioconjug. Chem.* 14, 979–988 (2003).

31.   Cordeiro, R. A., Serra, A., Coelho, J. F. J. & Faneca, H. Poly (β-amino ester )-based gene delivery systems: From discovery to therapeutic applications. *J. Control. Release* 310, 155–187 (2019).

32.   Green, J. J. *et al.* Combinatorial modification of degradable polymers enables transfection of human cells comparable to adenovirus. *Adv. Mater.* 19, 2836–2842 (2007).

33.   Green, J. J. *et al.* Electrostatic Ligand Coatings of Nanoparticles Enable Ligand-Specific\rGene Delivery to Human Primary Cells. *Nano Lett.* 7, 874–879 (2007).

34.   Sunshine, J. *et al.* Small-molecule end-groups of linear polymer determine cell-type gene-delivery efficacy. *Adv. Mater.* 21, 4947–4951 (2009).

35.   Segovia, N., Dosta, P., Cascante, A., Ramos, V. & Borrós, S. Oligopeptide-terminated poly (b-amino ester ) s for highly efficient gene delivery and intracellular localization. *Acta Biomater.* 10, 2147–2158 (2014).

36.   Dosta, P. *et al.* Delivery of Anti-microRNA-712 to Inflamed Endothelial Cells Using Poly(β-amino ester) Nanoparticles Conjugated with VCAM-1 Targeting Peptide. *Adv. Healthc. Mater.* e2001894 (2021) doi:10.1002/adhm.202001894.

37.   Fornaguera, C. *et al.* mRNA Delivery System for Targeting Antigen-Presenting Cells In Vivo. *Adv. Healthc. Mater.* 7, 1–11 (2018).

38.   Brugada-Vilà, P. *et al.* Oligopeptide-modified poly(beta-amino ester)s-coated AdNuPARmE1A: Boosting the efficacy of intravenously administered therapeutic adenoviruses. *Theranostics* 10, 2744–2758 (2020).

39.   Dosta, P., Segovia, N., Cascante, A., Ramos, V. & Borrós, S. Surface charge tunability as a powerful strategy to control electrostatic interaction for high efficiency silencing, using tailored oligopeptide-modified poly(beta-amino ester)s (PBAEs). *Acta Biomater.* 20, 82–93 (2015).

40.   Zugates, G. T. *et al.* Gene Delivery Properties of End-Modified Poly (Beta-amino ester)s. *Bioconjug. Chem.* 18, 1887–1896 (2007).

41.     Jones, C. H. *et al.* Structure – Function Assessment of Mannosylated Poly( β -amino esters) upon Targeted Antigen Presenting Cell Gene Delivery. *Biomacromolecules* 16, 1534–1541 (2015).

42.     Yoo, J., Park, C., Yi, G., Lee, D. & Koo, H. Active Targeting Strategies Using Biological Ligands for Nanoparticle Drug Delivery Systems. *Cancers.* 640, 1–13 (2019).

43.     Lori, F., Kelly, L. M. & Lisziewicz, J. APC-targeted immunization for the treatment of HIV-1. *Expert Rev. Vaccines* 3, 189–198 (2004).

44.     Irache, J. M., Salman, H. H., Gamazo, C. & Espuelas, S. Mannose-targeted systems for the delivery of therapeutics. *Expert Opin. Drug Deliv.* 5, 703–724 (2008).

45.     Keler, T., Ramakrishna, V. & Fanger, M. W. Mannose receptor-targeted vaccines. *Expert Opin. Biol. Ther.* 4, 1953–1962 (2004).

46.     Diebold, S. S., Plank, C., Cotten, M., Wagner, E. & Zenke, M. Mannose Receptor-Mediated Gene Delivery into Antigen Presenting Dendritic Cells. *Somat. Cell Mol. Genet.* 27, 65–74 (2002).

47.     Jones, C. H. *et al.* Mannosylated poly (beta-amino esters) for targeted antigen presenting cell immune modulation. *Biomaterials* 37, 333–344 (2014).

48.     Liu, Y., Li, Y., Keskin, D. & Shi, L. Poly (β -Amino Esters ): Synthesis, Formulations, and Their Biomedical Applications. *Adv. Healthc. Mater.* 8, 1–24 (2019).

49.     Jewell, C. M., Zhang, J., Fredin, N. J. & Lynn, D. M. Multilayered polyelectrolyte films promote the direct and localized delivery of DNA to cells. *J. Control. Release* 106, 214–223 (2005).

50.     Bechler, S. L. & Lynn, D. M. Characterization of degradable polyelectrolyte multilayers fabricated using DNA and a fluorescently-labeled Poly(B-amino ester): Shedding light on the role of the cationic polymer in promoting surface-mediated gene delivery. *Biomacromolecules* 13, 542–552 (2012).

51.     Yu, Y., Si, Y., Bechler, S. L., Liu, B. & Lynn, D. M. Polymer Multilayers that Promote the Rapid Release and Contact Transfer of DNA. *Biomacromolecules* 16, 2998–3007 (2015).

52.     Demuth, P. C. *et al.* Polymer multilayer tattooing for enhanced DNA vaccination. *Nat. Mater.* 12, 367–376 (2013).

53.     Kim, N. W. *et al.* Polyplex-releasing microneedles for enhanced cutaneous delivery of DNA

vaccine. *J. Control. Release* 179, 11–17 (2014).

54. DeMuth, P. C. *et al.* Polymer multilayer tattooing for enhanced DNA vaccination. *Nat. Mater.* 12, 367–76 (2013).

55. Demuth, P. C., Garcia-Beltran, W. F., Ai-Ling, M. L., Hammond, P. T. & Irvine, D. J. Composite dissolving microneedles for coordinated control of antigen and adjuvant delivery kinetics in transcutaneous vaccination. *Adv. Funct. Mater.* 23, 161–172 (2013).

56. Demuth, P. C., Su, X., Samuel, R. E., Hammond, P. T. & Irvine, D. J. Nano-layered microneedles for transcutaneous delivery of polymer nanoparticles and plasmid DNA. *Adv. Mater.* 22, 4851–4856 (2010).

57. Su, X., Kim, B. S., Kim, S. R., Hammond, P. T. & Irvine, D. J. Layer-by-layer-assembled multilayer films for transcutaneous drug and vaccine delivery. *ACS Nano* 3, 3719–3729 (2009).

58. Kim, Y.-C., Park, J. H. & Prausnitz, M. R. Microneedles for drug and vaccine delivery. *Adv. Drug Deliv. Rev.* 64, 1547–1568 (2012).

59. Suh, H., Shin, J. & Kim, Y. Microneedle patches for vaccine delivery. *Clin. Exp. Vaccine Res.* 3, 42–49 (2014).

60. Pulit-Penaloza, J. A. *et al.* A protective role of murine langerin+ cells in immune responses to cutaneous vaccination with microneedle patches. *Sci. Rep.* 4, 1–9 (2014).

61. Oosterhuis, K., Berg, J. H. van den, Schumacher, T. N. & Haanen, J. B. A. G. DNA Vaccines and Intradermal Vaccination by DNA Tattooing. *Curr. Top. Microbiol. Immunol.* 351, 3–32 (2010).

62. Ita, K. Transdermal Delivery of Drugs with Microneedles-Potential and Challenges. *Pharmaceutics* 7, 90–105 (2015).

63. Donnelly, R. F. *et al.* Hydrogel-Forming Microneedle Arrays for Enhanced Transdermal Drug Delivery. *Adv. Funct. Mater.* 22, 4879–4890 (2012).

64. Mccrudden, T. C. *et al.* Hydrogel-Forming Microneedles Prepared from '"Super Swelling"' Polymers Combined with Lyophilised Wafers for Transdermal Drug Delivery. *PLoS One* 9, e111547 (2014).

65. Rzhevskiy, A. S., Raghu, T., Singh, R., Donnelly, R. F. & Anissimov, Y. G. Microneedles as the technique of drug delivery enhancement in diverse organs and tissues. *J. Control. Release* 270, 184–202 (2017).

66.    Chang, H. *et al.* A Swellable Microneedle Patch to Rapidly Extract Skin Interstitial Fluid for Timely Metabolic Analysis. *Adv. Mater.* 29, 1–8 (2017).

67.    Zhu, J. *et al.* Gelatin Methacryloyl Microneedle Patches for Minimally Invasive Extraction of Skin Interstitial Fluid. *Small* 16, 1905910 (2020).

68.    Samant, P. P. *et al.* Sampling interstitial fluid from human skin using a microneedle patch. *Sci. Transl. Med.* 12, 1–16 (2020).

69.    Kalekar, L. A. & Rosenblum, M. D. Regulatory T cells in inflammatory skin disease: From mice to humans. *Int. Immunol.* 31, 457–463 (2019).

70.    Sakaguchi, S., Yamaguchi, T., Nomura, T. & Ono, M. Regulatory T Cells and Immune Tolerance. *Cell* 133, 775–787 (2008).

71.    Kang, S. M., Tang, Q. & Bluestone, J. A. CD4+CD25+ regulatory T cells in transplantation: Progress, challenges and prospects. *Am. J. Transplant.* 7, 1457–1463 (2007).

72.    Hartwig, T. *et al.* Regulatory T Cells Restrain Pathogenic T Helper Cells during Skin Inflammation. *Cell Rep.* 25, 3564–3572 (2018).

73.    Trüeb, R. M. & Dias, M. F. R. G. Alopecia Areata: a Comprehensive Review of Pathogenesis and Management. *Clin. Rev. Allergy Immunol.* 54, 68–87 (2018).

74.    Castela, E. *et al.* Effects of low-dose recombinant interleukin 2 to promote T-regulatory cells in alopecia areata. *JAMA Dermatology* 150, 748–751 (2014).

75.    Fisher, J. D. *et al.* In situ recruitment of regulatory T cells promotes donor-specific tolerance in vascularized composite allotransplantation. *Sci. Adv.* 6, (2020).

76.    Montane, J. *et al.* CCL22 Prevents Rejection of Mouse Islet Allografts and Induces Donor-Specific Tolerance. *Cell Transplant.* 24, 2143–2154 (2015).

77.    Montane, J. *et al.* Prevention of murine autoimmune diabetes by CCL22-mediated Treg recruitment to the pancreatic islets. *J. Clin. Invest.* 121, 3024–3028 (2011).

# Chapter II: PBAE-derived polyplexes for targeted transdermal vaccination

This chapter is submitted to Molecular Systems Design & Engineering as: *Poly(β-amino ester)s-based delivery systems for targeted DNA vaccination*

Authors: Núria Puigmal, Víctor Ramos and Salvador Borrós

This page left blank intentionally

## 2.1  Introduction

Nucleic acid vaccination has received increasing attention since first surfacing more than two decades ago, when DNA injection was confirmed to prompt *in situ* production of antigens and therapeutic proteins.[1] From that time, genetic vaccines have been reassured as a promising strategy to target a plethora of conditions including immune dysfunctions, cancers, infectious diseases and allergies.[2] Nucleic acid vaccination offers an attractive alternative to traditional vaccines which entail major drawbacks such as complex manufacturing, limited cell-mediated immunity, and safety concerns due to potential genomic integration and/or morph to pathogenic forms.[3,4]

Contrastingly, genetic vaccination promised enhanced biocompatibility, cost-efficient production, extended shelf-life and the capacity to engender both cellular and humoral immune responses,[5] opening up their potential for both prophylactic and therapeutic avenues. Their ease of construct design and safety profile has made them gamechangers for targeting epidemic or emerging diseases as evidenced throughout the COVID-19 pandemic,[6] where rapid design and manufacturing of the vaccines has been critical. In cancer settings, induction of specific and long-lasting immune responses against tumor antigens (TAs) could now be possible thanks to personalized vaccines that target the individual's exact TAs.[7] Only in the US, more than 50 clinical trials exploring gene-based vaccines are currently active, highlighting their relevance over their protein- and peptide-based counterparts.

Transcutaneous immunization with nucleic acids has been deemed as a superior route of administration over the subcutaneous or intramuscular due to the rich network of APCs residing in the dermal compartment and specialized in cascading immune responses.[8] Indeed, the promise of activating the humoral and cellular compartments of the immune system has pushed the development of two therapeutic candidates; DNA and mRNA vaccines.[9] Both vaccines share many similitudes, yet the main difference resides in the target location; the nucleus for DNA-based vaccines and the cytosol for the mRNA-based ones.[10] This distinguishing feature provides a substantial advantage to mRNA vaccines as their therapeutic cargo does not need to penetrate the nuclear membrane nor interacts with the genome, making them the safest and preferred choice among the scientific community.[11]

Despite their promise, first-generation vaccines proved to be poorly immunogenic in humans, which was hypothesized to stem from inefficient delivery of the cargo and weak transfection of cells.[12] Hence, delivery platforms were evidenced as critical to attain intracellular release of nucleic acids and

the subsequent expression of antigens,[13] evidencing the need for more refined vectors that could maximize the levels of immunization.

Viral vectors derived from adenoviruses and adeno-associated viruses first arose as strong contenders for delivery purposes due to their highly evolved machinery capable of transferring foreign genetic information to cells, along with the ability of the immune system of the host to respond to them.[14] However, several limitations and risks associated with their use rapidly surfaced including carcinogenesis, immunogenicity, broad tropism, limited gene packaging capacity and difficult vector production.[15] Though originally disregarded due to their poor performance, improved synthetic vectors displaying outstanding transfection efficiencies renewed the interest towards them,[16] since they overcame most of the caveats associated with viral delivery.

Poly(β-amino ester)s are a particular class of cationic polymers highly regarded as delivery vectors due to their excellent biocompatibility, biodegradability, an ease of synthesis without solvents nor catalysts.[17–19] Thanks to their chemical flexibility, extensive libraries of PBAEs can be generated by combinatorial end-modification to fine-tune their physicochemical properties such as size or zeta potential and favor cell-specific delivery of nucleic acids.[20] Moreover, other pendant chains such as ligands and endosomolytic moieties can be incorporated for superior cell-specificity transfection, a much needed tool when targeting elusive cellular subsets such as APCs in the context of transdermal vaccination.

Langerhans cells (LCs) are a subset of dendritic cells residing in the epidermis layer that have been long appreciated for their role in linking the innate and the adaptive immunity,[21] making them a prime cellular target for vaccination. Upon encounter with epicutaneous antigens, immature LCs internalize them, triggering their migration through dermal lymphatic vessels to the draining lymph nodes where naïve T cells will be primed and immune responses elicited.[22] Langerin (CD207), a type II lectin receptor expressed by LCs, plays a pivotal role in the recognition of antigens.[23] This receptor possesses mannose-binding specificity via highly conserved carbohydrate recognition domains, offering an excellent opportunity for ligand-mediated delivery of antigens.[24,25] Besides from langerin, numerous endocytic receptors belonging to the lectin family can capture antigens and transport them into specialized antigen-processing compartments as seen in **Figure II-1**.[26] More importantly, many of them also display mannose-binding affinity such as the mannose receptor, the analogous of langerin in dermal dendritic cells and macrophages.[27] Hence, mannose has been deemed as a universal ligand for targeted APC vaccination which, upon interaction with lectin-type receptors, promotes antigen processing via MHCI/MHCII presentation and the generation of more efficient immune responses.
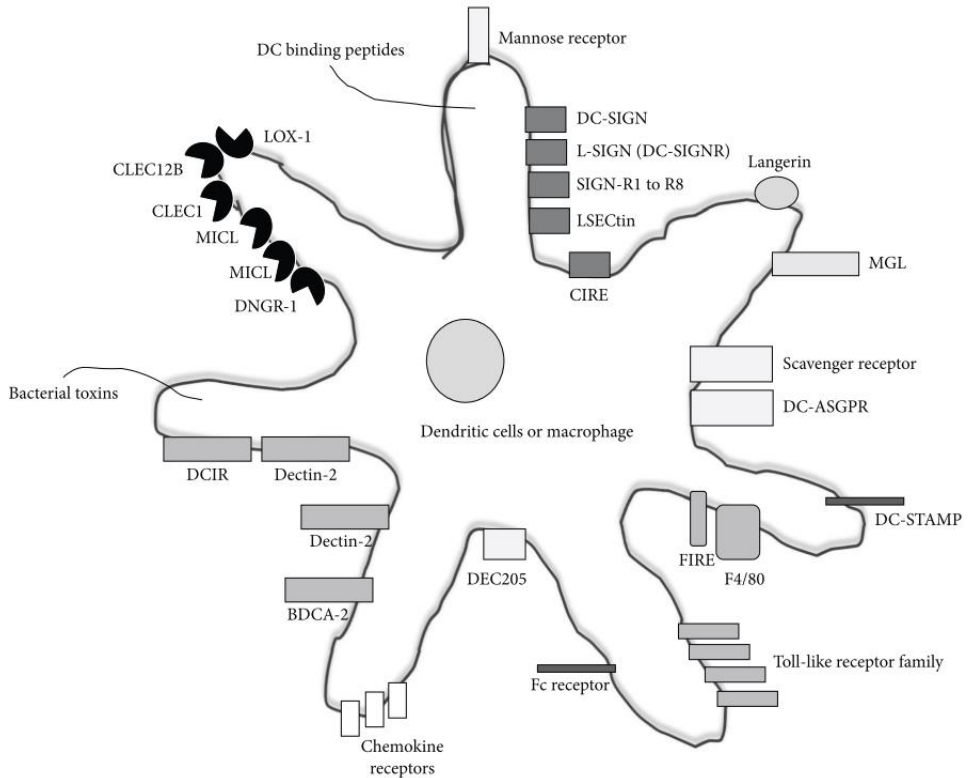
**Figure II-1: Schematic representation of the main receptors for antigen targeting.**[26] Professional APCs including dendritic cells and macrophages express a great variety of cell surface receptors that can be targeted using carbohydrate ligands such as mannose for nucleic acid vaccination.

Our group previously confirmed end-modification of PBAEs with amine-rich oligopeptides as a powerful tool to improve endosomal escape and biocompatibility while drastically boosting transfection efficiency in a cell-type-specific manner.[28–32] In this chapter, the use of oligopeptide modified (OM)-PBAEs will be expanded to target APCs residing in the dermal milieu and to examine whether oligopeptide decoration could suffice to actively target the immune cell reservoir of the skin. Complimenting this strategy, we will also leverage the binding-affinity of mannose to surface receptors of DCs and other auxiliary cells. Specifically, the library of OM-PBAEs previously developed by our group will be upgraded and the influence of mannose in their final transfection yield investigated. Therefore, the main objective of this chapter is the **design and screening of a new family of APC-targeting PBAEs for DNA/mRNA-based vaccination**. Employing the lessons learned from our group in chemical decoration of PBAEs, the newly synthesized library will integrate different

oligopeptides moieties and mannose as targeting ligands and its impact on cell transfection will be studied in different subsets of professional APCs and accessory dermal cells (**Figure II-2**).
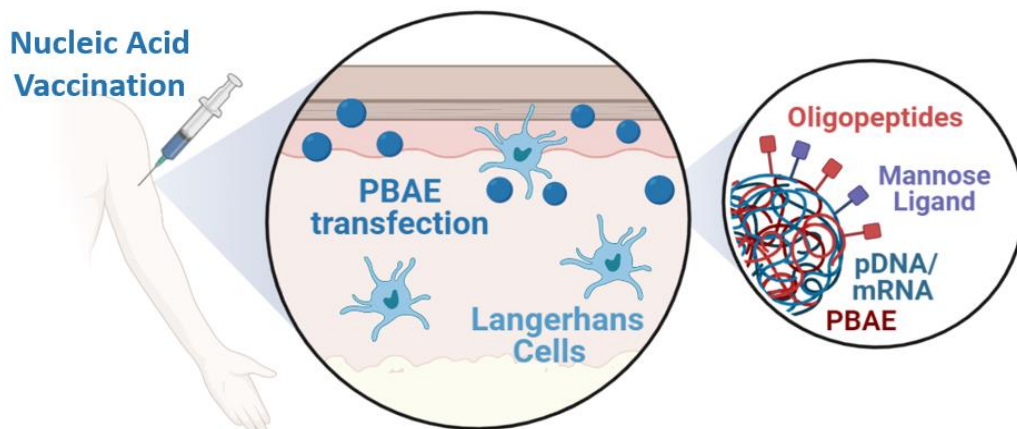


**Figure II-2. Chapter II graphical abstract.** Throughout this chapter, a new library of PBAEs decorated with oligopeptides and mannose as targeting ligands has been developed for targeted DNA/mRNA vaccination.

## 2.2  Aims

The main objective of the present chapter is the development of a new family of APC-targeting PBAEs including oligopeptides and mannose for DNA/mRNA-based vaccination. To do so, the following tasks were proposed:

- ✓ Synthesis of a new family of PBAEs decorated with oligopeptides moieties and the targeting ligand mannose and study of their physicochemical properties.

- ✓ Evaluation of transfection efficacy of the new OM- and MM-PBAEs *in vitro* using human models of the main cell phenotypes supporting antigen presentation in the skin.

- ✓ Comparison of transfection efficiency when complexing pDNA or mRNA in APCs.

- ✓ Assessment of transfection performance *in vivo* using OM- and MM-PBAEs.

## 2.3 Materials and Methods

### 2.3.1 Materials

Reagents and solvents used for polymer synthesis were purchased from Sigma-Aldrich and Panreac. Oligopeptide moieties used for polymer decoration (H-Cys-Arg-Arg-Arg-NH$_2$, H-Cys-Lys-Lys-Lys-NH$_2$, H-Cys-His-His-His-NH$_2$, and H-Cys-Asp-Asp-Asp-NH$_2$) were obtained from GL Biochem Ltd with a purity higher than 98%. The MUTZ-3 cell line was purchased from DSMZ (Braunschweig, Germany) while the rest of cell lines were obtained from ATTC (Manassas, Virginia). Human monocyte-derived Langerhans cells (MoLCs) and dendritic cells (MoDCs) obtained from healthy donors were kindly provided by Dr. Francesc Català (IDIBELL). Plasmid reporter green fluorescent protein (pmaxGFP, 3486 bp) was purified using the NucleoBond® Xtra Midi Plus EF kit (Macherey-Nagel) from competent Escherichia coli cells. mRNAs used in this study were eGFP (CleanCap Enhanced Green Fluorescent Protein mRNA 5-methoxyuridine) and Fluc (CleanCap Fluc mRNA 5-methoxyuridine) from TriLink. Chemokines for cell line differentiation were acquired from Peprotech.

### 2.3.2 Methods

#### 2.3.2.1. Animals

Adult 6–8 weeks old Balb/c mice were purchased (Envigo) and kept under pathogen-free conditions in laminar flow boxes. Animal maintenance and experiments were performed in accordance with established guidelines of the Catalan Government and following protocol number 8856, approved by the Direcció General del Medi Natural.

#### 2.3.2.2. Synthesis of oligopeptide-modified PBAEs (OM-PBAEs)

Oligopeptide-terminated PBAEs were synthesized as described by Dosta and colleagues.[33] Briefly, end-modified PBAE polymers were obtained by Michael addition via a two-step synthetic strategy. First, the acrylate-terminated polymer (C6) was obtained by addition of primary amines to diacrylates (1:1.2 M ratio of amine:diacrylate) at 90°C for 24 hours. Secondly, acrylate moieties were end-capped with oligopeptides (1:2.5 M ratio of acrylate:oligopeptides) in dimethyl sulfoxide (DMSO). The mixture was stirred overnight at room temperature and the resulting polymer was precipitated with a mixture of diethyl ether and acetone (70:30 v/v). Oligopeptides used for the end-capping reaction were: Cys + 3Arg (R), Cys + 3Lys (K), Cys + 3His (H) and Cys + 3Asp (D).

### 2.3.2.3. Synthesis of mannose-modified PBAEs (MM-PBAEs)

Synthesis of a second generation of oligopeptide-modified PBAEs including mannose moieties was performed as follows. Stock solutions of tri-arginine and tri-lysine end-modified PBAEs (R-C6, K-C6) were dissolved in anhydrous DMSO with allyl-α-D-Mannopyranoside (ADM) and triethylamine (1:4:10 M ratio). Reactions were allowed to proceed overnight at room temperature under stirring and resulting polymers were precipitated with a mixture of diethyl ether and acetone (70:30 v/v). Synthesized structures were confirmed by $^1$H NMR recorded in a 400 MHz Varian (NMR Instruments, Claredon Hills, IL) with methanol-d4 as a solvent.

### 2.3.2.4. Nanoparticle formation and characterization

Complexes containing pDNA (encoding for the green fluorescence protein) were obtained by mixing equal volumes of nucleic acid solution (0.5 mg mL$^{-1}$) and PBAE stock solution (100 mg mL$^{-1}$ in DMSO) to achieve the desired polymer-to-nucleic acid ratio (w/w). Briefly, the pDNA solution was added over the polymer solution, both diluted in sodium acetate buffer (AcONa buffer; 12.5 mM, pH=5), mixed by vigorous pipetting and allowed to react for 15 min at room temperature. Similarly, nanoparticles complexing mRNA were prepared following the same protocol but in a 25:1 polymer-to-mRNA ratio per our previous data.[31] Combinations of polymers used for nanoparticle formation were prepared as follows. Positively charged OM-PBAEs (CR3-, CK3-, CH3-C6 and their mannosylated counterparts) were mixed in a 50:50 ratio whereas pairs including both cationic and anionic polymers (CR3-, CK3, CH3-, Man-CR3- or Man-CK3-C6 with CD3-C6) presented a 70:30 ratio.

Resulting nanoparticles were characterized by agarose gel electrophoresis and dynamic light scattering (DLS). Nucleic acid retardation was assessed by loading PBAE-derived polyplexes into the wells of agarose gels (0.8% w/v) using different polymer-to-nucleic acid ratios. Particle size distribution and zeta distribution of resulting polyplexes was evaluated by DLS in a Nanosizer ZS Instrument (Malvern Instruments, UK) using different polymer:pDNA/mRNA ratios ranging from 5:1 to 150:1.

### 2.3.2.5. Generation of Langerhans Cells (LCs) from a human leukemia-derived cell line

Differentiation of the MUTZ-3 cell line into a reproducible human model for LCs was conducted as described elsewhere.[34] Cells were cultured in minimal essential medium alpha (MEM-α) supplemented with 20% v/v heat-inactivated FBS, 20% v/v conditioned medium collected from the human renal carcinoma cell line 5637, 1% penicillin-streptomycin and 2 mM L-glutamine. MUTZ-3 cells were seeded at a concentration of 0.25 x 10$^6$ cells/well in a 12-well plate and differentiated by culturing them for 7 days in conditioned MEM-α supplemented with 50 µM β-mercaptoethanol (2-

ME), 100 ng/mL human granulocyte-macrophage colony-stimulating factor (GM-CSF), 10 ng/mL transforming growth factor β1 (TGF-β1) and 2.5 ng/mL tumor necrosis factor α (TNF-α).

### 2.3.2.6. Generation of dermal dendritic cells (dDCs) from a human leukemia-derived cell line

Generation of dendritic cell lines from a human myeloid leukaemia cell lines (THP-1) was conducted as described elsewhere.[35] Briefly, $5 \times 10^5$ cells/ml were differentiated for 7 days in Dulbecco's Modified Eagle Medium in the presence of recombinant human GM-CSF (150 ng/ml) and IL-4 (50 ng/ml) into immature DCs.

### 2.3.2.7. Generation of monocyte-derived Langerhans cells (MoLCs) and dendritic cells (MoDCs)

Human monocyte-derived Langerhans cells (MoLCs) and dendritic cells (MoDCs) obtained from healthy donors were kindly provided by Dr. Francesc Català (IDIBELL), following approved guidelines. Primary cells were purified from peripheral blood mononuclear cells of healthy donors by magnetic-activated cell sorting according to the manufacturer's instructions (Miltenyi Biotec). CD14$^+$ monocytes were purified and cultured for 5 days in complete Dulbecco's Modified Eagle Medium supplemented with GM-CSF with TGF-β to generate MoLCs or with IL-4 to generate immature MoDCs.[36]

### 2.3.2.8. Transfection efficiency studies *in vitro*

Transfection efficiency of the OM- and MM-PBAEs libraries was examined using human models of the main cell phenotypes supporting antigen presentation in the skin. Cells were seeded in a 96-well plate 24 hours prior to the transfection assay to reach an 80% confluence by the following day. 15000 cells per well were seeded for the COS-7, HaCaT and HNDF cell lines while 20000 cells/well were seeded for MUTZ3, THP-1, MoLCs and MoDCs. Cells were incubated with 0.3 μg of pDNA or 0.15 μg of mRNA per well encapsulated in the OM- and MM-PBAEs. These were prepared at a 50:1 polymer-to-DNA ratio or 25:1 polymer-to-mRNA ratio and triplicates were assayed for each formulation. Briefly, cells were washed with PBS and 200 μL of supplemented media including the polyplexes were added. Cells remained incubated at 37°C in 5% $CO_2$ atmosphere until analysis 48 hours post-transfection. Untreated cells were used as negative control while the arginine-terminated PBAE CR3-C32 served as positive control group. Lipofectamine3000 (Thermo Fisher Scientific, Spain) was also used as a commercial control and incubated at 0.1 μg μl$^{-1}$ (concentration recommended by the manufacturer's guidelines). Gene delivery was analyzed by flow cytometry (BD LSR Fortessa™) and fluorescence microscopy (Nikon Eclipse TE2000-U) 48 hours post-transfection.

### 2.3.2.9. Cell viability assays

Cytotoxicity of the PBAE-pDNA polyplexes was evaluated using the MTT colorimetric assay. Cellular metabolic activity was measured 48 hours post transfection. Briefly, cells were washed with PBS 1X and incubated in complete medium supplemented with MTT solution (5 mg ml$^{-1}$), added at 10% v/v for 2 hours at 37°C and 5% $CO_2$. Afterwards, cell-grade DMSO was added to solubilize the resulting intracellular formazan crystals and optical absorbance was measured at 550 nm using a microplate reader (Elx808 Biotek Instruments Ltd, USA). Absorbance values were converted to percentage of cell viability relative to untreated cells. Previous tests were conducted using increasing incubation times (from 1 to 3 hours) with the MTT solution to determine the saturation point of the culture.

### 2.3.2.10. Lyophilization of PBAE polyplexes

Lyophilization of the nanoparticle was performed using the method previously optimized by our group.[31] Briefly, the initial volume of nanoparticles ($V_i$) was mixed and nanoprecipitated in an equal volume ($V_i$) of DEPC water. Next, same volume ($V_i$) of a HEPES 0.02M + 4 wt % sucrose solution was also added as cryo- and lyo-protectors. Then, nanoparticles were freeze-dried and the lyophilized powder was kept at −20°C until use. Reconstitution of the freeze-dried polyplexes was performed using a $V_i$ volume of DEPC water.

### 2.3.2.11. Biodistribution studies by *in vivo* bioluminescence

PBAEs were administered to mice (n=1) via intramuscular injection or transdermal injection using the Mantoux technique. Briefly, mice were injected with 10 µg (100 µL in DEPC water) of mRNA encoding for firefly luciferase complexed with OM- or MM-PBAE selected polymers. Radiance was measured by bioluminescence imaging *in vivo* 24 hours post injection. Briefly, mice were anesthetized and injected intraperitoneally with 150 µL of luciferin (Regis Technologies) (16.7 mg ml$^{-1}$ in PBS). Animals were placed in a high efficiency ImagEM X2 C9100-23BEM-CCD Imaging System (Hamamatsu Photonics) and images were acquired from the ventral direction. Quantification and analysis of photons recorded in images was done using the Wasabi image analysis software (Hamamatsu Photonics).

### 2.3.2.12. Statistical Analysis

Statistical analyses were carried out using Graph-Pad Prism 8 (GraphPad Software). All data are reported as mean + SD. For *in vitro* experiments, a minimum of n=3 biological replicates were used per condition in each experiment. Pairwise comparisons were performed using Student t-tests. No

specific pre-processing of data was performed prior to statistical analyses. Differences between groups were considered significant at p-values below 0.05 (* $p < 0.05$, ** $p < 0.01$, *** $p < 0.001$).

## 2.4   Results and Discussion

### 2.4.1   Synthesis of mannose-modified PBAEs

Our group has previously confirmed end-capping of PBAEs with oligopeptides moieties as a powerful strategy for cell-specific targeting, with PBAEs displaying a viral-like tropism yet without necessitating ligand-mediated mechanisms.[28,30,31] Thus, we aimed to harness the oligopeptide modified (OM)-PBAE library obtained from the top performing C6 polymer[33] as the starting point in the design of enhanced vectors for a DC-targeting vaccination technology, with a special focus in LCs. Given the scarcity of our cellular target, only accounting for 1.86% of all epidermal cells,[37] the former family of OM-PBAEs was further iterated to deliver polyplexes containing a mannose targeting ligand to enhance the receptor-mediated gene delivery route via langerin internalization.

Polymerization of new mannosylated candidates was performed as described in Materials & Methods. First, the C6 acrylate-terminated polymer was obtained by conjugate addition of hydrophilic/hydrophobic 5-amino-1-pentanol and hexylamine in a stoichiometric proportion along with a slight excess of 1,4-butanediol (**Figure II-3**). Here, hydrophobization of the polymer backbone via addition of pendant methyl groups is crucial to increase the stability and efficacy of resulting polyplexes,[16,33,38,39] which are especially susceptible to premature disassembling due to unspecific interactions with glycosaminoglycans and other densely charged proteins present in the extracellular matrix of the skin.



**Figure II-3: Synthesis of the acrylate-terminated poly(β-amino ester) C6 via Michael addition**. Reaction proceeded overnight under magnetic stirring at 90°C maintaining an inert atmosphere. The resulting polymer was precipitated, dissolved in anhydrous DMSO (100 µg/µL) and preserved at -20°C until further use.

Next, the end-acrylate groups of the C6 polymer were further modified with oligopeptide moieties using a molar excess to ensure full capping of the acrylate termini and avoid cytotoxicity issues (**Figure II-4**). From now on, CR3 and CK3 oligopeptides will be classified as cationic whereas CH3 and CD3 will be neutral or anionic, respectively. ^{1}H-NMR spectroscopy confirmed the disappearance of acrylate signals after end-capping while peaks associated to oligopeptides surfaced as reported before.[28]
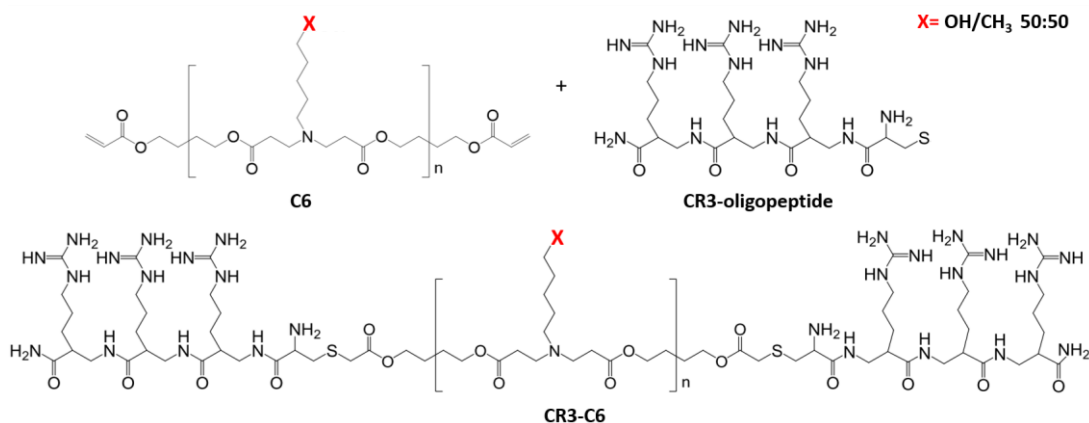


**Figure II-4. Synthesis of the arginine-terminated poly(β-amino ester) C6.** Modification of the tri-arginine oligopeptide is shown as an example. Briefly, both the acrylate-terminated C6 polymer and the oligopeptide moiety were dissolved in anhydrous DMSO and mixed at a 1:2.5 ratio (acrylate:oligopeptide). Mixtures remained under magnetic stirring overnight at room temperature and the resultant product was recovered by precipitation.

Finally, both CR3- and CK3-terminated PBAEs were further reacted with allyl-α-D-Mannopyranoside. Here, the acrylate chain acted as a Michael acceptor allowing the modification of amine groups present in the polymer backbone with mannose groups (**Figure II-5**). Sites of mannosylation were predicted to be dictated by the delicate equilibrium between nucleophilicity and steric hindrance. Again, ^{1}H-NMR spectroscopy was performed to properly define the chemical structure of the resulting polymer, yet its complex chemical backbone made this task troublesome. For this reason, further analysis by mass spectrometry or other sophisticated techniques might be more advisable. Moreover, given the influence of ligand valency on the targeting of human APCs with mannose,[40,41] a thorough screening and tuning of the degree of mannosylation could prove extremely beneficial in the future to refine the performance of the polymers. Of note, the reaction for mannose-decoration was only conducted on the CR3- and CK3-derived PBAEs as they will be the predominant constituents of future polyplexes.
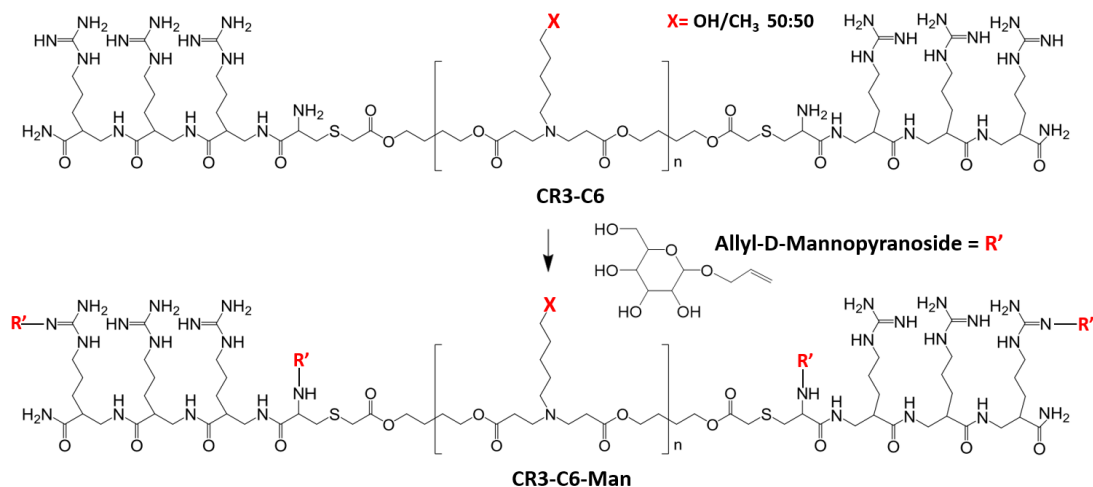
**Figure II-5 Synthesis of mannose-modified PBAEs from OM-C6 polymers.** Decoration of the arginine-modified PBAE is shown as an example. OM-PBAEs were dissolved in anhydrous DMSO with allyl-α-D-Mannopyranoside (ADM). Reactions were allowed to proceed overnight at room temperature under stirring and resulting polymers were precipitated with a mixture of diethyl ether and acetone (70:30 v/v). Red R's indicate the most provable site of reaction.

## 2.4.2  Biophysical characterization of OM- and MM-PBAEs

Our group previously demonstrated the capacity of OM-PBAEs derived from the C6 polymer to condensate RNAi drugs[33], microRNA[30] and mRNA[31] into discrete particles. Here, the capability of OM-C6-PBAEs along with their mannosylated counterparts to bind DNA was evaluated by gel retardation assay. For clarity, polyplexes assessed in this and further assays are detailed in **Table 1**. Specifically, screened polyplexes were either formulated with a single polymer or with a pair since our previous studies suggested that the properties of OM-PBAE could be additive.[28]

Overall, OM-C6-BAEs rendered polyplexes with higher complexation efficiencies if compared with those obtained from its predecessor, the C32 polymer,[28] as DNA migration was impeded at ratios as low as 5:1 (w/w), suggesting that the inclusion of hydrophobic chains can be harnessed to enhance encapsulation (data not shown). Results also showed that mannosylation of OM-PBAEs did not interfere with DNA complexation (**Figure II-6**) as particles condensed at the same ratios as their non-mannosylated counterparts did. Specifically, the presence of guanidinium groups and primary amines is known to facilitate the protonation of the CR3- and CK3-C6 polymers and in consequence, favor the interaction with the negatively charged phosphate groups present in the nucleic acids.

Contrarily, the limited protonation capacity of the CH3-C6 polymer and the negatively charged aspartic acid residues in the CD3-C6 polymer were expected to hamper DNA complexation. Our results showed that most polyplexes formulated with single-end or mixtures of OM-and MM-PBAEs blocked DNA migration at the lowest ratio evaluated (5:1). If minimal, it was observed that the addition of anionic groups delayed DNA complexation for K/H-Man- and R/H-Man-derived PBAEs.

**Table 1.List of screened polyplexes derived from single or multiple OM- and MM-PBAEs. (Man=mannosylated).**

**Single OM-/MM-polyplexes**

|  | Oligopeptide 1 |
| --- | --- |
| R | Cys + 3Arg |
| K | Cys + 3Lys |
| R-Man | Cys + 3Arg-man |
| K-Man | Cys + 3Lys-man |

**Multiple OM-/MM-polyplexes**

|  | Oligopeptide 1 | Oligopeptide 2 | Ratio |
| --- | --- | --- | --- |
| R/D | Cys + 3Arg | Cys + 3Asp | 70/30 |
| K/D | Cys + 3Lys | Cys + 3Asp | 70/30 |
| R/K | Cys + 3Arg | Cys + 3Lys | 50/50 |
| K/H | Cys + 3Lys | Cys + 3His | 50/50 |
| R/H | Cys + 3Arg | Cys + 3His | 50/50 |
| R/D-Man | Cys + 3Arg-man | Cys + 3Asp | 70/30 |
| K/D-Man | Cys + 3Lys-man | Cys + 3Asp | 70/30 |
| R/K-Man | Cys + 3Arg-man | Cys + 3Lys-man | 50/50 |
| R/H-Man | Cys + 3Arg-man | Cys + 3His | 50/50 |
| K/H-Man | Cys + 3Lys-man | Cys + 3His | 50/50 |

Complexes were further examined by DLS to evaluate their size and zeta potential. Screening of polyplexes prepared at a 50:1 polymer-to-DNA ratio using either single or mixtures of OM- and MM-PBAEs revealed that end-modifications had a notorious influence on their final physicochemical properties in agreement with previously published data.[28–31,33] The hydrodynamic diameter of polyplexes derived from OM- and MM-PBAEs ranged from 100 to almost 300 nm and interestingly, mannosylation did not appear to impact their final size in a defined pattern as some formulations experienced variations whether others did not (**Figure II-7A**). A subtle increase was observed for polyplexes formulated with the anionic CD3-PBAE, which was hypothesized to originate from repulsive forces with the negatively charged DNA backbone, hence the increment in particle size.
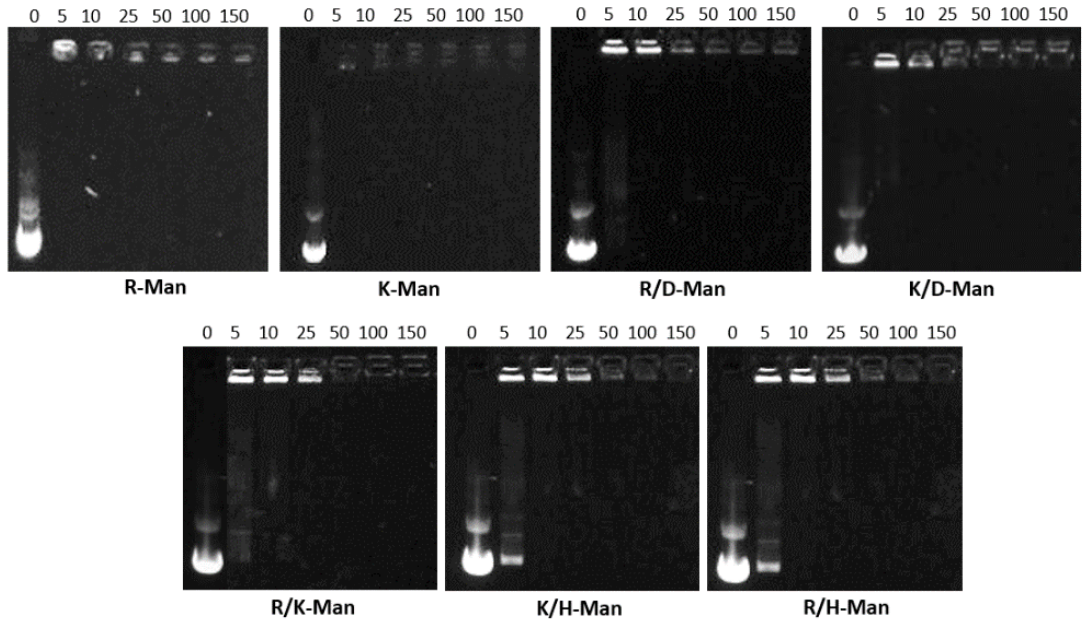
**Figure II-6. Gel retardation assays of polyplexes formulated with MM-PBAEs.** Polyplexes were prepared using increasing polymer-to-pDNA ratios (5:1 to 150:1) and loaded in agarose gels (0.8% w/v). Retention of the nucleic acids in the wells indicates full complexation. An equivalent concentration of free pDNA was used as migration control.

Regarding their surface charge, results showed that decorative oligopeptides had a dramatic influence, where arginine-bearing polyplexes presented the most positive potential, followed by lysine- and the pairs including histidine groups (**Figure II-7B**). Thought not significant, a trend was observed as most of the polyplexes derived from MM-PBAEs presented lower surface charges if compared with their homologous. Hence, these data hinted that the inclusion of mannose might be playing a shielding effect as suggested by others,[42] a desirable feature in future studies to limit the inherent cytotoxicity of densely charged particles.[43]

## 2.4.3 Analysis of cell viability

Next, cell viability studies were performed to examine the impact of oligopeptide modification and ligand targeting on nanoparticle toxicity. To do so, the HaCaT cell line was proposed as a representative tissue of the epidermal milieu (being the most abundant) and that will be used in this
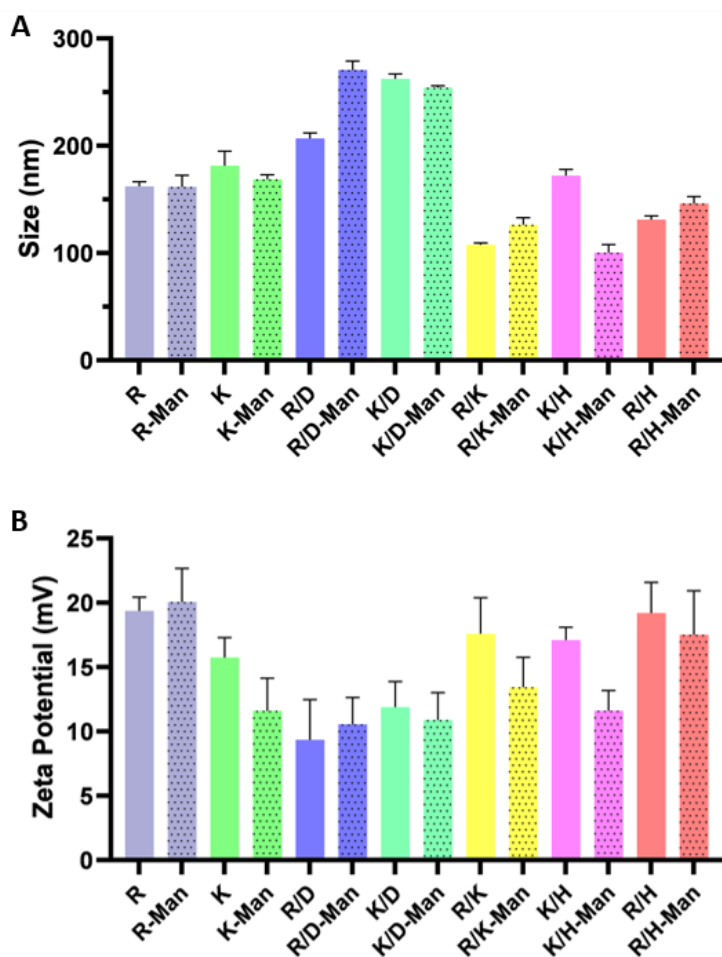
**Figure II-7: Average hydrodynamic diameter (A) and zeta-potential (B) distributions analyzed by Dynamic Light Scattering.** Polyplexes deriving from the complexation of pDNA with OM-PBAEs and MM-PBAEs were prepared at a 50:1 polymer:pDNA ratio. Polydispersity index (PDI) values were lower than 0.3 for all measurements. Results are shown as mean and standard deviation of triplicates.

and further studies as a model cell line. Briefly, HaCaT cells were incubated with the OM- and MM-PBAE libraries and the percentage of viable cells following transfection was assessed using the MTT assay. Significant differences in cell viability were not observed if comparing formulations against their mannosylated counterparts (**Figure II-8**). These results are in accordance with our DLS studies (**Figure II-7B**), as mannosylation decreased but did not significantly reduce the zeta potential of polyplexes, which closely relates with nanoparticle toxicity.[43]

In contrast, oligopeptide modification appeared to have a stronger influence in the average number of viable cells, as viability percentages ranged from a fair 40% to a 90% when compared to untreated control cells. As suggested by our group before,[29] the nature and distribution of the chemical groups originating the positive charges may be exerting a greater influence on the zeta potential of the nanoparticles and in turn, on the cell compatibility rather than their absolute charge. This could explain why formulations ought to be densely charged with positive groups such as the lysine-/arginine-modified PBAEs were less toxic than formulations including anionic moieties (R/D- and R/D-Man PBAEs). Overall, none of the screened formulations induced harmful levels of cytotoxicity, which may have been mitigated thanks to the inclusion of oligopeptides,[28,29] but also to the presence of mannose molecules in some formulations and its suggested "shielding" role.[44]
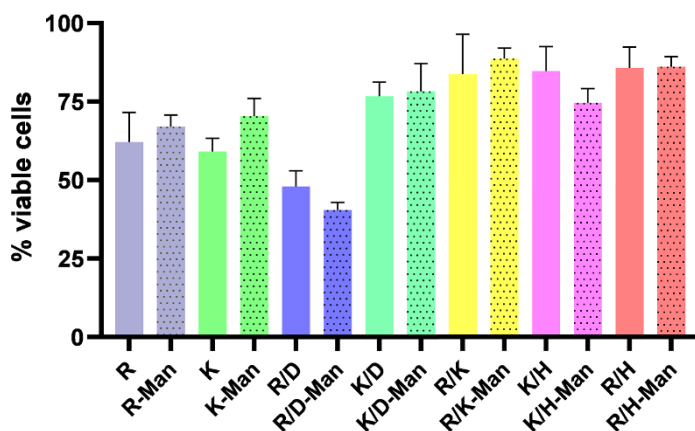


**Figure II-8. Cell proliferation assay (MTT) in HaCaT cells.** Viability of cells following transfection with OM- and MM-PBAEs was examined in the highly permissive HaCaT cell line. 15000 cells per well were seeded in a 96-well plate and incubated with polyplexes complexing 0.3 µg pDNA per well. Viability was determined at 48 hours post-transfection and plotted as percentage of viable cells relative to control untreated cells. No significant differences were observed when comparing formulations against their mannosylated counterpart (pairwise comparisons with Student's T test).

## 2.4.4   Gene delivery studies in professional APCs (Langerhans cells)

Transfection efficiency of the newly synthesized family of OM- and MM-PBAEs was tested in MUTZ-3 cells. This human myeloid-derived cell line can be differentiated into a LC-like phenotype under cytokine induction, displaying a high resemblance with their primary counterparts in terms of phenotypic plasticity and functional/transcriptional profiles.[35] When differentiated in a TGF-β-dependent fashion, MUTZ-3 cells express Langerin,[45] which possesses mannose-binding affinity[23,46] and is hypothesized to favor receptor-mediated pathways of nanoparticle internalization. In the

context of this work, the use of an immortalized cell line was supported by the reported disadvantages in the development of standardized DC vaccine technologies when monocyte-derived models are utilized, such as inter-/ intra-donor variability and their limited availability[47].

Screening of the non-targeted and mannosylated-libraries of PBAEs revealed that only one formulation bearing both cationic and anionic oligopeptides was capable of inducing significant levels of gene expression in our LCs model (**Figure II-9A**). Polyplexes derived from lysine- and aspartic acid-modified PBAEs, along with the mannose-modified pair, achieved percentages of GFP-positive cells around 2 and 4 % respectively, while the rest of formulations barely mediated gene transfer. Our data confirmed the potential of oligopeptide-capping for cell-specific gene delivery while the addition of targeting ligands prompted even higher transfection efficiencies. It was hypothesized that mannose was boosting the engulfment of polyplexes via clathrin- and scavenger receptors-dependant pathways as they are reported to dominate particle internalization in DCs when particles are sized around 250 nm or less.[48]

Regarding surface chemistry, both charge and the ligand organization pattern have an impact on nanoparticle internalization by DCs.[49] In accordance with our previous results, it appeared that charge distribution rather than the absolute zeta potential might be driving particle uptake,[29] which could hint why just a single formulation could effectively transfect LCs. Polyplexes decorated with lysine and acid aspartic residues might be displaying more positive groups in the surface and facilitate interaction with the negatively charged membrane of the cells. Finally, the inclusion of anionic groups in a defined distribution is known to enhance the penetration and further endosomal scape.[50] This could explain why other polyplexes similarly formulated with cationic and anionic moieties (R/D and R/D-Man) mediated little gene transference if compared with K/D- or K/D-Man-PBAEs.

Gene delivery efficiency of OM- and MM-PBAEs was also screened in human monocyte-derived Langerhans cells (MoLCs) (**Figure II-9B,C**). Despite the disadvantages mentioned herein, monocyte-derived models could provide a better correlation with *in vivo* settings than immortalized APCs models as the last have been suggested to lose their avidness for nanoparticles.[51] Assessment of gene transference revealed similar results when comparing both models of LCs. Once again, polyplexes formulated with the mixture of lysine- and acid aspartic-modified PBAEs (K/D and K/D-Man) outperformed the rest of their counterparts.

Here, mannosylation had a bigger influence if compared to MUTZ3 cells, achieving a three-fold improved transfection efficiency. Overall, the percentages of transfected cells increased in MoLCs, highlighting the need to account for model variability in gene delivery studies.
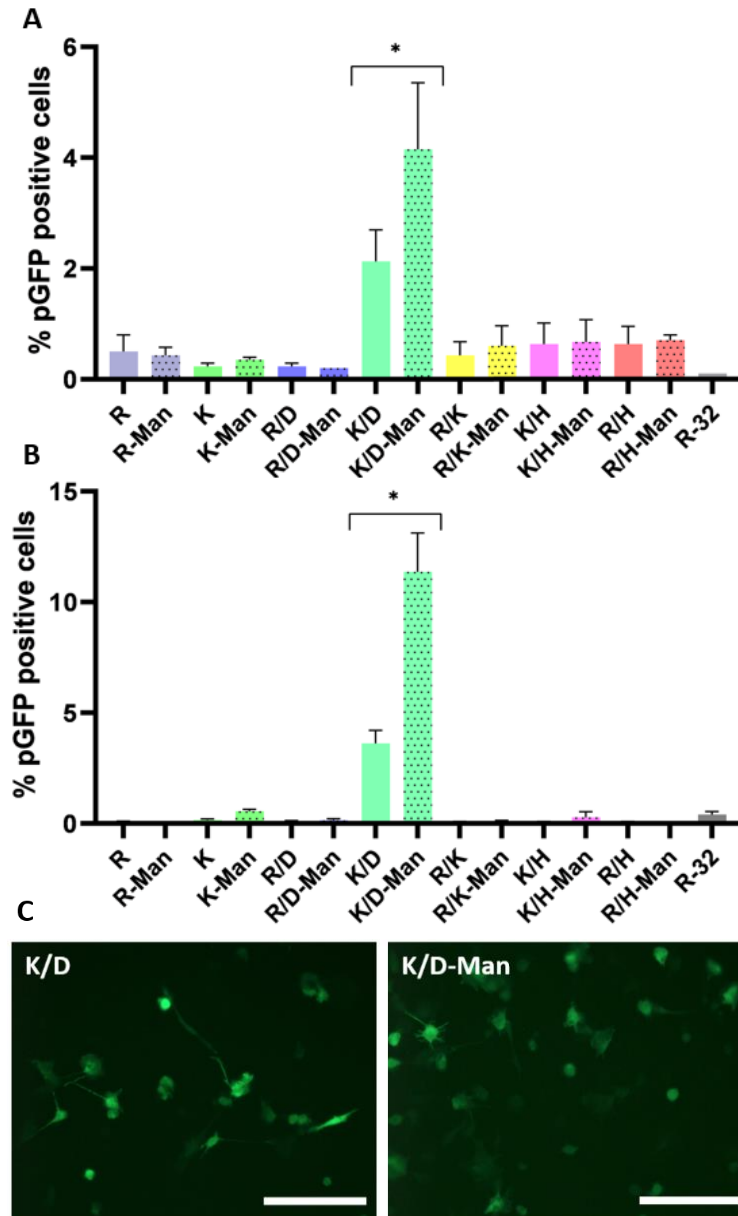
**Figure II-9. Assessment of PGFP gene expression by flow cytometry in Langerhans-like cells.** MUTZ-3 cells (**A**) and MoLCs (**B**) after transfection using the library of OM- and MM-PBAEs. Cells were transfected by adding 0.3 µg pDNA/well at a 50:1 polymer:DNA weight ratio. Results are presented as mean and standard deviation of triplicates. Fluorescence microscopy of MoLCs transfected with top formulations (C). Scale bar = 100 µm. Statistical significance was compared between MM-PBAEs and their non-modified counterpart. *p<0.05.

## 2.4.5   Gene delivery studies in professional APCs (dermal dendritic cells)

Professional APCs other than LCs can also mediate antigen presentation such as dermal DCs (dDCs), so the capability of the new libraries of PBAEs to target them was next explored given their key role in governing immune responses in collaboration with other APCs (**Figure II-10**).
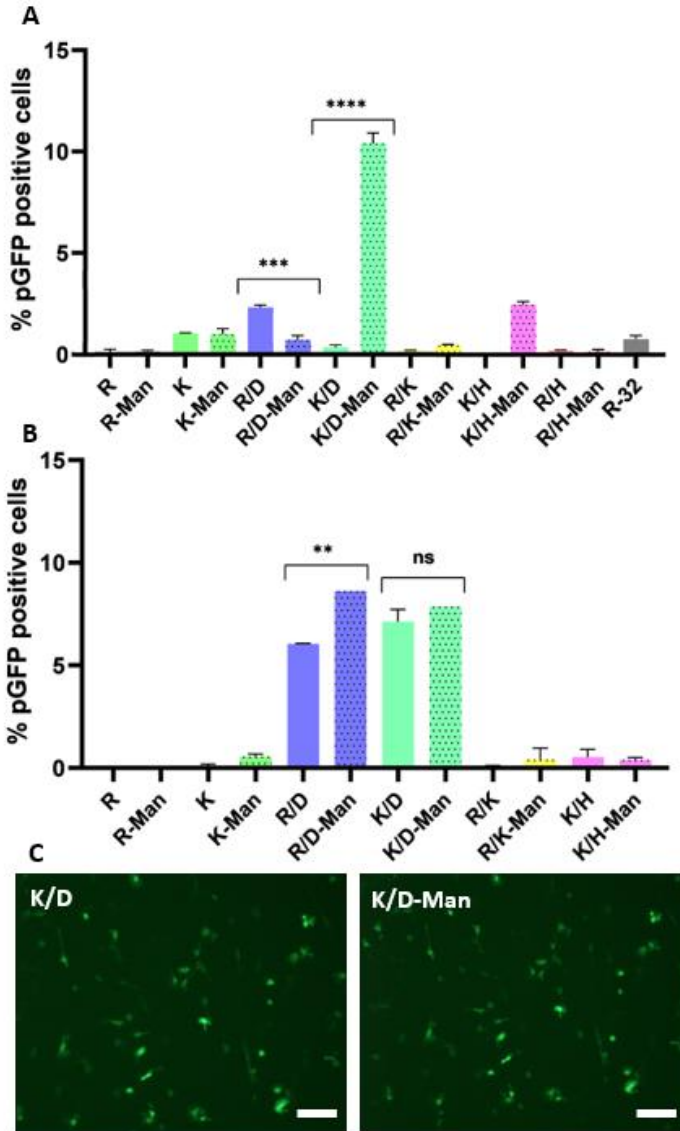


**Figure II-10. Assessment of PGFP gene expression by flow cytometry in dermal dendritic-like cells.** Immature THP-1 cells (**A**) and MoDCs (**B**) after transfection using the library of OM- and MM-PBAEs. Cells were transfected by adding 0.3 µg pDNA/well at a 50:1 polymer:DNA weight ratio. Results are presented as mean and standard deviation of triplicates. Fluorescence microscopy of MoDCs transfected with top formulations (**C**). Scale bar = 50 µm. Statistical significance was compared between MM-PBAEs and their non-modified counterpart. *p<0.05.

Unlike LCs, which have been recognized for many years, dDCs have only been studied in detail recently.[21] Although a great heterogeneity has been described among dDCs subsets and their functions, the simplest distinctive marker used to isolate them is between those that express Langerin (LCs) and those that do not (dDCs).[52] These cells can migrate to skin-draining lymph nodes both in the steady-state and in response to inflammation to present antigens acquired in the periphery to T cells.[24] In contrast with LCs, they arrive at the lymph nodes more quickly and can be identified within 18 hours after stimulation,[21] so the potential of the newly synthesized PBAEs to transfect them was examined following a similar strategy as for the gene delivery studies in LCs using dendritic-like cells derived from a myeloid leukaemia cell line (THP-1) and from monocytes (MoDCs).

Leukaemia-derived cell lines are able to differentiate into functional DCs, opening avenues for the development of highly reproducible DC vaccines and providing *in vitro* model systems for in-depth studies about DC physiology.[47] The THP-1 cell line is a common model to evaluate immune modulation as it can be rapidly differentiated into dendritic-like and macrophage-like phenotypes in a cytokine-dependent manner.[53,54] Following incubation with IL-4 and GM-CSF, THP-1 cells display the morphologic, phenotypic, molecular, and functional properties of DCs and more importantly, *de novo* cell-surface expression of receptors including the mannose receptor (CD207) and DC-sign (CD209).[54] These receptors can internalize antigens via MHC class I and class II presentation and possess mannose-binding affinity,[41] so it was expected that the inclusion of targeting ligands would boost transfection efficiencies in this cell line as well. Nevertheless, transfection studies using OM- and MM-PBAEs revealed an erratic profile in terms of protein expression. K/D-Man PBAEs mediated the highest levels of gene transference (10.4% GFP-positive cells), yet barely any was observed for their non-mannosylated counterparts (0.35% positive cells) (**Figure II-10A**). Other formulations showed timid gene expression (R/D- and K/H-Man-derived polyplexes) yet these results did not appear to be governed neither by mannosylation nor oligopeptide decoration. Transfection assays with differentiated THP-1 cells were conducted multiple times only to reveal inconclusive expression profiles after each attempt, which left us questioning whether the differentiation process was compromised. For this reason, alternative studies involving inhibition assays or flow-cytometry phenotyping could prove useful in the future to decipher the cause of such errant behavior in terms of transfectability.

Given the inconclusive results obtained from immortalized cells, we moved to study the transfection capacity of OM- and MM-PBAEs in MoDCs. Unlike for MoLCs, where a single formulation proved effective in mediating gene transference, the two candidates containing both cationic and

anionic oligopeptides dramatically outperformed the rest of the formulations (**Figure II-10B,C**), which mediated negligible levels of gene transfer. Considering that nanoparticle size and zeta potential can dictate cell-specific targeting per se without additional active targeting,[29] it does not come as a surprise that the two winning formulations displayed matching physicochemical properties when characterized prior in this chapter (**Figure II-7**). R/D- and K/D-derived polyplexes along with their mannosylated pairs presented the highest diameter and the lowest surface charge, distinctive features that could explain the targeting specificity for this cell line. Transfection efficiency in dDCs appeared to be mostly influenced by oligopeptide decoration rather than mannosylation, specially for polyplexes bearing lysine residues since significant differences were not observed between the non-decorated and the mannosylated candidate. These results suggest that polyplexes might be internalized using mechanisms other than clathrin-mediated endocytosis as others have discussed in more detail.[49]

## 2.4.6   Gene delivery studies in accessory dermal cells

Dendritic cells including LCs are known to dominate antigen presentation in the milieu of the skin epidermis and dermis,[55] yet other accessory dermal cells such as fibroblasts or keratinocytes are also orchestrators in the elicitation of immune responses via secretion of co-stimulatory molecules or by priming naïve-reactive T cells.[56–58] Therefore, the transfection capacity of our OM- and MM-PBAEs loaded with pDNA was also investigated with human fibroblast and keratinocyte models *in vitro*.

The inclusion of mannose moieties to the PBAEs backbone was confirmed to be an effective synthetic strategy to boost transfection levels in human normal fibroblast cells (hNDF) **(Figure II-11A,B)**. The greatest improvement was observed in histidine-bearing polyplexes, which went from registering the worst performance to double their transfection levels after mannosylation. It was hypothesized that the expression of polysaccharide-binding receptors on the surface of fibroblasts may be favoring cellular uptake as they can internalize glycosylated ligands from the extracellular space[44,59] and in turn, favor specific routes for polyplexes to enter into the intracellular space. Transfection assays using HaCaT cells revealed a similar trend as for the fibroblast model, with polyplexes derived from MM-PBAEs inducing the greatest levels of gene expression **(Figure II-11C, D)**. Polyplexes formulated with mixtures of OM- and MM-PBAEs –especially when containing both cationic and anionic oligopeptides– outperformed those single-ended, reaching a 75% percentage of GFP-positive cells for the K/D-Man PBAEs.
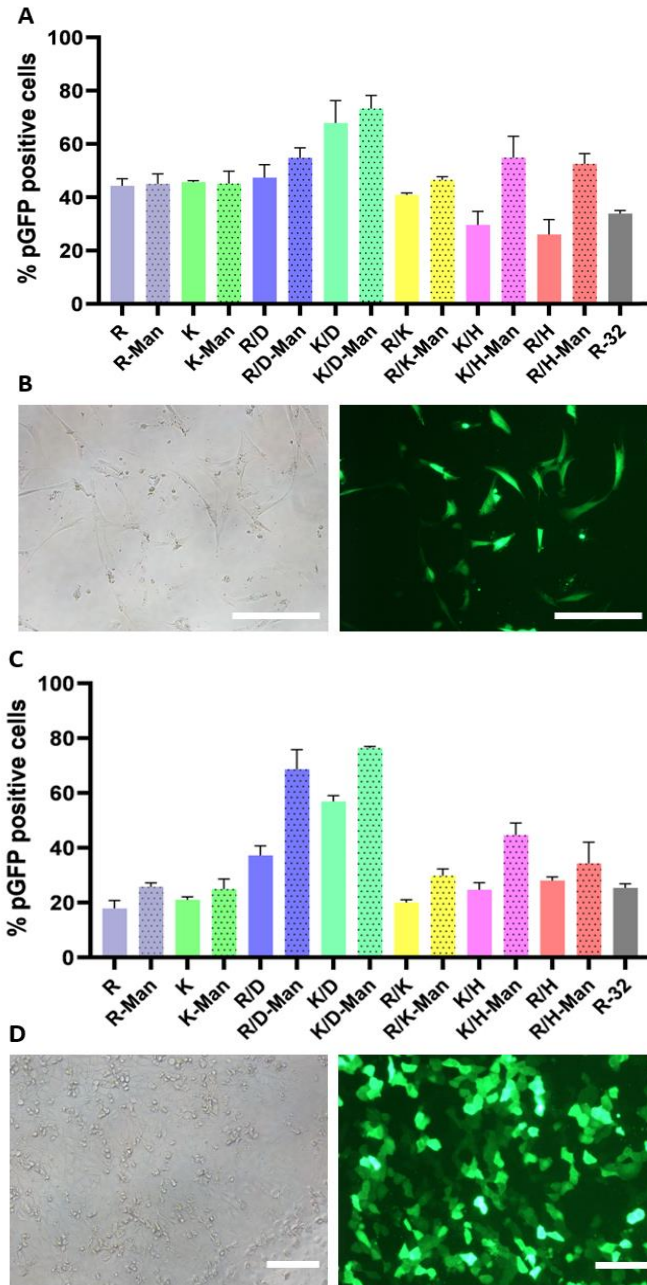
**Figure II-11. Evaluation of PGFP gene expression in accessory dermal cells by flow cytometry.** 15000 cells (hNDFs) were seeded in a 96-well plate and transfected with both OM- and MM-PBAEs by adding 0.3 µg pDNA/well at a 50:1 polymer-to-pDNA weight ratio (**A**). Light and fluorescence microscopy of fibroblast transfected with K/D-Man polyplexes. Scale bar = 100 µm (**B**). Quantification of GFP positive cells following transfection of HaCat cells with OM- and MM-derived polyplexes using 0.3 µg pDNA per well and presented as mean and standard deviation of triplicates (**C**). Light and fluorescence microscopy of immortalized keratinocytes transfected with K/D-Man polyplexes. Scale bar = 50 µm (**D**).

Both mannosylation and oligopeptide-modification had a great influence in the performance of polyplexes, although cell-specific targeting was mostly driven by the latest. Expression of the mannose receptor by keratinocytes[44] could be favoring the engulfment of mannose-modified polyplexes and ultimately, transfection efficiency when compared to the non-modified formulations. Finally, the overall increased transfection levels in keratinocytes if compared to fibroblast could be tentatively explained by their higher cell turnover rate and transfectability.

## 2.4.7  mRNA-based vaccination using OM- and MM-PBAEs as delivery vectors

As a rapidly emerging class of therapeutics, both DNA- and mRNA-based vaccines have gained great success as alternatives to subunit and attenuated vaccines, yet it has been mRNA vaccination the strategy that progressed the most towards widespread clinical use.

The main beneficial feature of mRNA vaccines is their instant translation in the cytosol rather than the nucleus, facilitating transfection of quiescent and slow-proliferating cells while excluding any risk of insertional mutagenesis.[60] Systematic improvement of the intracellular stability and translational efficiency of mRNAs using synthetic cap analogues, regulatory elements, and Poly(A) tails also helped in overcoming premature RNase cleavage and to down-modulate their immunogenicity for increased safety profiles.[61] In addition, mRNA vaccines allow for rapid, inexpensive and scalable manufacturing owing to the superior yields of *in vitro* transcription reactions,[11] providing a paradigm for rapid vaccine development and pandemic preparedness.[6]

Given the relevance of mRNA as genetic vector, the performance of the newly synthesized families of PBAEs was evaluated when complexing mRNA for APC-targeted vaccination. Our group has previously confirmed the superiority of OM-PBAEs to target APCs when administered systemically,[31] yet their potential as transdermal vectors has never been explored.

### 2.4.7.1  Gene delivery studies in professional APCs

First, transfection studies were conducted using the OM- and MM-PBAEs libraries in MoLCs and MoDCs as key elicitors of antigen presentation. Per our preliminary data and available literature,[31] the administered dose was halved if compared to that used in pDNA delivery studies due to the increased potency of mRNA. Results hinted a correlation between the DNA- and the mRNA-based gene delivery studies since the gene expression profile throughout the different formulations was

fairly similar, although some differences are of note. For our LC-like model, polyplexes bearing lysine and aspartic acid moieties (K/D- and K/D-Man-PBAEs) could not be rivalled again and more than a 30% of pGFP-positive cells was observed (**Figure II-12A**), reaffirming once again oligopeptide decoration as the driving force dictating transfection efficiency. Unlike for pDNA delivery studies, where the inclusion of the mannose ligand had doubled gene expression levels, significant differences between the original and the mannosylated candidate were not observed when delivering mRNA. Other formulations managed to mediate transfection but the levels were almost residual (4.14% positive cells for R/D-PBAEs and 5.25% for K/H-Man) if compared to the top-performing pair. Studies in MoDCs also revealed some discrepancies if comparing the results with those obtained from pDNA-based transfection. Again, polyplexes combining cationic and anionic oligopeptides surpassed the rest of the formulations but contrastingly, the K/D-Man formulation mediated twice as much gene expression as that induced by the original counterpart (**Figure II-12B**).

Reported differences in transfection efficiency among formulations when comparing DNA (**Figure II-9**) versus mRNA (**Figure II-12**) delivery studies and between DCs subsets were hypothesized to arise from the distinct target location for oligonucleotide delivery and the selective expression and internalization properties of C-type lectin receptors such as langerin or the mannose receptor. Indeed, it has been reported a great diversity in the intracellular routing of lectin receptors, even within the same receptor depending on the ligand that it engages with and that will ultimately dictate antigen presentation.[27] Internalization of nanoparticles by DCs is generally mediated through clathrin- or caveloae-mediated endocytosis for nanoparticles sizing 250 nm or less,[48] yet it has been reported that mannose-decorated antigens can also be taken up through receptor-independent mechanisms such as macropinocytosis regardless of their size.[62,63] Moreover, and depending on the route of choice, mannose-binding receptors can either traffic antigens directly to late endosomes (e.g., DC-SIGN) or rapidly recycle them via early endosomes (e.g., MR, Langerin).[27,41] All of the above evidences the intricate mechanisms pursued by DCs to internalize nanoparticles as a function of their size, charge and ligand motifs, which highlights the need for systematic screening to understand how nanoparticle internalization and endosomal scape influences in their final transfection efficiency.

Lastly, it should also be noted that the levels of transfection mediated by mRNA-complexing polyplexes duplicated or even triplicated those achieved by the corresponding pDNA-complexing ones for both LCs and DCs, confirming the superiority of mRNA to mediate gene transference in hard-to-transfect cell lines such as primary culture cells.
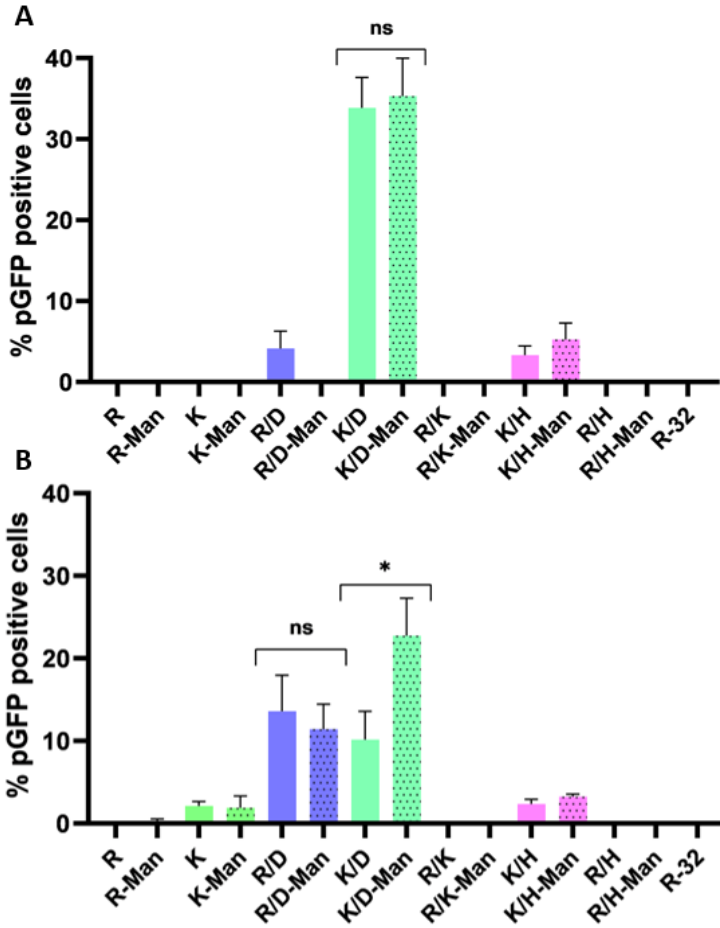
**Figure II-12. Analysis of gene expression following transfection with PBAE:mRNA polyplexes in professional APCs.** MoLCs (**A**) or MoDCs (**B**) were seeded and incubated with the OM- and MM-PBAEs libraries complexing mRNA encoding for GFP. Briefly, polyplexes prepared at a 25:1 polymer-to-mRNA ratio were incubated 48 hours with monocyte-derived cells (0.15 μg of mRNA per well) and gene expression was analyzed by flow cytometry. Data are represented as mean ± SD (experimental triplicates).

### 2.4.7.2 Characterization of lyophilized PBAEs for *in vivo* studies

Throughout this chapter, polyplexes formulated with lysine- and aspartic acid-modified PBAEs, along with their mannosylated variations, vanquished the rest of the formulations in terms of transfection efficiency. For this reason, their performance was next evaluated *in vivo*. Although not crucial, nanoparticle lyophilization has proved very useful to enable long-term storage time and concentration of their volume for high-dose administration, so the physicochemical properties of the polyplexes following lyophilization were examined to confirm that their tailored features remained unperturbed after the freeze-drying step. K/H- and K/H-Man-derived polyplexes were included as positive control of transfection in this and further studies per our previous data.[31]

Measurement of the polyplexes size by DLS did not reveal notable differences in their hydrodynamic diameter following lyophilization (**Figure II-13**). Slight fluctuations were observed in most formulations, although a trend could not be established. The most dramatic change was registered in the PDI values, as most of the formulations experienced an increase after nanoparticle reconstitution. In most cases, PDI values remained below 0.3 which is the consensus value for acceptable nanoparticle polydispersity. Overall, all the formulations endured the process of lyophilization and were deemed adequate for *in vivo* administration.
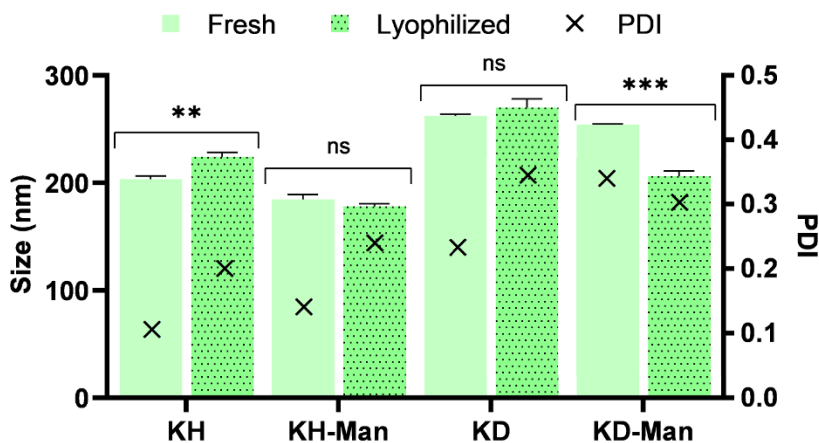


**Figure II-13. Particle size distribution analyzed by DLS.** Variations in the zeta potential of OM- and MM-PBAEs prior and after lyophilization were studied by DLS. Freshly prepared polyplexes (25:1 PBAE:mRNA ratio) were measured by DLS, freeze dried and subsequently reconstituted in DEPC water for the second measurement using the same samples. Comparisons were performed using one-way Student's t-tests. (ns = non-significant, *p < 0.05, **p < 0.01, ***p < 0.001).

### 2.4.7.3  *In vivo* gene delivery studies

Following completion of the characterization studies, the potential of our top candidates to mediate gene transference was examined *in vivo*. As a preliminary screening, biodistribution of the polyplexes was evaluated by bioluminescence in an immunocompetent mouse model. Polyplexes encapsulating mRNA were administered via intramuscular injection, as the preferred route of choice for vaccine administration, or via intradermal injection using the Mantoux technique.

Overall, absolute levels of gene expression were limited regardless of the site of administration (**Figure II-14**). The recorded bioluminescence signal in those mice receiving the intramuscular injection could not be distinguished from the background noise so this group was excluded from analysis. Regarding the intradermal injection, only the lysine-/aspartic acid-modified formulation appeared to induce fair levels of bioluminescence which remained localized around the area of injection as expected. Interestingly, expression of the reporter gene was not detected in those mice receiving the mannosylated version, which had been a top candidate throughout the *in vitro* screenings. Given the minimal number of mice used for this experiment and repetitions though, it would be unwise to make comparisons between the two of them or with the K/H-derived polyplexes.

The tentative explanation for the reduced gene expression observed *in vivo* could involve several factors such as the reduced delivered dose (accounting for just a fifth of the standard regimen)[31] and the difficulty to administer the nanoparticles by Mantoux injection. This technique requires extensive training and is difficult to accomplish reproducibly since insertion of the needle in a wrong angle can compromise the whole experiment. If too deep, deposition of the vaccine ends up being subcutaneous rather than intradermal which, despite the resemblance, it does not contain the cellular subsets the vaccine was aimed to target. Oppositely, shallow injections can result in leakage of part of the dose out of the skin during the injection or after the needle is removed, which unfortunately, occurred while performing this study. To address the limited control and reproducibility of this method of vaccine delivery, the use of alternative devices might be advisable as will be discussed in following chapters. It should also be noted that the assessment of gene expression by bioluminescence may not have been the most adequate method neither, owing to the scarcity of our cellular target and the targeting nature of our vector so intense signals might not have occurred at all even if the delivered dose was augmented.

In light of these findings, using alternative techniques including flow cytometry or immunohistochemistry along with other reporter genes such as fluorescent proteins may provide a better insight on whether cells are being transfected and, in case they are, which ones.
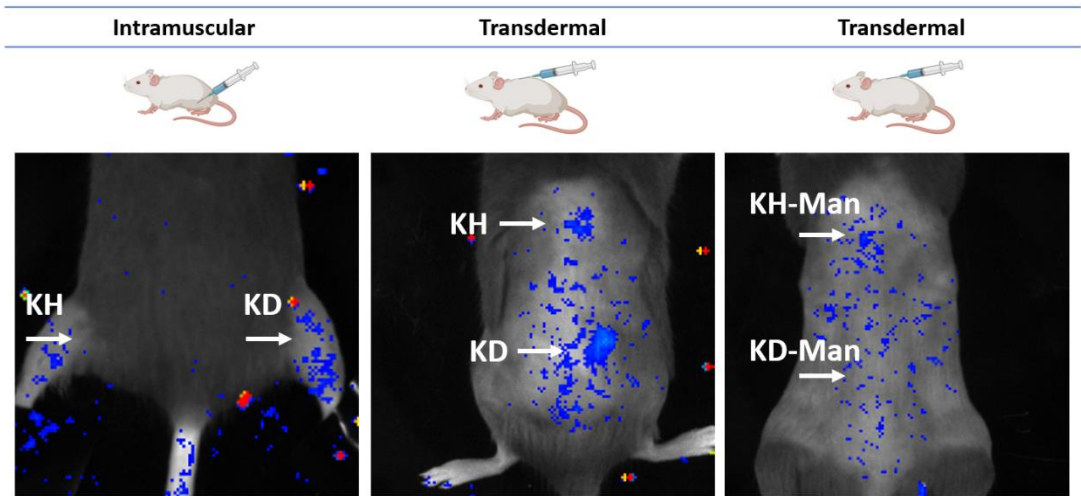
**Figure II-14. Bioluminescent images of a representative animal following PBAE injection.** BALB/c mice were administered intramuscularly or transcutaneously 10 µg (100 µL) of mRNA encoding for firefly luciferase complexed with OM- or MM-PBAE selected polymers. Radiance measurement was performed 24 hours after injection (n=1).

In conclusion, a thorough screening of the two new families of PBAEs designed in this chapter confirmed the potential of selected candidates to transfect the main cellular types dominating antigen presentation in the skin using *in vitro* human models. When translated into *in vivo* settings, the obstacles encountered to administer these polyplexes intradermally evidenced the need for alternative formulations and delivery methods that can allow effective targeting of the APCs residing in the most outer layers of the skin. For this reason, the following chapter will explore solvent-free methods avoiding the use of hypodermic needles to deliver nucleic acid therapeutics to dermal APCs.

## 2.5   Concluding remarks

The results of this chapter prove that chemical engineering of PBAEs with active-targeting ligands along with oligopeptides moieties renders superior delivery vectors with cell-specific transfection ability. Chemical linkage of mannose was confirmed to boost the transfection efficiency of the PBAEs, yet it was the inclusion of oligopeptides what ultimately provided cell-specific targeting.

Modification of the former family of OM-PBAEs with the targeting ligand mannose was achieved via Michael addition. When mixed with pDNA, the newly mannosylated candidates could efficiently encapsulate the nucleic acids at the same ratios as their non-mannosylated counterparts as evidenced by gel retardation assay. In addition, formulation of OM- and MM-PBAEs with pDNA resulted in monodisperse nanoparticles in the nanometric range and where mannosylation did not have a significant influence in their final physicochemical features. Contrarily, inclusion of oligopeptides provided means to fine-tune the nanoparticle properties, especially their surface charge, which closely depended on the nature of the amino acids.

Transfection efficiency of the newly synthesized library was thoroughly examined *in vitro* in the main cellular phenotypes initiating antigen presentation in the skin. Assays in immortalized (MUTZ3 cells) and primary (MoLCs) Langerhans-like cells proved the unmatchable superiority of polyplexes bearing lysine and aspartic acid moieties and where mannosylation, if helpful, was not the sole factor dictating transfection efficiency. Similar results were observed in transfection studies using dendritic-like cells, where it was confirmed that the combination of positively- and negatively-charged oligopeptides rendered the most efficient polyplexes (R/D- and K/D-derived PBAEs). Studies in other accessory cells lines such as fibroblasts and keratinocytes showed the same trend, with the mixtures of cationic and anionic PBAEs inducing the highest levels of gene transference.

In a similar fashion, the newly developed MM-PBAEs could efficiently complex mRNA and if necessary could be lyophilized without compromising their physicochemical features. Transfection studies using monocyte-derived models confirmed the superiority of the K/D- and K/D-Man-derived polyplexes again and where the levels of transfected cells triplicated those achieved by PBAE:pDNA complexes even when using half of the dose which could be attributed to the easier translation of mRNA that does not entail nuclear penetration.

Finally, *in vivo* bioluminescence studies revealed that top-performing polyplexes induced timid levels of gene expression when administered using conventional needles through the intradermal

route. While premature, this study evidenced the need for an alternative to nanoparticulate delivery that eliminates the use of hypodermic needles due to their limited accuracy and invasiveness.

In conclusion, we have developed a new family of PBAE candidates including oligopeptide moieties and a mannose ligand for cell-specific targeting of APCs in the dermal milieu. The capacity of discrete OM- and MM-PBAE formulations to selectively target different subsets pertaining to a same cellular type (DCs) proved the level of refinement that can be attained when combining oligopeptide and ligand decoration as synthetic strategies for PBAE design. These tools could be leveraged to rationally deliver prophylactic or therapeutic vaccines. In the future, a curated selection of the PBAE-derived vector may offer to opportunity to favor certain mechanisms for antigen presentation and in turn, the concomitant induction of helper immune responses with antibody production and cytotoxic cellular responses for the generation of long-term and robust immunity.

Given their flexibility of formulation, alternative PBAE-derived systems complexing nucleic acids will be explored in the next chapter using solvent-free strategies to enhance their stability and shelf-life while allowing integration with transdermal devices for efficient administration through the skin.

## 2.6  References

1.  Wolff, J. A. *et al.* Direct gene transfer into mouse muscle in vivo. *Science* 247, 1465–1468 (1990).

2.  Liu, M. A. DNA vaccines: an historical perspective and view to the future. *Immunol. Rev.* 239, 62–84 (2011).

3.  Metcalfe, S. M. & Fahmy, T. M. Targeted nanotherapy for induction of therapeutic immune responses. *Trends Mol. Med.* 18, 72–80 (2012).

4.  Nguyen, B. D. N., Green, J. J., Chan, J. M., Langer, R. & Anderson, D. G. Polymeric Materials for Gene Delivery and DNA Vaccination. *Adv. Healthc. Mater.* 20, 1–21 (2008).

5.  Hobernik, D. & Bros, M. DNA Vaccines — How Far From Clinical Use? *Int. J. Mol. Sci.* 19, 3605 (2018).

6.  Corbett, K. S. *et al.* SARS-CoV-2 mRNA vaccine design enabled by prototype pathogen preparedness. *Nature* 586, 567–572 (2020).

7.  Lopes, A., Vandermeulen, G. & Préat, V. Cancer DNA vaccines: current preclinical and clinical developments and future perspectives. *J. Exp. Clin. Cancer Res.* 1, 146 (2019).

8.  Kaurav, M. *et al.* Nanoparticulate mediated transcutaneous immunization: Myth or reality. *Nanomedicine NBM* 12, 1063–1081 (2016).

9.  Liu, M. A. A Comparison of Plasmid DNA and mRNA as Vaccine Technologies. *Vaccines* 7, 1–20 (2019).

10. Reichmuth, A. M., Oberli, M. A., Jaklenec, A., Langer, R. & Blankschtein, D. mRNA vaccine delivery using lipid nanoparticles. *Ther. Deliv.* 7, 319–334 (2016).

11. Pardi, N., Hogan, M. J., Porter, F. W. & Weissman, D. mRNA vaccines — a new era in vaccinology. *Nature* 17, 261–279 (2018).

12. Ferraro, B. *et al.* Clinical applications of DNA vaccines: Current progress. *Clin. Infect. Dis.* 53, 296–302 (2011).

13. Kim, N. W. *et al.* Polyplex-releasing microneedles for enhanced cutaneous delivery of DNA vaccine. *J. Control. Release* 179, 11–17 (2014).

14. Thomas, C. E., Ehrhardt, A. & Kay, M. A. Progress and problems with the use of viral vectors

for gene therapy. *Nat Rev Genet* 4, 346–358 (2003).

15. Yin, H. *et al.* Non-viral vectors for gene-based therapy. *Nat. Rev. Genet.* 15, 541–555 (2014).

16. Incani, V., Lavasanifar, A. & Uludağ, H. Lipid and hydrophobic modification of cationic carriers on route to superior gene vectors. *Soft Matter* 6, 2124–2138 (2010).

17. Anderson, D. G., Lynn, D. M. & Langer, R. Semi-automated synthesis and screening of a large library of degradable cationic polymers for gene delivery. *Angew. Chemie Int. Ed.* 42, 3153–3158 (2003).

18. Green, J. J. *et al.* Electrostatic Ligand Coatings of Nanoparticles Enable Ligand-Specific\rGene Delivery to Human Primary Cells. *Nano Lett.* 7, 874–879 (2007).

19. Zugates, G. T. *et al.* Gene Delivery Properties of End-Modified Poly (Beta-amino ester)s. *Bioconjug. Chem.* 18, 1887–1896 (2007).

20. Sunshine, J. *et al.* Small-molecule end-groups of linear polymer determine cell-type gene-delivery efficacy. *Adv. Mater.* 21, 4947–4951 (2009).

21. Kaplan, D. H. In vivo Function of Langerhans Cells and Dermal DC. *Trends Immunol.* 31, 446–451 (2010).

22. ER, T. *et al.* Exploitation of Langerhans cells for in vivo DNA vaccine delivery into the lymph nodes. *Gene Ther.* 21, 566–574 (2014).

23. Valladeau, J. *et al.* Langerin, a Novel C-Type Lectin Specific to Langerhans Cells, Is an Endocytic Receptor that Induces the Formation of Birbeck Granules. *Immunity* 12, 71–81 (2000).

24. Romani, N. *et al.* Targeting Skin Dendritic Cells to Improve Intradermal Vaccination. *Curr. Top. Microbiol. Immunol.* 351, 113–138 (2012).

25. Stoitzner, P., Sparber, F. & Tripp, C. H. Langerhans cells as targets for immunotherapy against skin cancer. *Immunol. Cell Biol.* 88, 431–437 (2010).

26. Apostolopoulos, V., Thalhammer, T., Tzakos, A. G. & Stojanovska, L. Targeting Antigens to Dendritic Cell Receptors for Vaccine Development. *J. Drug Deliv.* 2013, 869718 (2013).

27. Keler, T., Ramakrishna, V. & Fanger, M. W. Mannose receptor-targeted vaccines. *Expert Opin. Biol. Ther.* 4, 1953–1962 (2004).

28. Segovia, N., Dosta, P., Cascante, A., Ramos, V. & Borrós, S. Oligopeptide-terminated poly (b-amino ester) s for highly efficient gene delivery and intracellular localization. *Acta Biomater.*

10, 2147–2158 (2014).

29. Dosta, P., Segovia, N., Cascante, A., Ramos, V. & Borrós, S. Surface charge tunability as a powerful strategy to control electrostatic interaction for high efficiency silencing, using tailored oligopeptide-modified poly(beta-amino ester)s (PBAEs). *Acta Biomater.* 20, 82–93 (2015).

30. Dosta, P. *et al.* Delivery of Anti-microRNA-712 to Inflamed Endothelial Cells Using Poly(β-amino ester) Nanoparticles Conjugated with VCAM-1 Targeting Peptide. *Adv. Healthc. Mater.* e2001894 (2021) doi:10.1002/adhm.202001894.

31. Fornaguera, C. *et al.* mRNA Delivery System for Targeting Antigen-Presenting Cells In Vivo. *Adv. Healthc. Mater.* 7, 1–11 (2018).

32. Brugada-Vilà, P. *et al.* Oligopeptide-modified poly(beta-amino ester)s-coated AdNuPARmE1A: Boosting the efficacy of intravenously administered therapeutic adenoviruses. *Theranostics* 10, 2744–2758 (2020).

33. Dosta, P., Ramos, V. & Borrós, S. Stable and efficient generation of poly(β-amino ester)s for RNAi delivery. *Mol. Syst. Des. Eng.* 3, 677–689 (2018).

34. Ouwehand, K., Spiekstra, S. W., Waaijman, T. & Scheper, R. J. Langerhans cells derived from a human cell line in a full-thickness skin equivalent undergo allergen-induced maturation and migration. *J. Leukoc. Biol.* 90, 1027–1033 (2011).

35. Larsson, K., Lindstedt, M. & Borrebaeck, C. A. K. Functional and transcriptional profiling of MUTZ-3, a myeloid cell line acting as a model for dendritic cells. *Immunology* 117, 156–166 (2006).

36. Caucheteux, S. M. *et al.* Polypropylene Sulfide Nanoparticle p24 Vaccine Promotes Dendritic Cell-Mediated Specific Immune Responses against HIV-1. *J. Invest. Dermatol.* 136, 1172–1181 (2016).

37. Jurgen Bauer, Friedrich A. Bahmer, Jurgen Worl, Winfried Neuhuber, G. S. & Manigé, F. A Strikingly Constant Ratio Exists Between Langerhans Cells and Other Epidermal Cells in Human Skin. A Stereologic Study Using the Optical Disector Method and the Confocal Laser Scanning Microscope. *J. Invest. Dermatol.* 116, 313–318 (2001).

38. Sunshine, J. C., Akanda, M. I., Li, D., Kozielski, K. L. & Green, J. J. Effects of base polymer hydrophobicity and end-group modification on polymeric gene delivery. *Biomacromolecules*

12, 3592–3600 (2011).

39. Liu, Z., Zhang, Z., Zhou, C. & Jiao, Y. Hydrophobic modifications of cationic polymers for gene delivery. *Prog. Polym. Sci.* 35, 1144–1162 (2010).

40. Espuelas, S., Thumann, C., Heurtault, B., Schuber, F. & Frisch, B. Influence of ligand valency on the targeting of immature human dendritic cells by mannosylated liposomes. *Bioconjug. Chem.* 19, 2385–2393 (2008).

41. Irache, J. M., Salman, H. H., Gamazo, C. & Espuelas, S. Mannose-targeted systems for the delivery of therapeutics. *Expert Opin. Drug Deliv.* 5, 703–724 (2008).

42. Jones, C. H. *et al.* Structure – Function Assessment of Mannosylated Poly( β -amino esters) upon Targeted Antigen Presenting Cell Gene Delivery. *Biomacromolecules* 16, 1534–1541 (2015).

43. Fröhlich, E. The role of surface charge in cellular uptake and cytotoxicity of medical nanoparticles. *Int. J. Nanomedicine* 7, 5577–5591 (2012).

44. Jones, C. H. *et al.* Mannosylated poly (beta-amino esters) for targeted antigen presenting cell immune modulation. *Biomaterials* 37, 333–344 (2014).

45. Masterson, A. J. *et al.* MUTZ-3, a human cell line model for the cytokine-induced differentiation of dendritic cells from CD34+precursors. *Blood* 100, 701–703 (2002).

46. Tada, Y. *et al.* Identification and characterization of endogenous Langerin ligands in murine extracellular matrix. *J. Invest. Dermatol.* 126, 1549–58 (2006).

47. Santegoets, S. J. a M., van den Eertwegh, A. J. M., van de Loosdrecht, A. a, Scheper, R. J. & de Gruijl, T. D. Human dendritic cell line models for DC differentiation and clinical DC vaccination studies. *J. Leukoc. Biol.* 84, 1364–73 (2008).

48. Zhang, L. W., Wolfgang Bäumer & Monteiro-Riviere, N. A. Cellular uptake mechanisms and toxicity of quantum dots in dendritic cells. *Nanomedicine* 6, 777–791 (2011).

49. Jia, J. *et al.* Interactions Between Nanoparticles and Dendritic Cells: From the Perspective of Cancer Immunotherapy. *Front. Oncol.* 8, 1–11 (2018).

50. Verma, A. *et al.* Surface-structure-regulated cell-membrane penetration by monolayer-protected nanoparticles. *Nat. Mater.* 7, 585–595 (2008).

51. Silva, J. M., Vandermeulen, G., Oliveira, V. G., Pinto, S. N., Rodrigues, C., Salgado, A., Afonso, C. A., Viana, A. S., Jérôme, C., Silva, L. C., Graca, L., Préat, V., & Florindo, H. F. Development

of Functionalized Nanoparticles for Vaccine Delivery to Dendritic Cells: A Mechanistic Approach. *Nanomedicine* 9, 2639–56 (2014).

52.  Romani, N., Clausen, B. E. & Stoitzner, P. Langerhans cells and more: langerin-expressing dendritic cell subsets in the skin. *Immunol. Rev.* 234, 120–141 (2010).

53.  Chanput, W., Mes, J. J. & Wichers, H. J. THP-1 cell line: An in vitro cell model for immune modulation approach. *Int. Immunopharmacol.* 23, 37–45 (2014).

54.  Berges, C. *et al.* A cell line model for the differentiation of human dendritic cells. *Biochem. Biophys. Res. Commun.* 333, 896–907 (2005).

55.  Liard, C. *et al.* Intradermal immunization triggers epidermal langerhans cell mobilization required for CD8 T-cell immune responses. *J. Invest. Dermatol.* 132, 615–625 (2012).

56.  Heath, W. R. & Carbone, F. R. The skin-resident and migratory immune system in steady state and memory: Innate lymphocytes, dendritic cells and T cells. *Nat. Immunol.* 14, 978–985 (2013).

57.  Kündig, T. M. *et al.* Fibroblasts as efficient antigen-presenting cells in lymphoid organs. *Science* 268, 1343–7 (1995).

58.  Brian S Kim, Fumi Miyagawa, Young-Hun Cho, Clare L Bennett3, Björn E Clausen, S. I. K. Keratinocytes function as accessory cells for presentation of endogenous antigen expressed in the epidermis. *J Invest Dermatol.* 129, 2805–2817 (2009).

59.  Sheikh, H., Yarwood, H., Ashworth, A. & Isacke, C. M. Endo180, an endocytic recycling glycoprotein related to the macrophage mannose receptor is expressed on fibroblasts, endothelial cells and macrophages and functions as a lectin receptor. *J. Cell Sci.* 113, 1021–1032 (2000).

60.  Zhang, C., Maruggi, G., Shan, H. & Li, J. Advances in mRNA Vaccines for Infectious Diseases. *Front. Immunol.* 10, 594 (2019).

61.  Guan, S. & Rosenecker, J. Nanotechnologies in delivery of mRNA therapeutics using nonviral vector-based delivery systems. *Gene Ther.* 24, 133–143 (2017).

62.  Hillaireau, H. & Couvreur, P. Nanocarriers' entry into the cell: Relevance to drug delivery. *Cell. Mol. Life Sci.* 66, 2873–2896 (2009).

63.  Manzanares, D. & Ceña, V. Endocytosis : The Nanoparticle and Submicron Nanocompounds Gateway into the Cell. *Pharmaceutics* 12, 1–22 (2020).

# Chapter III: Transdermal PBAE-derived platforms for targeted vaccination

Authors: Núria Puigmal, Víctor Ramos and Salvador Borrós

This page left blank intentionally

## 3.1 Introduction

In the previous chapter, systematic screening of OM- and MM-PBAEs lead to the identification of superior formulations in the form of polyplexes for transcutaneous immunization. Typically, PBAE nanoparticle formation is driven by electrostatic interactions occurring between the cationic polymers and the negatively charged nucleic acids, which allows for effortless production and high throughput screening of numerous candidates to investigate their therapeutic efficacy. Nevertheless, the utilization of polyplexes as vaccine delivery vehicles is suboptimal due to their short half-life in solution, "cold-chain" requirements and their limitation to encapsulate negatively charged cargos,[1] preventing them from incorporating adjuvants other than nucleic acids —a much needed element in many vaccine formulations to couple a robust early innate immune response to the adaptive immune activation.[2] Due to their outstanding chemical flexibility, PBAEs offer alternative design opportunities that can be tailored depending on their final application and which could ultimately benefit vaccine widespread adoption and acceptance. Besides from polyplexes, other PBAE-based systems include micelles, gels, fibers, nanochaperones and films.[3]

The use of PBAEs as polyelectrolyte films (also known as polyelectrolyte multilayers, PEMs) was first reported by Lynn's research group in 2004,[4] becoming an elegant alternative to release therapeutic cargos from substrates under physiological conditions and promote localized delivery in a target area such as the skin (**Figure III-1**). PEMs are nanostructured films formed by iterative adsorption of alternately charged polymers and biological cargos such as nucleic acids onto substratum surfaces.[5,6] Assembly of the films using the "Layer-by-Layer" (LbL) method allows to fine-tune the film thickness and thus, drug loading, by changing the number of adsorbed polycation/polyanion layers.[7] Moreover, several layers of multiple therapeutic agents can be combined simultaneously or sequentially apart to manage complex therapeutic contexts necessitating multiple drugs.[8] Thus, drug release kinetics can be tailored as a function of film architecture/composition, allowing to regulate the release of each individual component and avoid diffusion-related burst release for an optimal therapeutic response.[9] The versatility of this system has stimulated a broad interest for translational development and commercialization given its facile scale-up production in mild manufacturing conditions and at ambient temperature, which ensures the preservation of the payload activity.[10]

Additionally, PEMs can faithfully coat any surface including topologically complex substrates such as those of interventional medical devices. In the context of gene vaccination, PEMs offer an opportunity for solvent-free delivery of nucleic acids that would allow for extended storage, reduced costs and the potential for cold chain independency,[11] all of them desirable advantages over nanoparticle-based systems, particularly for developing countries.
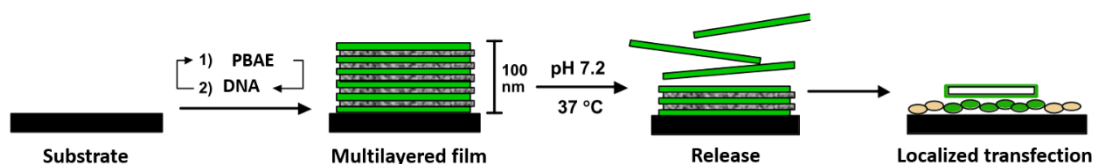


**Figure III-1. Idealized scheme of PEMs deposition for localized gene delivery.**[7] Sequential adsorption and deposition of PBAEs and bioactive cargos such as DNA onto substratum surfaces renders multi-layered films that can serve as delivery vehicles for direct and localized transfection.

Uniform and reproducible coating of substrates with PEMs is essential if translated to clinical settings. Over the years, numerous treatments have been proposed to improve the properties of the substrates of medical devices such as biocompatibility, reactivity, or adhesion. These, being fundamentally surface properties, can be modified in the near-surface region without compromising desirable bulk properties of the material.[12] Strategies such as plasma surface treatments can be used to remove loosely bonded surface contamination of the substrate and provide intimate contact between two interacting materials on the molecular scale;[13] here, (1) the surface of medical devices and (2) the cationic polymers integrated in the PEMs. Indeed, newly-generated functional groups after plasma treatments can serve as anchoring sites for PBAEs and other bioactive molecules to improve PEMs adhesion to the substrate's surface and prospectively, transfection efficiency.

New insights in vaccine development, the need for safe, economic, and non-invasive vaccine administration and the increasing mechanistic knowledge of immune responses when targeting the intradermal route, rather than the intramuscular or systemic, have all motivated the engineering of novel systems for transcutaneous gene vaccination.[11] Disrupting the skin barrier with physical methods can be useful to generate transport pathways across the stratum corneum for antigen permeation and in turn, a more readily access to LCs and other APCs.[14,15] Cutaneous methods of immunization include liquid jet injection, ballistic methods (also known as epidermal powder immunization) and topical methods, which deliver the therapeutic cargo via passive diffusion or facilitated transdermal transport (**Figure III-2**).[16]
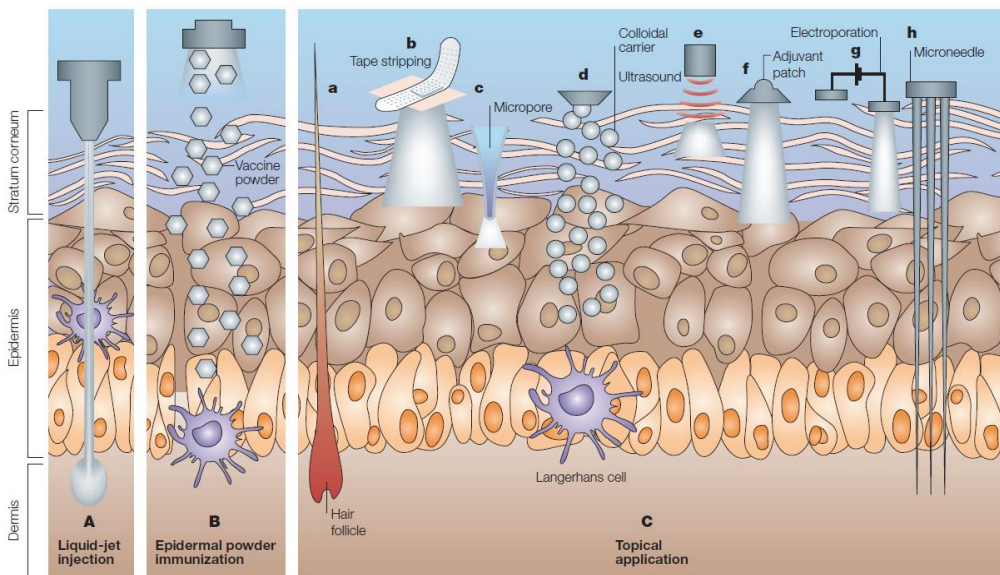
**Figure III-2. Schematic representation of the main approaches to overcome the stratum corneum.** [16] Vaccination technologies that facilitate intradermal administration and targeting of APCs in the dermal milieu can be categorized depending on their tissue target (SC, epidermis, and dermis) or mechanism of action.

Among these, microneedles (MNs) are considered as one of the most promising strategies to achieve systemic effects via transdermal delivery of drugs.[17] MNs are medical devices consisting in an array of needle-like projections in the micrometric range capable of disrupting the most outer layers of the skin to deliver vaccines, small molecules, proteins or nanoparticles.[18,19] With the emergence of microfabrication manufacturing technologies in the mid-1990's,[20] they became the subject of intense research for low-cost and minimally-invasive drug delivery.[21] Because of their size, MNs are painless as they avoid contact with the nervous terminations and pain receptors that populate the underlaying epidermis,[22] improving patient adherence while also allowing self-administration for a user-friendly experience. Indeed, MN administration overcomes many of the disadvantages associated with conventional hypodermic needles including needle phobia, the need of trained medical personnel for administration, sharps waste management, and hazards such as needle-stick injuries and needle-borne infections due to reuse.[11] Delivery of vaccines via MNs has been proven successful in enhancing immunogenicity (inducing stronger and less variable immune responses than those triggered via needle-based injection) while also reducing the number of immunizations needed for full seroconversion.[16] Moreover, MNs present dose-sparing advantages, in which the direct targeting of the rich network of immunogenic APCs present in the epidermis —instead of the sparse population

residing in the skeletal muscle— generates superior immune responses.[23] Five different types of MN designs are described in the literature, namely solid, coated, hollow, dissolvable and hydrogel-forming MNs.[24] Solid and hollow MNs were first proposed and are generally fabricated with glass, silicon or stainless-steel yet their use has been limited by their inherent poor biocompatibility, multi-step administration and the potential for infection due to reuse.[19] Contrarily, coated-, dissolvable-, and hydrogel-based MNs offer controlled drug release profiles, better dose accuracy and have been extensively described along with PBAEs as a therapeutic tandem in the context of gene vaccination.[9,25–28]

Previously in this work, we confirmed the potential of OM- and MM-PBAEs as a LC-targeting vaccination technology when encapsulating nucleic acids such as pDNA and mRNA as polyplexes. Considering these findings, we propose to expand the use of PBAEs as PEMs, while also exploring their therapeutic potential when integrated with transdermal medical devices such as MNs. The main objective of this chapter is **the development and optimization of new formulations of PBAE-derived PEMs for solvent-free nucleic acid vaccination**. Moreover, plasma surface techniques will be used to functionalize the substrates of medical devices and examine their impact on surface-mediated transfection. Employing the lessons learned during this and the previous chapter, PEMs-derived systems along with polyplexes will then be coupled to MNs and other transdermal devices to engineer a translational platform for transdermal immunization.

## 3.2 Aims

The main objective of the present chapter is to expand the library of OM- and MM-PBAE polymers for solvent-free transfection using PEMs while integrated in interventional medical devices. To do so, the following tasks were proposed:

- ✓ Development of a solvent-free delivery system using the newly synthesized families of OM- and MM-PBAEs as vectors.

- ✓ Study the impact of substrate decoration via plasma surface modifications as means to enhance transfection efficiency.

- ✓ Fabrication and characterization of polymeric transcutaneous devices for needle-free immunization.

- ✓ Comparison of the transfection efficiency of OM-and MM-PBAEs when integrated as PEMs or polyplexes in transcutaneous devices using a three-pronged approach (*in vitro*, *ex vivo* and *in vivo*).

## 3.3 Materials and Methods

### 3.3.1 Materials

Reagents and solvents used for polymer synthesis and rod/MN fabrication were purchased from Sigma-Aldrich and Panreac. Cell lines were obtained from ATTC (Manassas, Virginia). Human monocyte-derived Langerhans cells (MoLCs) obtained from healthy donors were kindly provided by Dr. Francesc Català (IDIBELL). Plasmid reporter green fluorescent protein (pmaxGFP, 3486 bp) was purified using the NucleoBond® Xtra Midi Plus EF kit (Macherey-Nagel) from competent Escherichia coli cells. mRNA used in this study was eGFP (CleanCap Enhanced Green Fluorescent Protein mRNA 5-methoxyuridine) and was acquired from TriLink.

### 3.3.2 Methods

#### 3.3.2.1. Animals

Adult 6–8 weeks old C57BL/6 mice were purchased (Envigo) and kept under pathogen-free conditions in laminar flow boxes. Animal maintenance and experiments were performed in accordance with established guidelines of the Catalan Government and following protocol number 8856, approved by the Direcció General del Medi Natural.

#### 3.3.2.2. Fabrication of polymeric rods

Polymeric rods mimicking the features of subcutaneous contraceptive delivery systems were fabricated using a stainless-steel rotary extruder. Polycaprolactone (PCL) pellets were charged in the loading container of the extruder and melted at 80°C for 10 min. Next, the instrument was allowed to cool down for safe manipulation and PCL strands were extruded and cut rendering 1 cm-rods with 1 mm diameter.

#### 3.3.2.3. Fabrication of solid and dissolvable MNs

Stainless steel microneedles ranging 500 µm used for cosmetic purposes served as positive molds and also were used as solid MNs for *ex vivo* and *in vivo* studies. Female molds were fabricated by pouring a PDMS solution (prepared as recommended by the manufacturer) over the positive mold, allowing it to cure for 24 hours at room temperature. To fabricate solid PLGA-based microneedles, a 15% w/v solution of PLGA (Resomer® RG 858 S, Sigma-Aldrich) was dissolved in acetonitrile, degasified for 30 min and casted on top of the molds. Solid MNs were allowed to dry under vacuum for 24 hours

and stored at room temperature. Dissolvable microneedles were fabricated in a similar fashion. Briefly, a premixed solution of poly(vinyl alcohol) (PVA) and glycerol (10% and 2% w/v respectively in deionized water) was combined with a suspension of PBAE-derived polyplexes and poured on the mold. Microneedles were allowed to dry likewise and stored until further use.

### 3.3.2.4. Layer-by-layer deposition of PBAEs and characterization on transcutaneous delivery devices

Manual deposition of polyelectrolyte multilayers of PBAE:pDNA on various substrates was adapted from elsewhere.[6] Substrates including extruded rods and solid polymeric MNs were immersed in a PBAE solution (2 mg ml$^{-1}$) in either AcONa Buffer or PBS for 5 min followed by two successive washing steps of 30 seconds each using the same buffer. Next, substrates were submerged in the pDNA solution (1 mg ml$^{-1}$) during 5 min and washed in the same fashion. This procedure was repeated multiple times until achieving the desired number of PBAE:pDNA bilayers and stored at room temperature until use. Characterization of *in situ* polyplex formation was assessed by DLS. Polymeric rods precoated with polyelectrolyte films were immersed in PBS for 30 min and supernatants were collected for DLS analysis. Quantification of deposited DNA was conducted using the Quant-iT™ dsDNA Assay Kit High Sensitivity (Thermo Fisher Scientific, Spain) following the manufacturer's instructions. Extruded rods were coated as described and placed in Eppendorf tubes containing 50 µL of PBS to allow film release for 30 min. Supernatant was next collected, stained with the kit, and analyzed by fluorescence (λ=485/530) using a plate reader (Elx808 Biotek Instruments Ltd, USA).

### 3.3.2.5. Plasma enhanced chemical vapor deposition (PECVD) and deep coating for substrate modification of MNs

The surface treatments carried out in this work were performed using a stainless-steel vertical plasma reactor manufactured by our group. This reactor consists in a stainless-steel chamber (diameter: 25.5 cm; length: 41.6 cm) vertical plate reactor. The ground electrode is the reactor chamber, and the radio frequency (RF) electrode is an aluminium plate, which is used to hold the samples for polymerization. Additionally, the RF electrode is connected to a RF pulse generator (13.56 MHz) via a matching box. Gases and monomers are supplied via a standard manifold with gas fluxes adjusted with a tree of needle valves. The system pressure is monitored using a vacuum gauge controller (MKS PDR900, Andover, MA, USA) connected with a cold cathode/micropirani vacuum transducer (MKS 972 DualMag) positioned at the center of the reactor. The system has a nitrogen

cold trap and a chemical trap filled with active carbon connected to prevent non-reacted monomer from reaching the pump (Trivac D 16BCS/PFPE Leybold, Cologne, Germany).

First, Pentafluorophenyl Methacrylate (PFM) (Sigma Aldrich) was plasma-polymerized (pp) via PECVD as follows. Briefly, PLGA-based MNs were treated by plasma activation at 15W, where a mixture of oxygen and argon (80:20 v/v) was fed until a working pressure of 0.15 mbar was achieved for the desired experimental time (10 min). Then, gas mixture was cut off and power generator was turned off to stop the formation of radicals on the substrate. Finally, PFM was regulated through the needle valve and introduced into the reactor chamber in vapor phase (heated at 75°C) at 0.15 mbar for the desired experimental time (3 min). Following modification, samples were removed from the reactor and stored with argon atmosphere until further use. Si-wafers (Wafer World, USA) were also introduced in the plasma reactor as controls in every batch for proof of effective functionalization.

Alternatively, dopamine and dopamine-conjugated hyaluronic acid were deposited onto the MN surface by deep coating. Here, MNs were first activated via plasma treatment using Argon/Oxygen (20:80) for 5 min. Activated MNs were next incubated 12 hours with a 2 mg mL$^{-1}$ solution of dopamine (Sigma Aldrich) or HADA kindly provided by Dr. Texidó and synthesized as described elsewhere.[29] Finally, samples were rinsed and preserved in argon atmosphere until further decoration with PEMs.

### 3.3.2.6. *Ex vivo* skin penetration studies

The ability of transdermal devices to penetrate the skin was tested *ex vivo* using 2 x 2 cm skin explants harvested from healthy C57BL/6 mice. PLGA-based and stainless steel MNs were thumb-pressed for 10 min whereas rods were implanted using an 18-gauge syringe. Transdermal skin penetration was confirmed by surface staining with Trypan blue (0.4%) (Gibco™, FisherScientific) and further imaged by optical microscopy.

### 3.3.2.7. Assessment of film deposition *ex vivo*

Film deposition following transdermal delivery was assessed by fluorescence microscopy. Briefly, devices were coated with PEMs as described before using fluorescently-labelled PBAEs. Once coated, the devices were either injected in the case of MNs or implanted for the rods as described before. Proof of film release was confirmed by fluorescence microscopy (Nikon Eclipse TE200-U).

### 3.3.2.8. *In vitro* transfection studies with transcutaneous devices

Transfection efficiency of coated transdermal devices was examined in HaCaT cells and MoLCs. PBAE-derived polyplexes were formulated and incubated as described in *Chapter II*. Devices functionalized with pDNA/mRNA:PBAE films were deposited gently on the wells of 48-well plates and were incubated for 48 hours at 37°C in 5% $CO_2$ atmosphere until analysis. Untreated cells were used

as negative control while Lipofectamine3000 (Thermo Fisher Scientific, Spain) served as positive control group. Gene delivery was confirmed by flow cytometry (BD LSR Fortessa™) and fluorescence microscopy (Nikon Eclipse TE2000-U) 48 hours post-transfection.

### 3.3.2.9. *Ex vivo* transfection studies with transcutaneous devices

Analysis of transfection efficiency was studied *ex vivo* with murine cadaveric skin explants following a protocol adapted from elsewhere.[30] Skin was harvested from healthy C57BL/6 mice and the subcutaneous fat was scrapped off to expose the basal layer. Next, 1 x 1 cm skin explants were sutured to stainless steel mesh to allow gas exchange and incubated in 24-well plates with Dulbecco's Modified Eagle Medium (DMEM) supplemented media. The height of the steel mesh was carefully adjusted so the epidermis would be facing up in the air-liquid interface to mimic physiological conditions. Then, transdermal devices were implanted (rods) or administered (PLGA MNs, stainless steel MNs, and hypodermic injection) as described to deliver pDNA-complexing PBAEs encoding for GFP. 24 hours post-treatment, skins were digested or cryosectioned for successive analysis.

### 3.3.2.10. *In vivo* transfection studies using transcutaneous devices

All surgeries were performed in a sterile environment under anesthesia. C57BL/6 mice were shaved prior to the pDNA/mRNA-coated device implantation (mRNA encoding for GFP). PLGA-based MN arrays were administrated by gently pinching the skin of the back of the mice and pressing down using both thumb and index fingers. MNs were pressed for 10 seconds to secure their position and kept in place with medical-grade tape. Stainless steel MNs were pressed against the skin multiple times to promote the creation of microchannels and an aqueous solution containing the PBAEs was added dropwise on top of the treated area. To implant the polymeric rods, a 3 mm incision was performed and the outer layers of the skin excluding the basal layer were separated using blunt-tipped forceps to create a small cavity. Coated-roads were placed in the cavity and these were sutured with prolene suture. 24 hours post-surgery, mice were sacrificed and the skin of the treatment area was harvested for further analysis. Mice from the control group were administered PBAE-derived polyplexes using the Mantoux technique as previously described in *Chapter II*.

### 3.3.2.11. Cryopreservation and cryosectioning of skin explants

Upon harvesting, skin explants were preserved in chilled supplemented media until processing. First, connective, adipose, and panniculus carnosus tissues below the basal layer were cleared using blunt-tipped forceps. Next, skins were incubated in formaldehyde (40%) for 2-4 hours at 4°C without agitation to prevent the skin from rolling over itself followed by two consecutive washes in phosphate

buffer (0.1M) of 20 min each. Skins were next submerged in a 30% sucrose solution in 0.1M phosphate buffer for 48 hours. After that, skins were dried with a tissue, placed in PVC tissue cassettes for O.C.T. embedding (Sakura Finetek, Europe) and frozen at -80$^{\circ}$C. 10-, 20-, and 50-µm sized lateral sections were cut using a Leica CM3050S cryostat.

### 3.3.2.12. Immunohistofluorescent (IHF) staining of skin explants

Frozen slides were allowed to thaw at room temperature for 20 min before proceeding with the staining. Nuclei were stained with 4',6-diamidino-2-phenylindole (DAPI, 1 mg/ml, Sigma) for 3 min at room temperature and washed with PBS (15 min). Microscope slides were mounted with Fluoromount™ Aqueous Mounting Medium (Southern-Biotechnology Associates, UK) and stored in the dark until analysis. Tissue sections were imaged by either fluorescent (Nikon Eclipse TE2000-U) or confocal (Leica SP8 Lightning resonant-scanning confocal spectral microscope) microscopy to confirm gene expression.

### 3.3.2.13. Statistical analysis

Statistical analyses were carried out using Graph-Pad Prism 8 (GraphPad Software). All data are reported as mean + SD. For *in vitro* experiments, a minimum of n=3 biological replicates were used per condition in each experiment. Pairwise comparisons were performed using Student t-tests. No specific pre-processing of data was performed prior to statistical analyses. Differences between groups were considered significant at *p*-values below 0.05 (* $p < 0.05$, ** $p < 0.01$, *** $p < 0.001$).

## 3.4 Results and Discussion

### 3.4.1 Engineering solvent-free delivery vectors using OM- and MM-PBAEs

Systematic screening of the transfection efficacy of OM- and MM-PBAEs in *Chapter II* confirmed the superiority of polyplexes bearing lysine and aspartic acid moieties, along with their corresponding mannosylated counterpart. In light of these findings, we compared the potential of this formulation pair as an LC-targeting vector for gene vaccination when used as solvent-free PEMs instead. First, a new system for surface-mediated transfection was developed and characterized using the top-performing PBAE formulations recently identified and with pDNA as a therapeutic model. Characterization of PBAE:pDNA films was first conducted on polymeric, polycaprolactone (PCL)-based, rods resembling an existing subcutaneous delivery device;[31] contraceptive implants. Our choice was motivated by utilitarian reasons as their easy fabrication and low-cost offered an excellent opportunity to investigate the performance of PBAE-derived PEMs in a translational device.

#### 3.4.1.1 Physicochemical characterization of PBAE:pDNA PEMs

Hydrolytically degradable films consisting in bilayers of OM- and MM-PBAEs and pDNA were fabricated as detailed in the Methods section. LbL-deposition of oppositely charged polyelectrolyte materials was conducted through serial dipping steps manually, yet this procedure could be easily automated using slide stainers as others before.[28]

Next, a physicochemical characterization of the films was conducted starting by their ability to engender polyplexes following film erosion from the rods (**Figure III-3A**). In consonance with others,[6,7,26] analysis of eroded films by DLS showed a high polydispersity in all the samples (PDI ≥ 0.3) and where aggregates ranging from 250 to 550 nm were observed regardless of the buffering solution utilized during their fabrication. These results were consistent with the view that pDNA could be released as part of a polymer aggregate or that it aggregates once in solution when both polymer and DNA have been released following a mechanism coined as "*in situ* polyplex formation".[6] However, it should be noted that characterization via DLS cannot provide direct insight into the composition of these aggregates and the exact mechanisms remain unclear. Mannosylation did not appear to influence the final size of the aggregates whereas the dipping buffer did, since significantly higher aggregates were engendered when using AcONa. For this reason, the use of PBS was preferred over

AcONa in further studies to fabricate the PEMs since the hydrodynamic diameter of the resulting aggregates was in the same range as to that observed for their corresponding polyplexes (**Figure II-7A**), whereas the size of AcONa-derived PEMs had doubled.

Next, pDNA deposition on the polymeric rods was quantified by dipping them with an increasing number of bilayers (**Figure III-3B**). Fluorescence analysis of supernatants recovered from eroded PBAE:pDNA films showed a correlation between the mass of pDNA deposited and the number of bilayers, hinting that film growth was occurring although statistically significant differences could not be claimed among all groups.
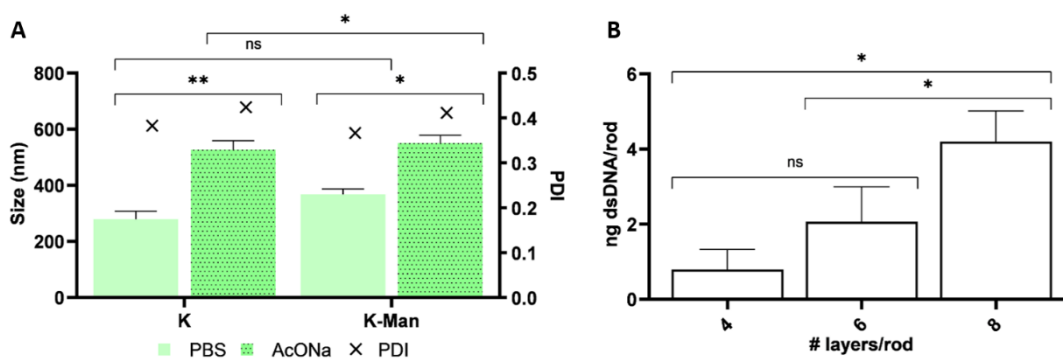


**Figure III-3. Physicochemical characterization of PBAE-derived PEMs upon release from PCL rods.** Hydrodynamic diameter of polyplexes released from PBAE:pDNA films using either PBS or AcONa as dilution buffer. PBAE:pDNA bilayers of K- and K-Man-PBAEs were deposited in a 2:1 polymer-to-DNA ratio (**A**). Fluorescence quantification of dsDNA recovered from eroded films. (**B**) Coated rods were prepared by depositing an increasing number of PBAE:pDNA bilayers using PBS as dilution buffer. DsDNA was quantified using the High Sensitivity Quant-iT™ dsDNA Assay Kit by fluorescence (λ=485/530) in plate reader. Data are shown as mean and standard deviation of triplicates.

### 3.4.1.2 Assessment of transfection efficiency using PEMs-derived PBAEs

Next, transfection efficiency of the polyelectrolyte films was evaluated as a function of bilayer number and dipping buffer using a permissive cell line (HaCaT). Flow cytometry results following transfection assays first pointed at the buffer as a critical parameter in the mediation of gene delivery. Our data showed that the percentage of transfected cells when using AcONa-derived films was significantly lower if compared to those achieved when fabricating the films with PBS (**Figure III-4A, B**), which might be caused by their higher diameter and the incapacity of cells to internalize such aggregates. A trend was also evidenced between the number of bilayers and the percentage of transfected cells, were the highest number of GFP positive cells was registered for those rods

accumulating more layers and thus, more pDNA. Finally, cells located under the functionalized substrates were preferentially transfected as predicted if compared to those in distant regions of the well confirming that transfection was driven by surface-mediated mechanisms (**Figure III-4C**).
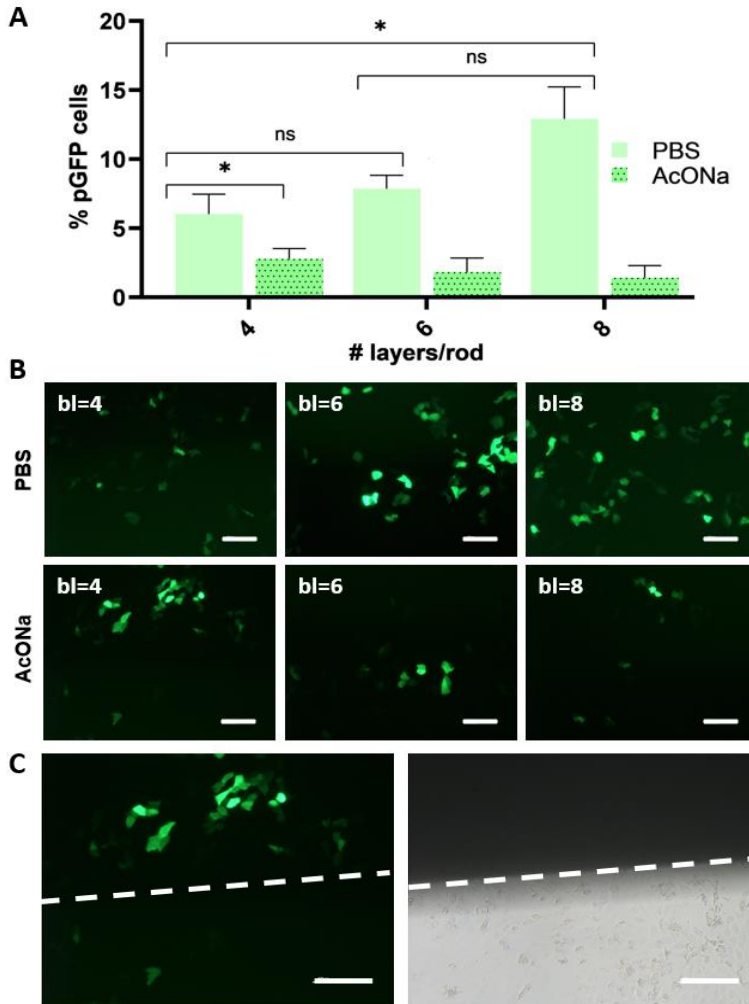


**Figure III-4. Transfection efficiency of PBAE:pDNA-coated rods as a function of bilayer number.** An increasing number of bilayers were piled on PCL-extruded rods using PBS or AcONa. 40000 HaCaT cells were seeded in 48-well plates and incubated with the coated rods for 48 hours. GFP gene expression was quantified by flow cytometry **(A)** and fluorescence microscopy **(B)** Scale bar = 50 μm. Fluorescence versus bright field microscopy served to confirm local transfection. Top area corresponds to the site of rod deposition. Scale bar = 50 μm. **(C)**

In light of these findings, PBS was reaffirmed as the buffer of choice in future studies given the superior performance of the resulting PEMs. Regarding the number of PBAE:pDNA bilayers, a total number of 8 was fixed where we compromised maximization of transfection studies while keeping PEM fabrication a time- and cost-effective procedure. Both dsDNA quantification following film erosion and analysis of gene expression suggested that higher number of bilayers rendered superior PEM-derived vectors in terms of transfection efficiency, yet piling more layers was not feasible if performed manually. Therefore, further studies using automated systems might be of interest in the future to examine the effect of the number of PBAE:pDNA pairs in their final performance, but also to address the impact of other parameters such as the buffer's pH or the polymer-to-pDNA weight ratio which are known to have an influence.[5]

Decoration of polymeric rods allowed us to set the bases for surface-mediated transfection using PEMs. Nevertheless, other needle-free technologies enabling non-invasive vaccination might be of more interest, especially if envisioning widespread adoption of the vaccination platform. For this reason, the use of MNs as vehicles for transdermal vaccination was explored since they offer high patient compliance while enhancing efficacy and tolerability of the therapy by exposing it to the intended molecular targets; in this work, dermal APCs.[19]

Specifically, the transfection efficacy of PBAE-derived PEMs when deposited onto the surface of polymeric rods and MNs was examined and compared to that mediated by nanoparticles using polyplexes as positive control group (**Figure III-5**, top panel). Briefly, MNs arrays were fabricated using PLGA, a biocompatible polymer only soluble in organic solvent, which allowed us to coat them with aqueous solutions containing the PBAEs and the pDNA without risks of eroding or compromising the geometry and tridimensional structure of the MN patch. Assessment of gene transfection by fluorescent microscopy confirmed that PBAE:pDNA polyelectrolyte films could induce gene expression when deposited into surfaces other than the rods (**Figure III-5**, bottom panel) and reaffirming their ability to conformally coat complex surfaces. Superior transfection levels were reported for coated polymeric MNs if compared to those promoted by coated PCL rods, which was attributed to the increased surface area of the MNs. Because of the patch indentations and its wider dimeter, the area that was in direct contact with the cells was superior for those wells containing MNs than for those incubated with rods. Finally, higher levels of transfection were observed for those cells incubated with polyplexes, which were predicted to be a consequence of the higher amounts of pDNA added per well in comparison to those added for the films.
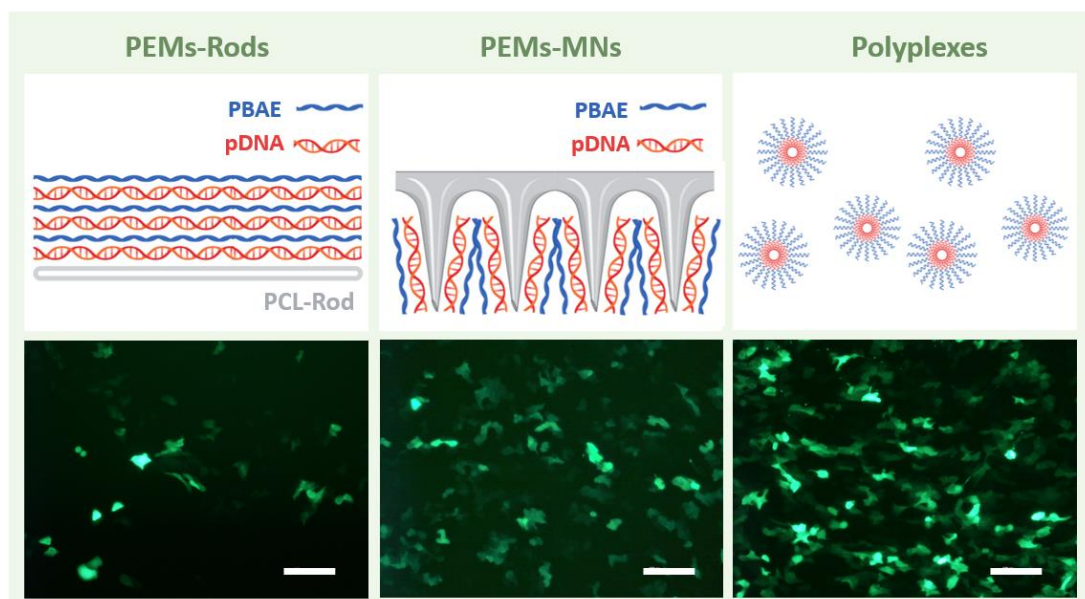
**Figure III-5. Analysis of gene expression in HaCaT cells using PBAE-decorated delivery systems.** Fluorescence microscopy following transfection with K/D-Man polymers as (1) PBAE:pDNA films when deposited in PCL rods and PLGA-based MNs or as (2) polyplexes. Scale bar = 50 μm.

## 3.4.2 Substrate decoration of transdermal devices via plasma treatment for enhanced PEM deposition

Surface functionalization via molecular design has been a key approach to incorporate new functionalities into existing biomaterials for biomedical applications. Some key technologies include chemical conjugation, self-assembled monolayers, LbL film deposition (as described here in this chapter), or plasma treatments.[32] The latest hold great potential since they enable chemical surface modification of various materials and can be applied on flexible and complex-shaped scaffolds such as MNs without cracking.

Hence, we decided to further iterate the design of the MNs by adding reactive polymeric coatings via plasma treatment so as to promote adhesion of PEMs to the MNs surface. In the previous section (**Figure III-5**), it was confirmed that transfection levels induced by PEM-coated MNs rivalled with those induced by polyplexes — even when far less pDNA was added. For this reason, it was hypothesized that pre-coating the MN surface with polymeric films displaying reactive anchorage points could boost even more PEM deposition and in turn, transfection efficacy, rendering a superior solvent-free platform for gene vaccination.

Given the expertise of our group in plasma surface modification, we first leveraged a well-described strategy based on plasma enhanced chemical vapor deposition (PECVD). By exposing a substrate to oxygen/argon plasma, highly reactive radicals are generated on its surface that can be used to graft various vaporized molecules such as pHEMA, Poly(acrylic acid), Allylamine, or Pentafluorophenyl Methacrylate (PFM).[33,34] PFM is known to preferably react with amine-bearing molecules to obtain biocompatible and bioactive surfaces,[35] so we decided to vaporize PMF onto the MN surface in an attempt to boost its interaction with the amine groups present in the PBAEs backbone. Following plasma treatment, MNs were decorated with PBAE:pDNA bilayers and incubated with HaCaT cells as our permissive cell line model to assess transfection efficiency.

Analysis of gene expression by fluorescence microscopy proved that dual coatings with plasma polymerized (pp)-PFM and PBAE derived PEMs could mediate substantial levels of gene transfer (**Figure III-6**, left). Results illustrated that transfection was confined to the areas in close contact with the MN arrays as confirmed before. Overall levels of gene transfection were notable, but still inferior to those achieved by polyplexes. If comparing pp-PEM-MNs to PEM-MNs, evident differences were not observed between the two of them, yet solely relying on qualitative assessment could be deceptive. For this reason, further quantification by flow cytometry would be necessary to confirm whether plasma modification is having a positive impact on transfection efficiency.

Analysis of cellular morphology by bright-field microscopy can be used to infer on cellular viability, where phenomena such as cell detachment or morphology change are well-accepted indicators to estimate cell toxicity. Here, surface modification via PECVD did not appear to induce significant cell toxicity in agreement with previous data from our group (**Figure III-6**, right).[35]

## Surface Modification by PECVD
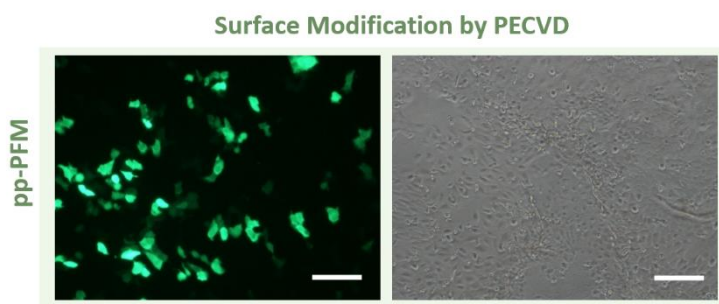


**Figure III-6. Surface decoration of PLGA-based MNs with PFM by PECVD.** MNs were activated in a vertical plasma reactor with an 80:20 mixture of oxygen and argon followed by PFM vaporization as described. Next, PBAE:pDNA-derived PEMs were deposited onto the MNs and these incubated with HaCaT cells for 48 hours. Transfection efficiency was qualitatively assessed by fluorescence microscopy. Scale bar = 50 μm.

We next proposed to immobilize the PEMs by wet/deep coating using dopamine as our coating layer. The various functional groups present in the dopamine backbone can react with a wide range of molecules, allowing the generation of biomaterials with specific functionalities. For instance, the oxidized quinone form of catechol can undergo reactions with various functional groups such as amines or thiols via Michael addition or Schiff base reaction.[32] Therefore, we proposed to leverage the reactivity of dopamine to form covalently grafted functional layers with the PBAEs, as it was hypothesized that the amine groups present in the lateral chains of the OM-/MM-PBAEs could again react with the dopamine coating following a Schiff base reaction.

Briefly, the surface of the MNs was activated via plasma treatment to improve wettability of the substrate and generate reactive radical species. Next, MNs were immersed in a dopamine solution to allow polymerization into polydopamine (PDA) to obtain a highly reactive coating.[36] Next, MNs were further decorated with PBAE:pDNA films and transfection efficiency was evaluated as before. Gene transference was confirmed to be mostly dependent on surface-mediated transfection mechanisms since most transfected cells were localized in those areas of the wells in intimate contact with the MNs patch, whereas GFP-positive cells were rare in those areas not covered with the MN arrays (**Figure III-7,** i). Again, this approach did not seem to surpass transfection levels induced by the non-functionalized MNs (**Figure III-5**). Regarding substrate biocompatibility, results showed that cells incubated with dopamine-coated MNs presented high levels of cellular death (**Figure III-7**, ii) which was predicted to be caused by the readily oxidation of dopamine and the subsequent generation of toxic superoxide radicals.[37]

In light of these findings, the use of a dopamine-modified hyaluronic acid (HADA) coating was proposed instead since the excellent biocompatibility of HA was predicted to surmount the inherent toxicity of dopamine. Transfection assays revealed that MNs coated with HADA induced lower levels of transfection if compared to PDA-coated MNs (**Figure III-7**, iii). It was hypothesized that the dopamine-coated MNs offered more reactive groups and in turn, might have favored PEM adhesion to the MN surface. On the contrary, the chemical linkage of hyaluronic acid may have reduced the number of available reactive groups and so, PEM accumulation. The silver lining was that the inclusion of HA moieties in the coating appeared to mitigate the inherent cytotoxicity of dopamine.[38] (**Figure III-7**, iv). In hopes of avoiding local toxicity, strategies using HADA would be preferable over dopamine-based if translating this platform to the clinic. Despite their worse performance in terms of transfection efficiency, we believe that biocompatibility should be prioritized over efficacy to avoid

toxic effects that could eventually induce skin irritation, inflammation or erythema following MN administration.
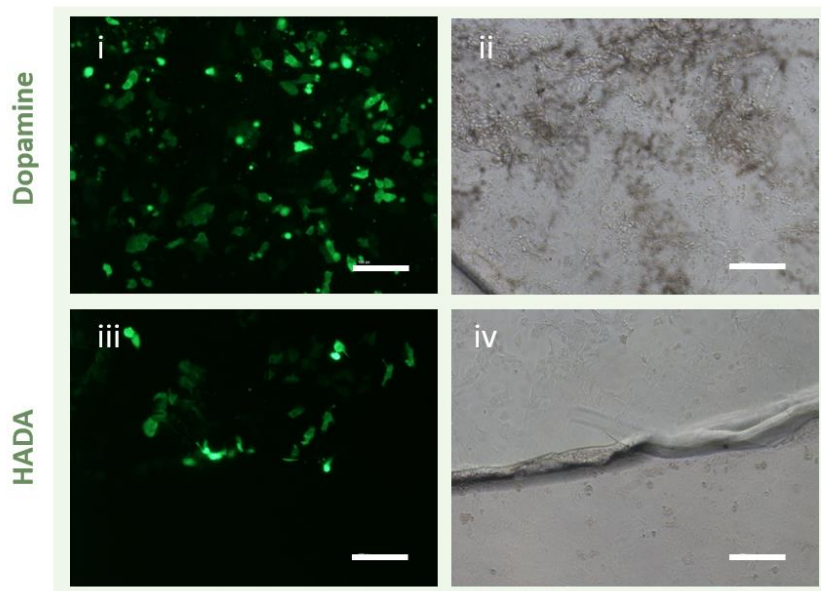


**Figure III-7. Modification of polymeric, PLGA-based MNs via plasma activation followed by deep coating with reactive monomers.** MNs were first treated by $O_2$/argon plasma activation to generate reactive radicals and were subsequently submerged in a 2 mg $mL^{-1}$ solution of either dopamine (top panel) or HADA (bottom panel) for 12 hours. Next, K/D-Man PBAE:pDNA films were deposited via LbL an incubated with HaCaT cells. Transfection efficiency was examined by fluorescence microscopy and cytotoxicity by bright field microscopy. Scale bar = 50 μm.

Per our preliminary screening, functionalization of the surface of MNs via plasma treatments did not appear to significantly improve the overall levels of transfection *in vitro*. For this reason, the plasma treatment step was obviated in future studies given its limited benefit to the overall performance of the platform and their reported cytotoxicity in some cases.

Nevertheless, a more thorough study would be advisable in the future to fully quantify the PEM deposition yield following surface decoration. We predict that these treatments, even if not impacting directly on transfection efficiency, could be useful for further translational steps to ensure uniformity and reproducibility of the LbL coatings.

### 3.4.3 Gene delivery studies using PBAE-decorated transdermal devices

Given the potential of OM- and MM-PBAE candidates to induce both nanoparticle- and surface-mediated transfection, their performance was examined using a three-pronged approach including *in vitro*, *ex vivo* and *in vivo* analysis. Specifically, transfection efficacy was compared when embedded or deposited into transdermal devices as optimized throughout this chapter.

#### 3.4.3.1 *In vitro* assessment of transfection efficiency in human Langerhans cells (MoLCs)

First, the transfection efficiency of the PBAE-based delivery systems was assessed using human-derived Langerhans cells (MoLCs), our main cellular target. Evaluation of GFP expression by flow cytometry confirmed the superiority of polyplexes (**Figure III-8A**), where the K/D-Man-PBAEs surpassed all the approaches screened and registered a ≈10-fold increased efficiency if compared to an advanced commercial vector (Lipofectamine3000). The unsurpassable performance of PBAE polyplexes encouraged us to include yet another transdermal approach based on nanoparticles in our studies; specifically, an array of dissolvable MNs made of poly(vinyl alcohol) (PVA) which embedded PBAE polyplexes in their matrix. Dissolvable MNs possess numerous advantages namely, low-cost, facile production by micromoulding and that the risk of leaving biohazardous sharp waste in the skin is eliminated as they dissolve upon contact with the skin interstitial fluid.[24] Surprisingly, gene expression was not observed when incubating the dissolvable MN arrays with MoLCs despite adding an equal amount of polyplexes as for the control group and which was hypothesized to be caused by a premature disassembling of the polyplexes during the fabrication process.

In parallel, PBAE:pDNA films also triggered notable levels of gene transference when deposited in both polymeric rods and solid MNs, which rivalled or even outperformed those obtained by the commercial control. No differences in gene expression were observed when using OM-PBAEs films (K/D) or their mannosylated counterparts (K/D-Man), evidencing the need for further studies to fully address the role of targeting moieties in surface-mediated transfection. Overall, levels of gene expression induced by PBAE:pDNA films were significantly lower if compared to those mediated by the corresponding PBAE-derived polyplexes. Reduced transfection percentages were attributed to the limited deposition yield of pDNA –being 100-times lower if normalized to the μg of pDNA added per well and compared to the ug added when using polyplexes. Nevertheless, such low deposition yield could be addressed in the future as it has been reported that up to 40 bilayers can be piled[9]. Also, the reduced surface area of the substrates limited the number of cells in close contact with them

for effective transfection as their area just accounted for a tenth of the total cell growth (for polymeric rods) or half (for MNs).
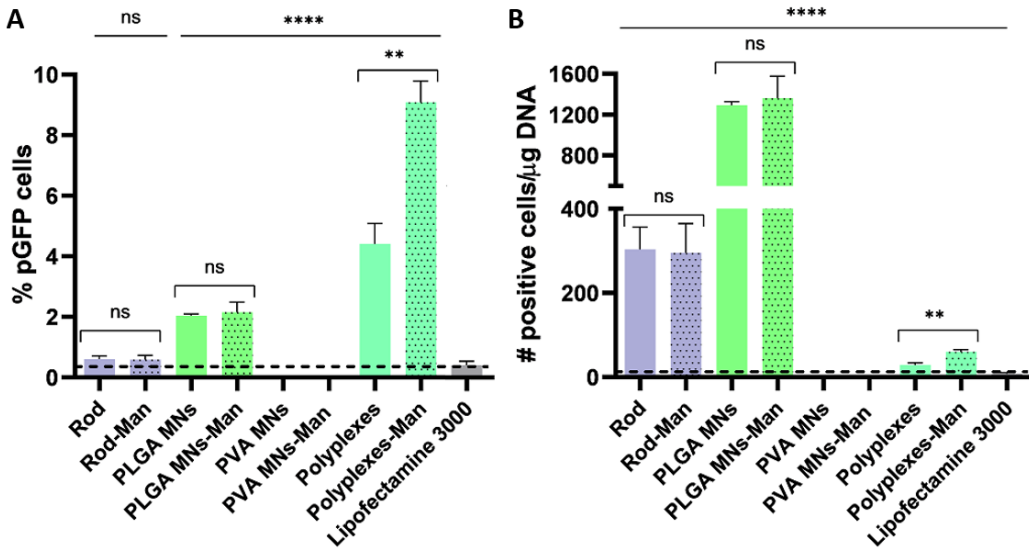


**Figure III-8. Screening of pGFP expression in MoLCs cells by flow cytometry following transfection with PBAE-based delivery systems.** Number of transfected cells are presented as total GFP-positive events (A) or theoretically normalized to the amount of pDNA added per well during transfection (B). Values from our previous dsDNA quantification assay in rods were extrapolated for coated MNs. Unless stated, statical significance was determined against Lipofectamine3000 as the control group. (ns = non-significant, $*p<0.05$, $**p<0.01$, $***p<0.001$, $****p < 0.0001$).

Using the same data as for **Figure III-8A**, the number of transfected cells was represented as a function of µg of DNA per well instead of total positive cells to obtain a more truthful insight into the actual transfection yields (**Figure III-8B**). Theoretically, delivery using PBAE:pDNA films appeared to dominate over nanoparticle-based strategies if normalizing transfection yields to mass of pDNA added per well, and where coated MNs induced the highest levels of gene delivery with a 100-fold increased efficiency. After them, polymeric rods also promoted notable levels of transfection, followed by polyplexes in the last place. More importantly, all PBAE-derived systems would appear to surpass the commercial standard for transfection (Lipofectamine 3000). While strictly theoretical, these results support the potential of polyelectrolyte films for solvent-free gene vaccination, especially when integrated with minimally-invasive devices such as MNs.

### 3.4.3.2 Evaluation of transfection efficiency *ex vivo* following transdermal gene delivery

We next added a layer of complexity to our model and proceeded to validate the potential of PBAE-derived systems *ex vivo* using murine skin explants. Driven by the lessons learned from previous experiments, both PEM-derived PBAEs and polyplexes were included in this study, yet the latest were repurposed given their poor performance when embedded in dissolvable MNs (**Figure III-8A**). Specifically, the use of solid, stainless-steel MNs was contemplated as means for "poke and patch". This approach leverages the mechanical strength of solid MNs to disrupt the skin and create microchannels. Following application, the MN array is retrieved and then the drug is applied in a conventional dosage form such as cream or emulsion; here, the PBAE solution.[39] Despite involving multiple steps and the increased risk of infection over other MN-based approaches,[17] its simplicity makes it highly attractive for translation into clinical settings.

Firstly, the ability of the medical devices to pierce the skin and deposit the PEMs/polyplexes was studied, both much needed abilities to ensure transdermal gene delivery. It was confirmed that polymeric rods could be easily implanted, yet the unavoidable invasiveness of these was expected to be a limiting factor for widespread adoption and patient acceptance (**Figure III-9**, top panel). Contrarily, MN administration was a user-friendly procedure that managed to effectively pierce the skin as evidenced by the presence of microconduits in the epidermis (**Figure III-9**, middle and bottom panel). We next examined whether PBAE:pDNA polyelectrolyte films would be released in the skin upon administration and whether polyplexes would be deposited using the "poke and patch" approach. Both polymeric rods and MNs were coated as described with bilayers of fluorescently-labelled polymer and pDNA and film deposition was confirmed by fluorescent microscopy (**Figure III-9**,vii, viii). Next, the devices were implanted in the skin explants and imaged likewise. Film release was especially evident for those explants pierced with the MNs, since the polymer could be observed all over the margins of the microconduit (**Figure III-9**, x, xi), confirming the adequacy of these approaches for future *in vivo* application. Similarly, disrupting the skin with solid MNs followed by the addition of polyplexes immediately after proved to be a feasible approach to fill the microconduits with prospective therapeutic products (**Figure III-9**, xii).
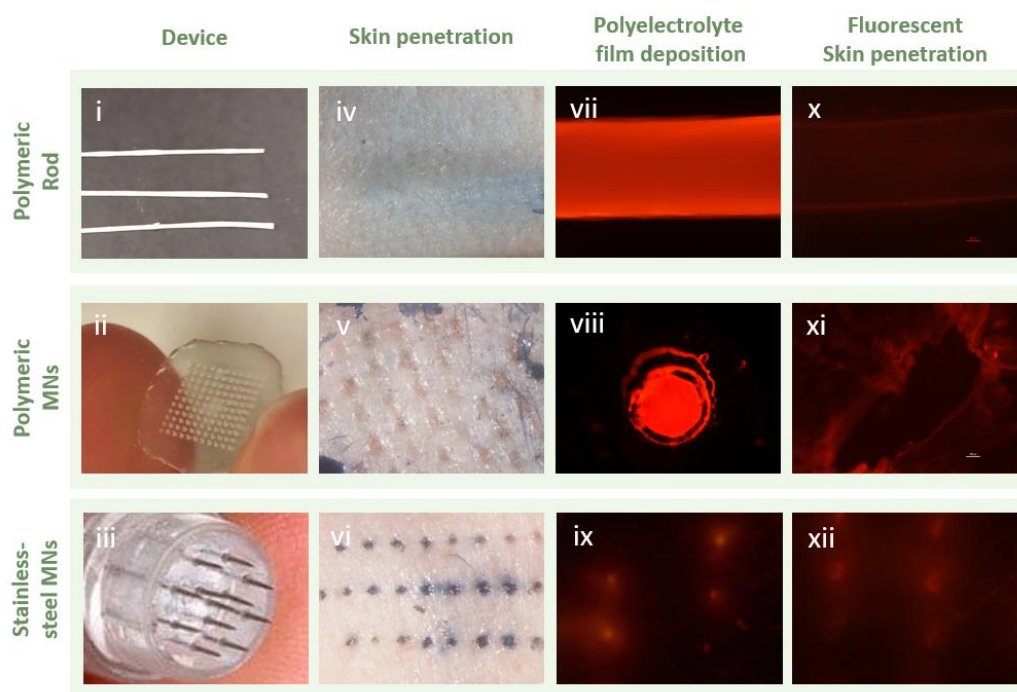
**Figure III-9.** *Ex vivo* **characterization of medical devices for prospective vaccine delivery using PBAE polyelectrolyte films.** Capacity of transdermal devices to effectively penetrate the skin was tested using cadaveric skin explants harvested from C57BL/6 healthy mice. Also, film and nanoparticles delivery using rods (top panel), solid PLGA-based MNs (middle panel) and stainless steel-MNs (bottom panel) was confirmed by fluorescence microscopy.

Transfection efficiency was then studied using an *ex vivo* model mimicking the physiological conditions of the skin by incubating the epidermis layer facing up to allow exposure to the liquid-air interface as others before (**Figure III-10**).[40] Maintenance of the skin structure using this model is ensured for up to 12 days,[30] making it a reliable model before moving forward with *in vivo* studies.



**Figure III-10.** *Ex vivo* **model for transdermal skin transfection.** Murine skin explants harvested from C57BL/6 healthy mice were sutured to steel mesh and incubated with supplemented media at the air-liquid interface.[30]

Skin explants were transfected via (1) nanoparticle-mediated strategies using polyplexes injected with hypodermic needles or with solid MNs using the "poke and patch" method or via (2) surface-mediated strategies including PEM-coated rods and MNs. In all cases, K/D and the K/D-Man PBAE formulations complexing pDNA were used. Mechanistic analysis were performed 24 hours post-transfection, where half of the skin explants were enzymatically digested and processed for single-cell flow cytometry whereas the other half was reserved for IHF.

Analysis of gene expression in the skin by flow cytometry was inconclusive (data not shown), since isolating GFP-positive events without a gating strategy was a gruesome task given the cellular complexity of the tissue. Hence, isolating the elusive APCs, owing to their scarce numbers, was not feasible without a prior staining to immunophenotype the different subsets. For this reason, future studies should be performed using surface receptors-staining panels for reliable insight on the transfection efficacy of each PBAE-derived system and the identity of the transfected cells.

Contrarily, promising results were observed when processing skin sections by fluorescence microscopy as positive events were identified scattered throughout the tissue slides (**Figure III-11**), although the total number of transfected cells was low. The majority of the events was concentrated in those explants treated with polyplexes yet none of the two strategies (hypodermic injection or MN-mediated administration) appeared to outperform the other in terms of transfection efficiency. Encountering GFP-positive cells was rare for those skin explants transfected with PEM-derived PBAEs regardless of the delivery device utilized. The tentative explanation for such low yield in all the treatments could be the higher transfectability of dividing cells than non-mitotic cells as plasmid DNA needs to reach the nucleus to induce gene expression, a phenomenon that mostly occurs during nuclear envelop disassembly when cells are dividing.[41] Here, cellular division could not be expected since an *ex vivo* model —rather than an *in vivo*—was used, thus limiting the opportunities for nuclear penetration. It was predicted that utilizing mRNA instead could improve overall levels of gene expression since translation of the therapeutic cargo occurs in the cellular cytosol rather than the nucleus so cell transfection should be facilitated.[42]

Finally, it was also of note the intense autofluorescence of the skin, a major experimental pitfall. Various parameters such as the fixation agent or incubation time were thoroughly adjusted in an attempt to minimize the interfering background fluorescence with little success. In future studies, using alternative methods such as immunohistochemistry (IHC) or secondary staining against pGFP by IHF could prove useful to augment the sensitivity of the analysis.
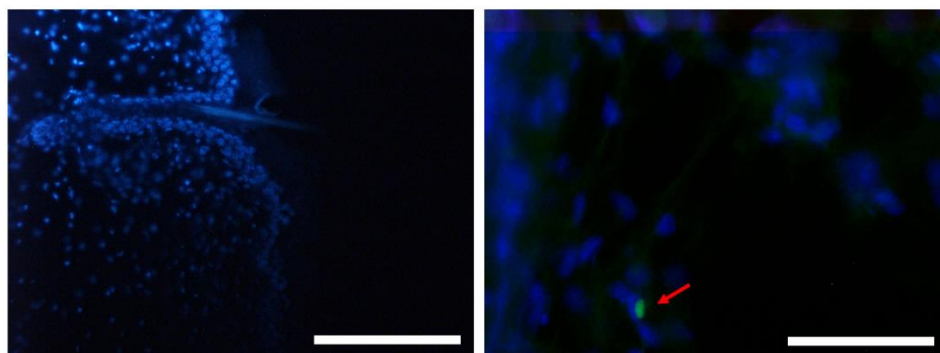
**Figure III-11.** *Ex vivo* **evaluation of transfection efficiency using PBAE-derived systems integrated in transdermal devices.** Cadaveric skin explants harvested from C57BL/6 healthy mice were administered one of the following treatments (n=2): (1) Injection of PBAE derived polyplexes using the Mantoux technique, (2) "poke and patch" solid MNs, (3) LbL-coated PLGA MNs and (4) LbL-coated rod implantation. Explants were cryosectioned 24 hours-post transfection and gene expression was assessed by microscopic fluorescence. Images depict 50 μm-skin slides corresponding to treatment (1). Scale bar = 200 μm (left), 50 μm (right).

### 3.4.3.3  *In vivo* gene delivery with PBAE-derived systems using the transdermal route

Lastly, the transfection efficiency of PBAE-derived systems when administered through the transdermal route was tested *in vivo* using a healthy murine model (**Figure III-12**). Same treatment groups were used as for the *ex vivo* assays, yet mRNA was complexed instead and the mechanistic analysis was restricted to fluorescence imaging by confocal microscopy for enhanced examination.
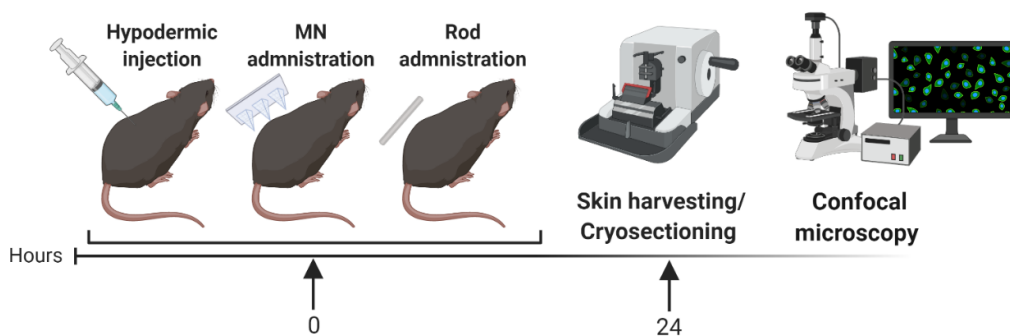


**Figure III-12. Schematic representation of the experimental design followed to assess gene transfection *in vivo*.** C57BL/6 healthy mice were administered one of the following treatments (n=1): (1) Injection of PBAE-derived polyplexes using the Mantoux technique, (2) Injection of PBAE polyplexes mediated by MNs (3) LbL-coated PLGA MNs and (4) LbL-coated rod implantation. 24 hours post-treatment, mice were euthanized and skin explants surrounding the area of treatment were harvested for mechanistic analysis. Skins were cryosectioned and imaged by confocal microscopy. Polyplexes and PEMs used for transfection derived from the K/D-Man-PBAE.

Administration of polyplexes was conducted via Mantoux injection or via "poke and patch" using stainless steel MNs. Again, transdermal injection using a hypodermic needle was highly technical whether the MN patch was easily applied in a minimally-invasive manner. Analogously, implantation of the LbL-coated rods required a sophisticated surgery while PEM-loaded MNs were thumb-pressed against the skin without further difficulties. When translated into clinical settings, we predict that invasiveness will be a determining factor for widespread acceptance. Therefore, using MNs — decorated with either polyplexes or PEMs— would represent an improvement upon current methods.

Gene expression following transdermal transfection was proven for all groups except for the rods coated with PBAE:mRNA films (**Figure III-13**). The most plausible explanation for such divergent outcome was the failure to implant the rods in the dermal compartment and that these remained lodged in the cavity below the subcutaneous fat layer instead, away from its intended cellular target. GFP-positive cells were observed after delivery with the rest of PBAE-derived platforms and where once again, the majority of positive events was concentrated in those mice treated with polyplexes; both via hypodermic- and MN-mediated injection. Our data pointed at the superiority of polyplexes to deliver nucleic acids *in vivo*, yet the low PEM deposition yields observed in previous experiments might be the most plausible explanation on why the threshold to attain effective transfection was barely met for coated-MNs. Hence, further efforts should aim to augment PEM deposition and so, boost their transfection capacity.
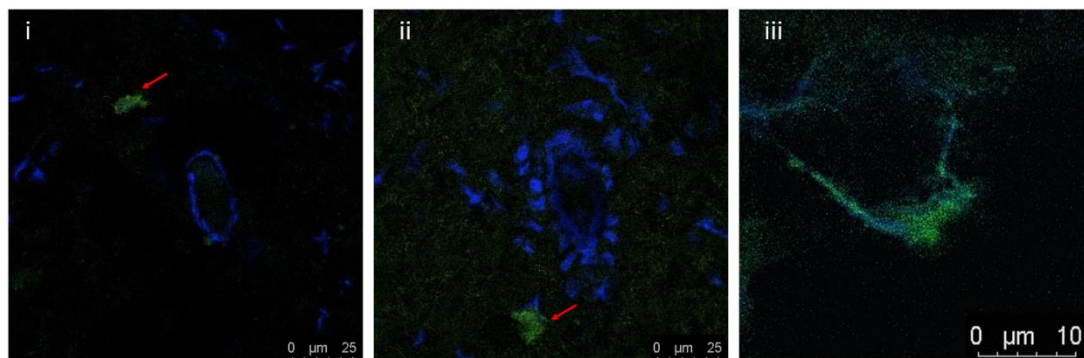


**Figure III-13. Assessment of gene expression following *in vivo* transdermal mRNA delivery.** Skin explants were harvested 24 hours post transdermal transfection and cryosectioned rendering 50 µm-thick tissue slides. Skin sections were stained using DAPI for nuclei visualization. GFP expression after transfection with PBAE-derived systems was confirmed by confocal microscopy. Confocal images are the merge of DAPI staining channel (blue) and FITC channel (green) and correspond to the mouse administered polyplexes via "poke and patch". Polyplexes and PEMs used for transfection derived from the K/D-Man-PBAE formulation.

A higher number of transfected cells was observed if compared to previous *ex vivo* transfection assays as evidenced by the presence of various positive cells across the same section **(Figure III-13**, ii), which was hypothesized to be induced by the use of mRNA as therapeutic model. Moreover, screening with high-power objectives allowed us to confirm the presence of transfected cells displaying dendrite-like structures, a feature shared by most professional APCs residing in the skin such as LCs or dDCs and which hinted that targeted gene vaccination might be achieved (**Figure III-13**,iii). Though preliminary, these results pointed at the potential of OM- and MM-PBAEs to mediate effective gene transfer in the skin using local, minimally-invasive transdermal delivery approaches.

## 3.5  Concluding remarks

The results of this chapter prove that the newly synthesized family of OM- and MM-PBAEs can be integrated with transcutaneous medical devices in the form of polyplexes or PEMs for local gene delivery. Capacity of OM- and MM-PBAEs to induce both nanoparticle and surface-mediated transfection was confirmed at *in vitro*, *ex vivo* and *in vivo* level.

Deposition of OM- and MM-PBAEs as PEMs was achieved using the Layer-by-Layer method. Mannosylation did not appear to impact *in situ* polyplex formation nor transfection efficiency when assessed in a permissive cell line. Contrarily, the dilution buffer used for PEM deposition had a clear influence, rendering bigger aggregates with poor performance when using AcONa if compared to PBS. The number of bilayers of the PEMs correlated with their transfection efficiency. PBAE-derived PEMs managed to coat geometrically complex medical devices such as MNs and polymeric rods for solvent-free gene delivery, with MNs displaying a superior performance owing to their increased surface area.

Surface modification via plasma treatment can be leveraged for biomedical applications. Decoration of the MN substrate with reactive functional groups did not appear to significantly improve overall levels of transfection, yet these techniques could prove useful for clinical translational of the platform to confer uniformity and reproducible PEM deposition.

Screening of the transfection efficiency of PBAE-derived systems *in vitro* using human Langerhans cells (MoLCs) proved the unmatchable superiority of these approaches over a commercial vector, Lipofectamine 3000, and where the percentage of transfected cells was 10-times higher when using the mannosylated polyplexes. Polymeric devices coated with PBAE:pDNA films also induced considerable levels of gene transfer, yet those were significantly lower when using total number of transfected cells as the biological readout. Contrarily, normalization of GFP-positive events per mass of pDNA added per well hinted that theoretically, surface-mediated transfection could trigger greater levels of gene transfer than their polyplex-based counterparts.

The capacity of PEMs-derived systems to penetrate the skin and deposit their therapeutic cargo was confirmed using skin explants as an *ex vivo* model. Likewise, the "poke and patch" was proven to penetrate the skin. Effective gene delivery was proven, yet the overall levels of transfected cells were poor which was hypothesized to stem from the low transfectability of non-mitotic cells.

In a similar fashion, *in vivo* studies confirmed the suitability of MN-mediated delivery over invasive approaches such as rod implantation or hypodermic vaccination. Overall levels of gene transfection

were superior when using PBAE:mRNA-derived systems *in vivo*, and where nanoparticles appeared to mediate enhanced levels of gene transfer. Transfection of cells displaying dendrite-like morphologies suggests the potential of OM-/MM-PBAE-derived systems for targeted gene delivery.

In conclusion, we have developed alternative methods based on PBAEs for gene vaccination using PEMs as our building block for nucleic acid adsorption. PBAE-derived PEMs induced gene transfer via surface-mediated transfection, proving the potential of PBAEs for nanoparticle- and solvent-free delivery. We confirmed that both polyplexes and PEMs could be coupled to medical transdermal devices for *in vivo* gene transfer and where minimally-invasive delivery using MNs induced comparable levels of transfection to those reported from invasive alternatives opening up potential avenues for needle-free prophylactic and therapeutic vaccination.

Here, we have proven the potential of PBAEs integrated with MNs platforms for transdermal immunization in the context of gene vaccination. In the next chapter, we will shift the focus to another immunotherapy, checkpoint blockade for cancer treatment, where hydrogel-based MNs loaded with PBAEs will be used to deliver nucleic acids serving as immunostimulatory drugs. Having confirmed their capacity for minimally-invasive delivery, we will also integrate a diagnostic compartment to our MN patch as part of a closed-loop system to simultaneously monitor the response to therapy.

## 3.6 References

1. Liu, Y., Li, Y., Keskin, D. & Shi, L. Poly (β -Amino Esters ): Synthesis, Formulations, and Their Biomedical Applications. *Adv. Healthc. Mater.* 8, 1–24 (2019).

2. Nguyen, B. D. N., Green, J. J., Chan, J. M., Langer, R. & Anderson, D. G. Polymeric Materials for Gene Delivery and DNA Vaccination. *Adv. Healthc. Mater.* 20, 1–21 (2008).

3. Iqbal, S. *et al.* Poly (β-Amino Esters) based Potential Drug Delivery and Targeting Polymer; An Overview and Perspectives. *Eur. Polym. J.* 141, 110097 (2020).

4. Zhang, J., Chua, L. S. & Lynn, D. M. Multilayered Thin Films that Sustain the Release of Functional DNA under Physiological Conditions. *Langmuir* 20, 8017 (2004).

5. Yu, Y., Si, Y., Bechler, S. L., Liu, B. & Lynn, D. M. Polymer Multilayers that Promote the Rapid Release and Contact Transfer of DNA. *Biomacromolecules* 16, 2998–3007 (2015).

6. Bechler, S. L. & Lynn, D. M. Characterization of degradable polyelectrolyte multilayers fabricated using DNA and a fluorescently-labeled Poly(B-amino ester): Shedding light on the role of the cationic polymer in promoting surface-mediated gene delivery. *Biomacromolecules* 13, 542–552 (2012).

7. Jewell, C. M., Zhang, J., Fredin, N. J. & Lynn, D. M. Multilayered polyelectrolyte films promote the direct and localized delivery of DNA to cells. *J. Control. Release* 106, 214–223 (2005).

8. Cordeiro, R. A., Serra, A., Coelho, J. F. J. & Faneca, H. Poly (β-amino ester )-based gene delivery systems: From discovery to therapeutic applications. *J. Control. Release* 310, 155–187 (2019).

9. Su, X., Kim, B. S., Kim, S. R., Hammond, P. T. & Irvine, D. J. Layer-by-layer-assembled multilayer films for transcutaneous drug and vaccine delivery. *ACS Nano* 3, 3719–3729 (2009).

10. Kyobum Kim, W., C.W. Chen, Y. H. & Wang, Y. Polycations and Their Biomedical Applications. *Prog. Polym. Sci.* 60, 18–50 (2016).

11. Kis, E. E., Winter, G. & Myschik, J. Devices for intradermal vaccination. *Vaccine* 30, 523–538 (2012).

12. Oehr, C. Plasma surface modification of polymers for biomedical use. *Nucl. Instruments Methods Phys. Res.* 208, 40–47 (2003).

13. Liston, E. M., Martinu, L. & Wertheimer, M. R. Plasma surface modification of polymers for improved adhesion: a critical review. *J. Adhes. Sci. Technol.* 7, 1091–1127 (1993).

14. Chen, Z. *et al.* Overcoming or circumventing the stratum corneum barrier for efficient transcutaneous immunization. *Drug Discov. Today* 23, 181–186 (2018).

15. Kaurav, M. *et al.* Nanoparticulate mediated transcutaneous immunization: Myth or reality. *Nanomedicine NBM* 12, 1063–1081 (2016).

16. Mitragotri, S. Immunization without needles. *Nat. Rev. Immunol.* 5, 905–916 (2005).

17. Guillot, A. J. *et al.* Microneedle-based delivery: An overview of current applications and trends. *Pharmaceutics* 12, 1–28 (2020).

18. Rzhevskiy, A. S., Raghu, T., Singh, R., Donnelly, R. F. & Anissimov, Y. G. Microneedles as the technique of drug delivery enhancement in diverse organs and tissues. *J. Control. Release* 270, 184–202 (2017).

19. Lee, K. J. *et al.* A practical guide to the development of microneedle systems – In clinical trials or on the market. *Int. J. Pharm.* 573, 118778 (2020).

20. Kim, Y.-C., Park, J. H. & Prausnitz, M. R. Microneedles for drug and vaccine delivery. *Adv. Drug Deliv. Rev.* 64, 1547–1568 (2012).

21. Ita, K. Transdermal Delivery of Drugs with Microneedles-Potential and Challenges. *Pharmaceutics* 7, 90–105 (2015).

22. Oosterhuis, K., Berg, J. H. van den, Schumacher, T. N. & Haanen, J. B. A. G. DNA Vaccines and Intradermal Vaccination by DNA Tattooing. *Curr. Top. Microbiol. Immunol.* 351, 3–32 (2010).

23. Suh, H., Shin, J. & Kim, Y. Microneedle patches for vaccine delivery. *Clin. Exp. Vaccine Res.* 3, 42–49 (2014).

24. Larrañeta, E., Lutton, R. E. M., Woolfson, A. D. & Donnelly, R. F. Microneedle arrays as transdermal and intradermal drug delivery systems: Materials science, manufacture and commercial development. *Mater. Sci. Eng. R* 104, 1–32 (2016).

25. Kim, N. W. *et al.* Polyplex-releasing microneedles for enhanced cutaneous delivery of DNA vaccine. *J. Control. Release* 179, 11–17 (2014).

26. DeMuth, P. C. *et al.* Polymer multilayer tattooing for enhanced DNA vaccination. *Nat. Mater.*

12, 367–76 (2013).

27. Demuth, P. C., Garcia-Beltran, W. F., Ai-Ling, M. L., Hammond, P. T. & Irvine, D. J. Composite dissolving microneedles for coordinated control of antigen and adjuvant delivery kinetics in transcutaneous vaccination. *Adv. Funct. Mater.* 23, 161–172 (2013).

28. Demuth, P. C., Su, X., Samuel, R. E., Hammond, P. T. & Irvine, D. J. Nano-layered microneedles for transcutaneous delivery of polymer nanoparticles and plasmid DNA. *Adv. Mater.* 22, 4851–4856 (2010).

29. Texidó, R., Orgaz, A., Ramos, V. & Borrós, S. Stretchable conductive polypyrrole films modified with dopaminated hyaluronic acid. *Mater. Sci. Eng. C* 76, 295–300 (2017).

30. Xu, W. *et al.* Application of a partial-thickness human ex vivo skin culture model in cutaneous wound healing study. *Lab. Investig.* 92, 584–599 (2012).

31. Vargason, A. M., Anselmo, A. C. & Mitragotri, S. The evolution of commercial drug delivery technologies. *Nat. Biomed. Eng.* (2021) doi:10.1038/s41551-021-00698-w.

32. Ding, Y. H., Floren, M. & Tan, W. Mussel-inspired polydopamine for bio-surface functionalization. *Biosurface and Biotribology* 2, 121–136 (2016).

33. Vasudev, M. C., Anderson, K. D., Bunning, T. J., Tsukruk, V. V & Naik, R. R. Exploration of Plasma-Enhanced Chemical Vapor Deposition as a Method for Thin-Film Fabrication with Biological Applications. *ACS Appl. Mater. Interfaces* 5, 3983–3994 (2013).

34. Texidó, R. & Borrós, S. Allylamine PECVD Modification of PDMS as Simple Method to Obtain Conductive Flexible Polypyrrole Thin Films. *Polymers* 11, 1–13 (2019).

35. Gilabert-Porres, J. *et al.* Design of a Nanostructured Active Surface against Gram-Positive and Gram-Negative Bacteria through Plasma Activation and in Situ Silver Reduction. *ACS Appl. Mater. Interfaces* 8, 64–73 (2016).

36. Hauser, D., Septiadi, D., Turner, J., Petri-fink, A. & Rothen-rutishauser, B. From Bioinspired Glue to Medicine: Polydopamine as a Biomedical Material. *Materials (Basel).* 13, 1–22 (2020).

37. Lih, E., Choi, S. G., Ahn, D. J., Joung, Y. K. & Han, D. K. Optimal conjugation of catechol group onto hyaluronic acid in coronary stent substrate coating for the prevention of restenosis. *J. Tissue Eng.* 7, 1–11 (2016).

38. Larrañeta, E. *et al.* Synthesis and characterization of hyaluronic acid hydrogels crosslinked

using a solvent-free process for potential biomedical applications. *Carbohydr. Polym.* 181, 1194–1205 (2018).

39.    Al-Zahrani, S. *et al.* Microneedle-mediated vaccine delivery: Harnessing cutaneous immunobiology to improve efficacy. *Expert Opin. Drug Deliv.* 9, 541–550 (2014).

40.    Mandal, A. *et al.* Cell and fluid sampling microneedle patches for monitoring skin-resident immunity. *Sci. Transl. Med.* 10, (2018).

41.    Mintzer, M. A. & Simanek, E. E. Nonviral Vectors for Gene Delivery. *Chem. Rev.* 109, 259–302 (2009).

42.    Reichmuth, A. M., Oberli, M. A., Jaklenec, A., Langer, R. & Blankschtein, D. mRNA vaccine delivery using lipid nanoparticles. *Ther. Deliv.* 7, 319–334 (2016).

# Chapter IV: PBAE-loaded hydrogel MNs for cancer immunotherapy

This page left blank intentionally

## 4.1  Introduction

The birth of cancer immunotherapy dates back to the 1900s with the pioneering —yet dangerous— use of bacterial "Coley's toxins" to unleash cytotoxic immune responses.[1] Today, harnessing the immune system to combat cancer is a clinical reality.[2] Traditionally, the hallmarks of cancer treatment included intravenous cytotoxic chemotherapy, radiation therapy and surgery,[3] yet their associated off-target effects and long-term sequela were a source of concern for both patients and clinicians. Instead, immunotherapies propose to deploy the patient's own immune system to attack malignant neoplasms in a targeted fashion.[4] Fueled by the striking results and improved prognosis of patients enrolled in clinical trials, immunotherapies are now a standard pillar of cancer treatment with checkpoint blockade immunotherapies amassing great popularity in the field.[2,5]

Activating antitumor immunity can be achieved by blocking immune checkpoints, inhibitory pathways used by cancer cells to elude and restrain the host's T-cell responses against the tumors.[6] Interrupting co-inhibitory signaling pathways with antibodies is now proven to restore immune-mediated eradication of tumor cells and achieve complete elimination of detectable tumor burden in the most favorable cases.[7] Originally, checkpoint inhibitors had been mostly directed into treating hematological cancers, but in recent years they have also shown great promise in the treatment of solid-tumor cancers and others not previously regarded as "immunogenic" such as lung cancer.[8,9] The most common checkpoint inhibition strategies include CTLA4 inhibition and PD1-PD-L1 blockade, with six inhibitors currently approved by the FDA owing to their superiority in extending patient survival.[10]

While efficacies of checkpoint inhibitors strongly depend on the cancer type, overall response rates have rarely exceeded 40%.[11] Such low responsiveness still evades understanding, though evidence points at tumor mutational burden, deregulation of checkpoints in both tumoral and T cells, and mechanisms of innate and adaptive resistance as the main orchestrators of such outcome.[9,11,12] Moreover, patient responsiveness might be dictated by the different tumor microenvironments and their immunosuppression level, as each possesses its own mechanisms to evade the immune system.[5]

Emerging evidence suggests that tumors with highly immunosuppressive microenvironments could benefit from multi-arm therapeutic regimens combining checkpoint inhibitor therapies with the delivery of immunostimulatory molecules.[13,14] These candidates can act as innate immune effectors and contribute to anti-tumor immunity,[15] eliciting a synergic effect with adaptive-mediated approaches such as checkpoint inhibitors to ultimately synchronize both compartments of the

immune system into fighting tumors. The increased responsiveness to combinatorial therapy is suspected to derive from the enhanced immunogenicity of tumors, increased presentation of tumor antigens and the abrogation of immunosuppressive signaling.[16] Proposed immunostimulatory therapeutics include STING agonists, biological agents such as oncolytic viruses, and oligonucleotide ligands/agonists of various immune receptors.[17]

Toll-like receptors (TLRs) are pattern recognition receptors (PRRs) intracellularly expressed by immune cells including dendritic cells, macrophages, natural killer cells, and other antigen-presenting cells and which function as primary sensors of the innate immune system.[18,19] TLRs recognize and can be activated by unmethylated cytosine-phosphate-guanine (CpG) oligodinucleotides (ODNs) which, upon binding, can initiate a cascade of innate and adaptive immune responses.[20] Among the ten TLRs discovered so far, TLR9 specifically activates plasmacytoid dendritic cells and B cells, resulting in potent T helper-1 (Th1)-type immune responses and antitumor responses (**Figure IV-1**).[21] Therefore, dual therapy including TLR9 agonists and checkpoint inhibitors represents a promising strategy to overcome checkpoint blockade resistance, particularly for T cell uninflamed tumors.[22]
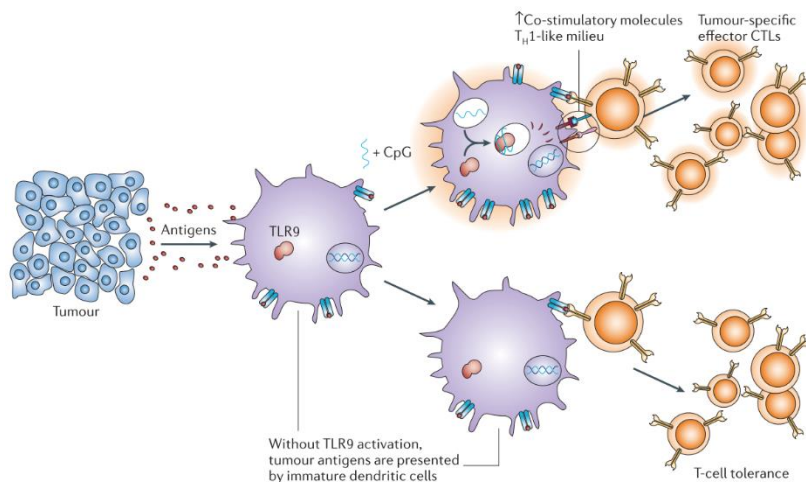


**Figure IV-1. Antitumor immunity can be induced via TLR9 activation using CpG ODNs.**[21] In the advent of disease, malignant cells suppress antitumor immunity to maintain tolerance and scape T-cell-mediated responses. Activation of DCs through TLR9 can up-regulate the expression of co-stimulatory molecules and shift T cell phenotype from tolerogenic to cytotoxic.

Traditionally, cancer treatments had prioritized systemic administration of therapeutics to ensure access to all sites of metastatic disease. Such approach could succeed when acting on pathways unique to tumor cells yet applying the same paradigm to checkpoint inhibitors can be problematic

since "taking the brakes off" of the host immune system leads to toxicities.[8] Existing literature delivering TLR9 agonists topically, subcutaneously and intratumorally versus systemically found that local administration can result in diminished off-target effects, greater tumor rejection and, in some instances, potent abscopal effects in distant non-treated tumors.[18] In light of these findings, the ability of biomaterials to direct immunomodulators to tumors has been exploited to fabricate macroscale delivery devices such as MNs for local —instead of systemic— delivery of cancer therapeutics. Indeed, MNs can be used to administer small and macro-molecules, like chemotherapeutics, proteins, genetic material and nanoparticle-based vectors such as PBAEs (**Figure IV-2**).[23]
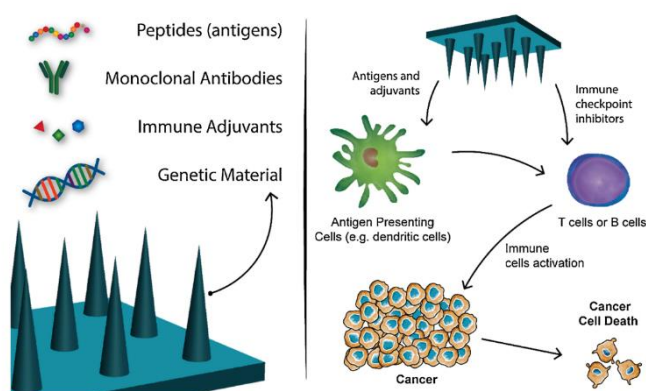


**Figure IV-2. Schematic representation of the cancer therapeutics delivered by MNs and their mechanisms of action.**[23] MNs are capable of delivering bioactive molecules to boost anticancer immunity while avoiding off-target toxicity.

Complimenting their therapeutic arm, MNs have been intensively investigated for minimally-invasive extraction of skin interstitial fluid (ISF) for clinical monitoring and early diagnosis of a wide range of pathologies including cancer.[24] ISF is the most prevalent and accessible fluid in the body, constituting a 75% of all extracellular fluid and 15- to 25% of the body weight.[25] ISF surrounds cells and tissues, functioning as a bridge between cells and blood as it is formed by blood transcapillary filtration.[26] Therefore, its biomarker composition is very similar to that in plasma and can reflect physiological function and health condition,[27] whereas alternative biofluids such as urine, sweat, tears or saliva correlate poorly with disease state and do not allow for analysis of the cellular compartment.[28] Historically, ISF had been underutilized as a source of biomarkers owing to the cumbersome methods available for ISF sampling such as suction blister, microdialysis, or open -flow micropercusion, which are time-consuming, patient-unfriendly and require medical expertise and equipment.[29] The emergence of MNs, —especially the hydrogel-forming type back in 2012[30]— allowed minimally-invasive ISF sampling, re-energizing the interest towards ISF as a valuable source

of biomarkers and a non-clotting alternative to blood for continuous monitoring of clinically relevant biomarkers.

Hydrogel MNs are the newest form of MNs first described by Donnelly and colleagues,[24] consisting of swellable polymers that are crosslinked to render hydrogels matrices in the form of MNs. In their dry state, MNs can effectively penetrate the stratum corneum barrier whereas upon insertion, they rapidly swell due to the hydrophilic nature of the hydrogels, forming hydrogels microconduits that can uptake ISF or release drugs in a controlled fashion.[30,31] After administration, hydrogel MNs are removed intact from skin, leaving no polymer residue behind but sufficiently softened to prevent reinsertion and the risk of reinfection.[31] Previous attempts to use MNs for ISF sampling have mainly focused on the extraction of soluble biomarkers from ISF, designing MNs for *in situ* detection of metabolites,[32,33] or necessitating downstream processing that involved harsh physical methods such as high-speed centrifugation[29,34] or heat treatments[35] to recover the soluble biomarkers. Alternatively, monitoring the cellular compartment of ISF could be leveraged to immunosurveil the immune status of the patient and inform on the progression of the disease and the response to therapy. However, sampling the immune cellular fraction from ISF requires highly intricated MN designs such as digestible MN platforms to retrieve and analyze the cells while preserving their viability and phenotype.[36] In the context of cancer diagnosis, immunosurveillance of the tumor microenvironment (or its surroundings) by monitoring prognosticative biomarkers such as the CD8+/CD4+ T-cell ratio can be used to assess responsiveness to immunotherapy.[37]

In previous chapters, the potential of OM-PBAEs to specifically direct nucleic acid therapeutics into the immune cells residing in the dermal milieu was proven. Moreover, these vectors could be integrated with MNs for transdermal delivery. Considering these findings, PBAEs will be leveraged once again in the context of cancer immunotherapy to deliver immunostimulatory nucleic acids using hydrogel-based MNs. In parallel, a diagnostic compartment will be included into the MN platform to sample the immune cellular compartment of ISF to monitor the response to therapy. Specifically, the main objective of this chapter is the **design of a novel theranostic MN platform offering (1) transdermal delivery of immunomodulators (ODNs) encapsulated in PBAEs to augment innate anticancer immunity and (2) ISF immunosurveillance for minimally-invasive biopsy of the tumor surroundings** (**Figure IV-3**). Using hyaluronic acid (HA) as foundational polymer, MNs will be fabricated to allow on-demand digestion —upon retrieval— to recover cells from ISF and correlate its immune signature to that in the tumor.
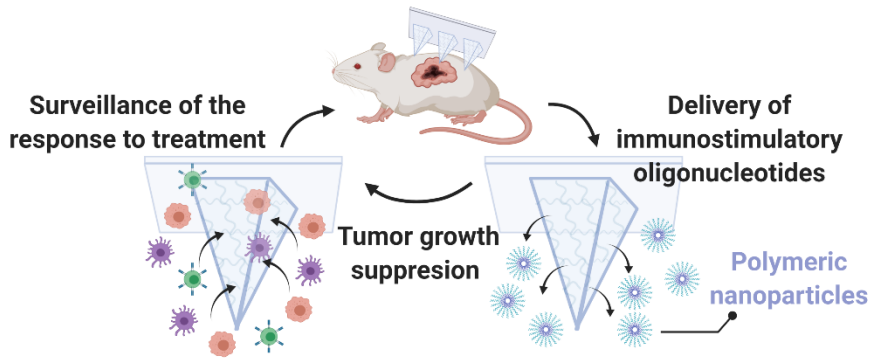
**Figure IV-3. Graphical abstract of Chapter IV.** Throughout this chapter, a new hydrogel-based MN platform has been engineered for transdermal delivery of PBAE-derived polyplexes encapsulating CpG ODNs for cancer treatment while simultaneously surveilling changes in the ISF immune profile as a response to therapy.

## 4.2 Aims

The main objective of the present chapter is the design of a novel MN-based platfrom for delivery of PBAE-complexed immunomodulators (TLR-9) and simultaneous uptake of ISF for *in situ* immune surveillance of the tumor surroundings. To do so, the following tasks were proposed:

✓ Development and screening of a novel family of hydrogel MNs using HA-modified polymers to identify highly swellable and digestible MNs for theranostic purposes.

✓ Characterization of the properties of $NH_2$-HA-derived MNs and study of the impact of the crosslinker on their swelling ability, digestion rate and mechanical properties.

✓ Assessment of the capacity of MNs to sample the cellular and soluble fraction of ISF.

✓ Characterization of OM-PBAEs encapsulating CpG ODNs.

✓ Assessment of the therapeutic potential of the MN platform for management of colorectal cancer macroscopically and at the cellular level.

✓ Analysis of the potential of MNs to continuously monitor the immune profiles in ISF and their changes as a response to immunotherapy.

## 4.3    Materials and Methods

### 4.3.1    Materials

All reagents and solvents were purchased from Sigma Aldrich unless otherwise stated. Sodium hyaluronate (60kDa) was obtained from LifeCore Medical with a purity of at least 95%. NHS-terminated 8-arm PEG was purchased from Creative PEG Works. MN PDMS custom-made molds (11 X 11 needles with height 600μm, base width 300 μm and tip to tip spacing of 600 μm) were obtained from Blueacre Technology. THP-1 cells were acquired from ATTC. ODN 1826-TLR9 ligand was purchased from InvivoGen (Ca, USA).

### 4.3.2    Methods

#### 4.3.2.1    Animals

Adult 6–8 weeks old C57BL/6 mice were purchased (Charles River) and kept under pathogen-free conditions at the animal facilities of the Koch Institute for Integrative Cancer Research (Cambridge, USA). Animal maintenance and experiments were performed under the protocol #1017-102-20 approved for this study by the Institutional Animal Care and Use Committee (IACUC) of the Massachusetts Institute of Technology (MIT).

#### 4.3.2.2    Synthesis of Amino-modified hyaluronic acid (HA-SS-NH$_2$) polymer

60 kDa-sodium hyaluronate (1% w/v in MES buffer) was activated with N-(3-(dimethylamino)propyl)carbodiimide (EDC) and N-hydroxysuccinimide (NHS) at a 1:4:2 molar ratio and reacted at room temperature for 30 min. The activated hyaluronic acid (HA) was then mixed with Cysteamine Dihydrochloride at 1:10 molar ratio and reacted at room temperature for 12 hours. HA-SS-NH$_2$ was purified by dialysis against deionized water for 6 days at room temperature, freeze dried, and stored at -20°C protected from humidity until use. For structural analysis, modified HA-SS-NH$_2$ was dissolved in D$_2$O and analysed by $^1$H-NMR, recorded using a Bruker Advance II 300MHz NMR.

#### 4.3.2.3    Synthesis of thiol-modified hyaluronic acid (HA-SS) polymer

Again, 60 kDa-sodium hyaluronate (1% w/v in MES buffer) was activated with N-(3-(dimethylamino)propyl)carbodiimide (EDC) and N-hydroxysuccinimide (NHS) at a 1:4:2 molar ratio and reacted at room temperature for 30 min. Next, the activated HA was reacted with Cysteamine Dihydrochloride in a 1:4 molar ratio. Finally, an equimolar amount of Tris(2-carboxyethyl)phosphine

hydrochloride (TCEP) was added to the reaction mixture to reduce the disulfide bound overnight and subsequently dialyzed against deionized water for 4 days at 4°C. Chemical structure was characterized by $^1$H-NMR (Bruker Advance II 300MHz NMR).

### 4.3.2.4  Synthesis of methacrylated hyaluronic acid (HA-Me)

4.0 g of 60 kDa-sodium hyaluronate were dissolved in 200 mL of deionized water and were left at 4°C under continuous stirring overnight. 133.3 mL DMF and 4.76 mL methacrylic acid were then added dropwise to the solution, respectively. The pH of the solution was regulated to pH 8-9 with 1M NaOH. The reaction was kept at 4°C under continuous stirring for another 18h. Subsequently, 9.88 g NaCl was added to the reaction solution to reach a NaCl concentration of 0.5 M before HA-Me was precipitated out in ethanol. The precipitate was washed with ethanol three 3 times before being dissolved in deionized water and the solution was dialyzed against deionized water for 7 days. The purified product was obtained by lyophilization and characterized by $^1$H NMR spectroscopy (Bruker Advance II 300MHz NMR) The degree of modification was determined by digital integration of the anomeric protons signals or methyl protons signals of HA and of the methacrylate proton signals at ~6.1, ~5.7, and ~1.9 ppm.

### 4.3.2.5  HA-based hydrogel disks fabrication

100 µL of hydrogel disks for streamlined screening were prepared by mixing equal volumes of HA-modified polymer (either amino- or thiol-terminated) (10% w/v) and the 8-arm-PEG crosslinker (10% w/v). Solutions were dissolved separately with phosphate buffer (pH=7.4) and vigorously mixed together for 10 seconds inside cylindrical plastic molds (diameter: 5 mm; height: 2.5 mm). Hydrogel disks were allowed to react for 5 min to ensure full gelation, freeze-dried, and stored at room temperature protected from humidity until use. Fabrication of HA-Me-derived disks was performed by dissolving HA-Me likewise and mixed with a 1% w/v solution of Irgacure®2959 and crosslinked for 1 min under UV light (UV Stratalinker™ 1800). Hydrogel disks were removed from the molds and stored until further use.

### 4.3.2.6  HA-based MN fabrication

Fabrication of HA-SS-NH2-derived MNs is described being the candidate of choice. MNs were produced using custom-made molds consisting in a 11 x 11 array of negative MNs projections, each one with a height of 600 µm and a radius of 150 µm. First, HA-SS-NH2 polymer (10% w/v in phosphate buffer, pH=7.4) was casted on top of the molds and centrifuged at 4200 rpm for 5 min. Excess polymer was removed, and molds were freeze- dried for 20 min. Then, 8-arm-PEG-NHS crosslinker (10% w/v in phosphate buffer, pH=7.4) was casted and forced by centrifugation through the mold under the

same conditions. This approach, together with the gradual gelation of hydrogel, ensured a successful polymerization of the matrix from "tip-to- top" of the MNs and a homogenous composition. Excess polymer was carefully removed, and molds were freeze-dried. If necessary, an aqueous solution containing PBAEs was deposited on the molds and briefly spined for 15 seconds. Immediately after, a polymeric backing layer of PLGA (Resomer® RG 858 S, Sigma-Aldrich, USA) at 15% (w/v) dissolved in acetonitrile was added dropwise until covering the whole area of the mold. Finally, HA-based MNs were allowed to dry at room temperature for 12 hours, peeled off the molds carefully, and stored at room temperature preserved from humidity.

### 4.3.2.7 On-demand digestion of HA-derived hydrogel matrices

HA-based MNs or HA-based hydrogels were incubated with 10 mM Tris (2-carboxyethil) phosphine (TCEP) solution in supplemented cell culture media or PBS at pH 7.4 (depending on whether cells were collected). HA-based MNs or HA-based hydrogels were incubated under rotation at 37°C for 10 min and the recovered suspension was filtered with a 70 μm cell strainer (BD bioscience) to remove any impurities.

### 4.3.2.8 Cell lines

Human monocyte THP-1 cells (ATTC) were maintained in RPMI 1640 supplemented with 10% FBS, 2 mM L-glutamine, 25 mM HEPES, 100 μg/mL Normocin™n (InvivoGen) and 100 U/mL penicillin and 100 μg/mL streptomycin. Cell lines were maintained in a humidified incubator at 37 °C, 5% $CO_2$.

### 4.3.2.9 *In vitro* cytotoxicity studies

THP-1 cells were incubated with different concentrations of digestion media (TCEP solution in supplemented media), ranging from 0.1 mM to 100 mM, for 10 min. Thereafter, digestion media was removed, and cells were washed with PBS and stained using the LIVE/DEAD fixable Violet Dead Cell Stain Kit (ThermoFisher Scientific, USA) following the manufacturer's guidelines. Dead cells were analyzed by flow cytometry using a BD LSRFortessa™ flow cytometer.

### 4.3.2.10 Swelling studies with HA-based hydrogel disks

HA-based hydrogels disks were incubated with PBS at 37°C and their weight was recorded over time ($W_i$) and normalized to their respective dry weight ($W_0$). Swelling percentage was assessed as a function of mass increase over time and calculated as: $W_i$ x 100/ $W_0$. For stability studies, hydrogel disk were left incubating at 37°C under gentle rotation and monitored daily until disappearance or termination of the study.

### 4.3.2.11 Recovery of immune cells from HA-based MNs *in vitro*

HA-based MN patches were incubated with $1 \times 10^6$ THP-1 cells per well for 24 hours. Then, MNs were washed with PBS to minimize unspecific interactions between cells and the MN backing layer and digested as previously described. After digestion, cells were pelleted and stained with the CellTrace CFSE Cell Proliferation Kit Protocol (ThermoFisher Scientific, USA) following the manufacturer's instructions. Total number of infiltrated cells was quantified by flow cytometry using a BD™ LSR II.

### 4.3.2.12 Recovery of soluble analytes in a mimetic skin model

Analyte recovery capacity of hydrogel-based MNs was conducted as detailed elsewhere using a skin model attempting to mimic the mechanical properties of the epidermis/ISF interface.[35,38] 1.4% w/v agarose hydrogels containing increasing amounts of the model metabolite Rhodamine B were polymerized in 30 mm x 15 mm petri dishes and covered with an stretched layer of Parafilm® aiming to emulate the properties of the water-impermeable stratum corneum. MN patches were left inserted in the agarose gels for two hours to reach a swelling plateau and subsequently digested as previously described. Finally, absorbance of the recovered analytes was measured in a plate reader ($\lambda$ = 553 nm) and correlated with the extracted mass.

### 4.3.2.13 Skin penetration studies

Penetration capacity of the HA-based MNs was tested *ex vivo* and *in vivo* in shaved C57BL/6 mice. HA-based MNs were applied and kept in place using medical-grade tape (FLEXcon, USA) for 1 hour. Skin penetration was confirmed by surface staining with blue Shandon™ Tissue-Marking Dye (ThermoFisher) and further imaged by optical microscopy.

### 4.3.2.14 CpG-PBAE nanoparticle formation and characterization

PBAEs polyplexes containing ODNs were obtained as previously described by mixing equal volumes of the ODN solution (0.5 mg mL$^{-1}$ diluted in DNase-free water) and CR3-C6 PBAE stock solution (100 mg mL$^{-1}$ in DMSO) to achieve the desired polymer-to-nucleic acid ratio (w/w). In brief, the pDNA solution was added over the polymer solution, both diluted in sodium acetate buffer (AcONa buffer; 12.5 mM, pH=5), mixed by vigorous pipetting and allowed to react for 15 min at room temperature. Resulting nanoparticles were characterized by nucleic acid retardation assay and dynamic light scattering (DLS). Briefly, CpG:PBAE polyplexes with ranging polymer-to-nucleic acid ratios were loaded in 4% E-Gel Precast Agarose Gels (Thermo Fisher). Next, gels were run following the manufacturer's instructions and visualized in fluorescence mode. Particle size distribution and zeta distribution of resulting polyplexes was evaluated by DLS in a Zetasizer Nano ZS Instrument

(Malvern Instruments Ltd, UK). Polyplexes were prepared as described and 100 µL of them were diluted in 900 µL of PBS.

### 4.3.2.15 *In vivo* murine model and therapeutic efficacy

The murine colorectal cancer model was generated by injecting MC38 cells constitutively expressing the mApple red fluorescent protein and which were kindly provided by the Miller Lab (MGH Center for Systems Biology, Boston). Briefly, 1 x 10^6 cells were injected subcutaneously in the right flank of the mice and allowed to grow until reaching 50-100 mm$^3$ (about 7 days post injection). Mice were anesthetized and administered CpG:PBAE polylexes via intratumoral injection (1 µg/ 50 µL/ dose), via hydrogel-based MNs (1 µg/ MN patch) or left untreated as control group (n=10 mice per group). MNs were administered on top of the tumor by thumb-pressing them against the skin, or in the surrounding areas as the study progressed since the morphology of the growing lumps impeded proper attachment. MNs were secured with medical-grade tape (FlexCon, USA) for 24 hours. On the following day, MNs were retrieved and a second set of empty MNs were applied to all the groups following the same procedure for diagnosis. Mechanistic analysis were performed by flow cytometry on day 14 after commencing the treatment (n=4). In parallel, the tumor size was measured every other day via caliper measurements (n=6), and the tumor volume was calculated using the equation V = (Length × Width t× Height)/π ÷ 6. Body weight was measured contemporaneously with tumor volume. Mice were euthanized when tumors reached a volume of 1000 mm$^3$ or when poor body condition were observed following the guidelines.

### 4.3.2.16 Recovery and immunophenotyping immune cell infiltrates in MNs

24 hours-post administration, MNs were retrieved from the mice and incubated in Hanks' Balanced Salt solution (HBSS) with Calcium and Magnesium (Gibco, ThermoFisher) until processing. MNs were next digested as described until obtaining a cell suspension. Cells were stained with fluorescently-labelled primary antibodies at a concentration of 1 × 10^6 cells/mL in 100 µL of cell staining buffer (BioLegend). Intracellular staining was performed using FoxP3 Staining Buffer Set (Miltenyi) according to the manufacturer's protocol. The following anti-mouse antibodies were used for flow cytometry and purchased from BioLegend: CD45 APC-Cy7 (clone 30-F11), , CD45 BV785 (clone 30-F11), CD11b BV421 (clone M1/70), Gr-1 APC-Cy7 (clone RB6-8C5), CD8a BV421 (clone 53-6.7), CD86 BV510 (clone GL-1), CD206 PE (clone C068C2), CD11c APC (clone N418). The following anti-mouse antibodies were purchased from BD Biosciences: CD3 BB700 (clone 17A2), CD4 BUV395 (clone GK1.5), CD8a BUV737 (clone 53-6.7), CD80 BUV737 (clone 16-10A1). Live cells were gated using LIVE/DEADTM (Thermo Fisher) aqua (cat. no. L34966), green (cat. no. L34970) or near-IR (cat. no.

L34976). Cells were stained according to the following panels detailed in **Table 2**. Samples were analyzed by flow cytometry with a BD LSR Fortessa™ (BD Biosciences) and data processed with FlowJo version 10 (Flowjo LLC).

**Table 2: Immunophenotyping panels for flow cytometry analysis.**

| Panel | Biomarkers |
|---|---|
| **T lymphocytes** | CD45, CD3, CD4, CD8 |
| **Granulocytes and Myeloid-derived suppressor cells (MDSCs)** | CD45, CD11b, Gr-1 |
| **Dendritic cells** | CD45, CD11c, MHCII, CD8alpha, CD86 and CD80 |

### 4.3.2.17 Harvesting and immunophenotyping of tumors and skin explants

Mechanistic analysis were performed on day 14 where mice were sacrificed and their organs harvested including spleens, tumors, tumor-draining lymph nodes and skin explants corresponding to the area of application. Lymph nodes were gently smashed against a 40 μm cell strainer and rinsed with PBS to recover the maximum amount of cells. Cell suspensions from spleens were further treated with 1X ACK Lysis buffer (Gibco, ThermoFisher) for 1 min to lyse red blood cells. Then, cells were centrifuged at 300g for 5 min and resuspended in 100 μL of staining buffer ($1 \times 10^6$ cells/mL) until staining. MC38 tumors were harvested, chopped and digested in a solution of HBSS supplemented with collagenase I, II and IV (100 ng/mL), and DNase I (1 μg/mL) for 2 h at 37°C. Tumor cells were further treated with ACK Lysing Buffer (Gibco) and resuspended in staining buffer ($1 \times 10^6$ cells/ mL) until staining. Finally, skin explants were processed using the human whole skin dissociation Kit (Miltenyi) following the manufacturer's guidelines specifically, the overnight incubation protocol for maximum cell yield. After that, mouse CD45 MicroBeads (Miltenyi) were used to positively select CD45+ leucocytes and the recovered fraction was resuspended in staining buffer. All cell suspensions were stained using the same set of panels described in the previous section.

### 4.3.2.18 Analysis of tumor proliferation by immunohistochemistry

Skin tissue sections were processed and imaged by the Hope Babette Tang Histology facility at the Koch Institute of Integrative Cancer Research at MIT (Cambridge, USA). Briefly, 1 cm$^3$ tumor sections were harvested on the day of mechanistic analysis were embedded in O.C.T. in plastic base molds for tissue embedding. Samples were flash frozen in a bath of dry ice and preserved at -80°C until sectioning. Tumors were cryosectioned into 20 μm-wide tissue sections and proliferation was

assessed via H&E staining and Ki-67 staining. Processing of the microscopic images was performed using the Aperio ImageScope 12.3.3 software (Leica).

### 4.3.2.19 Statistical analysis

Statistical analyses were carried out using Graph-Pad Prism 8 (GraphPad Software). All data are reported as mean + SD. For *in vitro* experiments, a minimum of n=3 biological replicates were used per condition in each experiment. Multiple comparisons among groups were determined using one-way ANOVA followed by a post-hoc test. Pairwise comparisons were performed using Student t-tests. For *in vivo* experiments, a minimum of n=4 biological replicates were used per condition in each experiment. No specific pre-processing of data was performed prior to statistical analyses. Differences between groups were considered significant at p-values below 0.05 (* $p < 0.05$, ** $p < 0.01$, *** $p < 0.001$).

## 4.4   Results and Discussion

### 4.4.1   Synthesis of a new family of HA-modified hydrogel MNs for theranostics

Selection of the hydrogel matrix constituting the MNs was considered a decisive factor for succeeding in the development of the theranostic MN platform. Indeed, using biocompatible polymers is mandatory since MNs disrupt the epidermis and thus, act as a foreign entity. Also, accidental breakage of the MNs inside the skin should not trigger immunogenic responses; instead, invading MNs should be degraded naturally to prevent negative effects for the patient.[39] Most polymers utilized in hydrogel-based MN fabrication have been extensively used for other biomedical purposes, with typical matrices including poly(methylvinylether/ maelic acid) (PMVE/MA), poly(2-hydroxyethyl methacrylate) (pHEMA) or hyaluronic acid (HA), mostly methacrylated.[24] HA has been an old favorite to fabricate hydrogel MNs due to its biocompatibility, non-immunogenicity and its natural ability to bind large volumes of water,[40] making it the ideal candidate for rapid ISF uptake. HA is a glycosaminoglycan that can function as a natural ligand of the ubiquitous CD44 receptor,[40,41] providing a binding motif for the immune cells present in ISF. Owing to its chemical flexibility, the HA structure can be easily modified rendering highly swellable hydrogels.

First, a new library of HA-modified polymers was synthesized to include pendant groups such as amines, thiols or a methyl methacrylate to generate hydrogels upon crosslinking with other agents (**Figure IV-4A**). Some of these candidates such as the methacrylated HA have been long described in the literature for MN fabrication,[29,34,35,42] whereas the synthesis of the amino-modified HA is reported here for the first time as further detailed. Next, each of these polymers was rationally paired with crosslinking agents and the resulting hydrogel MNs were broadly examined to identify a candidate meeting all the necessary requirements for our envisioned theranostic MN platform (**Figure IV-4B**).

It is of note that this preliminary screening aimed to discard suboptimal formulations early on in the project by answering basic yes-no questions such as (1) is MN fabrication possible?; (2) can cells infiltrate in the MN matrix? or (3) can MNs be digested to recover cellular biomarkers from ISF? In future sections of this chapter, a more detailed insight into the MNs features and the rationale behind our choices will be included.

**A**



**B**

| Hydrogel | Fabrication | Cell infiltration | Digestion | Swelling |
|---|:---:|:---:|:---:|:---:|
| HA-SS-NH$_2$-c-NHS | + | + | + | + |
| HA-SH-OPSS | - | + | + | + |
| HA-Me | + | + | - | + |
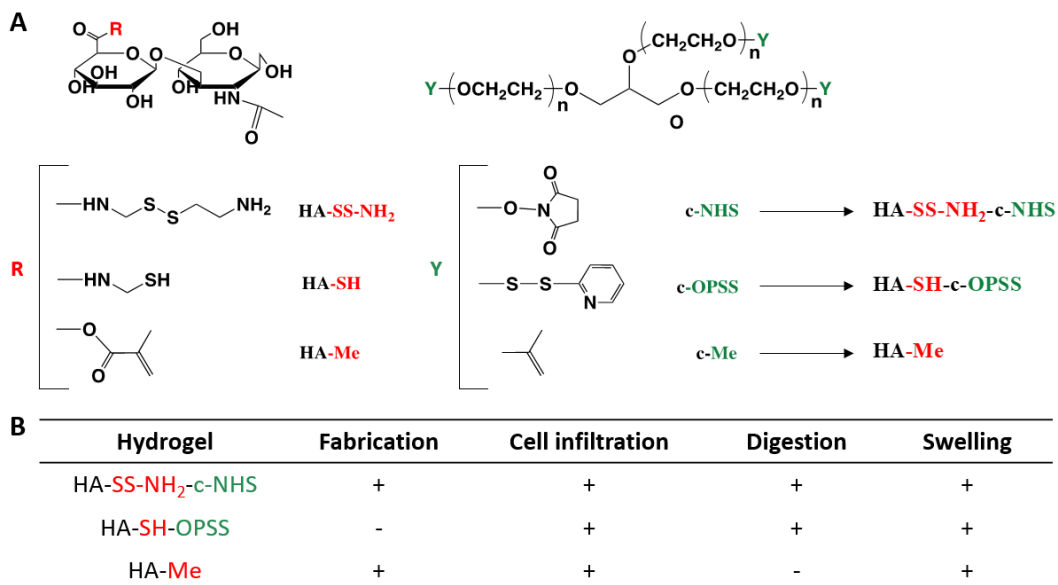
**Figure IV-4. Newly synthesized family of HA-derived MNs for *in situ* drug delivery and ISF sampling.** HA was modified via EDC/NHS activation using amino- and thiol- groups or a with methyl methacrylate to generate a library of hydrogel formulations for MN fabrication (**A**). Candidates were prescreened to identify outperforming formulations for theranostic purposes where [+] indicated a positive readout whereas [-] meant that the hydrogels did not met the needed requirements (**B**).

First, it was studied whether the HA candidates could be casted into molds for MN fabrication. All but the thiol-modified HA succeeded in generating hydrogel MNs, which was caused by its instant gelation upon contact with the crosslinker and which prevented it from being shaped into MNs.

Next, cell penetration inside the HA-derived hydrogels was evaluated since these had to allow immune cell infiltration for future diagnostic purposes. Briefly, hydrogel disks were incubated with an immune cell line *in vitro* and penetration of the cells into the hydrogels was confirmed by microscopy. Results revealed that all formulations allowed cell infiltration, yet some differences were observed in the overall numbers (**Figure IV-5**). It was hypothesized that preferential cell infiltration towards specific hydrogels might stem from the different functional groups used to decorate the HA backbone and which might have promoted attracting forces with the negatively-charged membrane of the cells.

Next, on-demand hydrogel digestion was investigated, being a much needed feature for recovery of cellular biomarkers from ISF upon retrieval of the MN patch. For the HA-SS-NH$_2$-NHS- and the HA-SH-OPSS-derived hydrogels, digestion was easily achieved in mere minutes by incubating them under reducing conditions. As later discussed, the presence of disulfide bond in their tridimensional matrix

—provided by either the HA backbone or the crosslinker— allowed to dissolve them when treated with a reducing agent. Contrarily, degradation of HA-Me was pursued via enzymatic digestion using hyaluronidase, yet we promptly realized that it was unattainable since the optimum pH for enzyme activity (pH = 4.5-6) was too acidic for cells to survive. If adjusting the pH of the enzymatic solution to the physiological range, the digestion rate was slowed down and it was predicted that days, instead of minutes, would have been needed to fully degrade the MNs, making the HA-Me useless if exploited for *ex vivo* recovery of cells.
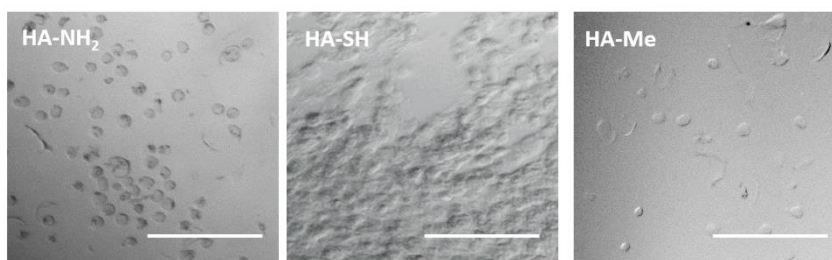


**Figure IV-5. Analysis of cell infiltration into HA-derived hydrogels.** Hydrogel disk obtained from the different HA-derived candidates were incubated with THP1 cells (1 x 10$^6$ cells per well) to allow cell penetration. Next, hydrogels were gently washed with PBS to remove loosely attached cells and imaged by bright-field microscopy. Scale bar=200 μm.

Finally, all hydrogel candidates were confirmed to be highly swellable, another crucial requirement for maximizing biomarker recovery and in turn, the sensitivity of further analysis.

To sum up, engineering the HA chemical backbone with functional groups was confirmed as a powerful tool to design swellable polymers for MN fabrication. The HA-SS-NH$_2$-NHS candidate was selected as our hydrogel of choice to develop a MN platform for cancer immunotherapy as it met all the necessary requirements. Despite not making the cut, the rest of the hydrogels candidates with distinct features could still prove useful in other settings, upon refinement of their chemical structure, were only the therapeutic or the diagnostic compartment are needed separately.

## 4.4.2   Characterization of the novel NH$_2$-HA-derived MN platform

As discussed before, a rational design of the polymer architecture was necessary to deliver a digestible MN platform capable of releasing immunomodulators while simultaneously sampling immune cells from ISF. Per our preliminary screening, the amino-modified HA polymer held the greatest potential in generating MNs for a prospective theranostic platform, so a thorough characterization of its properties was next conducted.

### 4.4.2.1 Design of a highly swellable MN platform with on-demand degradation for theranostics

The new HA-SS-NH$_2$ polymer was designed by leveraging its chemical flexibility —thanks to the presence of acid groups— to include a lateral chain. First, HA was activated and a cysteamine dihydrochloride molecule was covalently linked via EDC/NHS activation (**Figure IV-6A**). The newly added chain harbored both a primary amine group (for hydrogel formation) and a disulfide bond (for hydrogel degradation). To form the hydrogel, primary amines were reacted with the 8-arm-PEG-NHS crosslinker containing a succinimidyl functional group, allowing for spontaneous hydrogel gelation without the use of external triggers such as UV light, an attractive advantage over methacrylated HA. Next, a MN fabrication method was optimized by tunning the centrifugation and freeze-drying steps to deliver consistent and homogeneous MNs (**Figure IV-6B**).
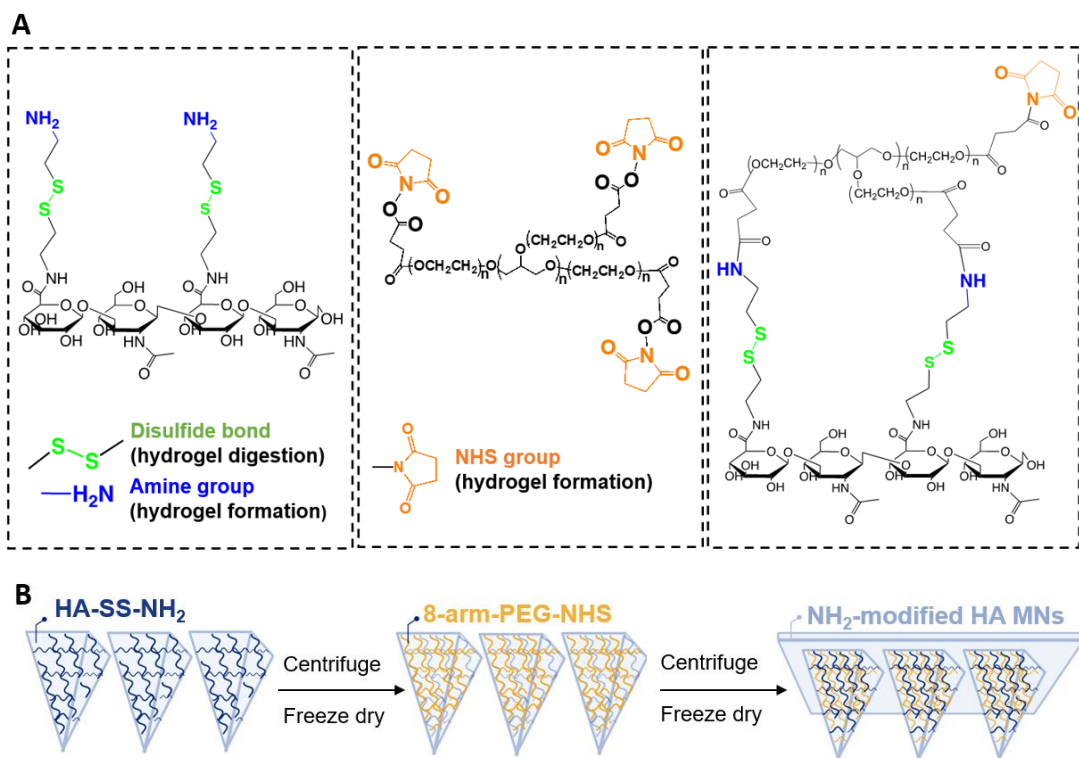


**Figure IV-6. Design and fabrication of a novel MN platform using amino-modified HA.** Chemical backbone of the HA polymer was engineered to include an amine group (for hydrogel formation) and a disulfide bond (for hydrogel digestion). When reacted with an 8-arm-PEG crosslinker, a highly swellable hydrogel was generated (**A**). Schematic representation of the fabrication method via successive addition of the two hydrogel components (**B**).

The optimal procedure consisted in a first set of steps where the HA-derived polymer was casted into a mold, centrifuged at high speed, and freeze-dried, creating a porous matrix that would provide with a scaffold for the subsequent components to be added. Next, the crosslinking agent was added by centrifugation again, which forced its diffusion through the whole HA matrix. This approach, together with the gradual gelation of the hydrogel, ensured a successful polymerization of the matrix from "tip-to-top" of the MNs and a homogenous composition if scanning the MN profile. At this point, the fabrication method branched depending on the final application of the platform. If restricted to ISF sampling, a polymeric backing layer made of PLGA was deposited, serving as an anchor for MN administration and retrieval. If aimed for theranostic purposes instead, an aqueous solution was added similarly containing the therapeutic agent of interest, the TLR-9 agonist complexed in PBAEs, followed by drop-wise deposition of the polymeric backing layer.

### 4.4.2.2 Biophysical characterization of the HA-derived MNs

Next, the properties of the MN platform such as MNs swelling capacity, mechanical strength, and ability for on-demand digestion were characterized. First, the influence of the crosslinking agent in the swelling capacity of the HA-NH2-derived hydrogels was investigated as a function of weight gain over time. Three different crosslinking agents were screened, differing in their molecular weight: (1) 40 kDa-8-arm-PEG-NHS (40 kDa-PEG), (2) 10 kDa-8-arm-PEG-NHS (10 kDa- PEG) and (3) their combination 70:30 wt % of 40 kDa:10 kDa-PEG. The utilization of hydrogel disks (rather than MNs) was preferred in this study since they displayed about a 30-fold increase in volume and therefore facilitated the screening.

The crosslinker type was not found to affect the initial swelling phase — an average swelling ratio of about 800% in less than an hour was observed for all hydrogels (**Figure IV-7**). However, the crosslinking agent had a marked influence on swelling at later time points with ratios of 1073% ± 58% and 1592% ± 36% for hydrogels derived from the from the 10 kDa-PEG and the 40 kDa-PEG, respectively. As expected, when the mixture of both crosslinkers was used, the swelling ratio was in between these values; 1191% ± 59%. These results showed that the choice of crosslinker — specifically, its molecular weight— allowed to tailor the swelling ability of the HA-derived hydrogels without the need of adding osmolytes such as sucrose or maltose to increase the osmotic pressure.[34]
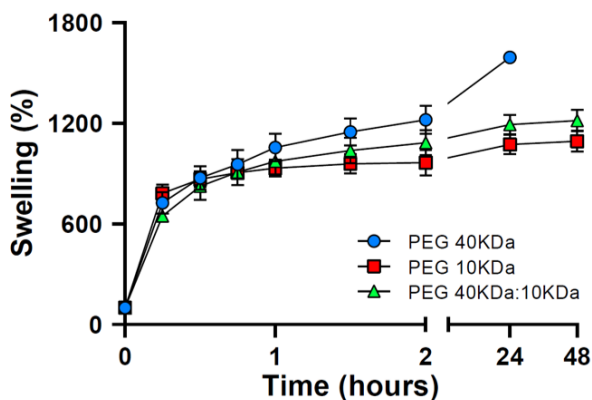
**Figure IV-7. Swelling rate of the HA-based hydrogels composed of amine-modified HA polymer.** The HA polymer was crosslinked with NHS-terminated 8-arm PEG crosslinkers differing in molecular weight. Weight of the hydrogels was recorded as a function of time using PBS as a buffer mimicking ISF. Data are represented as mean ± SD (n = 3).

Similar swelling phenomena were observed in stability studies when hydrogels were incubated in physiologically-relevant conditions (**Figure IV-8**). The PEG-40 kDa-derived-hydrogels dissolved after 48 hours of incubation as a consequence of their massive swelling. Contrarily, the volume of the other hydrogels remained unchanged for extended periods of time. Specifically, changes in the PEG-10 kDa-derived-hydrogels were not observed for more than 3 weeks when the experiment was finalized.
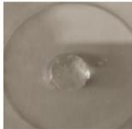


**Figure IV-8. Hydrogel disks stability when incubated in physiological-relevant conditions.** Hydrogels were incubated in PBS at 37°C under gently rotation and monitored daily.

Next, the capacity of the MN patch to penetrate the skin was evaluated both *ex vivo* and *in vivo* using a healthy murine model. Fine-tuning the crosslinking agent, both in terms of molecular weight and relative ratio, served as a powerful strategy to improve the mechanical strength of our MNs, avoiding the use of solid core/shells and irreversible crosslinking strategies.[36,43] It was expected that the ability to fill the entire needle with a hydrogel matrix would provide with a higher volume for

entrapment of ISF biomarkers, both cellular and soluble. In turn, higher amounts of sampled ISF could benefit successive analysis in terms of sensitivity, as more biomarkers would be available. *Ex vivo* studies revealed that MNs containing 10 kDa-PEG (alone or when mixed with the 40 kDa-PEG) could efficiently disrupt the stratum corneum as confirmed by the accumulation of blue Tissue-marking dye inside the micro conduits (**Figure IV-9A**), while those that were solely crosslinked with the PEG-40 kDa could not penetrate the viable skin. Similar results were observed *in vivo* (**Figure IV-9B**). Thus, we chose to continue our studies with the MNs crosslinked with the 70:30 mixture of 40kDa:10kDa-8-arm-PEG-NHS, which provided with both high swelling capacity and adequate mechanical properties, enabling to pierce the mouse skin. Finally, it was confirmed that the integrity of the MNs was maintained after administration *ex vivo*. As depicted in **Figure IV-9C**, HA-derived MNs fabricated with mixed crosslinkers significantly swelled and lost their characteristic pointed shape as expected. A few needles of the array appeared to be broken yet the majority of them remained intact (>90%).



| A | B | C |
|---|---|---|
| *EX VIVO* | *IN VIVO* | **BEFORE** **AFTER** |
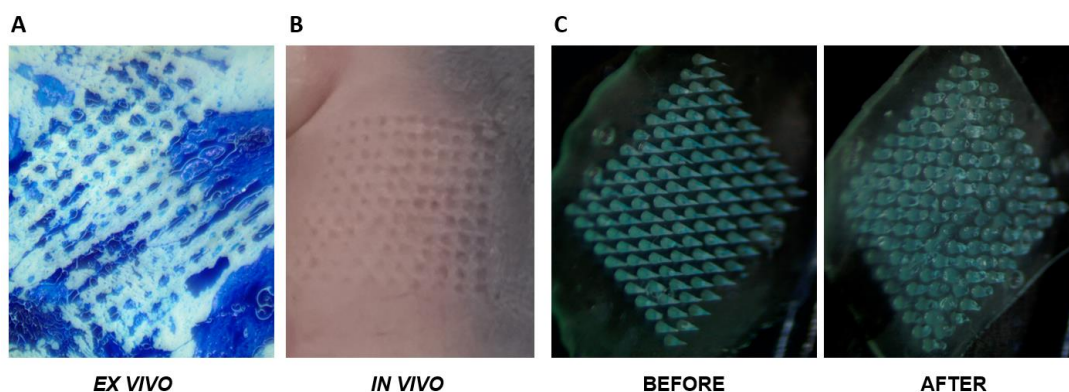
**Figure IV-9. Assessment of the mechanical strength of HA-derived MNs *ex vivo* and *in vivo*.** Effective skin disruption was observed both *ex vivo* (**A**) and *in vivo* (**B**) as evidenced by the presence of microconduits. Murine cadaveric skin explants were stained with blue Tissue-marking dye for enhanced visualization. Integrity of the MNs after *ex vivo* skin penetration was confirmed by optical microscopy (**C**).

The last imperative of our platform was on-demand degradation of the MN patch upon retrieval for *ex vivo* ISF recovery. As discussed, EDC/NHS activation of the HA polymer allowed to integrate a redox-sensitive side chain containing a disulfide bond that can be cleaved if incubated with a reducing agent. When reduced, the covalent bonds intertwining both crosslinker and polymer are dissolved cascading the collapse of the tridimensional structure of the hydrogel MNs and in turn, the release of the entrapped cells (**Figure IV-10A**). Here, the reducing agent of choice was tris (2-carboxyethil) phosphine (TCEP), a water-soluble and non-toxic reagent widely used for biochemical applications.[44]
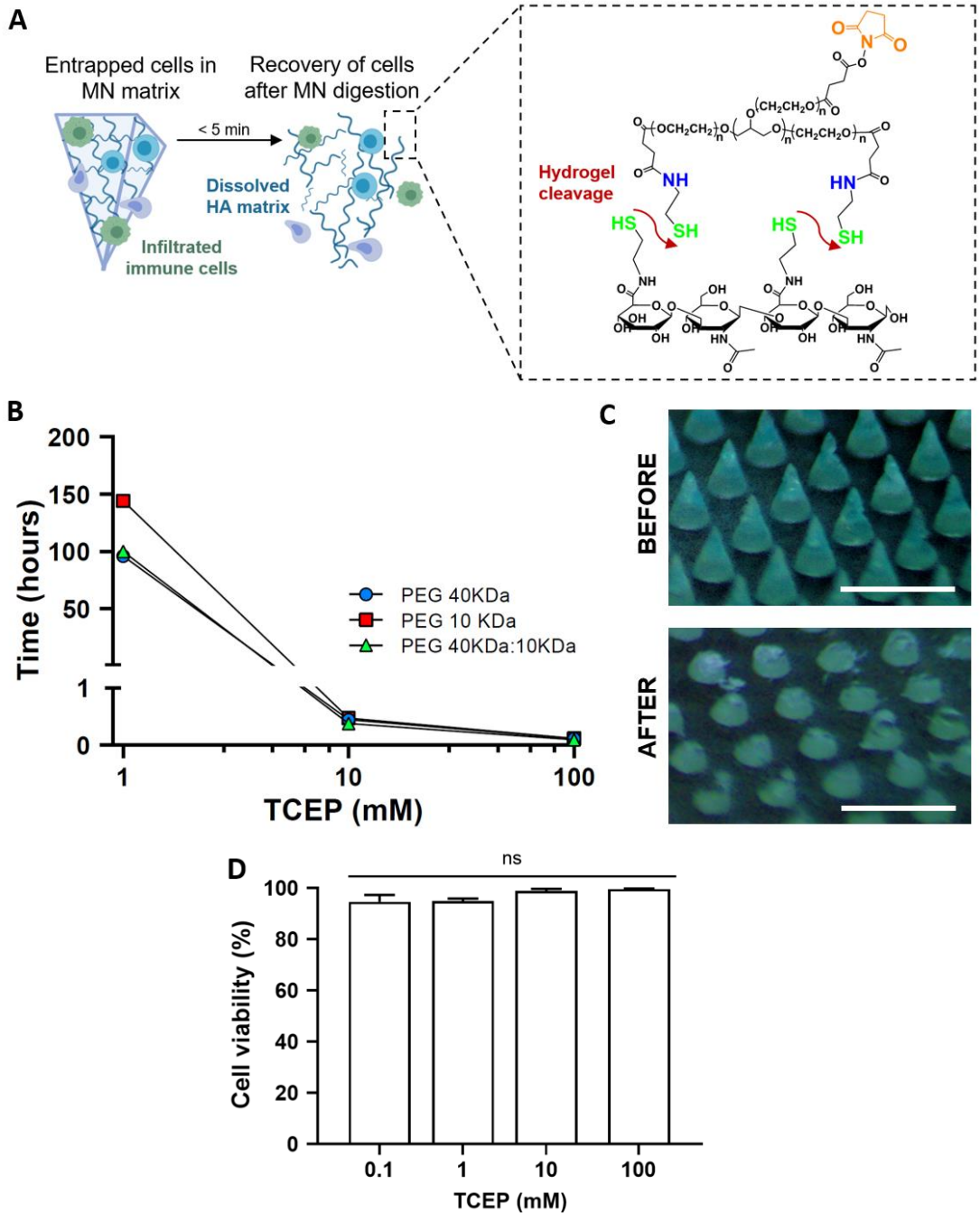
**Figure IV-10. On-demand digestion of HA-derived MNs for minimally-invasive ISF sampling.** Following administration, intact MNs entrapping ISF and cellular biomarkers can be retrieved and digested *ex vivo* upon the addition of a reductive agent (**A**). Incubation with the reducing agent TCEP triggered the degradation of HA-derived hydrogels (**B**) and MNs (**C**) in less than 5 minutes. Cell toxicity was not reported when incubating immune cells with experimentally-relevant concentrations of TCEP (**D**). Data are represented as mean ± SD (n = 3).

First, the digestion kinetics of HA-derived hydrogels as a function of TCEP concentration were analyzed (**Figure IV-10B**). Similar digestion profiles were observed regardless of the molecular weight of the crosslinker. A linear correlation between TCEP concentration and the time needed for full hydrogel digestion was also confirmed, where high concentrations of TCEP (>10 mM) ensured complete digestion in half an hour whereas hydrogel digestion was not accomplished, or was far too long, when TCEP concentration was lower than 1 mM. In light of these findings, the working concentration for further studies was established at 10 mM TCEP. The digestion kinetics of HA-derived hydrogels when in a MN form was also analyzed using fluorescently-labelled MNs for facile examination. Complete digestion of the MN array was confirmed in less than 5 minutes, as evidenced by the disappearance of the needle-like projections (**Figure IV-10C**).

As expected, the higher surface-are-to-volume ratio of the MNs, along with their overall low volume (~3 µL) if compared to the hydrogel disks, facilitated the penetration of the reducing agent and accelerated their digestion. Also, their on-demand digestibility was also gauged by comparing the fluorescence levels of TCEP-digested MNs versus that of control MNs incubated in PBS. Analysis of the supernatants showed a significant increase in fluorescence for MNs treated with TCEP whereas only residuals levels were measured for the control ones, which were suspected to be artifacts caused by the presence of unconjugated dye (data not shown). A pre-wash treatment with PBS to remove the dye excess followed by digestion of the MNs confirmed our hypothesis and proved that digestibility was strictly triggered by the reducing agent.

Finally, cytotoxicity of TCEP when incubated at experimentally-relevant concentrations was studied using THP-1 cells as a cellular model for immune cells (**Figure IV-10D**). Cell toxicity was not reported for any of the screened concentrations and TCEP was found highly compatible in agreement with previous data from the group.[45]

### 4.4.2.3  HA-derived MNs for sampling of the cellular and soluble fraction of ISF

Despite being a sought-after technology, MN-based platforms displaying both therapeutic and diagnostic capacities within the same device have rarely been explored since synchronizing both arms has been proven challenging.[46] However, preliminary data from the group had proven this possible since HA-derived hydrogels could release PBAE-based nanoparticles embedded in their matrix.

Having secured the therapeutic compartment of the platform, this section focused on the study of diagnostic capacity of the platform and its ability to extract ISF in the absence of chemotactic agents, which was theorized to be driven by the swelling ability of the MNs. First, extraction of the cellular component of ISF was assessed *in vitro* by incubating the arrays of MNs in monocyte-like cell suspensions followed by their digestion to collect and measure the infiltrated cellular fraction. Arrays of solid MNs were also incorporated to the analysis as controls to discern whether recovered cells were embedded within the hydrogel matrix or originated from unspecific interactions with the MN walls. Prior to MN digestion, MN arrays were also washed in PBS to remove weakly-attached cells that might be interacting with the backing layer, but also as means to normalize sample recovery. Microscopy analysis confirmed cell infiltration in the hydrogel (**Figure IV-11A**). Also, quantification of the digested MN suspension by flow cytometry depicted that cells were diffusing into the hydrogel MNs and remained inside the matrix (**Figure IV-11B**). Expectedly, the number of cells recovered from the solid arrays was practically negligible. Results also pointed at a correlation between the swelling ability of the hydrogel and its permissiveness to cell infiltration. A higher number of cells appeared to be infiltrated within MNs formulated with the 40 kDa-crosslinker if compared against the other formulations. As discussed before, it was hypothesized that functional groups such as amines might be playing a key role in mediating cell infiltration and more importantly, cell retention inside the hydrogel matrix. In future studies, it might be of interest to keep exploring chemical decoration of HA with other moieties as means to boost cell penetration and enhance the diagnostic capacity of MNs.
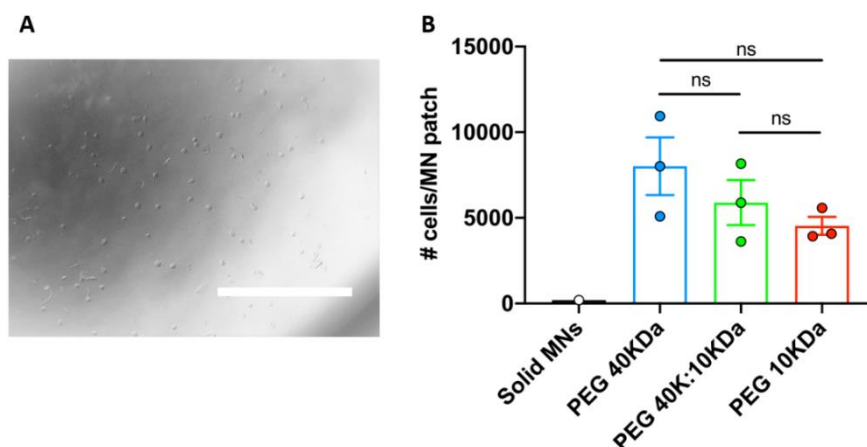


**Figure IV-11. Hydrogel-based MNs can sample cellular biomarkers *in vitro*.** Cell infiltration inside the HA-derived hydrogels was confirmed by optical microscopy (**A**) and by flow cytometry (**B**). MNs were incubated with THP-1 cells for 24 hours to allow cell penetration and digested under reducing conditions. Recovered cells were quantified by flow cytometry using solid, PLGA-based, MN arrays as control. Data are represented as mean ± SD (n = 3). Multiple comparisons among groups were determined using either one-way ANOVA followed by a post-hoc test or non-parametric t test (Mann-Whitney) when applicable.

Finally, the capacity of the platform to sample the soluble biomarkers from ISF was examined. Despite not being a diagnostic target in this project, analysis of soluble biomarkers is the subject of much current interest,[25] so it seemed only fit to include this parameter to our study. Sampling with MNs was investigated using a mimetic skin model as others before.[34,35] Briefly, agarose gels mimicking the mechanical properties of the epidermis/ISF were covered with a stretched layer of parafilm that emulated the water-impermeable stratum corneum. Hydrogel-based MNs were then applied to the skin model containing a model analyte, Rhodamine B (RhoB), which was recovered after digestion of the patches. Differences in RhoB concentration could be easily detected by gross observation as evidenced by the change in color intensity of the MN matrix after administration (**Figure IV-12A**). Quantification of the analyte absorbance confirmed a linear correlation between the concentration of RhoB in the skin-mimetic hydrogel and the concentration of the retrieved ISF when sampled using the PEG-40 kDa:10 kDa-derived MNs (**Figure IV-12B**).
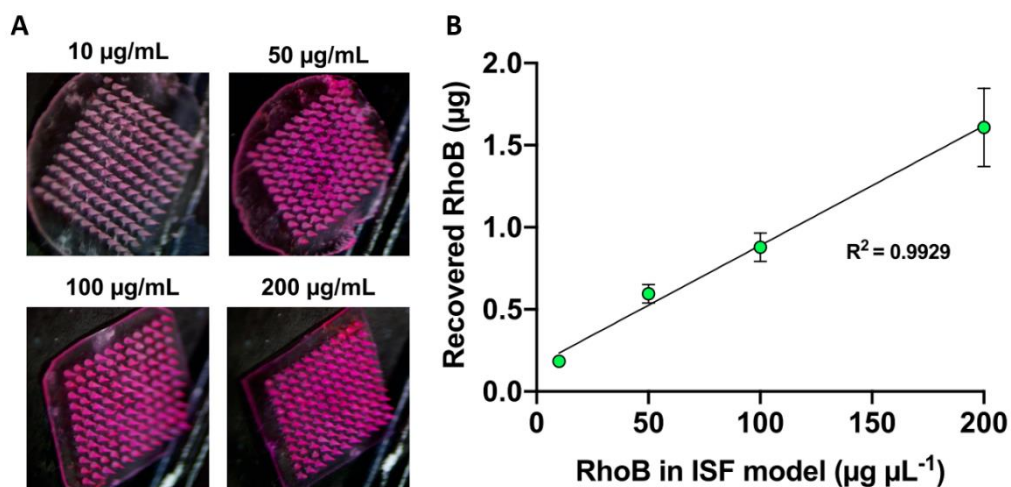


**Figure IV-12. Analyte recovery (RhoB) from mimetic skins with HA-derived MNs.** Increasing intensities in color were observed when sampling ranging concentrations of Rho with the MNs (**A**) Detected RhoB concentration was quantified by absorbance and compared to the real RhoB concentration in HA-based MNs, $R^2 = 0.9929$ (**B**) Data are represented as mean ± SD (n = 3).

Summarizing, characterization of the HA-derived MN platform confirmed its potential to disrupt the skin for transdermal delivery of immunomodulators while allowing superior ISF extraction. The novel mechanism for on-demand degradation allowed recovery of both soluble and cellular fraction of ISF entrapped in the MN matrix without compromising the viability of the latest. Following characterization of the platform, MNs integrating both a therapeutic and a diagnostic arm were fabricated for simultaneous drug delivery and monitoring of the response to therapy.

### 4.4.3 Use of HA-derived MNs for cancer theranostics

#### 4.4.3.1 Characterization of CpG-complexing PBAE polyplexes

The use of the ODN 1826 CpG, a class B TLR9 agonist, was proposed as an anti-tumor immunotherapy owing to its proven ability to enhance tumor responsiveness to checkpoint inhibitor therapeutics[14] and radiotherapy[47] when delivered as a multi-arm therapy. CpG ODNs are single-stranded short synthetic DNA molecules making their phosphodiester bond of native DNA especially prone to premature clearance by endonucleases if delivered as free drugs,[48] thus a delivery vector was necessary. Specifically, it was proposed to utilize the triarginine-modified C6 PBAE (CR3-C6) as delivery vehicle since previous data from the group proved that it could effectively delivery cyclic dinucleotides (CDNs) binding to STING,[49] another innate signaling pathway used in cancer treatment. Given its similarities with TLR9 agonists in inducing inflammation and immunity, it was hypothesized that this formulation could be an excellent starting point for this application too.

Although TLR9 receptors reside predominantly in the endoplasmic reticulum in resting cells, recognition of CpGs occurs in endolysosomes.[50] Activation of TLR9 by CpG requires the acidification of endosomes and lysosomes,[51] which our group has long reported that can be controlled via chemical decoration of PBAEs with oligopeptides to tune their buffering capacity.[52,53] After completion of this study with the CR3-C6 polymer, it could be of interest to conduct a methodical screening using other OM- and MM-formulations to favor this phenomenon. Moreover, the lessons learned throughout this work in terms of cell-specificity and transfection efficiency as a function of oligopeptide decoration and mannosylation could be of use here to promote specific targeting of the immune compartment.

First, a retardation gel assay was performed to establish the PBAE-to-ODN ratio required for full complexation of the therapeutic nucleic acid (**Figure IV-13A**). Again, the presence of guanidinium groups and primary amines was predicted to facilitate the protonation of the CR3-C6 polymers and in consequence, electrostatic binding to the ODNs. DNA migration was impeded at weight ratios higher than 50:1 PBAE:CpG ODN, thus becoming the ratio of choice throughout the rest of the study. Analysis by DLS confirmed the encapsulation of CpG ODN into discrete and monodisperse particles (PDI > 0.3) in the nanometric range (hydrodynamic diameter = 99.57 nm) (**Figure IV-13B**). Assessment of the surface charge of the nanoparticles confirmed that they were positively charged (zeta potential = 18.5 mV) as expected due to the presence of protonable groups in the oligopeptides.
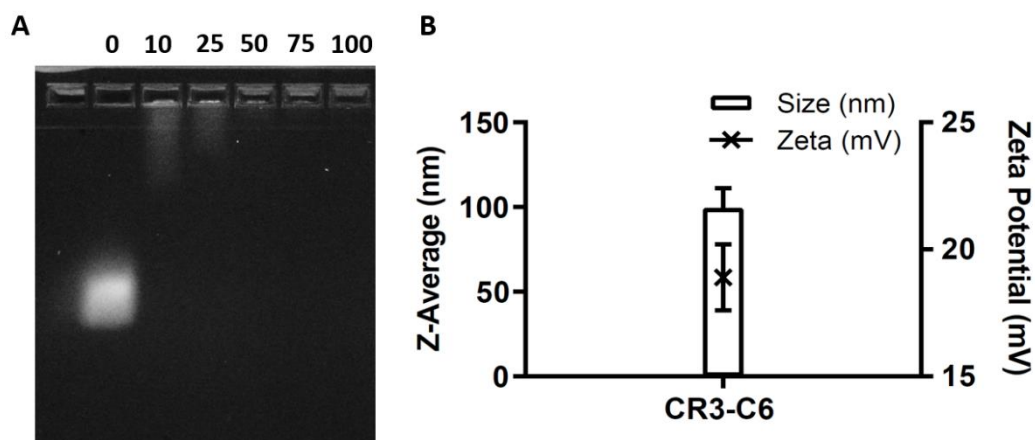
**Figure IV-13. Physicochemical characterization of PBAE:CpG ODN nanoparticles.** Gel retardation assay of CR3-C6 derived polyplexes using increasing polymer-to-ODN ratios (**A**). The average hydrodynamic diameter and zeta-potential distributions were analyzed by Dynamic Light Scattering (**B**). Polydispersity index (PDI) values were lower than 0.3 for all measurements. Results are shown as mean and standard deviation of triplicates.

#### 4.4.3.2   Model justification and experimental design to assess the theranostic capacity of HA-MNs

Next, the theranostic potential of the HA-based MNs loaded with PBAE:CpG ODN polyplexes was examined in a colorectal cancer model. Here, a murine cancer model using MC38 colon adenocarcinoma cells was generated since it is a highly immunosuppressive model and poorly responsive to checkpoint inhibitor therapies in clinical settings.[54] Specifically, the low densities of CD8+ T cells and the overwhelming number of suppressor cells, constituting more than 50% of all CD45+ immune cells in tumors,[55] generate strongly immunosuppressive microenvironments within the tumors that here were challenged via MN-based delivery of immunostimulatory therapeutics. CpG ODNs were used as a monotherapy to test the feasibility and therapeutic potential of MNs when delivering this immunomodulator using the transdermal route. However, it should be noted that TLR9 agonists, particularly in combination with checkpoint inhibitors,[18] have demonstrated their highest potential as a synergistic treatment, which our group expects to explore in the future.

The experimental design pursued for the *in vivo* studies has been detailed in **Figure IV-14**. Briefly, C57BL/6 mice were injected MC38 cells in their flanks to induce a subcutaneous tumor model. Seven days-post induction, the therapeutic regimen was commenced for three groups (n=10) treated with (1) PBAE:CpG ODN polyplexes delivered via MNs, (2) PBAE:CpG ODN polyplexes delivered intratumorally via hypodermic injection or (3) a control group without any type of treatment that was

used to define the baseline immunity of the cancer model. On the following day, therapeutic MNs were removed and a new set of empty MNs (diagnostic MNs) was applied to all groups to surveil the changes in their immune profiles as a response to therapy by flow cytometry. Sampled ISF from the therapeutic MNs could have been used to that end since HA-MNs allow for simultaneous drug delivery and ISF sampling yet 24 hours between the treatment and the sampling timepoint were allowed and a new set of MNs was used as it was predicted that fluctuations in the immune profiles would be more evident. This protocol was repeated 5 times until day 13 post-therapy initiation where half of the mice were used for macroscopic examination of the therapeutic efficacy which was daily monitored by tracking their survival and tumor growth once the therapeutic regimen was completed. The other half of mice were reserved for mechanistic analysis to evaluate the therapy efficacy at the cellular level by flow cytometry and IHC analysis. Specifically, the cellular immune signature of MN-sampled ISF was compared with that obtained from the tumors, and the skin surrounding them, to address whether a correlation could be established between them and to prove the diagnostic potential of ISF as source of biomarkers. Ultimately, it was hypothesized that MNs could provide means for non-invasive immunosurveillance and continuous monitoring of the response to therapy if positive correlations were to be stablished between MN-sampled ISF and the tumor microenvironment, becoming an alternative to current invasive approaches.
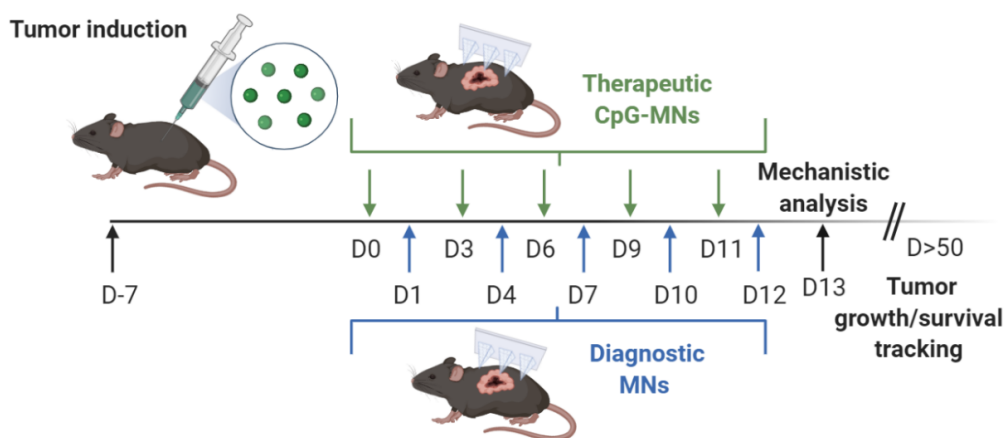


**Figure IV-14.** *In vivo* **assessment of the theranostic potential of HA-based MNs embedded with PBAE:CpG ODN polyplexes in a murine colorectal model (MC38)**. PBAE:CpG ODN polyplexes were administered using the HA-derived MNs or via intratumoral injection as a control group (1 µg/ dose) (n=10 mice/group). Changes in the immune profiles were monitored every other day in ISF by flow cytometry using the HA-based MNs as a minimally-invasive platform for ISF extraction. Mechanistic analysis were performed at day 13 by flow cytometry and IHC while tumor growth/survival was tracked until termination of the experiment by day ≈50.

#### 4.4.3.3 Macroscopic assessment of the therapeutic efficacy of the MNs *in vivo*

Fist, we focused on the therapeutic compartment of the MN platform and its ability to instigate antitumor immune responses that resulted in tumor growth suppression. When administrating the MNs, it was attempted to localize the therapeutics as proximal to the tumor site as possible since the use of a subcutaneous cancer model —instead of an orthotopic— prevented from localizing the therapy intratumorally if delivered with the MN platform. MNs could be administrated on top of the tumors and "wrap" them to maximize the treated area. The flexibility of the polymeric backing layer allowed to intimately adjust the MN array to the geometry of the tumor. Contrarily, the needle-like projections of the patch were robust enough to effectively pierce the skin (**Figure IV-15**). As the experiment went by, an experimental limitation was encountered since increasing tumor sizes impeded full coverage and prompted premature detachment of the edges of the patch, which was predicted to result in the delivery of suboptimal dosages. In those cases, MN patches were accommodated in the neighboring areas surrounding the tumor rather than on top in an attempt to ameliorate this issue.
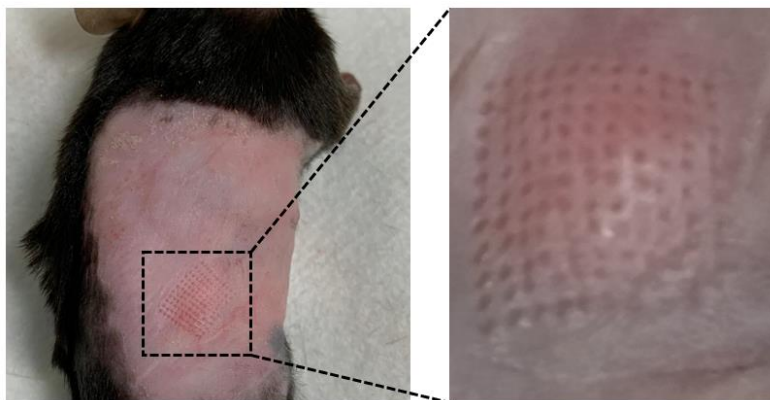


**Figure IV-15. Assessment of effective skin penetration in a tumor model using HA-based MNs.** Macroscopic images confirming *in vivo* penetration of the skin when using hydrogel MNs. Effective disruption of the skin was evendiced by the presence of microconduits surrounding the tumor.

Following completion of the treatment delivered via MNs or intratumoral injection (as positive control), tumor growth suppression was monitored daily via caliper measurement. Tumor growth measurements confirmed that control tumors left untreated grew rapidly as expected, whereas PBAEs complexing CpG ODN showed great potential in delaying tumor growth regardless of the administration route (**Figure IV-16A**). Results showed that tumor burden was inhibited in the

treatment groups while actively treating the individuals and variations in the tumor volume could only be noticed once the treatment was ceased. By contrary, tumor volumes in the untreated group were significantly higher by day 17 post-tumor induction already. Overall, local delivery of PBAE:CpG ODNs polyplexes via intratumoral injection inhibited tumor growth more efficiently than when using MNs. Regardless of the administration route, the therapeutic merit of PBAE-derived polyplexes was irrefutable since a 3-fold and a 20-fold reduction in tumor volume was registered by the end of the experiment when delivered transdermally ($\approx$200 mm$^3$) and intratumorally ($\approx$30 mm$^3$), respectively. It is worth of mention that the therapeutic potency of the TLR9 agonist when encapsulated in OM-PBAEs surpassed that from previous studies employing the same therapeutic agent and cancer model,[14] with the added value that here it was administered as a monotherapy whereas in previous attempts it had been pursued as part of a multi-arm therapy combining the immunostimulatory molecule, the ODN 1826 TLR9 agonist, with a checkpoint blockade immunotherapy (CTLA4) known to synergically drive antitumor immunity.[5,15] In light of these findings, the potential of OM-PBAEs as delivery vehicles for anticancer immunotherapies was reasserted, supporting that localization of the immunostimulant within the endolysosomal compartments, where TLR9 is preferentially expressed, can favor tumor growth suppression.[56] In agreement with others,[14] nanoencapsulation of the CpG ODN also induced suppressive effects at much lower doses than those needed when delivered intratumorally as free drugs.[57]

The distinct performances of the PBAE vectors depending on the administration route might be explained by various reasons. First and foremost, localizing the therapy at the site of neoplasia via intratumoral injection is expected to increase the bioavailability and in turn, the potency of the treatment yet not without limitations. While intratumoral delivery of immunotherapy drugs is increasing rapidly in both the investigational and standard of care domains, especially for palpable subcutaneous lesions, the feasibility and safety of these interventions for deeper lesions such as colorectal cancer that require image-guidance remains unknown.[58] Given that most intratumoral immunotherapy clinical protocols typically require repeated drug administrations, legitimate concerns have arisen regarding the risks of bleeding and organ injury due to frequent, repeated needle punctures. Contrarily, unleashing antitumor immunity with MNs would be a minimally-invasive, needle-free approach that could generate an almost-abscopal effect when signaling and priming the immune subsets present in the dermal compartment.[18] Experimentally, quantifying the total amount of PBAEs embedded in the MNs matrix was not possible so it could only be confirmed theoretically that the dosages delivered using the HA-MNs were equal to those injected

intratumorally. For this reason, it would be premature to claim that the overall performance of CpG-loaded MNs was inferior to that mediated intratumorally. Similarly, including an extra control group administered PBAE:CpG ODNs polyplexes by subcutaneous injection, instead of intratumoral injection, might have provided a deeper insight into the impact of the administration route on the overall therapy efficacy.

The suppression of tumor growth observed in individuals treated with the TLR9 agonist had an obvious impact on their survival. Animal survival in the untreated group was significantly reduced in compared to the treated groups, which registered more than a 2-fold increase in survival frequencies when treated with PBAE:CpG-loaded MNs (**Figure IV-16B**). A dramatic improvement in survival was also observed in control mice administered PBAE polyplexes intratumorally, where only 1 out 6 mice had to be euthanized by the end of the study. The rest of individuals were predicted to have survived for a few extra weeks given their minimal tumor size at the time of experiment completion (30 mm$^3$).
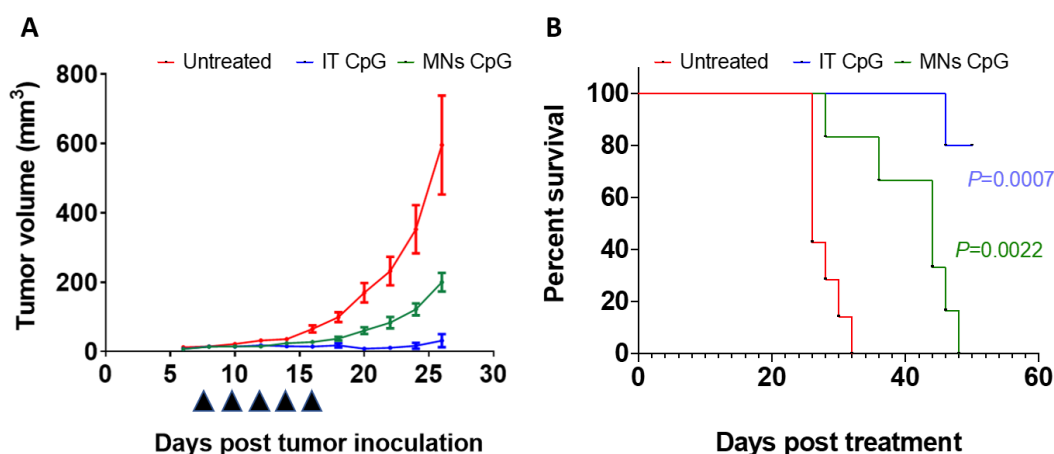


**Figure IV-16. Analysis of tumor growth suppression following delivery of PBAE:CpG polyplexes via MNs.** CR3-C6 PBAEs complexing CpG ODNs were delivered via HA-based MNs or intratumorally as a control group. 1 μg ODN encapsulated in PBAEs were administered five times every other day. Tumor growth was monitored by caliper measurements (**A**). Data are represented as mean ±SD (n=6). Kaplan–Meier survival curves of mice treated with the indicated formulation using a 1000 mm3 tumor volume or poor body condition as the endpoint criteria (**B**) Statistical analysis (n=6) was performed using a Log-Rank Mantel–Cox test.

### 4.4.3.4   Analysis of the therapeutic potential of MNs to modulate the tumor microenvironment

Antitumor immunity, and its impact on tumor growth suppression, was also examined at the cellular level by immunohistochemical analysis using H&E and Ki-67 staining as representative

biomarkers of proliferation. In agreement with the macroscopic findings, it was found that the tumor microenvironment (TME) of tumors treated with PBAE:CpG ODNs polyplexes had lower frequencies of proliferating cells compared to untreated tumors (**Figure IV-17**). Intracellular expression was significantly higher in the untreated group whereas differences between MN- versus intratumoral-delivery were not observed.
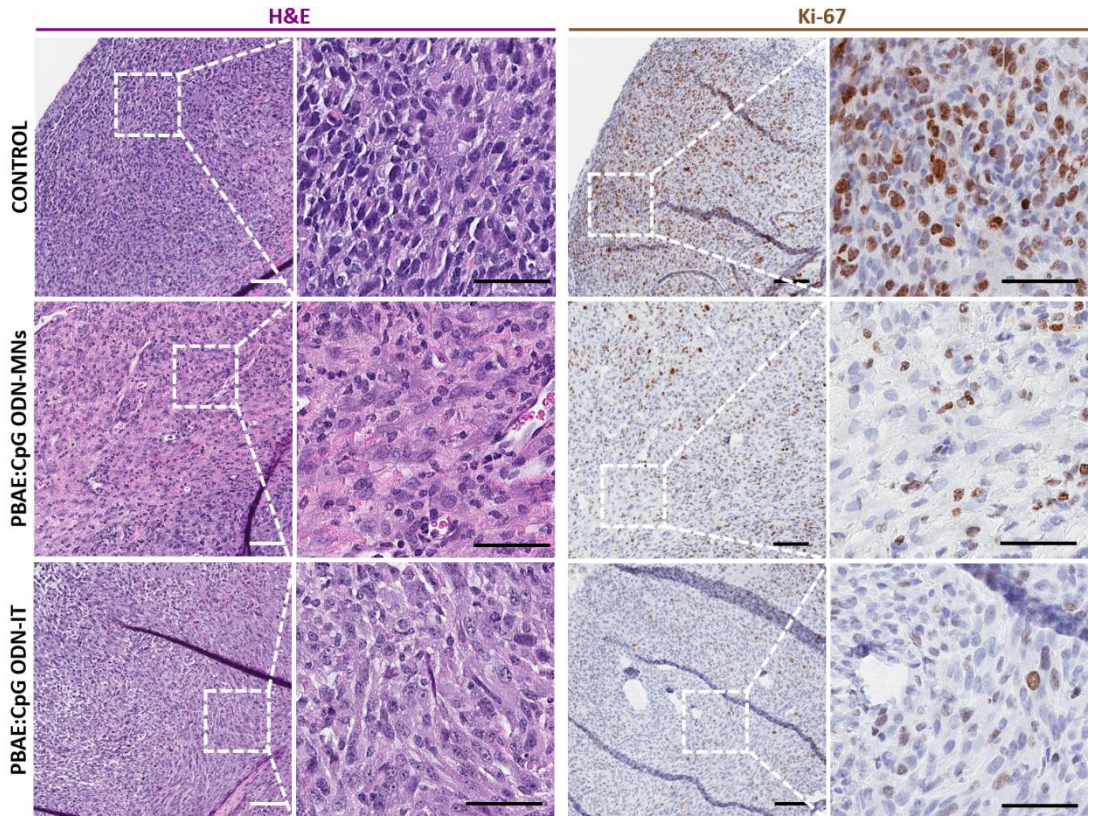


**Figure IV-17. Evaluation of the changes in the tumor microenvironment following delivery of CpG ODNs.** Tumors from each group were harvested on the day of mechanistic analysis and cryosectioned in 20-μm tissue slides for IHC analysis. Staining for H&E and Ki-67 were performed as proliferation biomarkers. Scale bar = 100 μm.

Next, the ability of the PBAE:CpG ODNs polyplexes to modulate the tumor microenvironment (TME) when delivered using HA-based MNs was examined by flow cytometry immunophenotyping. An increase in activated granulocytic cells (CD11b+ Gr-1+, which includes monocytes, neutrophils, eosinophils and myeloid-derived suppressor cells) was evident in both treatment groups (p=0.007 for MN-based delivery and p=0.509 intratumoral (**Figure IV-18A**). These results were consistent with the notion that granulocytes, particularly neutrophils, are among the first responders that migrate to the site of inflammation[59] —in this case induced by TLR activation.[60] Various studies have reported the
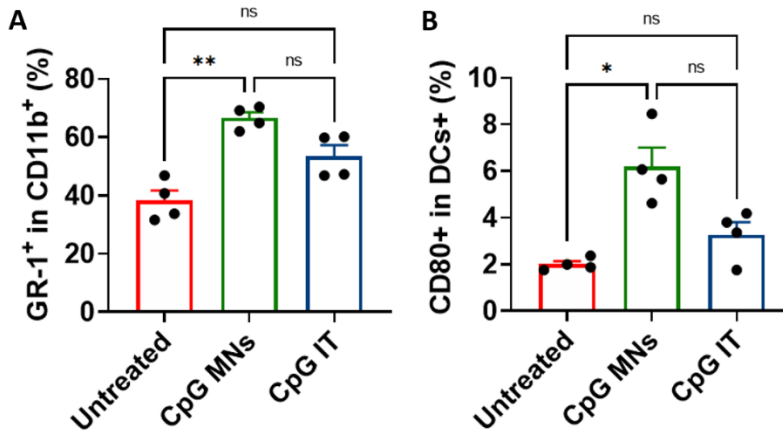
**Figure IV- 18. Immunophenotyping by flow cytometry of tumor lysates following treatment with PBAE: CpG polyplexes.** 13 day post treatment initiation, tumors from the three experimental groups were harvested and digested enzymatically. Cell phenotypes composing the tumor were enumerated by flow cytometry. Flow cytometry quantification of granulocytic cells (**A**) (CD11b$^+$, Gr-1$^+$) and DCs (**B**) (CD80$^+$ cells in CD11c$^+$ MHCII$^+$). Data are represented as mean ± SEM (n = 4). Multiple comparisons among groups were determined using one-way ANOVA followed by Kruskal-Wallis test. P-value: *$p < 0.05$, **$p < 0.01$.

antitumor properties of tumor-associated neutrophils such as direct toxicity towards malignant cells and abrogation of metastasis.[61] However, the exact role of neutrophils in cancer has long been a matter of controversy. On the other side of the coin, neutrophils also appear to support tumor progression and high frequencies have been correlated with poor patient prognosis. [62] Indeed, their functional plasticity has been recently demonstrated as they can undergo alternative activation — towards a pro- or an antitumor phenotype— depending on the cues found in the TME.[63] In agreement with others, [55] our results confirmed that granulocytic cells accounted for at least a 40% of the CD45+ cell compartment within the TME (**Figure IV-18A**). Such dominance supports their foreseen potential as a therapeutic target for next generation immunotherapies,[64] specially in tumors with low T cell densities showing poor responsiveness to current strategies.[54]

TLR agonists can provoke distinct immune stimulatory effects depending on their structural and biological properties. So far, three main families have been described —CpG ODN class A, B, and C— where each of them has a differential influence on interferon gamma (IFN-α) secretion and DC activation.[51] In this study, the ODN 1826 belonging to class B was used, which are known to be weak inducers of IFN-α production but strong stimulators of DC maturation and as a consequence, expression of costimulatory molecules such as CD80, CD86 or CD40.[65] Aimed at demonstrating such immune stimulatory capacity, expression of the CD80 (B7-1) receptor on DCs was also assessed.

Analysis of the enzymatic lysates of the tumors by flow cytometry confirmed a significant increase in CD80 expression in those mice administered the PBAE:CpG ODNs polyplexes using MNs (p=0.015) (**Figure IV-18B**). CD80 expression was also higher on mice treated via intratumoral injection if compared to the untreated group, yet significant differences could not be claimed in this case. Augmented expression of proinflammatory molecules when delivering the polyplexes transdermally may be explained by the fact that the skin harbors a richer immune population of DCs, if compared to the scarce reservoir in the tumor, which may have facilitated nanoparticle uptake by DCs and their maturation as a response to the inflammatory signals; here, the CpG ODNs.

Finally, fluctuations in the T cell compartment of the TME induced by the immune stimulators were examined. Infiltration of CD8+ cytotoxic T cells into the TME is a hallmark of antitumor immunity as they play essential roles in killing tumoral cells.[66] Complimenting their effector sister lineage, CD4+ T cells provide with "helper" functions such as antibody and cytokine production to boost the cytotoxic responses.[67] Overall, our results confirmed that immune T cell infiltrates in the TME were minimal (accounting for less than 1% of all CD45 + cells), a feature commonly described as "immune-desert" and which characterizes T cell uninflamed tumors such as in colorectal cancer.[7] For both CD8+ and CD4+ T cells, a moderate increase was observed in their frequencies, especially in mice administered the polyplexes intratumorally, although significant differences between MN-treated and untreated mice could not be claimed (**Figure IV-19**).
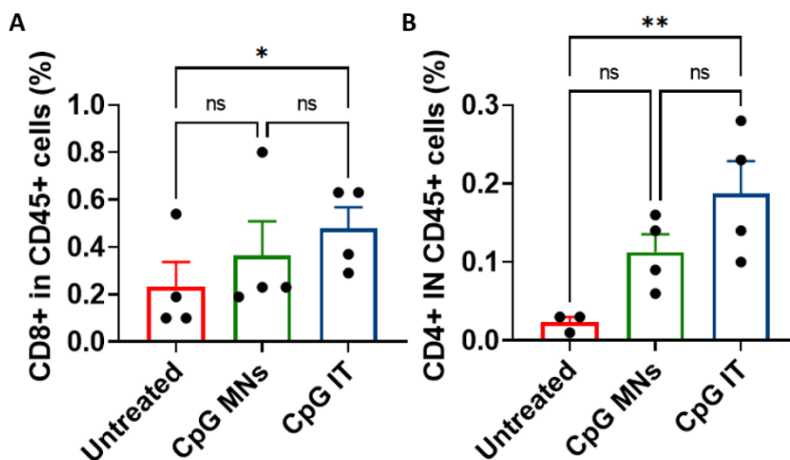


**Figure IV-19. Analysis of the immune T cell compartment in the TME following immune stimulation with CpG ODNs.** Harvested tumors were processed as described and the resulting cellular suspensions were stained for flow cytometry immunophenotyping. Quantitative representation of CD8+ T cells (CD45+ CD3+ CD8+) (**A**) and CD4+ T cells (CD45+ CD3+ CD4+) (**B**) Data are represented as mean ± SEM (n = 4). Multiple comparisons among groups were determined using one-way ANOVA followed by Kruskal-Wallis test.

Given the ability of CpG ODNs to enhance immune stimulation, higher CD8^{+} T cell infiltrates had been expected in the treatment groups, a hypothesis supported by the proven efficacy of the therapy in terms of tumor growth suppression and prolonged survival. On the one hand, it was theorized that the use of CpGs belonging to class A or class C, which sustain secretion of type I IFN more effectively than class B,[51] may have boosted higher levels of CD8^{+} T cell proliferation. Since type I IFN induces optimal signaling for cross-priming of CD8^{+} T cells by DCs,[68] an enhanced first-step of immune priming could have led to superior T cell activation and infiltration into the TME. On the other hand, it may be advisable to redesign the experimental plan since performing the mechanistic analysis one day after finishing the treatment might have been too premature or too late to see any remodeling of the T cell immune composition in the TME. Therefore, surveilling the fluctuations in the T cell composition at earlier or later time points could help elucidate the immunomodulatory role of the therapy.

Moreover, it would be beneficial in future studies to include another experimental group receiving combination therapy with checkpoint inhibitors. As previously discussed, the maximum therapeutic efficacy of CpGs has been accomplished when administered as the adjuvant component of multi-arm immunotherapies. Evidence supports that the synergistic effect with checkpoint blockade improves both the quantity and quality of CD8^{+} T cells, becoming polyfunctional and with superior ability to suppress tumor growth in colorectal cancer models.[69] For this reason, it was predicted that differences in the frequencies of CD8^{+} T cells would be more noticeable in groups receiving combination treatments.

Regarding the CD4^{+} T cell fraction, a more evident increase of its frequency was reported, especially in mice receiving the control intratumoral injection. These results are supported by the literature, since the class B TLR used for this study is known to promote activation of B cell and results in potent T helper-1-type immune responses.[51]

### 4.4.3.5  *In vivo* assessment of the potential of the MNs for immune surveillance

Once confirmed the therapeutic merit of the MNs to suppress tumor growth and immunomodulate the TME, their diagnostic ability to uptake ISF as means for minimally-invasive immunosurveillance was tested. As described herein, the immune profiles of ISF were originally aimed to be contrasted with those from the tumors and the skin surrounding the area of MN administration. Unfortunately, the immunophenotyping results obtained from the harvested skins were inconclusive

due to an experimental drawback and comparison of the skin immune signature against ISF, which was ought to share the most similarities with, was not possible.

On the day of mechanistic analysis, the last set of MNs applied to all treatment groups were retrieved and digested under reducing conditions to isolate the cellular fraction of ISF. Next, the cellular suspensions obtained from the MNs were stained along with those isolated via enzymatic digestion of the tumors. Comparison of the T cell immune profiles from ISF and tumors revealed a similar distribution of the T cells frequencies. If normalizing the CD8+ T cell population to CD3+ cells, significant differences among treatment groups compared to the untreated mice could not be claimed in ISF nor in the tumors (**Figure IV-20**, left panels). A similar trend was also confirmed for the CD4+ T cell population (**Figure IV-20**, middle panels).
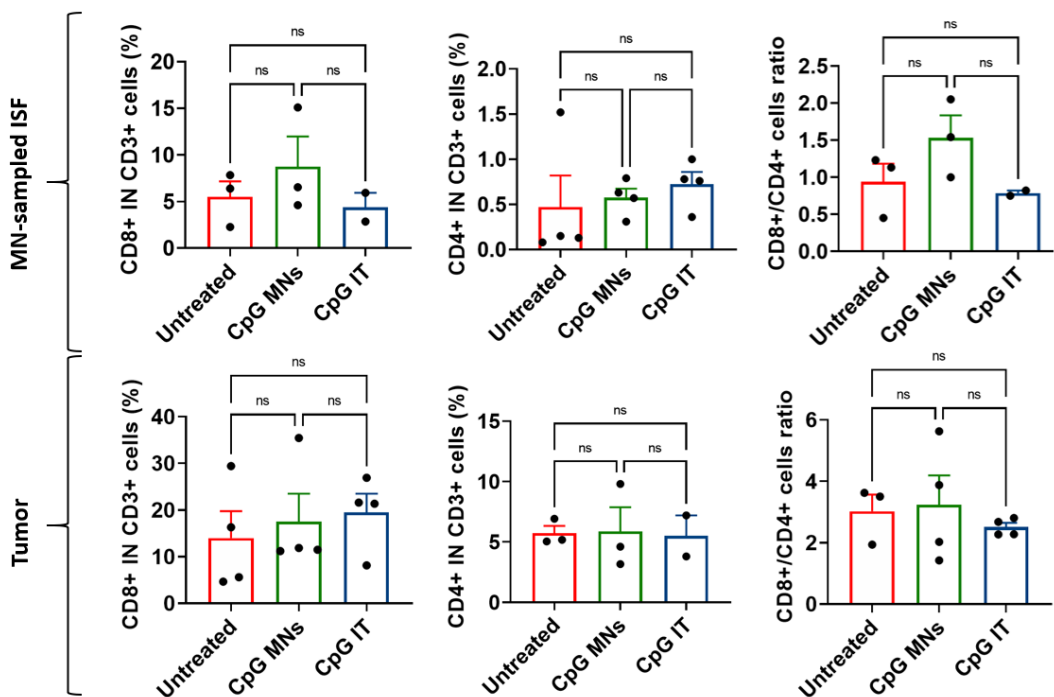


**Figure IV-20. Analysis of the immune T cell signature in MN-sampled ISF and tumors.** MNs retrieved on the day of mechanistic analysis were digested under reducing conditions and stained for immunophenotyping along with tumor lysates. Immune profiles compared included CD8+ T cells, CD4+ T cells and CD8+-to-CD4+ T cell ratio. MNs corresponding to 3-4 mice were pooled together and represented as experimental triplicates. Each replicate from tumor lysates correspond to one mouse (n = 4). Multiple comparisons among groups were determined using one-way ANOVA followed by Kruskal-Wallis test.

In primary colorectal cancers, tumor infiltrating lymphocytes have been proven as a robust prognostic biomarker with higher accuracy than clinicopathologic characteristics.[70,71] Therefore, changes in the CD8+-to-CD4+ T cell ratio were measured as a common prognosticative biomarker of responsiveness to immunotherapy.[72] Quantification by flow cytometry of the cell infiltrates in MN-sampled ISF and in tumors revealed no significant increase of the CD8+/ CD4+ ratio following immunotherapy (**Figure IV-20**, right panels). If not significant, analysis of the MN-sampled ISF showed a higher ratio in mice treated with PBAE-loaded MNs if compared to untreated mice. In light of these findings, it may be of interest to sample ISF multiple times —both at early and late time points— to assemble an immune temporal profile and assess whether MNs could inform earlier on the immune state of the individual since they collect circulating cells that may be on their way to the site of threat.

Interestingly, the magnitude of the deviations registered in the frequencies of T cells when sampled with the MNs did not differ from those observed in the tumors, supporting the potential of the MNs as a mode of tissue surveillance. Specific differences in the overall numbers could be explained by two main hypothesis. On the one hand, the samples recovered from ISF and tumors were processed in different manners, which may have left to experimental differences. Cellular suspensions from 3 or 4 MN patches applied to mice of the same group were pooled together in order to have experimental triplicates with sufficient events to make strong statistical claims. Contrarily, each event represented in the quantification of T cells in tumors corresponds to a single individual. For this reason, increasing the n of each group may be helpful in future studies so tumor suspensions of various animals can also be pooled for a more accurate comparison. On the other hand, the correlations between the TME and ISF remain largely unknown, especially when sampled from distal sites such as the skin. To our knowledge, correlation of the ISF composition with the physiological and pathological state of the tumor has only been attempted using soluble biomarkers such as proteins and nucleic acids.[73,74] In that case, a positive correlation was stablished in a breast cancer model yet ISF was sampled from inside the tumor and the proteome, but not the immune cell composition, was discussed.

To sum up, our results supported the use of HA-based MNs for surveilling the immune cell compartment of ISF. If tentatively, the resemblance in the T cell immune signature of MN-sampled ISF with that from the tumors hinted at the potential of this platfrom for monitoring progression of the disease in cancer settings. Nevertheless, further studies are needed to confirm whether immune profiling of the ISF in distal sites with MNs could serve as a prognosticative tool to infer on the state of tumor and the prognosis of the individual.

## 4.5  Concluding remarks

The results of this chapter prove the potential of PBAE-complexed immunostimulatory drugs to unleash antitumor immunity when delivered transdermally with MNs. Hydrogel-forming MNs loaded with OM-PBAEs were capable of inhibiting tumor growth suppression and modulate the tumor microenvironment while allowing *in situ* ISF extraction for immune surveillance.

Engineering the chemical backbone of HA via click chemistry allowed to generate multiple candidates for fabrication of hydrogel-based microneedles. Thiol-terminated and methacrylated candidates did not met the needed requirements for theranostics whereas the amino-modified HA polymer rendered highly swellable MNs allowing cell infiltration and on-demand digestion. Chemical linkage of a lateral chain allowed to introduce a primary amine group (for hydrogel formation) and a disulfide bond (for hydrogel degradation).

Swelling ability, mechanical strength and on-demand digestibility of the MNs was thoroughly examined as a function of the crosslinking agent. Molecular weight of the crosslinker had a notorious impact on both swelling ability and mechanical strength of the HA-derived MNs, supporting the use of MNs crosslinked with a 70:30 mixture of 40kDa:10kDa-8-arm-PEG-NHS in future studies. Digestion studies proved efficient MNs digestion —in less than 5 minutes— of the whole hydrogel matrix.

The capacity of the MNs to recover cellular and soluble biomarkers from ISF was examined *in vitro*. Following MN digestion, effective recovery of cells was confirmed by flow cytometry and where the amount of extracted cells correlated with the swelling ability of the hydrogel. Recovery of soluble biomarkers was proven using an *in vitro* model mimicking the ISF/epidermis. The extracted mass of the analyte, RhoB, correlated with that originally present in the skin model.

The therapeutic potential of HA-based MNs was examined in a colorectal cancer model *in vivo* using immunostimulatory nucleic acids (CpG ODNs) as an adjuvant model for improved responsiveness to checkpoint inhibitors. PBAE:CpG ODNs polyplexes delivered with MNs induced significant tumor growth suppression as evidenced by macroscopic measurements of the tumor volume over time. In agreement, increased survival frequencies were registered for the treated group administered therapeutic polyplexes via MNs or intratumorally as a control if compared to untreated individuals. Moreover, IHC studies confirmed tumor growth suppression at the cellular level as evidenced by the significant reduction of proliferation biomarkers.

Immunomodulation of the TME was examined by flow cytometry immunophenotyping. Augmented levels of granulocytes were observed in those mice administered PBAE:ODNs polyplexes. Moreover, an increase in the expression of the proinflammatory receptor CD80 by DCs was proven, supporting the immunostimulatory role of the CpG ODNs and their ability to promote DC maturation, particularly when delivered via MNs.

The T cell uninflamed nature of the tumors was demonstrated by flow cytometry analysis since T cells accounted for less than 1% of all CD45+ events. Moreover, delivery of immune stimulators did not promote infiltration of CD8+ T cells into the tumor regardless of the delivery route.

The ability of HA-based MNs to sample ISF for *in situ* immunosurveillance was proven. MNs allowed to sample the cellular compartment of the ISF from the tumor and retrieve the immune cells for immunophenotyping by flow cytometry. Comparison of the T cell frequencies in ISF and in tumor lysates revealed a correlation between both tissues, since no significant differences where observed between treated/untreated individuals, supporting their use as a mode of tissue surveillance.

In conclusion, we have engineered a novel MN platfrom with a dual function for therapy and immune surveillance in cancer settings. MNs allowed the delivery of PBAEs complexing a TLR agonist, mediating tumor growth suppression and immunomodulation of the TME in a minimally-invasive way. Simultaneously, MNs allowed for *in situ* recovery of immune cells from ISF, opening up potential avenues for monitoring the response to immunotherapy. In light of these findings, the use of HA-based MNs for immunosuppression, instead of immune stimulation, will be proposed in the next chapter; specifically, for the management of skin transplant rejection.

## 4.6 References

1.    McCarthy, E. F. The toxins of William B. Coley and the treatment of bone and soft-tissue sarcomas. *Iowa Orthop. J.* 26, 154–158 (2006).

2.    Mellman, I., Coukos, G. & Dranoff, G. Cancer immunotherapy comes of age. *Nature* 480, 480–489 (2011).

3.    Arruebo, M. *et al.* Assessment of the evolution of cancer treatment therapies. *Cancers* 3, 3279–3330 (2011).

4.    Waldman, A. D., Fritz, J. M. & Lenardo, M. J. A guide to cancer immunotherapy: from T cell basic science to clinical practice. *Nat. Rev. Immunol.* 20, 651–668 (2020).

5.    Hargadon, K. M., Johnson, C. E. & Williams, C. J. Immune checkpoint blockade therapy for cancer: An overview of FDA-approved immune checkpoint inhibitors. *Int. Immunopharmacol.* 62, 29–39 (2018).

6.    Pardoll, D. M. The blockade of immune checkpoints in cancer immunotherapy. *Nat Rev Cancer* 12, 252–264 (2016).

7.    Darvin, P., Toor, S. M., Nair, V. S. & Elkord, E. Immune checkpoint inhibitors: recent progress and potential biomarkers. *Exp. Mol. Med.* 12, 1–11 (2018).

8.    Milling, L., Zhang, Y. & Irvine, D. J. Delivering safer immunotherapies for cancer. *Adv. Drug Deliv. Rev.* 114, 79–101 (2017).

9.    Riley, R. S., June, C. H., Langer, R. & Mitchell, M. J. Delivery technologies for cancer immunotherapy. *Nat Rev Drug Discov* 18, 175–196 (2019).

10.   Ellis, P. M., Vella, E. T. & Ung, Y. C. Immune Checkpoint Inhibitors for Patients With Advanced Non–Small-Cell Lung Cancer: A Systematic Review. *Clin. Lung Cancer* 18, 444–459 (2017).

11.   Barrueto, L. *et al.* Resistance to Checkpoint Inhibition in Cancer Immunotherapy. *Transl. Oncol.* 13, 100738 (2020).

12.   Nowicki, T. S., Hu-Lieskovan, S. & Ribas, A. Mechanisms of Resistance to PD-1 and PD-L1 Blockade. *Cancer J.* 24, 47–53 (2018).

13.   Duan, X. *et al.* Immunostimulatory nanomedicines synergize with checkpoint blockade

immunotherapy to eradicate colorectal tumors. *Nat. Commun.* 10, 1899 (2019).

14.   Buss, C. G. & Bhatia, S. N. Nanoparticle delivery of immunostimulatory oligonucleotides enhances response to checkpoint inhibitor therapeutics. *Proc. Natl. Acad. Sci. U. S. A.* 117, 13428–13436 (2020).

15.   Moynihan, K. D. & Irvine, D. J. Roles for innate immunity in combination immunotherapies. *Cancer Res* 77, 5115–5221 (2017).

16.   Sharma, P. & Allison, J. P. Immune Checkpoint Targeting in Cancer Therapy: Towards Combination Strategies with Curative Potential. *Cell* 161, 205–214 (2015).

17.   He, M. *et al.* Immune Checkpoint Inhibitor-Based Strategies for Synergistic Cancer Therapy. *Adv. Healthc. Mater.* 2002104 (2021) doi:10.1002/adhm.202002104.

18.   Karapetayan, L., Luke, J. J. & Davar, D. Toll-Like Receptor 9 Agonists in Cancer. *Onco. Targets. Ther.* 13, 10039–10060 (2020).

19.   Bhardwaj, N., Gnjaitc, S. & Sawhney, N. B. TLR AGONISTS: Are They Good Adjuvants? *Cancer J.* 16, 382–391 (2011).

20.   Krieg, A. M. Toll-like receptor 9 ( TLR9 ) agonists in the treatment of cancer. *Oncogen* 27, 161–167 (2008).

21.   Krieg, A. M. Therapeutic potential of Toll-like receptor 9 activation. *Drug Discov.* 5, 471–484 (2006).

22.   Koch, M. *et al.* Tumor Infiltrating T Lymphocytes in Colorectal Cancer. *Ann. Surg.* 244, 986–993 (2006).

23.   Moreira, A. F. *et al.* Microneedle-based delivery devices for cancer therapy : A review. *Pharmacol. Res.* 148, 1–11 (2019).

24.   Turner, J. G., White, L. R., Estrela, P. & Leese, H. S. Hydrogel-Forming Microneedles : Current Advancements and Future Trends. *Macromol. Biosci.* 21, 1–18 (2021).

25.   Samant, P. P. *et al.* Sampling interstitial fluid from human skin using a microneedle patch. *Sci. Transl. Med.* 12, 1–16 (2020).

26.   Wiig, H. & Swartz, M. A. Interstitial fluid and lymph formation and transport: physiological regulation and roles in inflammation and cancer. *Physiol Rev* 92, 1005–1060 (2012).

27.   Niedzwiecki, M. M. *et al.* Human Suction Blister Fluid Composition Determined Using High-Resolution Metabolomics. *Anal. Chem.* 90, 3786–3792 (2018).

28. Yang, Y. & Gao, W. Wearable and flexible electronics for continuous molecular monitoring. *Chem. Soc. Rev.* 48, 1465–1491 (2018).

29. Zheng, M. *et al.* Osmosis-Powered Hydrogel Microneedles for Microliters of Skin Interstitial Fluid Extraction within Minutes. *Adv. Healthc. Mater.* 9, 1–11 (2020).

30. Donnelly, R. F. *et al.* Hydrogel-Forming Microneedle Arrays for Enhanced Transdermal Drug Delivery. *Adv. Funct. Mater.* 22, 4879–4890 (2012).

31. Mccrudden, T. C. *et al.* Hydrogel-Forming Microneedles Prepared from '"Super Swelling"' Polymers Combined with Lyophilised Wafers for Transdermal Drug Delivery. *PLoS One* 9, e111547 (2014).

32. Zhang, X., Chen, G., Bian, F., Cai, L. & Zhao, Y. Encoded Microneedle Arrays for Detection of Skin Interstitial Fluid Biomarkers. *Adv. Mater.* 31, 1–8 (2019).

33. Al Sulaiman, D. *et al.* Hydrogel-Coated Microneedle Arrays for Minimally Invasive Sampling and Sensing of Specific Circulating Nucleic Acids from Skin Interstitial Fluid. *ACS Nano* 13, 9620 (2019).

34. Chang, H. *et al.* A Swellable Microneedle Patch to Rapidly Extract Skin Interstitial Fluid for Timely Metabolic Analysis. *Adv. Mater.* 29, 1–8 (2017).

35. He, R. *et al.* A Hydrogel Microneedle Patch for Point-of-Care Testing Based on Skin Interstitial Fluid. *Adv. Healthc. Mater.* 9, 1–11 (2020).

36. Mandal, A. *et al.* Cell and fluid sampling microneedle patches for monitoring skin-resident immunity. *Sci. Transl. Med.* 10, (2018).

37. Rudqvist, N., Pilones, K. A., Lhuillier, C. & Wennerberg, E. Radiotherapy and CTLA-4 blockade shape the TCR repertoire of tumor-infiltrating cells. *Cancer Immunol. Res.* 6, 139–150 (2019).

38. Chang, H. *et al.* A Swellable Microneedle Patch to Rapidly Extract Skin Interstitial Fluid for Timely Metabolic Analysis. *Adv. Mater.* 29, 1702243 (2017).

39. Donnelly, R. F., Raghu, T., Singh, R. & Woolfson, A. D. Microneedle-based drug delivery systems: Microfabrication, drug delivery , and safety. *Drug Deliv.* 17, 187–207 (2010).

40. Larrañeta, E. *et al.* Synthesis and characterization of hyaluronic acid hydrogels crosslinked using a solvent-free process for potential biomedical applications. *Carbohydr. Polym.* 181, 1194–1205 (2018).

41. Misra, Suniti, Hascall, Vincent, Markwald, R. R. & Ghatak, S. Interactions between hyaluronan and its receptors (CD44, RHAMM) regulate the activities of inflammation and cancer. *Front. Immunol.* 6, 1–10 (2015).

42. Zhu, J. *et al.* Gelatin Methacryloyl Microneedle Patches for Minimally Invasive Extraction of Skin Interstitial Fluid. *Small* 16, 1905910 (2020).

43. Lee, K. J. *et al.* A Patch of Detachable Hybrid Microneedle Depot for Localized Delivery of Mesenchymal Stem Cells in Regeneration Therapy. *Adv. Funct. Mater.* 30, 1–11 (2020).

44. Cline, D. J. *et al.* New Water-Soluble Phosphines as Reductants of Peptide and Protein Disulfide Bonds: Reactivity and Membrane Permeability. *Biochemistry* 43, 15195–15203 (2004).

45. Dosta, P. *et al.* Scale-up manufacturing of gelatin-based microcarriers for cell therapy. *J Biomed Mater Res* 7, 2937 (2020).

46. Howells, O. *et al.* Microneedle Array-Based Platforms for Future Theranostic Applications. *ChemBioChem* 20, 2198–2202 (2019).

47. Yuan, S., Qiao, T. & Chen, W. CpG Oligodeoxynucleotide 1826 Enhances the Lewis Lung Cancer Response to Radiotherapy in Murine Tumor. *Cancer Biother. Radiopharm.* 26, (2011).

48. Yin, H. *et al.* Non-viral vectors for gene-based therapy. *Nat. Rev. Genet.* 15, 541–555 (2014).

49. Dosta, P. *et al.* Delivery of Stimulator of Interferon Genes (STING) Agonist Using Polypeptide-Modified Dendrimer Nanoparticles in the Treatment of Melanoma. *Adv. NanoBiomed Res.* 2100006 (2021) doi:10.1002/anbr.202100006.

50. Latz, E. *et al.* TLR9 signals after translocating from the ER to CpG DNA in the lysosome. *Nat. Immunol.* 5, 190–198 (2004).

51. Murad, Y. M. & Clay, T. M. CpG Oligodeoxynucleotides as TLR9 Agonists Therapeutic Applications in Cancer. *Biodrugs* 23, 361–375 (2009).

52. Dosta, P., Segovia, N., Cascante, A., Ramos, V. & Borrós, S. Surface charge tunability as a powerful strategy to control electrostatic interaction for high efficiency silencing, using tailored oligopeptide-modified poly(beta-amino ester)s (PBAEs). *Acta Biomater.* 20, 82–93 (2015).

53. Segovia, N., Dosta, P., Cascante, A., Ramos, V. & Borrós, S. Oligopeptide-terminated poly (b-amino ester) s for highly efficient gene delivery and intracellular localization. *Acta Biomater.*

10, 2147–2158 (2014).

54. Postow, M. A., Callahan, M. K. & Wolchok, J. D. Immune Checkpoint Blockade in Cancer Therapy. *J. Clin. Oncol.* 33, (2015).

55. Mosely, S. I. S. *et al.* Rational Selection of Syngeneic Preclinical Tumor Models for Immunotherapeutic Drug Discovery. *Cancer Immunol. Res.* 5, 29–42 (2017).

56. Radovic-Moreno, A. F. *et al.* Immunomodulatory spherical nucleic acids. *Proc. Natl. Acad. Sci. U. S. A.* 112, 3892–3897 (2015).

57. Switaj, T. *et al.* CpG immunostimulatory oligodeoxynucleotide 1826 enhances antitumor effect of interleukin 12 gene-modified tumor vaccine in a melanoma model in mice. *Clin. Cancer Res.* 10, 4165–4175 (2004).

58. Sheth, R. A. *et al.* Assessment of Image-Guided Intratumoral Delivery of Immunotherapeutics in Patients With Cancer. *JAMA Netw. open* 3, e207911 (2020).

59. Borregaard, N. Neutrophils, from Marrow to Microbes. *Immunity* 33, 657–670 (2010).

60. Hayashi, F. *et al.* Toll-like receptors stimulate human neutrophil function. *Blood* 102, 2660–2669 (2012).

61. Shaul, M. E. & Fridlender, Z. G. Tumour-associated neutrophils in patients with cancer. *Nat. Rev. Clin. Oncol.* 16, 601–620 (2019).

62. Uribe-Querol, E. & Rosales, C. Neutrophils in cancer: Two sides of the same coin. *J. Immunol. Res.* 2015, 1–21 (2015).

63. Granot, Z. & Fridlender, Z. G. Plasticity beyond cancer cells and the immunosuppressive switch. *Cancer Res.* 75, 4441–4445 (2015).

64. Ocana, A., Nieto-Jiménez, C., Pandiella, A. & Templeton, A. J. Neutrophils in cancer: Prognostic role and therapeutic strategies. *Mol. Cancer* 16, 1–7 (2017).

65. Lu, H. TLR agonists for cancer immunotherapy: Tipping the balance between the immune stimulatory and inhibitory effects. *Front. Immunol.* 5, 3–6 (2014).

66. Farhood, B., Najafi, M. & Mortezaee, K. CD8+ cytotoxic T lymphocytes in cancer immunotherapy: A review. *J. Cell. Physiol.* 234, 8509–8521 (2019).

67. Tay, R. E., Richardson, E. K. & Toh, H. C. Revisiting the role of CD4+ T cells in cancer immunotherapy—new insights into old paradigms. *Cancer Gene Ther.* 28, 5–17 (2021).

68.    Schiavoni, G., Mattei, F. & Gabriele, L. Type I interferons as stimulators of DC-mediated cross-priming: Impact on anti-tumor response. *Front. Immunol.* 4, 1–8 (2013).

69.    Wang, S. *et al.* Intratumoral injection of a CpG oligonucleotide reverts resistance to PD-1 blockade by expanding multifunctional CD8+ T cells. *Proc. Natl. Acad. Sci. U. S. A.* 113, E7240–E7249 (2016).

70.    Sideras, K. *et al.* Prognostic value of intra-tumoral CD8+/FoxP3+ lymphocyte ratio in patients with resected colorectal cancer liver metastasis. *J. Surg. Oncol.* 118, 68–76 (2018).

71.    Pagès, F. *et al.* Immune infiltration in human tumors: A prognostic factor that should not be ignored. *Oncogene* 29, 1093–1102 (2010).

72.    Diederichsen, A. C. P., Hjelmborg, J. V. B., Christensen, P. B., Zeuthen, J. & Fenge, C. Prognostic value of the CD4+/CD8+ ratio of tumour infiltrating lymphocytes in colorectal cancer and HLA-DR expression on tumour cells. *Cancer Immunol. Immunother.* 52, 423–428 (2003).

73.    Celis, J. E. *et al.* Proteomic characterization of the interstitial fluid perfusing the breast tumor microenvironment. *Mol. Cell. Proteomics* 3, 327–344 (2004).

74.    Espinoza, J. A. *et al.* Cytokine profiling of tumor interstitial fluid of the breast and its relationship with lymphocyte infiltration and clinicopathological characteristics. *Oncoimmunology* 5, e1248015 (14 (2016).

# Chapter V: From stimulation to immunosuppression: MNs for managing skin allograft rejection

Authors: Núria Puigmal, Pere Dosta, Zhabiz Solhjou, Karim Yatim, Cynthia Ramírez, John Y. Choi, Juliano B. Alhaddad, Ana Paula Cosme, Jamil R. Azzi, and Natalie Artzi

Patents:

- Microneedle-Based Platform for Simultaneous Local Delivery of Drugs and Skin Interstitial Fluid Extraction (63/154688)
- Microneedle-Based Platform for Simultaneous Local Delivery of Drugs and Interstitial Skin Fluid Sampling for Management of Immune Mediated skin diseases (63/154850)
- Microneedle-Based Platform for Simultaneous Local Delivery of Drugs and Skin Interstitial Fluid Extraction for Manegement of Skin Rejection (63/154690)

This page left blank intentionally

## 5.1 Introduction

Adoptive cell therapies are the third cornerstone of immunotherapy, consisting in the transference of autologous immune cells for either stimulation or immunosuppression of the immune system.[1] Their therapeutic success in the context of cancer treatment has been dramatic when delivering engineered cytotoxic T cells,[2] and it paved the way for alternative T cell-based therapies transferring regulatory T cells.[3] $CD4^+CD25^+FoxP3^+$ regulatory T cells ($T_{regs}$) are a subtype of T cells that suppress other activated immune cells and control the body's response to self and foreign antigens to prevent overactivated immune responses such as in the case of autoimmune disorders.[4] $T_{regs}$ account for one of the largest subsets of immune cells in the skin, promoting local immunological homeostasis and restoring normal function after a threat.[5,6] In the event of a challenge such as burn, autoimmune disease or foreign organ transplant, $T_{regs}$ can respond to the danger signals and resolve inflammation.[7,8] Upon antigen-specific activation, $T_{regs}$ exert suppression using either direct or indirect mechanisms, or by spreading their suppressive functions to neighboring cells via a phenomenon known as infectious tolerance (**Figure V-1**).[3,9] The increased proportion of $T_{regs}$ in skin-resident $CD4^+$ T cell population compared to other organs (20% in skin vs 5% in peripheral blood) also suggests an integral role for immune regulation in a tissue-specific manner.[10,11]
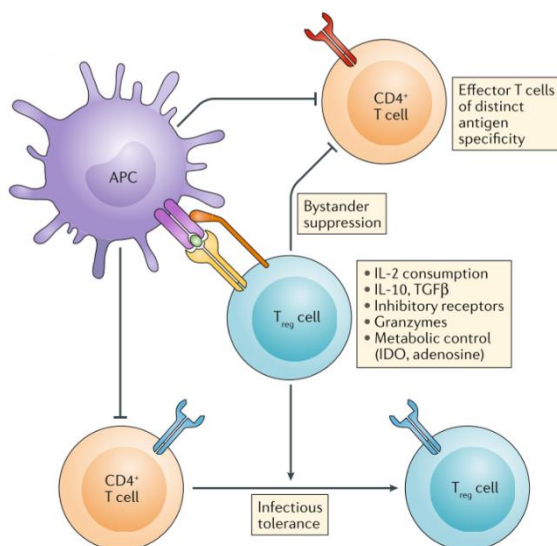


**Figure V-1. $T_{regs}$ and their mechanisms of immunosuppression.**[3] $T_{regs}$ exert their suppressive function at the site of inflammation via multiple mechanisms. $T_{regs}$ can release anti-inflammatory soluble mediators or target other T cells directly via bystander suppression or indirectly via APC binding. Finally, $T_{regs}$ modulate the tissue microenvironment to induce the generation of other immunosuppressive cell subsets following a mechanism coined as "infectious tolerance".

Indeed, disruption in skin $T_{reg}$ homeostasis —due to dysregulated $T_{reg}$ number or function— triggers disorders such as psoriasis,[12] alopecia areata,[13,14] diffuse systemic scleroderma, atopic dermatitis, or cutaneous lupus erythematosus.[5] Hence, pharmacologic $T_{reg}$ augmentation and adoptive $T_{reg}$ transfer have emerged as means to manage skin autoimmune disorders and skin transplantation.[3]

Skin allograft transplantation (from a genetically different individual) is the first-line therapy for severe burn patients and victims of traumatic injuries when autograft transplantation (from self) is not viable due to insufficient healthy tissue for excision, donor site morbidity, or poor tolerability to additional surgeries.[15–17] Despite advances in tissue engineering, usage of artificial skin is not a commonplace in clinical practice,[18] reaffirming allogenic skin transplantation as the cornerstone for the management of patients with extensive burns.[19] However, skin rejection following skin allotransplantation —the most immunogenic of all known allografts—is inevitable,[20] arising from the intense immunogenicity of transplanted allografts harboring immunogenic antigens presented to the recipient's immune system by DCs.[4] The current gold-standard therapy for the management of skin rejection is systemic immunosuppression, which partially suppresses rejection, at the cost of increasing the risk of opportunistic infections and incidence of malignancy.[21,22] Therefore, inducing immune regulation after allograft transplantation without impeding other protective immune functions is crucial to improve long-term outcome and donor-specific tolerance.

Adoptive $T_{reg}$ therapies aiming to expand skin-resident $T_{regs}$ within the skin allograft have shown potential in restoring immunological homeostasis at the site of alloimmunity.[21,23–25] However, widespread translation of these therapies into clinical settings has been limited by several challenges as $T_{regs}$ are extremely rare and heterogenous, rendering them difficult to isolate and expand *in vitro*.[26,27] Also, the infusion of 50 billion polyclonal $T_{regs}$ is needed to achieve therapeutic significance on top of their rapid clearance from serum following their transfer.[28]

Most importantly, $T_{regs}$ need a favorable immune environment including IL-2 to ensure their survival and phenotypic stability.[29] Post-transplant immunosuppressive therapies are known to generate a hostile IL-2 depleted milieu for $T_{regs}$ proliferation,[30,31] but attempting to counteract the levels of IL-2 via systemic administration has been constrained by risks of infection,[32] vascular leak syndrome,[33] and the expansion of other proinflammatory cell counterparts such as natural killer (NK) cells.[34] Previous studies have also shown an increase in $T_{reg}$ proliferation and population size in the spleen in response to systemic IL-2 delivery, while its effect on allograft survival was limited if compared to its broad range of side effects.[35,36] Since $T_{regs}$ mediate specific functions depending

entirely upon their residing tissues,[11] tissue-specific therapeutic approaches that locally target the skin should be favored instead, to maximize their efficacy and overcome the risks associated with systemic delivery. Besides from IL-2, another chemokine, CCL22, has been proposed as a powerful candidate to mediate migration of $T_{regs}$ to the site of inflammation and reestablish donor-specific tolerance in various transplant models including vascularized allograft composites[37,38] and pancreatic islets allografts.[39,40]

Prompt recognition of skin allograft rejection episodes is as critical as their management, particularly at early stages.[41,42] Current strategies to monitor skin transplant failure rely on gross observation and skin biopsies, yet rejection only becomes apparent late in the process when intervention can no longer be effective. Moreover, punch biopsies are highly invasive and their readout can be biased due to the limited area that is being analyzed, so diagnosing phenomena of partial rejection can be troublesome. Common biomarkers used to identify signs of rejection include pro-inflammatory molecules such as IL-6, IFN-γ, IL-17 or TNF-α.[43] Clinically, the $T_{reg}$-to-effector T cell ratio along with intragraft $T_{reg}$ infiltrates have also been used as prognosticative tools to assess the levels of rejection —or immunosuppression— in the allograft as a response to therapy.[44,45]

As previously described in this work, MN-based delivery allows precise tissue localization within the skin,[46,47] enhancing the efficacy and tolerability of the therapy by directly exposing it to the intended molecular targets and reducing the off-target effects associated with systemic approaches. The minimally-invasive and pain-free nature of MNs facilitates high patient compliance, while minimizing the risk of infections, which is of utter importance in this context given the increased recurrence in burn patients.[16] Moreover, MNs can be used as a minimally-invasive tool for ISF sampling to inform on the tissue physiology and in turn, report on the patient physiological state.[48,49]

Leveraging the lessons learned in *Chapter IV* on immunomodulation and immunosurveillance, the previously designed HA-based MNs have been proposed for the integral management of skin allograft rejection. The main objective of this chapter is the **fine-tuning of the MN-based platform to provide full coverage of the transplant area and homogenous drug delivery of: (1) CCL22 for the recruitment of adoptively transferred and endogenous $T_{regs}$, and (2) IL-2 to promote $T_{reg}$ stability and homeostasis at the site of alloimmunity**, tilting the $T_{reg}$-to-effector T cell ratio in favor of immunological homeostasis (**Figure V-2**). Moreover, the $T_{reg}$ homing process into the allograft is expected to be monitored by ISF sampling using the same MN patch. Studying the temporal immune

profile *in situ* could yield a more comprehensive picture of the state of rejection of the transplant and the opportunity to intercept the inflammatory process prior to reaching an irreversible state.
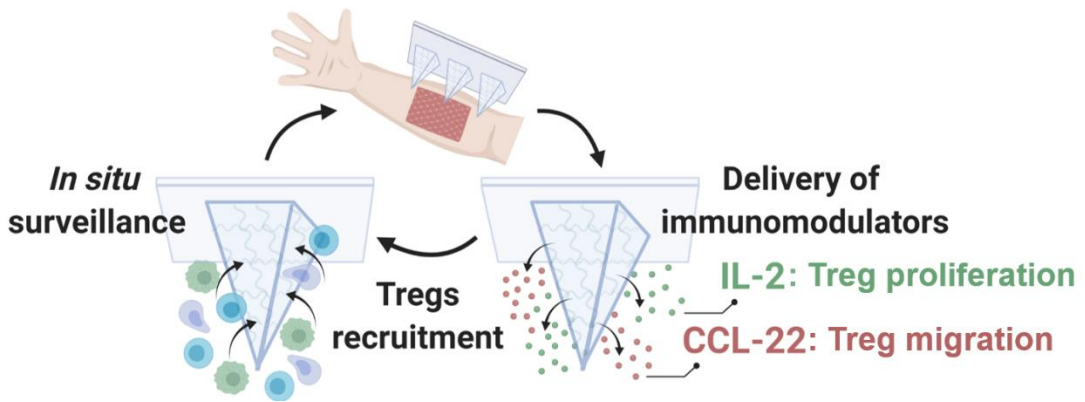


**Figure V-2. Graphical abstract of Chapter V.** HA-based MNs have been optimized in this chapter for simultaneous release of CCL22 (for $T_{reg}$ migration) and IL-2 (for $T_{reg}$ proliferation) to restore the immune homeostasis while monitoring the $T_{reg}$ homing process *in situ* via ISF sampling.

## 5.2 Aims

The main objective of this chapter is the iteration of the previously engineered HA-based MNs for delivery of chemokine immunomodulators to promote intragraft $T_{reg}$ proliferation while simultaneously retrieving ISF to monitor the $T_{reg}$ homing process as a response to therapy. To do so, the following tasks were proposed:

- ✓ Optimization of the HA-derived MN platform to deliver bioactive chemokines.

- ✓ Characterization of the delivery kinetics and loading capacity of the HA-derived MNs.

- ✓ Study the level of $T_{reg}$ recruitment and immunosuppression in the skin allografts following MN-based delivery of chemokines using a three-pronged approach: flow cytometry, RT-PCR and immunohistochemistry.

- ✓ Monitoring of $T_{reg}$ proliferation and T cell alloimmunity in peripheral organs

- ✓ Monitoring of the $T_{reg}$ homing process using the MN-based platform

- ✓ Assessment of the diagnostic potential of the MNs when compared to whole allograft biopsies.

## 5.3   Materials and Methods

### 5.3.1   Materials

All reagents and solvents were purchased from Sigma Aldrich unless otherwise stated. Sodium hyaluronate (60kDa) was obtained from LifeCore Medical with a purity of at least 95%. NHS-terminated 8-arm PEG was purchased from Creative PEG Works. MN PDMS custom-made molds (11 X 11 needles with height 600 μm, base width 300 μm and tip to tip spacing of 600 μm) were obtained from Blueacre Technology. CCL22 and IL-2 chemokines were purchased from Biolegend.

### 5.3.2   Methods

#### 5.3.2.1   Animals

C57BL/6J (B6 wild type; #000664), BALB/cJ (BALB/c wild type; #000651) and B6.129S7-Rag1tm1Mom (B6 Rag1$^{-/-}$, #002216) mice were purchased from The Jackson Laboratory (Bar Harbour, ME, USA) and housed under specific-pathogen-free conditions at the Brigham and Women's Hospital animal facility. All mouse work was performed in compliance with ethical regulations and was approved by the Institutional Animal Care and Use Committee of Brigham and Women's Hospital. Surgical procedures were performed under xylazine/ketamine anaesthesia. Age and sex-matched mice (6-8 weeks, male and female) were randomized into experimental and control groups for all experiments. Mice were euthanized in the animal care facilities by methods specified and approved by the HMA Standing Committee on Animals and consistent with the American Veterinary Medical Association guidelines (isoflurane or sodium pentobarbital).

#### 5.3.2.2   Synthesis of Amino-modified hyaluronic acid (HA-SS-NH$_2$) polymer

60 kDa-sodium hyaluronate (1% w/v in MES buffer) was activated with N-(3-(dimethylamino)propyl)carbodiimide (EDC) and N-hydroxysuccinimide (NHS) at a 1:4:2 molar ratio and reacted at room temperature for 30 min. The activated hyaluronic acid (HA) was then mixed with Cysteamine Dihydrochloride at 1:10 molar ratio and reacted at room temperature for 12 hours. HA-SS-NH$_2$ was purified by dialysis against deionized water for 6 days at room temperature, freeze dried, and stored at -20°C protected from humidity until use. For structural analysis, modified HA-SS-NH$_2$ was dissolved in D$_2$O and analysed by $^1$H-NMR, recorded using a Bruker Advance II 300MHz NMR.

### 5.3.2.3 HA-based MN fabrication

Fabrication of HA-SS-NH$_2$-derived MNs is described being the candidate of choice. MNs were produced using custom-made molds consisting in a 11 x 11 array of negative MNs projections, each one with a height of 600 μm and a radius of 150 μm. First, HA-SS-NH$_2$ polymer (10% w/v in phosphate buffer, pH=7.4) was casted on top of the molds and centrifuged at 4200 rpm for 5 min. Excess polymer was removed, and molds were freeze-dried for 20 min. Then, 8-arm-PEG-NHS crosslinker (10% w/v in phosphate buffer, pH=7.4) was casted and forced by centrifugation through the mold under the same conditions. This approach, together with the gradual gelation of hydrogel, ensured a successful polymerization of the matrix from "tip-to- top" of the MNs and a homogenous composition. Excess polymer was carefully removed, and molds were freeze-dried. If necessary, an aqueous solution containing appropriate concentrations of chemokines and glycine (10 ng mL$^{-1}$) was deposited on the molds and briefly spined for 15 seconds. Immediately after, a polymeric backing layer of PLGA (Resomer® RG 858 S, Sigma-Aldrich, USA) at 15% (w/v) dissolved in acetonitrile was added dropwise until covering the whole area of the mold. Finally, HA-based MNs were allowed to dry at room temperature for 12 hours, peeled off the molds carefully, and stored at room temperature preserved from humidity.

### 5.3.2.4 On-demand digestion of HA-derived hydrogel MNs

HA-based MNs were incubated with 10 mM Tris (2-carboxyethil) phosphine (TCEP) solution in supplemented cell culture media or PBS at pH 7.4 (depending on whether cells were collected). HA-based MNs or HA-based hydrogels were incubated under rotation at 37°C for 10 min and the recovered suspension was filtered with a 70 μm cell strainer (BD bioscience) to remove any impurities. Cell suspensions were next resuspended in media or FACs staining buffer for further analysis.

### 5.3.2.5 Murine skin transplantation

A fully MHC-mismatched murine skin transplant model was used in this work as previously described.[43] Briefly, full-thickness trunk skin grafts (1.0 cm by 1.5 cm) from BALB/c donors were harvested and connective, adipose, and panniculus carnosus tissues were cleared using blunt-tipped forceps. The fur of each anesthetized recipient Rag1$^{-/-}$ mouse was shaved at the dorsal trunk, 1.0 cm by 1.5 cm of the recipient mouse's skin was excised, and an equally sized skin graft was sutured onto the graft bed with 6-0 prolene suture (Ethicon, #8695G). Skin transplants were secured with dry gauze and bandaged for 7 days before adoptive cell transfer and MN application. The transplant state was closely monitored to intercept any signs of rejection.

### 5.3.2.6 Skin penetration studies on allografts

Penetration capacity of the HA-based MNs was tested *in vivo* using recipient Rag1^{-/-} mice. MN administration was performed in a sterile environment under anaesthesia. Mice were shaved one day prior to MN patch insertion. One MN patch sizing 1 cm$^2$ was applied in the center of the allograft by gently pinching the surrounding skin and pressing down the patch using both thumb and index. MN were pressed for 10 seconds to secure their position and kept in place with medical-grade tape (Flexcon, USA). To retrieve the MNs, mice were put under anesthesia and patches were removed by gently pulling the tape.

### 5.3.2.7 Analysis of the mechanical strength of the HA-derived MNs

Mechanical properties of the MNs when empty or chemokine-loaded were measured by a micro-force test station with a mechanical sensor (3400 Series, Instron, USA). Briefly, MN patches were placed on the surface of the platform with the needle-like projections facing up. Then, the MN patch was compressed by the vertical moving sensors at constant rate of 0.6 mm/min. The displacement and force applied on the MNs were recorded from the moment the sensors touched the uppermost tip of the MNs until a maximum force of ≈100 N was reached. After the test, the force-travel curves of MNs arrays were obtained accordingly by correlating the compressive strain or displacement (%) with the compressive stress (kPa). Finally, the Young's modulus or modulus of elasticity in tension was calculated from the slope in the elastic (or linear) portion of the physical stress-strain curve (GPa).

### 5.3.2.8 Recovery of soluble analytes in a mimetic skin model

Analyte recovery capacity of hydrogel- based MNs was conducted as detailed elsewhere using a skin model attempting to mimic the mechanical properties of the epidermis/ISF interface.[50,51] 1.4% w/v agarose hydrogels containing increasing amounts of the model metabolite Rhodamine B were polymerized in 30 mm x 15 mm petri dishes and covered with a stretched layer of parafilm aiming to emulate the properties of the water-impermeable stratum corneum. MN patches were left inserted in the agarose gels for two hours to reach a swelling plateau and subsequently digested as previously described. Finally, absorbance of the recovered analytes was measured in a microplate reader (λ = 553 nm) (Infinite 200 Pro, Tecan Austria) and correlated with the extracted mass.

### 5.3.2.9 Study of chemokine release kinetics

Recombinant human IL-2 was fluorescently labeled with the Lightning-Link® Rapid Alexa Fluor®594 kit (Novus Biologicals, USA) following the manufacturer's instructions. Release studies

were conducted with HA-based MNs loaded with labeled IL-2. IL-2-loaded MNs were placed in an Eppendorf tube, immersed with PBS (1 mL), and incubated under rotation at 37°C. 100 μL of PBS were replaced at predetermined time point, and IL-2 fluorescence corresponding to the released chemokine was measured at 650–665 nm using a Microplate Reader (Infinite 200 Pro, Tecan Austria).

### 5.3.2.10 Loading capacity of HA-based MNs loading capacity

HA-based MNs were fabricated as described and loaded with increasing amounts of fluorescently-labelled IL-2. IL-2-loaded MNs were digested as previously detailed under reducing conditions and the MN loading capacity was assessed by checking IL-2 fluorescence at 650–665 nm using a Microplate Reader (Infinite 200 Pro, Tecan Austria). Fluorescence values were converted to ng of IL-2 and compared against the original amount of loaded IL-2.

### 5.3.2.11 CCL22- dependent Transwell® migration assay

Recruitment of $T_{regs}$ as a function of CCL22 was assessed in a 24-well plate containing a 5 μm-pore polycarbonate transwell filter system (Costar transwell permeable support #3421). MNs loaded with incremental amounts of CCL22 (0, 10 and 100 ng) or an equivalent dose of soluble CCL22 were added in the receiver wells and incubated at 37 °C for 1 hour. $5x10^5$ CD3$^+$ T cells were magnetically isolated from C57BL/6 mice using the mouse T cell isolation kit (EasySep, #19851) and resuspended in full culture media and added to the top wells. Cells were then incubated at 37°C and 5% $CO_2$ for 3 hours. Cells in the receiver well were then harvested and stained with Fixed viability dye, anti-CD3, CD4, CD25, and FoxP3 antibodies (detailed hereinafter) and analyzed by flow cytometry.

### 5.3.2.12 Recovery and immunophenotyping of immune cell infiltrates by flow cytometry

- Recovery from skin allografts: A single cell suspension from skin grafts was obtained as previously described.[43] In brief, skin grafts were harvested, minced into 1 mm$^2$ fragments and digested in a solution of RPMI supplemented with 10% Fetal Bovine Serum, 1% Penicillin and Streptomycin (100 IU/ml Penn, 100 ug/ml Strep) and collagenase P (stock concentration 1mg/ml; Cat no: 11213865001, Roche) for 3 h at 37°C. Afterwards, skin grafts were re-incubated for 15 min at room temperature after adding 200 Kunitz Units/ml of recombinant DNase I (Cat no:10104159001, Roche) to reduce DNA fragments and clumping. The solution was then filtered through 70 μm mesh filters and centrifuged at 800 g for 8 min, then resuspended in Full media supplemented with 20% FBS and incubated at 37°C overnight to recover from enzymatic treatment. Then cells were resuspended in FACS staining buffer (1× DPBS,1.0% Bovine Serum Albumin,0.02% sodium azide (Sigma-Aldrich)) for flow cytometry analysis.

- Recovery from spleens: Spleens were gently smashed against a 40 µm cell strainer and rinsed with PBS to recover the maximum amount of cells. Cell suspensions were further treated with 1X ACK Lysis buffer (Gibo, ThermoFisher) for 1 min to lyse red blood cells. Then, cells were centrifuged at 300g for 5 min and resuspended in 100 µL of staining buffer ($1 \times 10^6$ cells/mL) until staining.

- Recovery from MNs: Cell suspensions were recovered as described in section 5.3.2.4. Recovered cell suspensions were counted manually using a hemocytometer and stained with fluorescent antibodies at a maximum concentration of $1 \times 10^6$ cells in 100 µL FACS staining buffer (BioLegend). The following anti-mouse antibodies were purchased from eBioscience: CD45 PE-Cy7(clone 30-F11), Foxp3 APC (clone FJK-16S), CD4 Pacific Blue (clone RM4-5), CD25 PE (clone PC61.5) and BD Biosciences: CD3 PerCP Cy5.5 (clone 500A2), CD8 Alexa Flour 488 (clone 53-6.7). Dead cells were stained using Fixed Viability Dye eFluor780 (eBioscience). Stained cells were analyzed by flow cytometry using a BD FACS Canto II cytometer (BD Biosciences) and all data were analyzed using FlowJo version 10 (Flowjo LLC) following the gating strategy outlined in **Figure V-3**.
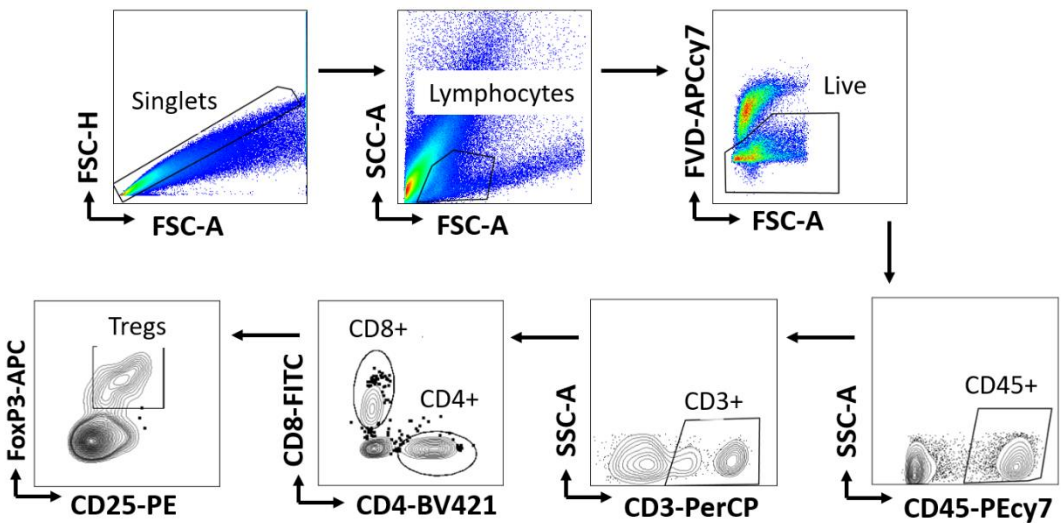


**Figure V-3. Representative FACs gating strategy.** Arrows indicate the sequence of steps. First, singlets were discriminated on the basis of forward (FSC-H) scatter followed by isolation of lymphocytes. Next, dead cells were excluded by their Phycoerythrin-Cy7 positivity. Finally, $T_{regs}$ were identified from CD45+, CD3+ and CD4+ cells and gated for APC/PE positivity.

### 5.3.2.13 Quantitative Real-time Polymerase Chain Reaction

Quantitative real-time polymerase chain reaction (qPCR) was used to assess the differential expression of mRNA transcripts between control (Empty MN) and CCL22+ IL-2 (10 or 100 ng) groups. A small piece of each allograft was kept in RNAprotect tissue reagent (Qiagen, Cat. #76104) on the same day skin allografts were harvested for digestion and flow cytometry analysis. Later, the skin

grafts were partially thawed and 1mm² pieces were cut to finer pieces. RNA was then isolated using RNA isolation kit (Qiagen RNeasy plus Mini Kit, Cat. #4136) following the manufacturer's protocol. Eluted RNA concentration was measured. The RNA concentration was measured with a NanoDropTM 2000 Spectrophotometer (Thermofisher Scientific, Waltham, MA, United States) and complementary DNA strands were reverse-transcribed with iScript Reverse Transcription Supermix (#1708841, Bio-Rad Laboratories) as per the manufacturer's protocol. Resulting cDNA was stored at -20°C till further use. Quantitative real-time PCR was performed in 0.1 mL MicroAmp™ Fast Optical 96-Well Reaction Plates (Applied Biosystems, #4346906) with 30 ng of ds-RNA per mRNA target, 500 nM forward and 500 nM reverse primers, and SsoAdvanced Universal SYBR Green Supermix  (#1725274, Bio-Rad Laboratories) diluted to 1X with PCR-grade water (#W4502, Sigma-Aldrich) in 10-µL reaction volumes. Primer pairs were based on OriGene's qSTAR qPCR Primer Pairs (Rockville, MD, United States) and synthesized through Integrated DNA Technologies (Coralville, IA, United States). Cycle threshold (Ct) values were measured with QuantStudio 3 (Thermofisher Scientific, Waltham, MA, United States). Ct values were then corrected with GAPDH housekeeping gene expression per replicate, per run, log2 normalized, averaged for the control replicates, and deviation from the average was calculated per condition, per replicate. Fold change of Foxp3 to CD3 was calculated by dividing fold change of Foxp3 to fold change of CD3 (each separately normalized to GAPDH) and fold change of IL-6 was presented after normalization to GAPDH.

### 5.3.2.14 Analysis of intragraft $T_{reg}$ infiltration by immunohistochemistry

Skin tissue sections were processed and imaged by the Hope Babette Tang Histology facility at the Koch Institute of Integrative Cancer Research at MIT (Cambridge, USA). Briefly, 0.5 cm² allograft sections harvested on the day of mechanistic analysis were embedded in OCT in plastic base molds for tissue embedding. Samples were flash frozen in a bath of dry ice and preserved at -80°C until sectioning. Allografts were cryosectioned into 20 µm-wide tissue sections and FoxP3 expression was confirmed via indirect staining using HRP-conjugated antibodies and visualized using DAB substrate. Slides were counterstained with Hematoxylin (coloring nuclei in blue) to help orient with respect to the FoxP3 staining. Processing of the microscopic images was performed using the Aperio ImageScope 12.3.3 software (Leica).

### 5.3.2.15 Statistical analysis

Statistical analyses were carried out using Graph-Pad Prism 8 (GraphPad Software). All data are reported as mean + SEMs. For *in vitro* experiments, a minimum of n=3 biological replicates were used per condition in each experiment. Pairwise comparisons were performed using Student t-tests.

Multiple comparisons among groups were determined using one-way ANOVA followed by a post-hoc test. For *in vivo* experiments, a minimum of n=4 biological replicates were used per condition in each experiment. Multiple comparisons among groups were determined using non-parametric t test (Mann-Whitney). No specific pre-processing of data was performed prior to statistical analyses. Differences between groups were considered significant at p-values below 0.05 (* $p < 0.05$, ** $p < 0.01$, *** $p < 0.001$).

## 5.4 Results and Discussion

### 5.4.1 Fine-tuning of the MN platform for delivery of bioactive chemokines and intragraft $T_{reg}$ proliferation

Throughout the previous chapter, the potential of the novel MN-based platform for cancer theranostics was acknowledged. Nevertheless, this platform was envisioned as a translational, modular device that could be exploited for alternative conditions still necessitating both therapeutic and diagnostic solutions, namely the management of skin allograft rejection. Hence, its use was proposed to deliver bioactive chemokines (CCL22 and IL-2) to promote intragraft $T_{reg}$ proliferation after adoptively transferring them to restore the immunological homeostasis while surveilling the $T_{reg}$ homing process.

In our previous studies, the use of PBAEs as delivery vectors was advisable to localize nucleic acid immunomodulators in the skin while preventing their premature clearance by endonucleases. In the context of transplantation, it was foreseen that delivering immunomodulatory chemokines as free drugs would be a more realistic strategy if aiming to resemble the physiological settings in which $T_{regs}$ uptake chemokines from the extracellular space, since these are excreted as exogenous molecules by mast cells, macrophages, and inflammatory dendritic cells.[52] Moreover, the analogous of endonucleases, proteases, were not deemed a threat since chemokines naturally-secreted by myeloid cells are still active and can recruit alloreactive T cells to induce rejection despite their high frequencies in actual burn wound/allograft environments.[19,53] Therefore, proteases were not expected to affect exogenous chemokines delivered "artificially" in a distinct manner.

#### 5.4.1.1 Characterization of the mechanical properties of chemokine-loaded MNs

Studies were initiated by fabricating chemokine-loaded MNs following the same method illustrated in **Figure IV-6B**. Briefly, the hydrogel matrix derived from the HA-SS-NH$_2$ polymer and the 8-arm-PEG-NHS was loaded with an aqueous solution containing both CCL22 and IL-2. As before, adding the therapeutics by high-speed centrifugation ensured a uniform distribution of the chemokines across the needle-like projections and thus, maximizing the potentially therapeutic surface-area of the device. Next, the mechanical properties of the MN patch were examined since the insertion ability of the MNs can be hampered in actively rejecting allografts as they tend to display

hardened areas and scabs that could impede proper skin penetration. Hence, a compression test was conducted to assess whether the inclusion of chemokines had a negative impact on their mechanical strength (**Figure V-4A,** left). Briefly, both empty and loaded MNs were compressed using increasing forces and the varying force and travel of the sensor was recorded to obtain the force-travel curves. Significant differences were not observed when comparing their Young's modulus, confirming that the mechanical properties of the patch remained unperturbed after addition of the therapeutic payload (**Figure V-4A,** right). These results were reaffirmed by testing their skin penetration capacity when administered into the allografts. Despite posing more challenges than healthy skin models, both formulations managed to effectively pierce the allografts as depicted in **Figure V-4B**.
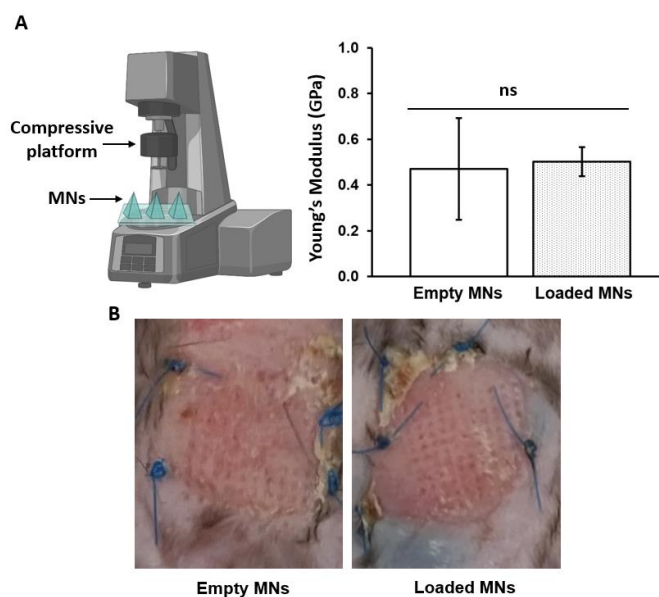


**Figure V-4. Assessment of the mechanical properties of hydrogel-forming MNs.** A compression test was performed using a micro-force test station to compare the mechanical strength of empty MNs versus chemokine-loaded ones (**A**, left). Young's modulus isolated from the slope of the linear part of the strain-stress curves (**A**, right). Macroscopic images of skin allografts after effective disruption of the outer layers of skin allografts using HA-derived MNs (**B**). Triplicates were used and data are represented as mean ± SD (n = 3).

### 5.4.1.2 HA-derived MNs for delivery of bioactive chemokines

When designing the MN platfrom, it was resolved that a rapid release of the therapeutic cargo from the MNs —in less than a day— would be more favorable to synchronize both therapeutic and diagnostic arms of the MN patch, so fluctuations in the prognosticative biomarkers could be monitored daily. This "almost continuous" vigilance over the allografts offered by the MNs —instead

of using biopsies spaced over time— could allow to intercept rejection prior to reaching an irreversible state. Therefore, the therapeutic compartment of the MNs was accommodated to the diagnostic, and not vice versa, by tailoring the MNs properties to allow a fast delivery of the chemokines.

The delivery kinetics of the chemokines when released from the MNs was studied by using fluorescently-labelled IL-2 as our chemokine model. As discussed previously in *Chapter IV*, the choice of crosslinker is known to influence the final properties of the MNs and here, the three different candidates previously explored were included in the analysis to assess their impact on the delivery kinetics. Interestingly, no IL-2 was released when using the original hydrogel formulations, which was attributed to the interaction between the IL-2-amine groups with unreacted free-NHS groups in the crosslinker, impeding its release (**Figure V-5**). The released protein observed from the 40 kDa-PEG-derived hydrogel starting at ≈ 6 hours was hypothesized to arise from artifacts of dissolved hydrogel rather than real chemokine release in accordance with our previous swelling studies (**Figure IV-7**). In light of these findings, the MN matrix was further iterated to ensure a fast release of the chemokines. Briefly, undesired interactions with the chemokines were impeded by treating the hydrogel matrix of the MNs with an end-capping agent, the amino acid glycine, whose amino-end groups would preferentially interact with the crosslinker's non-reacted NHS-terminal groups.
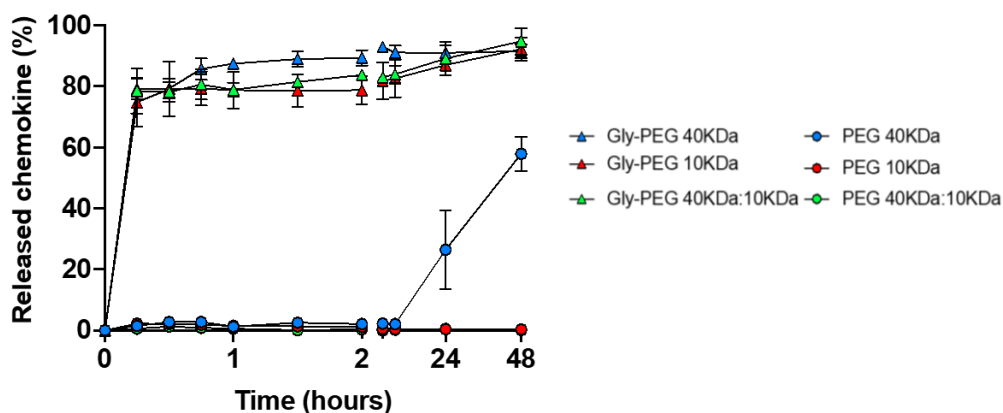


**Figure V-5. Chemokine release kinetics when delivered using HA-derived MNs *in vitro*.** MNs were loaded with fluorescently-labelled IL-2 and incubated under physiologically-relevant conditions. Release of the IL-2 from the HA-based MNs was quantified by tracking the fluorescence signal of the labeled IL-2 over time. Data are represented as mean ± SD (n = 3).

Indeed, end-capping the hydrogel matrix resulted in more than 80% of the cytokine being released within the first 30 min, making it the chosen strategy for further studies. Of note, differences in the release profiles were not observed regardless of the crosslinker agent used when end-capped with glycine. The fast release nature of the hydrogel matrix could hold great promise as it could result in

reduced administration times and in turn, mitigate the risk of infections caused by long-term administration of a foreign body.

Next, loading efficiency of chemokines in the MNs was examined, once again, using fluorescently-labelled IL-2 as our model. Briefly, MNs fabricated with increasing amounts of IL-2 were digested as described under reductive conditions and the amount of loaded chemokine was measured by fluorescence. Results illustrated a linear correlation between the loaded concentration and the retrieved one after digestion of the MN patches, proving the accuracy of the loading method and the potential to deliver chemokine payloads in the nanogram range (**Figure V-6**). Hydrogel-forming MNs not only have expanded the range of drugs that can be delivered but also facilitate the delivery of clinically-relevant doses.[54] Here, the capacity of the HA-based MNs to entrap biologically-relevant dosages of immunomodulators was proven, as they allowed to embed the amounts needed for future studies in murine models.
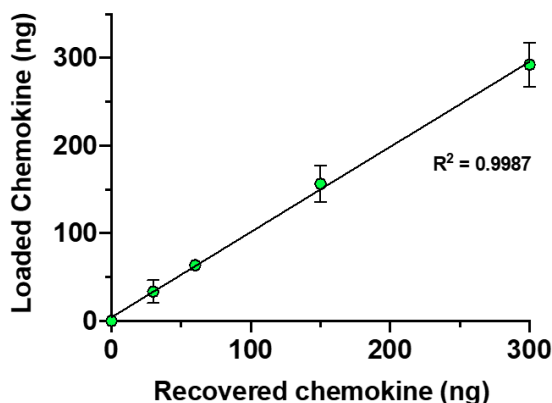


**Figure V-6. Analysis of the MNs loading capacity.** HA-based MNs loaded with fluorescently labelled IL-2 were digested under reducing conditions and the total amount of loaded IL-2 was quantified by fluorescence measurement at $\lambda$=665 nm. Data were plotted as initially loaded mass of IL-2 versus recovered mass of IL-2, $R^2$ = 0.9987 and represented as mean ± SD.

Finally, a functional assay was conducted to verify that the chemokines loaded in the MNs maintained their biological activity. Owing to the mild conditions of the fabrication method, using aqueous solutions and at room temperature, damages to the tridimensional structure and function of the chemokines were not expected. To test this hypothesis, a migration assay was conducted to assess the ability of CCL22 to mediate $T_{reg}$ recruitment when delivered using the MN platform or as soluble chemokines through a Transwell® migration assay while also comparing the rates of $T_{reg}$ migration as a function of CCL22 concentration. Briefly, ranging concentrations of CCL22, either MN-

loaded or soluble, were incubated with CD3+ T cells and the number of $T_{regs}$ migrated to the output wells was analyzed after 3 hours of incubation by flow cytometry. Results illustrated a dose-dependent increase of $T_{reg}$ migration for both soluble and MN-loaded CCL22 wells (P= 0.02 and 0.04 for soluble and MN-loaded respectively) (**Figure V-7**). Recruitment of $T_{regs}$ mediated by CCL22-loaded MNs was comparable to that observed when adding soluble CCL22 in the same dose (p=0.9, 0.2, 0.2 for 0, 10 and 100 ng/ml respectively). Interestingly, a trend of higher $T_{reg}$ recruitment in wells with CCL22-loaded MNs was observed if compared to soluble CCL22. It was theorized that these results could stem from the maintenance of higher gradient of CCL22 when released from the MNs compared to soluble CCL22. Results also suggested that chemokine functionality was not affected by the fabrication method nor by being stored at room temperature prior to the experiments (for about 1 week). Indeed, preliminary shelf-life studies showed that chemokines embedded in the MN hydrogel matrix could remain bioactive for up to 3 weeks post-MN fabrication at room temperature (data not shown). If premature, these results hinted at the translational potential of our platform and its cold-chain independency.
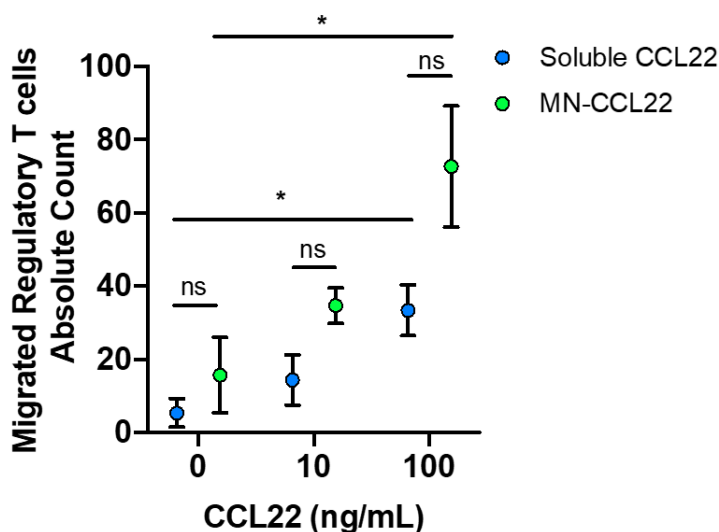


**Figure V-7. Comparison of $T_{reg}$ migration as a function of CCL22 concentration when soluble or MN-loaded.** CD3+ T cells isolated from C57BL/6 mice were plated in 24- well Transwell® while MNs loaded with CCL22 (or a soluble equivalent dose) were added in the receiver well. Migrated cells were harvested and quantified by flow cytometry. Data are represented as mean ± SD (n = 3). Multiple comparisons among groups were determined using either one-way ANOVA followed by a post-hoc test or non-parametric t test (Mann-Whitney) when applicable. P-value: ns = not significant, *p < 0.05, **p < 0.01.

## 5.4.2 Study of the on-target effect of MNs in promoting $T_{reg}$ migration *in vivo*

Once the ability of the HA-derived MNs to deliver bioactive chemokines was proven, their capacity to mediate $T_{reg}$ migration was studied *in vivo* using an adoptive transfer transplant model; specifically, in Rag1-/- mice receiving BALB/c skin allografts. The animal model of choice was a fully MHC-mismatched, immunocompromised murine model where rejection against the skin allograft is not mounted until its immune system is reconstituted via adoptive T cell transfer. The lack of an endogenous T cell compartment offered the opportunity to examine the kinetics and behavior of transferred $T_{regs}$ as a response to the therapy without the interference of endogenous T cells prior to moving to allogeneic models. First, a transplant model including two allografts was used to corroborate whether CCL22 could induce the recruitment of $T_{regs}$ to the site of alloimmunity when delivered with the MNs, and whether $T_{reg}$ migration was indeed site-specific (**Figure V-8A**).
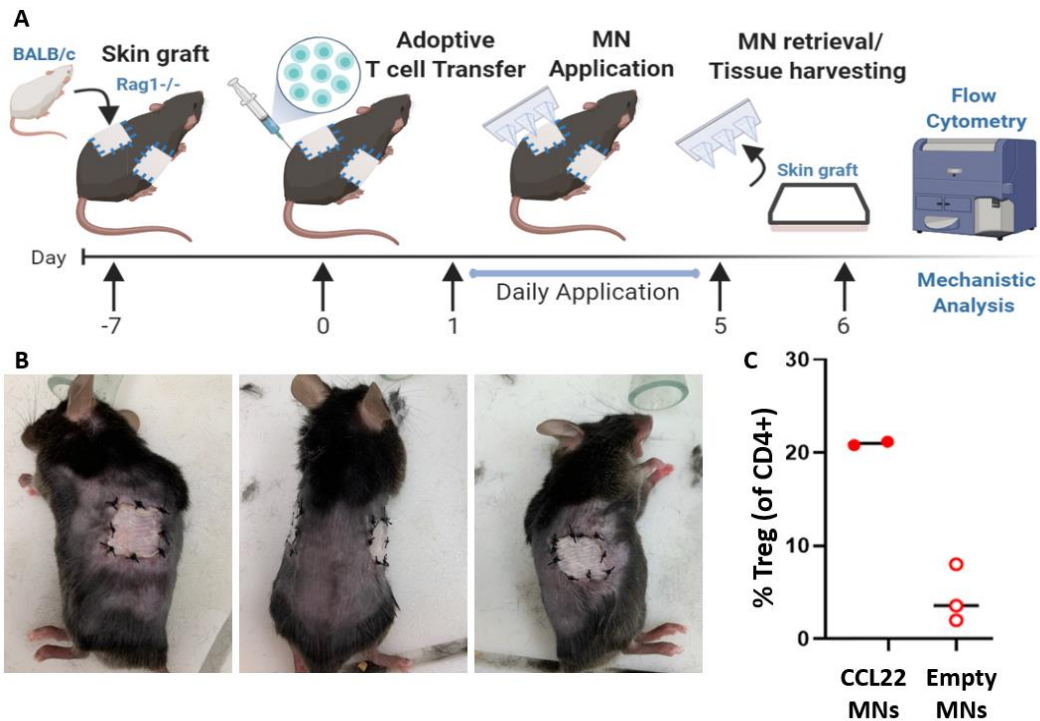


**Figure V-8. $T_{reg}$ migration to the skin allograft as a function of CCL22 is site-specific.** Experimental design using a two-grafted skin allograft model. Two skin patches from BALB/c mice were transplanted onto the dorsal trunk of a Rag1^{-/-} mouse on C57BL/6 background. On day 7 post-transplant, T lymphocytes were adoptively transferred and empty/loaded-MNs were applied consecutively for 5 days. At day 6 post adoptive T cell transfer, allografts were harvested and analyzed by flow cytometry (**A**). Macroscopic images of the murine model with two allografts at day 7 post-transplant (**B**). $T_{regs}$ were isolated from the skin allografts by enzymatic digestion and immunophenotyped by flow cytometry (**C**).

Transferring two allografts to the same individual allowed the inclusion of an internal control within the same individual to reaffirm the local action of the therapy, as opposed to systemic administration,[43] if delivered via MNs. Once the skin allografts were fully adhered (**Figure V-8B**), T cells were adoptively transferred and CCL22-loaded MNs where administered in one flank whereas empty ones were applied in the opposite. Lastly, whole allograft biopsies were performed and the immune profiles of the two grafts were contrasted. Analysis by flow cytometry of the isolated lymphocytes confirmed that MNs had a preferential, on-target, and allograft-specific effect as evidenced by the higher number of $T_{regs}$ in allografts treated with CCL22-loaded MNs (>20%) (**Figure V-8C**). By contrast, the proportion of $T_{regs}$ out of CD4+ cells was dramatically lower in the control allograft administered empty MNs, supporting the hypothesis that $T_{regs}$ can be recruited and focalized to the site of alloimmunity following delivery of chemoattractant chemokines with MNs.

## 5.4.3 Analysis of the immunosuppressive effect cascaded by $T_{regs}$ following CCL22/IL-2 MN-based delivery in skin allografts

### 5.4.3.1 Assessment of $T_{reg}$ proliferation in skin allografts via a three-pronged analysis

Next, a new set of *in vivo* experiments was conducted to shed light on the immune modulatory function of the MNs and their ability to promote $T_{reg}$ proliferation in the skin allografts (**Figure V-9**).
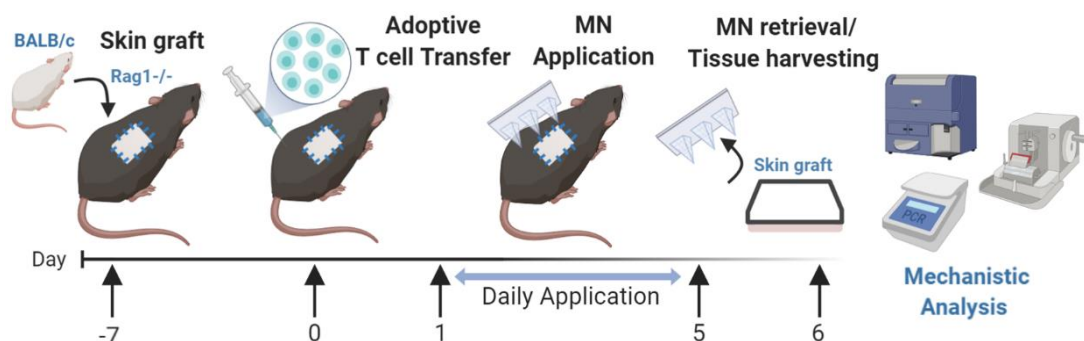


**Figure V-9. Assessment of $T_{reg}$ proliferation in an adoptive transfer transplant model via a three-pronged analysis.** A skin patch recovered from a BALB/c mouse was grafted onto the dorsal trunk of an immunodeficient Rag1^{-/-} mouse lacking both T and B cells. On day 7 post-transplant, $7x10^6$ magnetically isolated T lymphocytes were adoptively transferred to induce rejection in the allograft recipients as previously described.[43] Next, MNs ((1) 100 ng CCL22+10 ng IL-2 or (2) 100 ng CCL22+100 ng IL-2) were applied daily for five consecutive days, with one group receiving empty MNs as control. At day 7 post adoptive transfer, skin grafts were harvested and analyzed by quantitative PCR, flow cytometry and immunohistochemistry.

Recent studies have confirmed the utility of CCL22 and IL-2, when used individually, to restore immune homeostasis and prolong allograft survival without compromising other vigilant functions.[37,43,55] By contrast, in this work it has been proposed for the first time in literature the combination of both immunomodulators with the rationale being for CCL22 to enhance the recruitment of $T_{regs}$ to the site of alloimmunity,[38,56] the skin allograft, and for IL-2 to maintain $T_{reg}$ homeostasis *in vivo.*[30,31] Recruiting $T_{regs}$ (with CCL22) and then supporting their homeostasis (with IL-2) in the allograft was also expected to trigger a favorable infectious tolerant milieu, where $T_{regs}$ would convert nearby cells into suppressive agents thus generating long-lasting resident $T_{regs}$ and skin allograft tolerance and survival. MNs were loaded with either 10 or 100 ng of IL-2 since previous evidence proved that low-dose regimens of IL-2 can preferentially stimulate $T_{regs}$ over effector T cells, due to the selective enrichment of CD25 —the high-affinity receptor of IL-2—, on $T_{regs}$.[57] The regimens proposed in this studies were dramatically scaled-down if compared to systemic dosages with high hopes —and evidence—[58] that reduced amounts of IL-2 would not unleash dangerous activation of other proinflammatory cells sharing surface expression of CD25 with $T_{regs}$.

Quantitative PCR analysis were performed on harvested skin allografts to measure the differential expression of CD3 as the universal T cell biomarker (cell infiltrates inducing allograft rejection) and FoxP3 as a transcription factor differentiating $T_{regs}$ from conventional T cells (cell infiltrates suppressing rejection). Ratio of fold change in FoxP3 to CD3 expression was then used as an indicator of the impact of the delivered chemokines on $T_{reg}$ recruitment and proliferation within the T cell fraction. Skin allografts treated with CCL22/IL-2-loaded MNs showed significantly increased ratios of FoxP3 to CD3 if compared to allografts treated with empty MNs (**Figure V-10A**). These outstanding results confirmed the therapeutic merit of chemokine-loaded MNs to favor selective $T_{reg}$ proliferation in the allografts. Results illustrated that the ratio of fold change was more than doubled, or even tripled, in some individuals when comparing groups administered loaded-MNs against the control group. Comparison of FoxP3 expression in "high-dose" versus low-dose IL2-loaded MNs did not reveal significant differences and their fold-changes fluctuated around the same order of magnitude. These findings could prove highly beneficial when translating this platform into more allogeneic models since off-target activation of the inflammatory compartment might be mitigated, or even eliminated, without compromising therapeutic efficacy. Of note, registered heterogeneity among mice came as no surprise given the sophisticated animal models used in our studies, although observed levels did not differ from those registered in previous works of this field.[43]
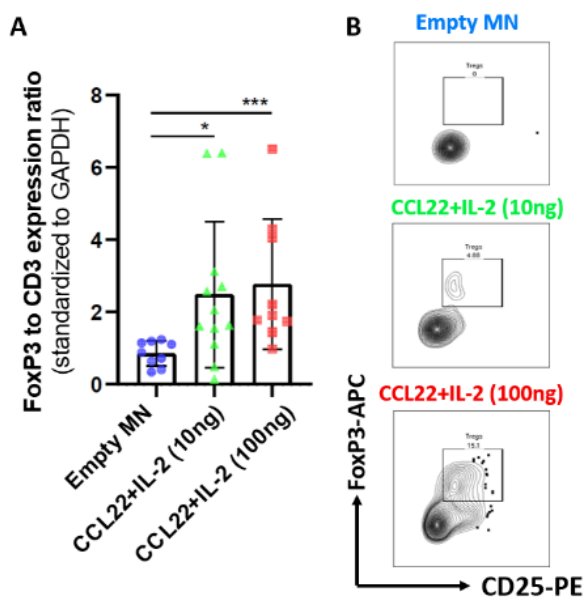
**Figure V-10. CCL22/IL-2-loaded MNs can mediate intragraft T$_{reg}$ proliferation.** Gene expression in harvested skin allografts was analyzed by RT-PCR (**A**). Fold change of Foxp3 to CD3 expression was calculated by dividing fold change of Foxp3 to fold change of CD3 (each separately normalized to GAPDH as housekeeping gene). Representative flow-cytometry-dot-plots following MN-based delivery of chemokines (**B**). Lymphocytes were isolated by enzymatic digestion and immunophenotyped to identify the T$_{reg}$ subset (gated as FoxP3-APC; CD25+-PE). A minimum of n=4 biological replicates were used per condition in each experiment (here pooled). Multiple comparisons among groups were determined using one-way ANOVA followed by a post-hoc test. (* p< 0.05, ** p<0.01, *** p<0.001).

Complimenting the analysis by PCR, the immune cell populations infiltrating into the allografts were also enumerated by flow cytometry (**Figure V-10B**). Specific gating of T$_{regs}$ (CD4+CD25+FoxP3+) among lymphocytes confirmed a correlation with our previous findings since T$_{reg}$ presence was only evident in those skin allografts administered chemokines with the MNs. Contrarily, events corresponding to T$_{regs}$ were not observed in the control group administered empty MNs.

Finally, intragraft T$_{reg}$ proliferation was gauged by immunohistochemistry, where staining for FoxP3 confirmed higher infiltration of T$_{regs}$ in treated allografts (**Figure V-11**). Interestingly, distribution of T$_{reg}$ infiltrates was not uniform nor scattered throughout the allograft; instead, clusters of T$_{regs}$ were observed. If preliminary, regions homing higher numbers of T$_{regs}$ appeared to be proximal to the microconduits left by the MNs after administration (**Figure V-11**, middle panel). As expected, T$_{reg}$ proliferation could not be observed in the control group. Following a three-pronged analysis, triple confirmation was obtained of the on-target effect of MNs in boosting T$_{reg}$ proliferation in allografts.
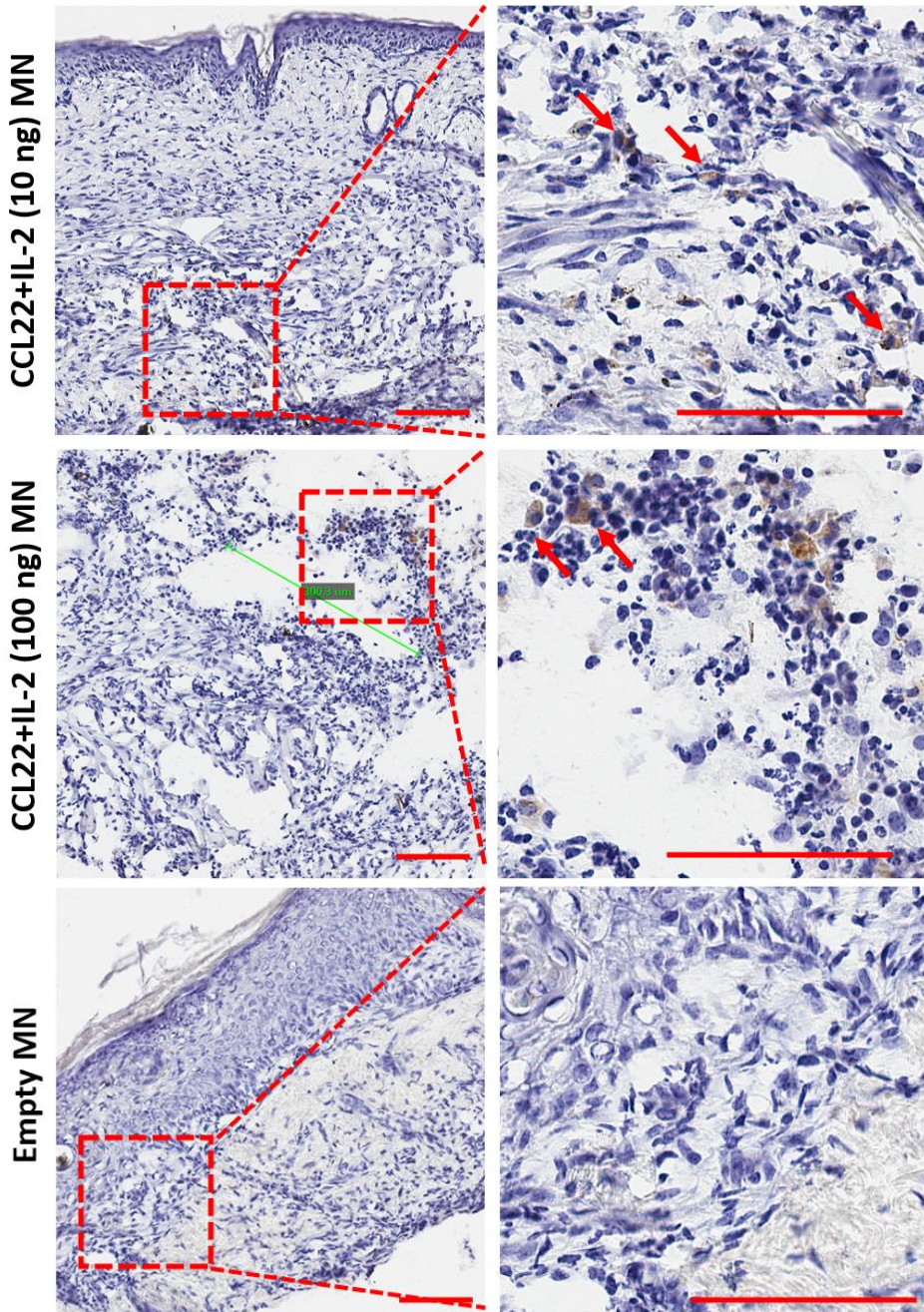
**Figure V-11. T$_{reg}$s proliferate at the site of alloimmunity following local MN-based delivery of immunomodulators.** Harvested skin allografts from treatment groups (CCL22 + IL-2-loaded MNs) and the control group were cryosectioned into 20 µm-thick slides. Staining against FoxP3 was used as a biomarker to evaluate intragraft T$_{reg}$ proliferation. FoxP3 expression was confirmed via indirect staining using HRP-conjugated antibodies and visualized using DAB substrate. Slides were counterstained with Hematoxylin (coloring nuclei in blue) to help orient with respect to the FoxP3 staining. Scale bar = 100 µm.

### 5.4.3.2 Examining local immunosuppression induced after T_{reg} proliferation in skin allografts

To demonstrate whether T_{regs} could induce an immunosuppressive effect within the allograft milieu, gene expression of IL-6 was measured being a commonly recognized indicator of inflammation. IL-6 is a key inflammatory cytokine linked with the augmentation of alloimmune responses in wounds/transplants and responsible for poorer burn patient prognosis when its levels are high.[59] Indeed, an increase of immunostimulatory cytokines such as IL-6 triggers a pro-inflammatory environment that tips the balance in favor of effector immune responses and ultimately instigates allograft rejection.[60] For this reason, the levels of IL- 6 gene expression in the previously harvested allografts were analyzed by quantitative PCR to determine the immunosuppressive scope induced by the platfrom (**Figure V-12**).
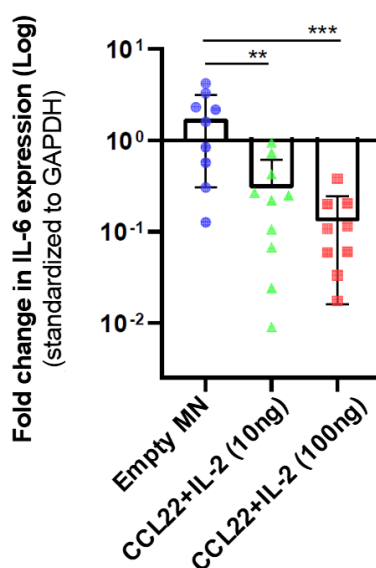


**Figure V-12. Intragraft T_{reg} proliferation ameliorated the proinflammatory environment at the site of alloimmunity.** IL-6 was used as a proinflammatory biomarkers. Gene expression of IL-6 was quantified by RT-PCR and normalized to the expression of the housekeeping gene GAPDH. A minimum of n=4 biological replicates were used per condition in each experiment (here pooled). Multiple comparisons among groups were determined using one-way ANOVA followed by a post-hoc test. (* p< 0.05, ** p<0.01, *** p<0.001).

Allografts administered immunomodulators experienced a dramatic decrease in their levels of IL-6 expression if compared to the control group, registering as much as a >5-fold and a >8-fold reduction (**Figure V-12**). In accordance with the increased T_{reg} percentages observed in **Figure V-10A**, it would appear that infiltrated T_{regs} ameliorated the proinflammatory environment at the site of alloimmunity,

with a few individuals registering about a 100-fold decrease in IL-6 expression. Such therapeutic milestone was predicted to have biological significance when translating our MN platform to fully allogeneic humanized models. When correlated with the values of $T_{reg}$ infiltration in the allograft, these results pointed at the downstream therapeutic effects of the MN-based platform and its capacity to locally promote immunosuppression without impeding regulatory functions.

### 5.4.3.3  Analysis of $T_{reg}$ expansion and systemic immunity in peripheral organs

Previous studies have demonstrated that systemic administration of IL-2 promoted $T_{reg}$ proliferation in the spleen but failed to do so in the skin allografts which aggravated their outcomes.[43] For this reason, the systemic effects triggered after local delivery of IL-2 with MNs were examined, using spleens as a distal site of alloimmunity. $T_{reg}$ expansion in the peripheral spleen was evaluated by harvesting the splenocytes from allograft recipients on day 7 post adoptive transfer. Data illustrated comparable $T_{reg}$ numbers for all the groups and no significant $T_{reg}$ expansion in the spleens (**Figure V-13**). Interestingly, mice treated with higher doses of IL-2 (CCL22 10ng + IL-2 100ng MNs) displayed overall decreased levels of $T_{regs}$ in the spleens. If not significant, this trend was intriguing as higher concentrations of IL-2, would be expected to elicit more substantial systemic effects, even if delivered locally. To sum up, systemic proliferation of $T_{regs}$ following MN-based delivery of IL-2 was not evidenced, pointing at the enhanced safety of this platform if compared to systemic routes and its potential to modulate immune cell composition and reduce inflammatory state locally.

To complete our studies, alloimmune memory responses were also examined via mixed lymphocyte reaction (MLR). Briefly, direct recognition of allogeneic molecules is assessed by co-culturing donor splenocytes (from the allograft donor) with recipient splenocytes (from the Rag1$^{-/-}$ host) and these are allowed to proliferate. Low levels of T cell expansion are considered a sign of over-immunosuppression, whereas high T cell expansion in response to donor antigens is read as increased risk of allograft rejection.[61] Here, splenocytes were harvested from the different groups of recipients (empty MNs, 100 ng CCL22+10ng IL-2 and 100 ng CCL22+100 ng IL-2) and incubated with irradiated donor splenocytes so only the recipient ones would proliferate. Significant changes were not observed in regards of alloimmune memory proliferation nor antigen-specific cell proliferation among groups. Taken together, these findings suggest that although CCL22 and IL-2 could effectively be delivered to the graft and impact on the inflammatory state, the MN platform does not seem to pose substantial systemic effects and could ultimately provide a safer platform for local delivery of targeted therapeutics.
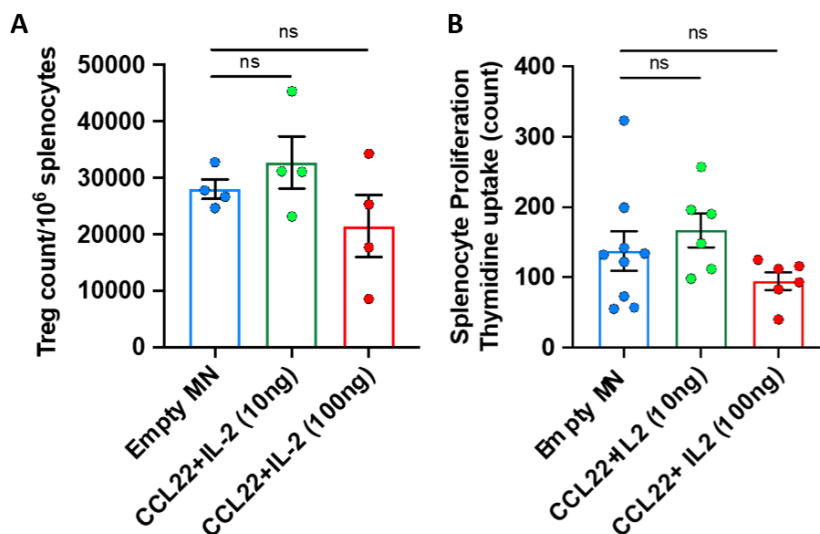
**Figure V-13. Analysis of distal and memory alloimmune responses following local MN-based delivery.** Flow cytometry quantification of $T_{reg}$ proliferation in peripheral sites (**A**). $T_{regs}$ total count was represented per million of splenocytes (FOXP3+; CD4+). Splenocyte proliferation study by MLR reaction (**B**). Data are represented as mean ± s.e.m. (n=4/9). Multiple comparisons among groups were determined using either one-way ANOVA followed by a post-hoc or non-parametric t test (Mann-Whitney) when applicable. P-value: ns = not significant, *p < 0.05, **p < 0.01.

### 5.4.4 Assessment of the diagnostic compartment of the HA-derived MNs

Once the therapeutic merit of the hydrogel-based MNs was demonstrated, their diagnostic capacity was examined. The ability of hydrogel-based MNs to sample ISF as a source of biomarkers is now well established.[62] In the context of skin transplantation, MNs have the overarching allure of being a minimally-invasive approach as opposed to punch biopsies —the current standard. Moreover, MNs could offer a detailed picture of the rejection state since they can provide full coverage of the transplant, avoiding the bias induced when only a limited biopsy area is evaluated. As discussed previously, using MNs to retrieve soluble biomarkers from ISF such as nucleic acids,[63,64] proteins[48] or metabolites[51,65,66] can be of interest, but not adequate to infer on the phenotypic and functional immune signature of the tissue. Instead, monitoring the immune profiles associated with early rejection —which are characterized by lack of $T_{regs}$ and the infiltration of tissue-resident memory T cells ($T_{RMs}$) from the donor—[67] could be useful to preemptively intervene before deterioration of the graft is macroscopically evident. At that stage, allografts are irremediably damaged and antirejection treatment starts when graft loss is mostly inevitable.[19] In clinical settings, we envisioned that local surveillance of infiltrating $T_{regs}$ and memory T cells within the skin graft using MNs could provide a

deeper insight of the rejection process, allowing for a further tailoring of the dose and timing of the immunosuppressive regimen to the extent of the underlying rejection process and the opportunity for early intervention.

As a proof-of-principle study, the MN platform was challenged to simultaneously sample the immune cellular fraction from ISF (for diagnostics) while delivering chemokine immunomodulators to the allograft (for therapeutics). A new set experiments was conducted on Rag1$^{-/-}$ mice transplanted with skin allografts aimed at demonstrating whether HA-derived MNs could monitor the $T_{reg}$ homing process and if the $T_{reg}$ immune signature obtained from MN-sampled ISF correlated with that from whole allograft biopsies. To this end, both empty and chemokine-loaded MNs were used to discretely monitor the changes in the ISF immune profiles, focusing on the variations in the allograft $T_{reg}$ infiltrates as a prognosticative readout. Following the same experimental design as in **Figure V-9**, MNs corresponding to the fifth day of treatment were retrieved from the allografts and digested to recover and enumerate by flow cytometry the cellular phenotypes infiltrated in the MNs, focusing on the $T_{reg}$ subset (**Figure V-14**). To validate that these reflected the immune state in the tissue, the presence of intragraft $T_{regs}$ was also evaluated by enzymatically digesting the skin allografts and immunophenotyping the isolated immune cell fractions to compare them with those from ISF.
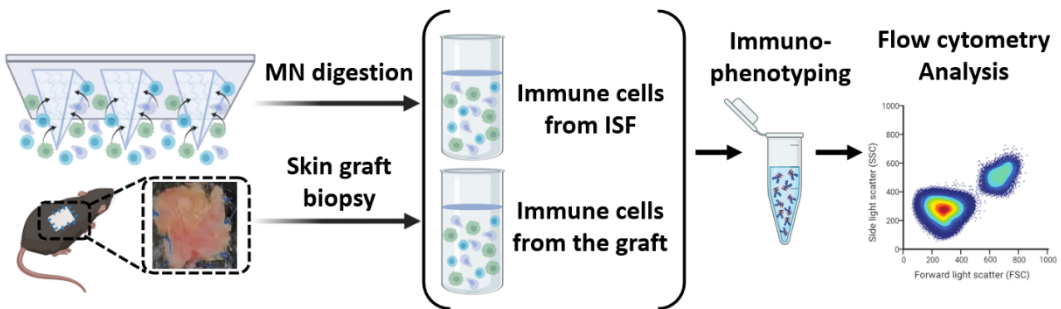


**Figure V-14.** *In vivo* **mechanistic analysis aiming to monitor $T_{reg}$ homing process into the allograft.** 7 days-post adoptive transfer, the last set HA-derived MNs used to deliver chemokines were digested under reducing conditions as described in Chapter IV to isolate the cellular fraction of the ISF. In parallel, whole allografts were digested and the infiltrated immune cells were stained along with those ISF-sampled and immunophenotyped by flow cytometry. A minimum of n=4 biological replicates were used per condition in each experiment.

Analysis by flow cytometry of the retrieved ISF following MN sampling confirmed the presence of a higher percentage of $T_{regs}$ in the allografts treated with CCL22/IL-2-loaded MNs if compared to those treated with empty MN as controls (**Figure V-15**, left panel). These results were in accordance with the immune profiles obtained from digested allografts, which also showed a significant increase of intragraft $T_{regs}$ when administered the chemotactic chemokines (**Figure V-15**, right panel).

**Figure V-15. Monitoring of the T$_{reg}$ homing process and the response to therapy using ISF-sampling MNs.** Representative flow-cytometry-dot-plots depicting CD8+, CD4+ and FoxP3+ cell populations extracted from ISF (left panel) and skin allograft (right panel). Immune profiles were compared between treatments (control versus loaded-MNs) and correlated between tissues (ISF versus allograft). A minimum of n=4 biological replicates were used per condition in each experiment.
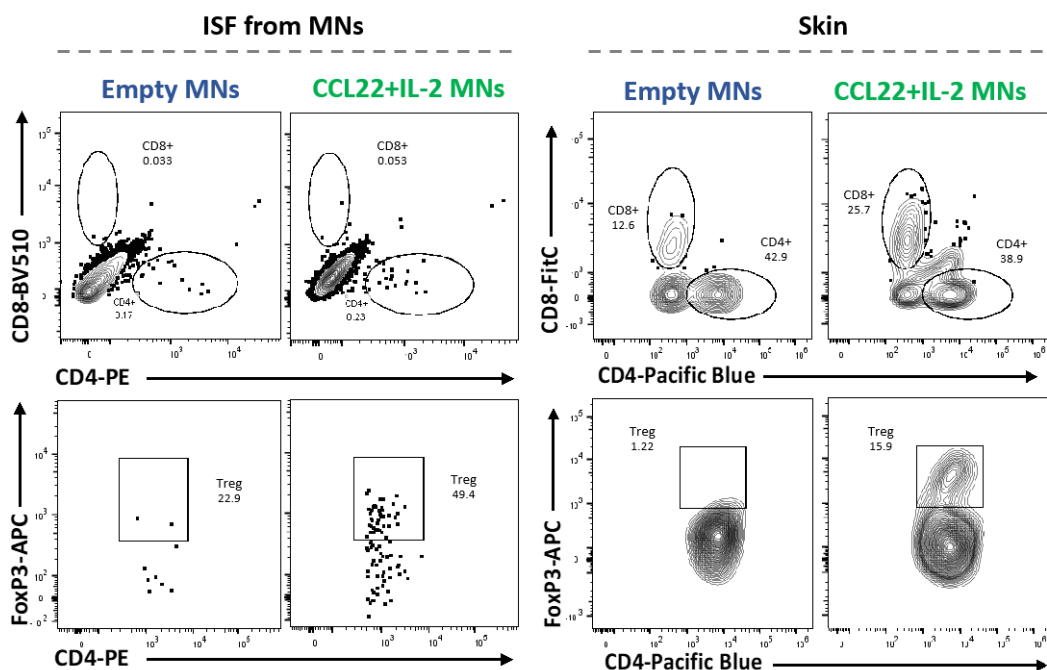
Unexpectedly, data were also in agreement with the previously registered behavior of T$_{regs}$ when studying the therapeutic arm of the MNs, since significantly higher expression of T$_{regs}$ biomarkers (FoxP3) had been also confirmed by RT-PCR (**Figure V-10A**) and IHC (**Figure V-11**) in treated allografts, proving an intimate correlation with the cellular composition in ISF.

Of note, the matching trend in terms of T$_{reg}$ proliferation observed when comparing ISF against skin as a function of the therapy was not applicable if comparing T$_{reg}$ relative percentages among CD4+ cells instead. Such variations were not unexpected since previous evidence has suggested that the frequencies of circulating immune cells in blood do not necessarily match the composition of resident immune populations in the ISF if comparing their absolute percentages.[68] Therefore, it was hypothesized that the absolute frequencies in ISF might not equate to those in the skin neither. Analogously, analysis of the soluble fraction of biomarkers in ISF had showed that 83% of proteins found in serum are also present in ISF; contrarily, 50% of proteins in ISF are not present in serum.[69] Such uniqueness might also extrapolate to the cellular compartment of ISF, highlighting the need for

systematic analysis to quantitively correlate the cellular composition of ISF to that from its harboring tissues. Historically, the lack of convenient methods to sample ISF had deterred researchers from using ISF as a source of biomarkers,[49] yet the irruption of MNs has re-energized this field and new ISF biomarkers with prognosticative value are already emerging.

Besides from the biologic rationale, differences in the relative percentages of $T_{regs}$ in representative samples of ISF (49.4%) and allografts (15.9%) could stem from experimental limitations of our animal model. Opting for a stringent murine model lacking both endogenous B and T cells, instead of a fully allogeneic model, offered a better insight into the behavior of $T_{regs}$ as a response to therapy without the interference of the endogenous fraction. However, this feature significantly reduced the available number of lymphocytes susceptible of being sampled and the overall extraction yield of the MNs significantly decreased if comparing absolute counts of extracted cells with those from the cancer model (*Chapter IV*). As a consequence, correlation between treatments and tissues could only be established qualitatively but not quantitively since the smallest differences had a tremendous impact on the final relative percentages and standard deviations. Far from discouraging us, future actions aiming to improve the statistical robustness of this study could involve increasing the size of the MN patch, sample pooling from multiple patches, and the integration of highly sensitive detection methods to the MN platform. Moreover, moving to fully allogeneic murine models containing richer populations of immune infiltrates (both the adoptively transferred and the endogenous) is expected to augment the overall yield and sensitivity of our platform.

To sum up, the diagnostic potential of the HA-derived MNs was proven as a mode of tissue immunosurveillance. Proof-of-principle studies allowed to surveil the $T_{reg}$ homing process into the allograft and the response to the immunotherapy *in situ*. In future studies, the diagnostic arm of the MN patch could surely be expanded to surveil other prognosticative biomarkers such as effector T cells or natural killers infiltrating into the allograft as crucial orchestrators of rejection so as to provide a comprehensive picture of the cellular dynamics driving allograft rejection in "almost" real-time.

## 5.5 Concluding remarks

The results of this chapter proved that HA-derived MNs can be used as an immunosuppressive platform for the management of skin allograft rejection. The delivery-and-sampling functions of the MNs allowed to regulate the immune system locally after skin transplantation while monitoring the efficacy of the immunotherapy via ISF sampling using a single, theranostic MN patch.

We confirmed that HA-based MNs can be loaded with particulate-free immunomodulators such as chemokines. Addition of chemokines into the MN matrix did not have an impact on their final mechanical properties. Engineering the hydrogel matrix of the MN patch allowed to tailor the delivery kinetics of the chemokines to obtain a fast release profile that would accommodate to the diagnostic compartment of the platform.

The refined method used for MN fabrication allowed to load bioactive chemokines in the therapeutic range. Transwell® migration assays revealed that loaded MN could mediate similar levels of $T_{reg}$ attraction to those induced by soluble chemokines in a dose-dependent manner, even if MNs remained stored at room temperature prior to the assay.

On-target effect of the MNs in mediating local $T_{reg}$ recruiting at the site of alloimmunity was examined using a stringent, adoptive transfer transplant model containing two skin allografts. Flow cytometry analysis of harvested skin allografts revealed that CCL22-loaded MNs could promote site-specific $T_{reg}$ recruitment as evidenced by the increase in intragraft $T_{reg}$ infiltrates. Contrarily, migration of adoptively transferred $T_{regs}$ to the opposite allograft administered empty MNs (internal control) was not observed, confirming the ability of the MNs to localize the therapy. Moreover, it was confirmed that MNs could be successively administrated into the skin allograft without causing major injury or bleeding.

The ability of chemokine-loaded MNs to promote $T_{reg}$ proliferation at the site of alloimmunity was proven by a three-pronged analysis including flow cytometry, RT-PCR, and IHC. An irrefutable increase in $T_{reg}$ proliferation was observed in those allografts delivered CCL22 (for $T_{reg}$ recruitment) and IL-2 (for $T_{reg}$ homeostasis) using the HA-derived MNs. Differences in the number of infiltrated $T_{regs}$ could not be discerned between the "high-" and the "low-dose" IL-2-loaded MNs suggesting that reduced, yet localized, treatment could maintain $T_{reg}$ homeostasis and promote their proliferation.

Gene expression of the proinflammatory cytokine IL-6 was significantly reduced in those allografts administered CCL22/IL-2-loaded MNs when analyzed by RT-PCR. These results, in agreement with the

increased percentage of $T_{regs}$ in the allografts, proved the immunosuppressive potential of the MN platform and therapeutic benefit of leveraging the regulatory compartment of the immune system.

Analysis of systemic and memory immunity in distal sites of alloimmunity (spleen) evidenced that local delivery of IL-2 using hydrogel-based MNs did not induce any systemic toxicity. Differences in the proliferation of $T_{regs}$ in the spleen were not observed when comparing treatment groups receiving CCL22/IL-2 to the control group (empty MNs), proving that $T_{reg}$ proliferation was not occurring in peripheral sites as opposed to systemic IL-2 administration. Results from the one-way MLR assay did not show significant differences in memory alloimmune responses hinting at the overall safety of the platform.

Analysis by flow cytometry of MN-sampled ISF confirmed a positive correlation between the frequencies of $T_{regs}$ present in ISF and those infiltrated in the skin allografts. Retrieved ISF displayed increased $T_{reg}$ frequencies when sampled from allografts treated with chemokine-loaded MNs in agreement with previous mechanistic analysis. MNs allowed ISF sampling to infer on the allograft state and to monitor the $T_{reg}$ homing process in a minimally-invasive way as opposed to graft biopsies.

In conclusion, we fine-tuned our theranostic HA-derived MN platform for the management of skin allograft rejection. The critical allure of this strategy is its universal application to many other immune mediated skin diseases, known to be caused by a defect in immunoregulation, most specifically in tissue resident $T_{regs}$. Restoring $T_{reg}$ number and function in diseased skin is the Holy Grail for many disorders such as Atopic Dermatitis, psoriasis and Alopecia Areata, so this MN platform could be leveraged as a leading solution for the management of autoimmune skin diseases. Here, MNs were proven to deliver bioactive immunomodulators other than nucleic acids into the skin allografts, and where the novel therapeutic pair of CCL22 and IL-2 can induce an immunosuppressive state in the allograft, unleashed by the proliferation of $T_{regs}$ following adoptive T cell transfer. $T_{reg}$ recruitment and expansion was restricted to the site of alloimmunity and did not induce systemic effects. Moreover, the HA-based MNs platform allows to surveil the $T_{reg}$ homing process, opening up potential avenues for the early detection of rejection episodes along with increased prospects of graft survival.

## 5.6   References

1.  Riley, R. S., June, C. H., Langer, R. & Mitchell, M. J. Delivery technologies for cancer immunotherapy. *Nat Rev Drug Discov* 18, 175–196 (2019).

2.  Milling, L., Zhang, Y. & Irvine, D. J. Delivering safer immunotherapies for cancer. *Adv. Drug Deliv. Rev.* 114, 79–101 (2017).

3.  Raffin, Caroline, Vo, Linda T. Bluestone, J. A. Treg cell-based therapies: challenges and perspectives. *Nat. Rev. Immunol.* 20, 158–172 (2020).

4.  Sakaguchi, S., Yamaguchi, T., Nomura, T. & Ono, M. Regulatory T Cells and Immune Tolerance. *Cell* 133, 775–787 (2008).

5.  Kalekar, L. A. & Rosenblum, M. D. Regulatory T cells in inflammatory skin disease: From mice to humans. *Int. Immunol.* 31, 457–463 (2019).

6.  Kang, S. M., Tang, Q. & Bluestone, J. A. CD4+CD25+ regulatory T cells in transplantation: Progress, challenges and prospects. *Am. J. Transplant.* 7, 1457–1463 (2007).

7.  Nguyen, A. V. & Soulika, A. M. The dynamics of the skin's immune system. *Int. J. Mol. Sci.* 20, 1811 (2019).

8.  Matejuk, A. Skin Immunity. *Arch. Immunol. Ther. Exp. (Warsz).* 66, 45–54 (2018).

9.  Jonuleit, H. *et al.* Infectious tolerance: Human CD25+ regulatory T cells convey suppressor activity to conventional CD4+ T helper cells. *J. Exp. Med.* 196, 255–260 (2002).

10. Wolff, M. J. *et al.* TH17, TH22 and Treg cells are enriched in the healthy human cecum. *PLoS One* 7, e41373 (2012).

11. Ali, N. & Rosenblum, M. D. Regulatory T cells in skin. *Immunology* 152, 372–381 (2017).

12. Hartwig, T. *et al.* Regulatory T Cells Restrain Pathogenic T Helper Cells during Skin Inflammation. *Cell Rep.* 25, 3564–3572 (2018).

13. Trüeb, R. M. & Dias, M. F. R. G. Alopecia Areata: a Comprehensive Review of Pathogenesis and Management. *Clin. Rev. Allergy Immunol.* 54, 68–87 (2018).

14. Castela, E. *et al.* Effects of low-dose recombinant interleukin 2 to promote T-regulatory cells in alopecia areata. *JAMA Dermatology* 150, 748–751 (2014).

15. Turissini, J. D., Elmarsafi, T., Evans, K. K. & Kim, P. J. Major Risk Factors Contributing to Split

Thickness Skin Graft Failure Skin. *Georg. Med. Rev.* 3, (2019).

16.  Uehara, M. *et al.* Anti-IL-6 eluting immunomodulatory biomaterials prolong skin allograft survival. *Sci. Rep.* 9, 6535 (2019).

17.  Rezaei, E. *et al.* Can Skin Allograft Occasionally Act as a Permanent Coverage in Deep Burns? A Pilot Study. *World J. Plast. Surg.* 6, 94–99 (2017).

18.  Pham, C., Greenwood, J., Cleland, H., Woodruff, P. & Maddern, G. Bioengineered skin substitutes for the management of burns: A systematic review. *Burns* vol. 33 946–957 (2007).

19.  Benichou, G. *et al.* Immune recognition and rejection of allogeneic skin grafts. *Immunotherapy* 3, 757–770 (2011).

20.  Klimczak, A. & Siemionow, M. Immune Responses in Transplantation: Application to Composite Tissue Allograft. *Semin. Plast. Surg.* 21, 226–233 (2007).

21.  Tang, Q. & Bluestone, J. A. Regulatory T-cell therapy in transplantation: Moving to the clinic. *Cold Spring Harb. Perspect. Med.* 11, a015552 (2013).

22.  Zhou, J., He, W., Luo, G. & Wu, J. Fundamental immunology of skin transplantation and key strategies for tolerance induction. *Arch. Immunol. Ther. Exp. (Warsz).* 61, 397–405 (2013).

23.  Wood, K. J., Bushell, A. & Hester, J. Regulatory immune cells in transplantation. *Nat. Rev. Immunol.* 12, 417–430 (2012).

24.  Kingsley, C. I., Karim, M., Bushell, A. R. & Wood, K. J. CD25 + CD4 + Regulatory T Cells Prevent Graft Rejection: CTLA-4- and IL-10-Dependent Immunoregulation of Alloresponses. *J. Immunol.* 168, 1080–1086 (2002).

25.  Zheng, X. X. *et al.* Favorably tipping the balance between cytopathic and regulatory T cells to create transplantation tolerance. *Immunity* 19, 503–514 (2003).

26.  Brunstein, C. G. *et al.* Umbilical cord blood-derived T regulatory cells to prevent GVHD: Kinetics, toxicity profile, and clinical effect. *Blood* 127, 1044–1051 (2016).

27.  Di Ianni, M. *et al.* T regulatory cell separation for clinical application. *Transfus. Apher. Sci.* 47, 213–216 (2012).

28.  Bluestone, J. A. *et al.* Type 1 diabetes immunotherapy using polyclonal regulatory T cells. *Sci. Transl. Med.* 7, (2015).

29.  Camirand, G. & Riella, L. V. Treg-Centric View of Immunosuppressive Drugs in

Transplantation: A Balancing Act. *Am. J. Transplant.* 17, 601–610 (2017).

30. Setoguchi, R., Hori, S., Takahashi, T. & Sakaguchi, S. Homeostatic maintenance of natural Foxp3+ CD25+ CD4+ regulatory T cells by interleukin (IL)-2 and induction of autoimmune disease by IL-2 neutralization. *J. Exp. Med.* 201, 723–735 (2005).

31. Boyman, O., Kovar, M., Rubinstein, M. P., Surh, C. D. & Sprent, J. Selective stimulation of T cell subsets with antibody-cytokine immune complexes. *Science (80-.* 311, 1924–1927 (2006).

32. Brunstein, C. G. *et al.* Adoptive transfer of umbilical cord blood-derived regulatory T cells and early viral reactivation. *Biol. Blood Marrow Transplant.* 19, 1271–1273 (2013).

33. Baluna, R. & Vitetta, E. S. Vascular leak syndrome: A side effect of immunotherapy. *Immunopharmacology* 37, 117–132 (1997).

34. Hirakawa, M. *et al.* Low-dose IL-2 selectively activates subsets of CD4+ Tregs and NK cells. *JCI Insight* 1, 1–18 (2016).

35. Grinberg-bleyer, Y. *et al.* IL-2 reverses established type 1 diabetes in NOD mice by a local effect on pancreatic regulatory T cells. *J. Exp. Med.* 207, 1871–1878 (2010).

36. Sather, B. D. *et al.* Altering the distribution of Foxp3+ regulatory T cells results in tissue-specific inflammatory disease. *J. Exp. Med.* 204, 1335–1347 (2007).

37. Fisher, J. D. *et al.* In situ recruitment of regulatory T cells promotes donor-specific tolerance in vascularized composite allotransplantation. *Sci. Adv.* 6, (2020).

38. Jhunjhunwala, S. *et al.* Bioinspired controlled release of CCL22 recruits regulatory T cells in vivo. *Adv. Mater.* 24, 4735–4738 (2012).

39. Montane, J. *et al.* CCL22 Prevents Rejection of Mouse Islet Allografts and Induces Donor-Specific Tolerance. *Cell Transplant.* 24, 2143–2154 (2015).

40. Montane, J. *et al.* Prevention of murine autoimmune diabetes by CCL22-mediated Treg recruitment to the pancreatic islets. *J. Clin. Invest.* 121, 3024–3028 (2011).

41. Joffre, O. *et al.* Prevention of acute and chronic allograft rejection with CD4 +CD25+Foxp3+ regulatory T lymphocytes. *Nat. Med.* 14, 88–92 (2008).

42. Ingulli, E. Mechanism of cellular rejection in transplantation. *Pediatr. Nephrol.* 25, 61–74 (2010).

43. Eskandari, S. K. *et al.* Regulatory T cells engineered with TCR signaling – responsive IL-2

nanogels suppress alloimmunity in sites of antigen encounter. *Sci. Transl. Med.* 12, 1–16 (2020).

44. Ding, R. *et al.* Messenger RNA for FOXP3 in the Urine of Renal-Allograft Recipients. *N. Engl. J. Med.* 353, 2342–2351 (2005).

45. Dahan, K., Matignon, M., Audard, V., Lang, P. & Grimbert, P. Intragraft Levels of Foxp3 mRNA Predict Progression in Renal Transplants with Borderline Change. *J Am Soc Nephrol* 19, 2277–2281 (2008).

46. Ye, Y., Yu, J., Wen, D., Kahkoska, A. R. & Gu, Z. Polymeric microneedles for transdermal protein delivery. *Adv Drug Deliv Rev* 127, 106–118 (2018).

47. Kim, Y.-C., Park, J. H. & Prausnitz, M. R. Microneedles for drug and vaccine delivery. *Adv. Drug Deliv. Rev.* 64, 1547–1568 (2012).

48. Zhang, X., Chen, G., Bian, F., Cai, L. & Zhao, Y. Encoded Microneedle Arrays for Detection of Skin Interstitial Fluid Biomarkers. *Adv. Mater.* 31, 1–8 (2019).

49. Samant, P. P. *et al.* Sampling interstitial fluid from human skin using a microneedle patch. *Sci. Transl. Med.* 12, 1–16 (2020).

50. Chang, H. *et al.* A Swellable Microneedle Patch to Rapidly Extract Skin Interstitial Fluid for Timely Metabolic Analysis. *Adv. Mater.* 29, 1702243 (2017).

51. He, R. *et al.* A Hydrogel Microneedle Patch for Point-of-Care Testing Based on Skin Interstitial Fluid. *Adv. Healthc. Mater.* 9, 1–11 (2020).

52. Eby, J. M. *et al.* CCL22 to Activate Treg Migration and Suppress Depigmentation in Vitiligo. *J. Invest. Dermatol.* 135, 1574–1580 (2015).

53. Neely, A. N. *et al.* Proteolytic activity in human burn wounds. *Wound repair Regen.* 5, 302–309 (1997).

54. Mccrudden, T. C. *et al.* Hydrogel-Forming Microneedles Prepared from '"Super Swelling"' Polymers Combined with Lyophilised Wafers for Transdermal Drug Delivery. *PLoS One* 9, e111547 (2014).

55. Pilat, N. *et al.* Treg-mediated prolonged survival of skin allografts without immunosuppression. 117, (2020).

56. Elhussein Mohamed, O. Y., Elazomi, A., Mohamed, M. S. & Abdalla, F. B. Local elevation of CCL22: A new trend in immunotherapy (skin model). *J. Cell. Immunother.* 2, 79–84 (2016).

57.     Matsuoka, K. I. *et al.* Low-dose interleukin-2 therapy restores regulatory T cell homeostasis in patients with chronic graft-versus-host disease. *Sci. Transl. Med.* 5, 1–12 (2013).

58.     Klatzmann, D. & Abbas, A. K. The promise of low-dose interleukin-2 therapy for autoimmune and inflammatory diseases. *Nat. Rev. Immunol.* 15, 283–294 (2015).

59.     Farina Jr, J. A. F., Rosique, M. J. & Rosique, R. G. Curbing Inflammation in Burn Patients. *Int. J. Inflam.* 2013, 715645 (2013).

60.     Murphy, S. P., Porrett, P. M. & Turka, L. A. Innate immunity in transplant tolerance and rejection. *Immunol. Rev.* 241, 39–48 (2011).

61.     Mehrotra, A., Leventhal, J. & Cravedi, P. Monitoring T cell alloreactivity. *Transpl. Rev* 29, 53–59 (2015).

62.     Turner, J. G., White, L. R., Estrela, P. & Leese, H. S. Hydrogel-Forming Microneedles : Current Advancements and Future Trends. *Macromol. Biosci.* 21, 1–18 (2021).

63.     Al Sulaiman, D. *et al.* Hydrogel-Coated Microneedle Arrays for Minimally Invasive Sampling and Sensing of Specific Circulating Nucleic Acids from Skin Interstitial Fluid. *ACS Nano* 13, 9620 (2019).

64.     Yang, B., Fang, X. & Kong, J. Engineered Microneedles for Interstitial Fluid Cell-Free DNA Capture and Sensing Using Iontophoretic Dual- Extraction Wearable Patch. *Adv. Funct. Mater.* 30, 1–13 (2020).

65.     Zheng, M. *et al.* Osmosis-Powered Hydrogel Microneedles for Microliters of Skin Interstitial Fluid Extraction within Minutes. *Adv. Healthc. Mater.* 9, 1–11 (2020).

66.     Zhu, J. *et al.* Gelatin Methacryloyl Microneedle Patches for Minimally Invasive Extraction of Skin Interstitial Fluid. *Small* 16, 1905910 (2020).

67.     Heidt, S. *et al.* Peripheral blood sampling for the detection of allograft rejection: Biomarker identification and validation. *Transplantation* 92, 1–9 (2011).

68.     Mandal, A. *et al.* Cell and fluid sampling microneedle patches for monitoring skin-resident immunity. *Sci. Transl. Med.* 10, (2018).

69.     Müller, A. C. *et al.* A comparative proteomic study of human skin suction blister fluid from healthy individuals using immunodepletion and iTRAQ labeling. *J. Proteome Res.* 11, 3715–3727 (2012).

This page left blank intentionally

**Chapter VI: Conclusions**

This page left blank intentionally

# Conclusions

Transdermal delivery platforms derived from poly(β-amino ester)s, either as free vehicles or integrated in microneedles, have been developed and described in this thesis. Immunomodulatory drugs have been delivered using the transdermal route for three cardinal applications of the immunotherapy field including: nucleic acid vaccination, cancer immunotherapy and adoptive cellular therapy.

Firstly, cell-specific targeting of APCs residing in the dermal milieu for nucleic acid vaccination has been achieved by decorating poly(β-amino ester)s with oligopeptide moieties and a mannose ligand for indirect and receptor-mediated targeting, respectively.

- *In vitro* transfection studies in cell types dominating antigen presentation in the skin corroborated that PBAEs including both cationic and anionic oligopeptides, along with their mannosylated counterparts, present superior transfection capacity.

- Analysis of gene expression in professional APCs such as Langerhans cells and dermal dendritic cells confirmed the unmatchable superiority of PBAEs bearing lysine and aspartic acid moieties following DNA/mRNA delivery studies.

- Results proved that mannosylation of PBAEs, if helpful for boosting overall transfection efficiencies, does not dictate cell-specific transfection; instead, oligopeptide decoration has been deemed as the main determinant in promoting targeted gene delivery.

Targeting PBAEs mediated modest levels of gene expression *in vivo* when delivered via hypodermic injection. Hence, integrating PBAEs into minimally-invasive transdermal platforms, in the form of polyplexes or as polyelectrolyte films, was proposed to facilitate delivery and localization of the therapeutics in the skin.

- PBAE polyelectrolyte films were efficiently deposited via the Layer-by-Layer method. Surface-mediated gene transfer has been achieved by using PBAEs as solvent-free delivery systems and where both the dilution buffer and number of bilayers impact transfection efficiency.

- Increased percentages of cell transfection have been reported when using polyplexes over PEMs in professional APCs. If normalizing the percentages per mass of nucleic acid, PBAE-derived PEMs appear to induce greater levels of gene expression.

- *Ex vivo* and *in vivo* transfection assays revealed that polyplexes promote higher levels of transfection while gene expression is similar if comparing invasive to MN-based delivery of nucleic acids, opening up therapeutic avenues for needle-free PBAE-based vaccination.

Next, the potential of MNs for cancer immunotherapy was explored, proposing the use of MNs integrating a diagnostic arm as part of a closed-loop system to simultaneously monitor the response to the immunotherapy.

- A digestible hydrogel-based MN platform has been successfully engineered for delivery of an immunomodulator while enabling sampling and recovery of the cellular fraction of ISF upon *ex vivo* digestion for immune surveillance.

- Swelling ability, mechanical strength, and on-demand digestibility of the MNs was thoroughly examined as a function of the crosslinking agent, which was confirmed to dictate the properties of the MN patch.

- Retrieval of both cellular and soluble biomarkers from ISF by the MNs has been confirmed *in vitro*. Following on-demand digestion of the patch under reducing conditions, such biomarkers are recovered in less than 5 minutes for further analysis.

- MN-based delivery of immunostimulatory nucleic acids, specifically a TLR-9 agonist complexed in PBAEs, has been demonstrated to prompt tumor growth suppression leading to a 3-fold reduction in tumor volume and a 2-fold increase in survival frequencies.

- MN-delivered ODNs managed to modulate the immunosuppressive tumor microenvironment by augmenting proinflammatory DCs. Moreover, an increase in the $CD8^+$ and $CD4^+$ T cell fraction was observed regardless of the administration route.

- Comparison of the immune profiles in ISF and the tumors suggests a correlation between the two tissues as observed by flow cytometry immunophenotyping, supporting the potential of MNs for minimally-invasive monitoring of the immune state.

Finally, leveraging the insights into immunomodulation and immunosurveillance using MNs, translation of the MN platform into an application that aimed for immunosuppression of the immune system, instead of its activation, was proposed.

- The previously developed MNs have been successfully fine-tuned for integral management of skin allograft rejection. *In vitro* functional studies proved that MNs can

deliver clinically-relevant doses of bioactive chemokines including CCL22 and IL-2. Tailoring of the delivery kinetics has been achieved via end-caping of the crosslinker as observed in release studies, shifting from a sustained to a burst-like release profile.

- *In vivo* studies using an adoptive transfer transplant model demonstrated that administering chemokine-loaded MNs to skin allografts unleashes an on-target, allograft-specific, and immunosuppressive effect. A three-pronged evaluation of the allograft state corroborated an increase in intragraft $T_{regs}$ infiltrates and a reduction in proinflammatory biomarkers.

- Mechanistic analysis performed on peripheral organs such as the spleens revealed that local delivery of IL-2 using MNs does not trigger systemic nor memory alloimmunity.

- An intimate correlation has been established between the immune profiles in skin allografts and those in ISF. Comparison of the cellular infiltrates from whole allograft biopsies and digested MNs revealed an increase in the frequencies of $T_{regs}$ in both allografts and ISF when therapeutic chemokines had been administered. Contrarily, only residual numbers of $T_{regs}$ were observed in the untreated group.

- The delivery-and-sampling functions of the MNs induced Treg proliferation in skin allografts to restore the immune homeostasis after transplantation and simultaneous monitoring of the therapy efficacy and the transplant state using a single, theranostic MN patch.

This page left blank intentionally